Study of Ozone Sensitivity to Precursors at High Spatial Resolution Using the Modified CMAQ-ADJ Model

by

Hongyan Dang

A thesis
presented to the University of Waterloo
in fulfillment of the
thesis requirement for the degree of
Doctor of Philosophy
in
Earth Sciences

Waterloo, Ontario, Canada, 2012

AUTHOR'S DECLARATION

I hereby declare that I am the sole author of this thesis. This is a true copy of the thesis, including any required final revisions, as accepted by my examiners.

I understand that my thesis may be made electronically available to the public.

Abstract

In this thesis, I apply the adjoint for the Community Multiscale Air Quality model (hereafter CMAQ-ADJ) in a high spatial resolution study of the sensitivity of ozone to several of its precursors in the regions surrounding the Great Lakes. CMAQ-ADJ was originally developed for low spatial resolution applications. In order to use it in high spatial resolution (12 km) studies, it was necessary to resolve a conflict between the pre-set fixed output time step interval in CMAQ-ADJ and the CMAQ-calculated irregular synchronization time-step and also to modify the meteorological interface for the backward model integrations. To increase computation efficiency, the chemistry time-step in the modified CMAQ-ADJ is checkpointed instead of being re-calculated in the backward part of the model as before.

I used the modified model to analyze the sensitivity of ozone to precursor species for cases of assumed high ozone episode in two target locations in southwestern and east-central Ontario. The studies examined the influence of pre-existing ozone, NO, CO, anthropogenic volatile organic compounds (VOCs) and isoprene on ozone level changes for the 69 hours immediately preceding the assumed high ozone event. The results are dominated by the long-distance advection, local meteorology (lake breezes), air temperature, the underlying surface features, and emissions in the pollutant pathway. Both production and titration of ozone by NOx is evident at different times and locations in the simulations. The industrial Midwest U.S. and Ohio Valley have been shown to be an important source of anthropogenic emission of NO and most VOCs that contribute to high ozone events in southwestern and east-central Ontario. Isoprene from the northern forest suppresses ozone in both target regions, with a greater magnitude in east-central Ontario. The response of ozone level in the two selected receptor regions in Ontario to different VOCs depends on the type of VOC, the time and location they are emitted, and the air temperature. Increasing VOC emissions in urban areas such as Toronto and Ottawa in the morning can enhance the ozone level by late afternoon. Increasing VOCs except ethylene and formaldehyde in regions with large VOC/NOx ratio in the morning tends to suppress the ozone level by late afternoon. Among all the species examined, NO has the largest impact on the target ozone level changes. CO is very unlikely to significantly influence the ozone level changes in southwestern or east-central Ontario.

Acknowledgements

First I would like to express my heartfelt gratitude to my supervisor Dr. James Sloan for the support of my Ph.D. study and research. Thanks for his financial support and guidance. Dr. Sloan has carefully supervised every step of my work so I can avoid many potential problems as early as possible. Thanks.

I also want to show my deep gratitude to my committee members Dr. Thomas Edwards, Dr. Andre Unger, and Dr. John Lin for their inspirations and help in my research and course works. I thank Dr. John Lin for sponsoring me using the SHARCNET cluster Brown. I would like to thank Dr. Michael Moran and Dr. Francis Poulin for their kindness for being the external examiners for my thesis.

I thank Dr. Amir Hakami heartily for providing the CMAQ-ADJ model, without which my thesis would not have been possible. His many suggestions in using and improving the CMAQ-ADJ model are also very grateful.

I truly appreciate Dr. Fan Meng's sharing with me all his experiences in using SMOKE and CMAQ-ADJ. Thank Dr. Zhuanshi He for providing meteorological data for my research. I thank him for his help in using CMAQ and NCL. Thank Dr. Deyong Wen, Alex Men, Dr. Thomas Kuhn, Jerry Hu, Dr. Lucas Neil, Yoga Arumugam, Zena Rebello, and Rabab Mashayekhi for their kind discussions. I thank the SHARKNET staff very much for their professional technique supports. I wish to thank Joshua Benmergui, William Sellier for proofreading my thesis.

Finally, I would like to thank my family and my friends for their endless support and encouragement.

Table of Contents

List of Figures

List of Tables

Chapter 1

Introduction

1.1 Motivation and objectives

Due to the complexity and nonlinearity of atmospheric physical and chemical processes, numerical air quality models (AQMs) have become one of the most important research tools to study the relationships between the emissions, transport, and transformation of air quality constituents.

AQMs have been extensively used in sensitivity studies of air pollution, i.e., how atmospheric pollutants respond to different perturbations such as emission changes or weather condition changes. There are two types of approaches in sensitivity studies using AQMs: direct sensitivity analysis and adjoint sensitivity analysis. A direct sensitivity analysis integrates AQMs forward in time and hence is a source-oriented approach. It is efficient when studying the response of all model variables to a small number of perturbations. Adjoint sensitivity methods are receptor-oriented backward approaches which are efficient to quantify the contribution from all sources to the perturbations in the target area at a specific time (target time). The adjoint for an AQM model can also be used to examine model parameters or further be applied to variational data assimilations due to its ability to calculate the derivatives of a cost function.

This thesis is based on the adjoint for the Community Multi-scale Air Quality (CMAQ) modeling system. The first version of the adjoint for CMAQ (hereafter CMAQ-ADJ) was published in 2007 by Hakami et al. (2007), which was developed from CMAQ both manually and with the help of a software "Kinetic Pre-Processor" for adjoint sensitivity analysis of chemical kinetic systems in three-dimensional air quality models (Daescu et al., 2003; Sandu et al., 2003). In addition to all the supporting libraries inherited from CMAQ, CMAQ-ADJ contains more than 160 subroutines with more than 60,000 lines of source codes in FORTRAN. In this thesis, three modifications are applied to CMAQ-ADJ code:

1. Modify the model code so that CMAQ-ADJ will not be restricted by model resolution, especially at high resolutions.
2. Modify the implementations of the horizontal advection in the original CMAQ-ADJ.
3. Find and fix other problems caused by using I/O API library.

After modifying CMAQ-ADJ, three scenarios were designed to examine the modified version of CMAQ-ADJ, as well as to apply the modified model to high resolution air quality sensitivity studies in Ontario.

The three scenarios designed for studying the sensitivities of ozone in the target regions (southwestern Ontario or east-central Ontario) to its precursor species and to the pre-existing ozone used meteorological and emission data of July 2007. The first scenario investigated under typical summer weather conditions, how the precursor species makes a contribution in the research domain to an assumed high ozone episode with a mixing ratio 100 ppb everywhere in the target region. The second scenario investigated a case that has the same meteorological conditions as Scenario 1, but different high ozone episode, i.e., ozone concentrations increases by 40 ppb everywhere in the target region. In the third scenario, the same ozone perturbation as Scenario 1 was used, but under different weather conditions than Scenario 1.

Furthermore, the modified CMAQ-ADJ was used to replace the CMAQ-ADJ in the 4D-Var modeling system of CMAQ (Singh and Sandu, 2007) to provide the community a scientific tool for high resolution four-dimensional data assimilation of CMAQ.

1.2 Contributions

A modified version of the adjoint for CMAQ is provided to the community. Compared with the original CMAQ-ADJ, the modified CMAQ-ADJ can work at any resolution under any weather conditions; therefore, the new version of the model makes sensitivity studies in nested regions possible. It can also be applied to high resolution variational data assimilation or parameter estimation studies. The modified CMAQ-ADJ has a modified meteorological

interface so that transport from distant regions to pre-set target regions can be detected. The chemistry time-step in the backward part of the modified CMAQ-ADJ uses the checkpointed data from the forward model, which is not re-calculated as in the original CMAQ-ADJ. The correct checkpointing of the chemistry time-step is essential for an air quality model as chemistry integration is the major process in such models. A high resolution 4D-Var data assimilation interface for the CMAQ model has also been provided in this thesis, the interface has been examined using dummy data.

Adjoint sensitivity studies of Ontario ozone to its influencing chemicals were conducted using the modified CMAQ-ADJ at high spatial resolution (12 km) in two-level nested domains. Compared to those sensitivity studies on Ontario ozone changes using forward sensitivity methods, the adjoint method has shown its high efficiency in calculating detailed spatial and temporal evolution features of all precursors so that ozone pollution can be studied systematically in a way that has not been done before.

Located downwind of the Great Lakes, southwestern Ontario and east-central Ontario are strongly influenced by local circulation that is related to lake effect. The sensitivity results have shown that pollutants can be trapped within the region for at least 69 hours under typical summer weather conditions in this area. Pollutants over lake regions have larger effect on ozone in Ontario than those over land regions. Pollutants can also be advected to this area from distant regions by large scale winds.

The pre-existing ozone transported along the northern side of the Great Lakes Basin can enhance the ozone level in east-central Ontario, but have little influence on ozone changes in southwestern Ontario. Enhanced pre-existing ozone levels in the industrial Midwest U.S. and Ohio Valley have less influence on the ozone level in east-central Ontario in the next 2 days to 69 hours than that in southwestern Ontario under the typical summer weather conditions used in this study. Increasing ozone in urban area such as Chicago, Detroit, or Toronto will suppress the ozone level in both target regions 2 days to 69 hours later. Newly increased ozone has a larger effect to local ozone increase than ozone added earlier.

By increasing nitrogen monoxide (NO) emission in northern Ontario, the ozone level in both southwestern and east-central Ontario can be enhanced in at least the next 2 days to 69 hours. In reality, northern Ontario has relatively little anthropogenic NO. Therefore, the high

ozone event in the above two Ontario regions should not be attributed to NO here, but to the large amounts of anthropogenic NO in Midwest U.S. and Ohio Valley, as the modified CMAQ-ADJ has calculated a large area of positive sensitivity of ozone to NO there. This implies that the industrial Midwest U.S. and Ohio Valley is an important source of ozone pollution in both southwestern and east-central Ontario. Increasing NO emission in urban areas such as Toronto can suppress later ozone formation. NO emissions in the morning or early afternoon have the largest potential to be transformed to ozone in the late afternoon. NO has largest influence on ozone formation among all the species examined.

Carbon monoxide (CO) enhances ozone formation in all cases in this study, but the magnitude is very small compared to that of NO and VOCs emissions. CO alone is very unlikely to cause a significant ozone increase in southwestern and east-central Ontario.

Additional VOC emissions from northern Ontario can suppress ozone formation in both southwestern and east-central Ontario. As there are little anthropogenic activities in northern Ontario, biogenic VOC emissions from vegetation and forest are left to become a possible sink for ozone in southwestern and east-central Ontario. Anthropogenic VOC emissions (except toluene) in the Midwest U.S. and Ohio Valley can enhance the ozone formation in southwestern and east-central Ontario. Toluene tends to suppress ozone production in the two target regions in Ontario except those emitted in urban areas several hours before the high ozone event.

The magnitude of ozone response to VOCs is a combined result of the type of VOC, the location of the VOC emission, the time when the VOC was emitted, and temperature. In the highly polluted area at Toronto, morning emissions of almost all VOCs enhance local ozone level by late afternoon, but those VOC emissions 2 days to 69 hours prior can suppress downwind ozone formation in the next 2 days to 69 hours. A morning release of carbon compounds in Ottawa can also enhance local ozone level by late afternoon. The magnitude of the ozone sensitivity to different VOCs and the area of the influencing region of different VOCs are different, which is related to the specific property of the VOC. A larger portion of carbon compounds contributes to later ozone formation in the selected receptor regions. A detailed summary can be found in the last Chapter of this thesis.

1.3 Structure of the thesis

This study will mainly focus on the improvement of CMAQ-ADJ model and the application of the modified version of CMAQ-ADJ at high spatial resolution to investigate the influencing factors that relate to the high ozone event in southwestern and east-central Ontario. The organization of this thesis is as follows.

Chapter 2 shows the importance of tropospheric ozone, and then reviews major research results about tropospheric ozone in the world and in Ontario. The formation of ozone from its precursors is provided, which will be the major theoretical basis for the rest of this thesis.

In Chapter 3, the formulation of the U.S. EPA's air quality forecast model CMAQ and its major processes are described. The construction of CMAQ-ADJ is based on these formulations. This chapter also introduces the necessary supporting sub-processors that drive both CMAQ and CMAQ-ADJ.

Chapter 4 will summarize direct sensitivity methods, adjoint sensitivity methods, and their applications in air quality studies. The original version of the adjoint for CMAQ (published in 2007) will be then introduced. Some of its major limitations and the solutions to remove these limitations will be given.

Chapter 5 will mainly focus on studying Ontario ozone sensitivities using the modified CMAQ-ADJ. To conduct further sensitivity study, it is essential to set the model correctly. The performance of CMAQ in the research domain was used to examine the model settings. Then the CMAQ-simulated VOC/NOx chemistry regimes that will be used to analyze the results of the modified CMAQ-ADJ were provided.

Ozone sensitivities in both southwestern and east-central Ontario will be investigated in three scenarios, separately. The spatial distribution and temporal evolution of the sensitivity fields of pre-existing ozone, ozone precursors NO, and organic compounds will be analyzed in detail for both target regions, ending with their individual summaries.

The scope and future work are presented in Chapter 6. Because another important application of an ajdoint model is 4D-Var data assimilation, it is necessary to combine the modified CMAQ-ADJ with an optimizer software to form a 4D-Var data assimilation system for CMAQ. Since no comprehensive applications using real observational data were

conducted, this work was presented in Chapter 6, but the code will be provided with the thesis.

Conclusions are provided in Chapter 7.

Chapter 2

Tropospheric ozone

2.1 Introduction

In the lower atmosphere, ozone has become the pollutant of concern in both industrial countries and developing countries. The long lifetime of ozone in the atmosphere (1 to 2 months in winter and 1 to 2 weeks in summer) makes it a global air quality issue (Brasseur et al., 1999). West et al. (2009) showed that with the increase in tropospheric ozone level in polluted regions since preindustrial times, the global background ozone has also increased. The surface ozone concentration has increased from ~10 to 15 parts per billion (ppb) since the industrial revolution to recent ~30 to 40 ppb in remote areas of the world (FinlaysonPitts and Pitts, 1997). It has been found that anthropogenic emissions of nitrogen oxides ($NOx = NO + NO_2$) and other ozone-related species such as non-methane volatile organic compounds (NMVOCs), CO, and CH_4 contribute to the increase in ozone pollution (Lelieveld and Dentener, 2000; Wang and Jacob, 1998). The northern-hemispheric ozone in the troposphere increases about 60±20% by the combined pollution emissions from North America, Europe, and Asia (Lelieveld and Dentener, 2000; Wang and Jacob, 1998). The elevation of tropospheric O_3 level in the tropical areas and southern hemisphere such as Indonesia, central Africal, Southern Africa, South America, and south Atlantic region has close relationship with biomass burnings in Africa, Indonesia, and South America, as reviewed by Chandra et al. (2002) and Fishman and Brackett (1997). A detailed summary of the long-term trends in tropospheric ozone trends at different locales in the world can be found in Forster et al. (2007).

As the major air pollution element, ozone is a respiratory irritant, it reduces human's lung function and increases respiratory symptoms (Ito et al., 2005; Lippmann, 1991). Chronic exposure to ozone is associated with exacerbation of asthma and premature mortality (Lippmann, 1993). Research by Bell et al. (2005) has shown strong evidence of a short-term association between ozone and cardiovascular and respiratory mortality. Gryparis et al. (2004) found that high ozone concentrations are associated with the increase in the total daily

number of deaths, cardiovascular deaths, and respiratory deaths. Ozone is also toxic to natural ecosystems and agriculture. Ozone can cause agricultural crop loss and plant damages (Heck et al., 1982; Krupa and Manning, 1988; Reich and Amundson, 1985). Ozone destroys other natural and man-made materials such as plastic, metallic materials and rubber (Altshuller et al., 1961; Andries et al., 1979; Layer and Lattimer, 1990).

Tropospheric ozone is also an important greenhouse gas. The increase in the large-scale background tropospheric ozone level causes positive radiative forcing. It heats the low level atmosphere through the greenhouse effect by trapping long-wave terrestrial radiation (Philander, 1998). Atmospheric models have estimated an increase in the radiative forcing at around +0.35 wm^{-2} due to the increase in tropospheric ozone levels since the Industrial Revolution in 1750 (Forster et al., 2007). In comparison, the estimated combined anthropogenic radiative forcing of the same period is around +1.6 wm^{-2} (Forster et al., 2007). There is a strong correlation between high-O_3 events with high temperature (Lin et al., 2000; Sillman and Samson, 1995), therefore, the warm climate caused by the increased ozone can favor the formation of more ground-level ozone, which results in a positive feedback loop. The surface ozone might not always increase when considering other effects of a warmer climate. For example, the isoprene emission also increases when the air temperature is high (Constable et al., 1999). Isoprene ozonolysis is an important O_3 loss pathway. Ozone production is suppressed when NOx is removed as organic nitrates by the direct reaction between isoprene and O_3, especially under isoprene-saturated chemical regime (Fiore et al., 2005).

In a hotter climate, there is more water vapour in the atmosphere. Water vapour is the major source of tropospheric hydroxyl radical (OH), which is initiated by the photodissociation of ozone by ultraviolet light (Lelieveld and Dentener, 2000; Monks, 2005):

$$\mathbf{O_3 + h\gamma \xrightarrow{\lambda<330\,nm} O + O_2} \qquad 2\text{-}1$$

$$\mathbf{H_2O + O \rightarrow OH + OH} \qquad 2\text{-}2$$

where hγ is the product of the Planck constant and the frequency of light at wavelength $\lambda < 330\,nm$. OH controls the atmospheric lifetime of many trace gases (Lelieveld and

Dentener, 2000) such as methane. Methane is also a greenhouse gas and takes part in global climate change (FinlaysonPitts and Pitts, 1997). OH further reacts with hydrocarbons to produce organic peroxy radicals (RO_2, details in Section 2.2), and takes part in complex nonlinear ozone production chemistry through NO-to-NO_2 conversion (Lelieveld and Dentener, 2000; Wennberg and Dabdub, 2008). Some researchers have shown that total tropospheric O_3 level can decrease due to the increase in temperature and water vapor (Brasseur et al., 1998; Johnson et al., 2001). Through the above positive and negative feedbacks, tropospheric ozone contributes to complex climate forcing. Climate change also influences the concentration and distribution of tropospheric ozone through a variety of direct and indirect processes such as non-linear microphysical processes, chemical transformations, and meteorological effects (Constable et al., 1999).

In Canada, ozonesondes from Canadian stations show that from 1980 to 1990, the tropospheric ozone level has a decreasing trend, but the trend rebounds to a positive trend between 1991 and 2001 (Tarasick et al., 2005). In Ontario, over the past three decades, the average ozone level in the lower atmosphere has risen by 30% in summer months and 65% in the winter months (Figure 1) (www.airqualityontario.com/press/publications.cfm). Although the ozone level can decrease through reducing its precursor emissions (FinlaysonPitts and Pitts, 1997), the increasing ozone trend in Ontario is opposite to the decreasing precursors. Over the 1998 to 2007 period, in Ontario, emissions of NOx were lowered by 30% and CO by 29% (www.airqualityontario.com/press/publications.cfm). Research by Geddes et al. (2009) shows that summer ozone levels do not show significant changes in the Greater Toronto Region due to the 30~40% decrease of precursor NOx and VOC since 2000. They concluded that this reflects the competing effects from complex NOx-VOC chemistry (details in Section 2.2) and transport from the west and the south. Galvez (2007) and Yap et al. (1988) suggested that transboundary transport of ozone and anthropogenic emissions of ozone precursors from the nearby U.S. states may be important contribution to summer high ozone episodes in southern Ontario. Brankov et al. (2003) used back-trajectory clustering analysis to study air mass flow and found that polluted air masses from the Ohio River Valley and the industrial U.S. Midwest can lead to significantly higher ozone concentrations at the CN tower site in Toronto. Cluster analysis of 10-year (1994-2003) data shows air flows from the

southwest passing over Michigan and entering southern Ontario, further influence ozone level in Eastern Canada (Johnson et al., 2007). The sensitivity study of (Fast and Heilman, 2005) in the Great Lakes regions revealed that increased anthropogenic emissions does not necessarily increase summer ozone production when the meteorological conditions are not favorable, i.e., when northwesterly flows brings cooler and wetter air parcels.

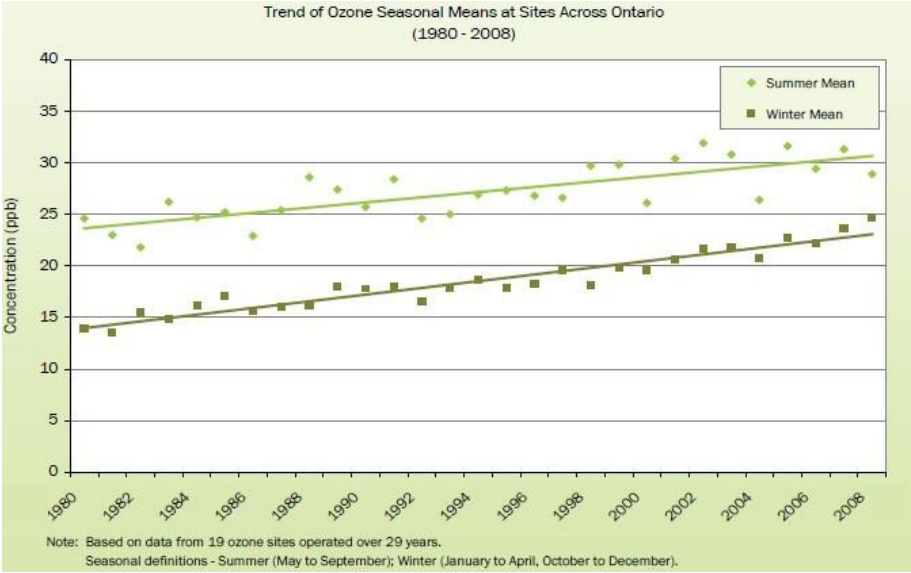

Figure 1. Averaged surface ozone trend in Ontario in warm and cold seasons. Reprint of Figure 2.6 of (AQO2008, 2010).

2.2 Tropospheric ozone chemistry

Ozone in the troposphere is a secondary air pollutant, it can be transported downward from the stratosphere (Junge, 1962; Logan, 1985). The main source of tropospheric ozone is formed through the *in situ* nonlinear photochemical reactions of carbon compounds and nitrogen oxides NO and NO_2 (Crutzen, 1973; Fishman et al., 1979). Lelieveld and Dentener (2000) concluded that about 90% of the boundary layer O_3 is formed this way. The ozone formation reactions almost always start by the oxidization of VOCs, hydrocarbons RH (H is a hydrogen atom. R is a carbon-containing fragment), or CO by the OH radical (Sillman, 1999):

$$\mathbf{VOC + OH \overset{O_2}{\rightarrow} RO_2 + H_2O} \qquad 2\text{-}3$$

$$\mathbf{CO + OH \overset{O_2}{\rightarrow} HO_2 + CO_2} \qquad 2\text{-}4$$

The peroxy radical $\mathbf{RO_2}$ represents any of a number of chains of organics with an $\mathbf{O_2}$ attached. Free radicals $\mathbf{HO_x}$ ($\mathbf{HO_2}$ or $\mathbf{RO_2}$) react with NO to form $\mathbf{NO_2}$. $\mathbf{OH}$ is regenerated in this process:

$$\mathbf{RO_2 + NO \xrightarrow{O_2} secondary\ VOC + HO_2 + NO_2} \quad 2\text{-}5$$

$$\mathbf{HO_2 + NO \xrightarrow{O_2} OH + NO_2} \quad 2\text{-}6$$

The secondary VOCs are intermediate organic species, typically including aldehyde and ketones (Sillman, 1999). NO_2 is photolyzed to generate NO and atomic oxygen. O_3 is formed when the oxygen atom combines with O_2 and a third body molecule M (N_2 or O_2):

$$\mathbf{NO_2 + h\gamma \xrightarrow{\lambda<430nm} NO + O} \quad 2\text{-}7$$

$$\mathbf{O + O_2 + M \rightarrow O_3 + M} \quad 2\text{-}8$$

The ozone formation rate is non-linear and depends on the rate of the initial reaction of VOC with OH. Normally, the time scale of this ozone formation reaction and the following ozone removal reaction occur on a time scale of 200s or less (Sillman, 1999). When the photolytic production of OH is shut down at night, the organics are oxidized by the nitrate radical NO_3, which is formed under the presence of sufficient concentrations of NO_2 and O_3 (FinlaysonPitts and Pitts, 1997).

Ozone concentrations can be suppressed through the process of NO_x tritration during which O_3 is removed by reacting with NO (Seinfeld and Pandis, 1998):

$$\mathbf{NO + O_3 \rightarrow NO_2 + O_2} \quad 2\text{-}9$$

Suppressed ozone concentrations are most likely to be observed at nighttime and in the immediate downwind vicinity of large point source emissions of NO such as in power plant plumes (Gillani and Pleim, 1996). In daytime, NO_x tritration is normally balanced by the photolysis of NO_2, except near large NO emission sources where there is net production of NO_2 from O_3. Nighttime ozone is a net removal process since photolysis rates are zero (Sillman, 1999).

As described above, the formation and destruction of ground-level ozone are the result of complex photochemical reactions between nitrogen oxides NO_x and VOCs. Local ozone levels are determined by these precursor species through a non-linear effect. Reduction in precursor concentrations hence does not necessarily lead to decreased ozone levels. An increase in ozone level may appear in some urban areas due to decreased ozone titration effect (Geddes et al., 2009). Meteorological condition such as wind is closely correlated to the increase in the background ozone transported from other regions (Chou et al., 2006; Geddes et al., 2009; Vukovich and Sherwell, 2003). Therefore, the emission and transport of NO and VOCs, as well as the transport of background ozone, are important issues for ozone sensitivity studies.

The Ontario Ministry of the Environment and Environment Canada issue several smog advisories to the public every summer when the ground-level ozone concentrations are forecasted to exceed the one-hour Ambient Air Quality Criteria (AAQC) of 80 ppb (AQO2007, 2008). Ozone alone can be the main driver of a summer smog in southwestern Ontario (BAQS, 2008). For example, ground-level ozone was responsible for 99% of the Ontario Ministry of the Environment standard (no particulate matter included) "poor" air quality hours in southern Ontario in summer 2001 (Galvez, 2007). In this thesis, I use a modified version of the CMAQ-ADJ and model-simulated summer data in 2007 to study the influencing factors of high ozone events in southwestern and east-central Ontario.

Chapter 3

MODELS-3/CMAQ

3.1 Framework of MODELS-3

The Models-3 Community Multi-scale Air Quality (M3-CMAQ) modeling system was developed by the United States Environmental Protection Agency (U.S. EPA) to describe the multi-scale spatial and temporal evolutions of more than 200 air quality constituents (depends on chemical mechanisms used) in the atmosphere, including the major pollutants such as tropospheric ozone and its precursor species NOx, VOCs, fine particles, toxics, acidic deposition, and visibility degradation (Byun and Young, 1999; EPA-SMOKE, 2007).

CMAQ contains three components (Models-3): meteorology, emission, and chemistry (Byun and Schere, 2006). The meteorological modeling system provides the atmospheric states and motions for the emission and the chemistry. The emission model deals with anthropogenic and natural emissions that are injected into the atmosphere. The CMAQ Chemical Transport Model (CCTM) simulates the pollutant chemistry and dynamics. As the center of CMAQ, CCTM can give a complete deterministic description of the processes of pollutant transport, chemical transformations of the gas and/or aqueous phase, aerosol chemistry and dynamics, and plume chemistry.

Since 2003, CMAQ has been adopted by the U.S. National Centers for Environmental Prediction (NCEP) to provide surface ozone concentration forecasts for up to 48 hours for the northeastern U.S. (Davidson et al., 2004). CMAQ became the operational air quality forecasting system at the U.S. NCEP in 2004. By now, CMAQ has been extensively examined and used by more than 1000 users throughout the world since its first release in June 1998 (http://www.epa.gov/AMD/peer/posters/Abstract_1.1.pdf). The Waterloo Centre for Atmospheric Sciences (WCAS) at the University of Waterloo has used CMAQ to study air quality issues since 2003 (Brulfert et al., 2007; Gbor et al., 2006; Gbor et al., 2007; Meng et al., 2007; Wen, 2006). The development of this thesis is based on CMAQ and its adjoint model CMAQ-ADJ (Byun and Schere, 2006; Hakami et al., 2007).

3.2 The Community Multi-scale Air Quality modeling system (CMAQ)

From 1998 to 2010, the U.S. EPA released 11 versions of CMAQ to the public with efficiency improvements, implementation modifications, and updates of science in all aspects to include the advancements in the science of aerosols, chemistry, process analysis, clouds, vertical diffusion, advection, and so on (http://www.cmaq-model.org/). A newer version of CMAQ does not always excel compared to the older versions in the model's performance with respect to the simulation of key pollutants (Foley et al., 2010).

In the CMAQ modeling system, air quality issues are solved numerically with finite difference approximations in "one-atmosphere" on 3-dimensional (3-D) Eulerian one-way monoscale grids.

3.2.1 Key model components and processes

The CCTM of CMAQ solves the trace concentration evolutions in the atmosphere. The science in CCTM explicitly corresponds to a hierarchical functional modular structure (Byun and Schere, 2006). These explicit scientific processes are the time rate of the change of concentration, horizontal advection, vertical advection, horizontal eddy (turbulent) diffusion, vertical eddy diffusion, production or loss from chemical reactions (gas-phase chemical reactions), emissions, aqueous transformations, plume-in-grid process, and the deposition and formation of aerosols. The model used in this study does not include the subgrid scale plume, aqueous-phase chemistry, or aerosol modules.

The advection and diffusion processes describe the transport of chemicals in the atmosphere (Byun et al., 1999). The mean-wind advection can transport a plume of pollutants a long distance without much change in the concentration. The turbulent-mixing diffusion makes the pollutant tend to mix quickly near the sources causing substantial concentration changes (Byun, 2002).

The 3-D advection processes in CMAQ is artificially decomposed to horizontal and vertical components. The horizontal advection is further split into x- and y- directions. The

two 1-D processes are solved separately, each solution acting as the other's initial condition (Byun et al., 1999).

Reynolds flux terms are produced when applying the ensemble averaging to decompose the velocity components and concentrations related nonlinear processes into mean and turbulent terms (Byun et al., 1999). CCTM simulates the turbulent diffusion processes in both horizontal and vertical directions in which the *K* theory is used to parameterize the turbulent flux terms. Molecular diffusion caused by the random motion of molecules is not included in CMAQ (Byun and Schere, 2006). The deposition process in CMAQ is considered to be the diffusion flux at the bottom of the model (Byun and Schere, 2006).

Since any flux from the bottom and the top of the atmosphere (100 hPa) is zero, CMAQ does not handle groundwater issues. Surface water flow is not considered either by CMAQ or the supporting meteorological model MM5 used in this thesis. When aqueous chemistry module is included in CMAQ, the concentration of chemical species will change, and these species take part in aqueous chemistry when they dissolve in cloud water droplets (Baek et al., 2011). In CMAQ, thermodynamic equilibrium controls the amount that gas-phase species dissolves into the cloud water, while accumulation-mode aerosols act as nucleation particles for cloud droplet formation and are assumed to be completely absorbed into the cloud water (Byun and Schere, 2006). Aqueous chemistry module in CMAQ is composed of equilibrium reactions including gas-liquid phase partitioning and dissociation, kinetic chemical reactions of S(IV) to S(VI), removal mechanisms such as wet deposition and scavenging, and SOA formation from methyl glyoxal and glyoxal (Baek et al., 2011). The CMAQ used in this thesis does not include aqueous chemistry, as detailed in Section 3.2.2.

3.2.2 Gas-phase chemical kinetics

As the essential component of an air quality model (AQM), gas phase chemical mechanisms describe the chemical reactions between reactive atmospheric species from a few up to more than 4000 depending on the complexity of the mechanism (Dodge, 2000). The involved reactions have various characteristic time scales that correspond to a set of nonlinear

ordinary differential equations and become a computationally intensive problem for AQMs (Mathur et al., 1998). Different chemical mechanisms may use different ways to simplify organic chemistry and use different parameterizations and approximations to solve the reaction rates, product mass, pressure and temperature dependence of rate constants, and photolysis parameters (Dodge, 2000; Kuhn et al., 1998). Production of the same species by different chemical mechanisms can have an uncertainty range of 30% or more (Russell and Dennis, 2000).

The chemical mechanisms that have been used in CMAQ include version 4 of the Carbon Bond (CB4) (Gery et al., 1989), CB05 which is an updated version of CB4 (Yarwood et al., 2005), and SAPRC-99 (Carter, 2000). The CB4 used in CMAQ has up to 14 species (46 in total, 30 of which are organic species) and 15 more reactions (96 in total) than its original version (Gison and Young, 1999). The domain extent has also been formulated not only for planetary boundary layer but also for the upper troposphere. Therefore, the updated CB4 is appropriate for regional scale modeling, in addition to the original urban scale modeling. There are 4 versions of CB4 in CMAQ, i.e., basic version, CB4-AQ (with aqueous chemistry processes), CB4-AE (with aerosol processes), and CB4_AQ_AE (with both aerosol and aqueous chemistry processes). CB05 further updated CB4's reaction rate constants, increased species to 59 kinds (10 organic species and radicals) , and increased the reactions to 156 (Yarwood et al., 2005). The SAPRC-99 in CMAQ has included the production of aerosol and organic acids; it has 80 species and 214 reactions. Compared with CB4 and CB05, SAPRC-99 has more detailed organic chemistry. The Carbon Bond mechanisms CB4 and CB05 use lumped structure techniques to group organic compounds into mechanism species based on the bond types associated with individual carbon atoms (Whiten et al., 1980). SAPRC-99 uses a lumped molecule approach (a generalized or surrogate species, i.e., a single species represents compounds of the same class) to represent similar organic compounds (Lurmann et al., 1987; Yu et al., 2010). Lumping chemical mechanisms in the atmospheric modeling of VOCs is done to ensure that the model is of reasonable size and complexity (Lewis et al., 2000).

These three mechanisms have been evaluated comprehensively regarding their performances on the prediction of ozone and ozone related species against measurements.

Faraji et al. (2008) found that for most urban areas in southeast Texas, CB4 and SAPRC-99 produce similar ozone concentrations. Luecken et al. (2008) found that except for many urban areas and the central U.S., CB4, CB05, and SAPRC predicted similar ozone concentrations for the rest of the United States. Yu et al. (2010) found that in terms of ozone prediction over the eastern United States, none of the above 3 mechanisms show better performance than others, CB4 has the best performance for observed ozone less than 75 ppb. The gas-phase photochemical mechanism used in this thesis is the basic CB4.

The basic CB4 mechanism contains 36 species and 93 reactions, 11 of these 93 reactions are photolytic reactions. The basic CB4 has nine primary organic species that are injected directly into the atmosphere. Except for the explicitly represented ethylene, isoprene, and formaldehyde, the other primary organic species represent carbon-bond types, i.e., the single bonds (paraffins), double-bonded carbon atoms (olefins), 7-carbon ring structures (toluene), and 8-carbon ring structures (xylene). The aldehydes represent the carbonyl group and adjacent carbon atom in acetaldehyde and higher molecular weight aldehydes (Gipson and Young, 1999). The species for the basic CB4 mechanism are listed in Table 1, the 93 reactions of CB4 are listed in Appendix A (Gipson and Young, 1999).

Table 1. **Species names for the CB4 core mechanism.**

Species Name	Description	Number of Carbons
NO2	Nitrogen dioxide	0
NO	Nitric oxide	0
O	Oxygen atom in the $O^3(P)$ electronic state	0
O3	Ozone	0
NO3	Nitrate radical	0
O1D	Oxygen atom in the $O^1(P)$ electronic state	0
OH	Hydroxyl radical	0
HO2	Hydroperoxy radical	0
N2O5	Dinitrogen pentoxide	0
HNO3	Nitric acid	0
HONO	Nitrous acid	0
PNA	Peroxynitric acid (HNO_4)	0
H2O2	Hydrogen peroxide	0
CO	Carbon monoxide	1
FORM	Formaldehyde	1
ALD2	Acetaldehyde and higher molecular weight aldehydes	2
C2O3	Acetylperoxy radical	2
XO2	NO to NO_2 conversion from alkylperoxy (RO_2) radical	0
PAN	Peroxyacetyl nitrate	2
PAR	Paraffin carbon bond (C-C)	1
XO2N	NO to organic nitrate conversion from alkylperoxy (RO_2) radical	0
ROR	Secondary alkoxy radical	0
NTR	Organic nitrate ((RNO_3))	1
OLE	Terminal olefin carbon bond (R-C=C)	2
ETH	Ethene	2

TOL	Toluene and other monoalkyl aromatics	7
CRES	Cresol and higher molecular weight phenols	8
TO2	Toluene-hydroxyl radical adduct	7
OPEN	Aromatic ring opening product	4
CRO	Methylphenoxy radical	7
XYL	Xylene and other polyalkyl aromatics	8
MGLY	Methylglyoxal and other aromatic products	3
ISOP	Isoprene	5
ISPD	Isoprene product (lumped methacrolein, methyl vinyl ketone, etc.)	4
SO2	Sulfur dioxide	0
SULF	Sulfuric acid (gaseous)	0

3.3 Supporting sub-processors

As a regional forecast model, the CMAQ chemistry transport model (CCTM) is driven by several offline input data (EPA-CMAQ, 2009): emissions, meteorological data, initial inputs, boundary conditions, and clear sky photolysis rates.

CMAQ is an emission-based model. Its air pollutant inputs come from pre-processed emission data such as point emission from individual facilities or a single sources, area emissions from stationary and diffuse sources over areas, biogenic emissions estimated by the Biogenic Emission Inventory System, Version 3 (BEIS3) (Geron et al., 1994; Guenther et al., 2000; Pierce et al., 1998; Williams et al., 1992), and mobile source emissions from on-road motor vehicles and other mobile equipment. Any available emission inventory data for the modeled year must be temporarily allocated to all grids in the simulation region from their geographic units. These data are allocated by annual, seasonal, weekly, or daily values (EPA-SMOKE, 2007). The Sparse Matrix Operator Kernel Emission (SMOKE) modeling system generates hourly gridded data of both individual chemical species and lumped (grouped) species defined by CMAQ (CMAQ, 2007).

The meteorological data calculated by meteorological modeling systems are pre-processed by the Meteorology-Chemistry Interface Processor (MCIP) to coordinate between available meteorology data and the requirements of CMAQ such as map projections, grid and coordinate transformations, parameters and variables necessary for CMAQ integration to maintain dynamic consistency and compatibility with the meteorology data. The offline meteorological data used in this thesis are calculated from the Fifth-Generation National Center for Atmospheric Research/Pennsylvania State University Meso-scale Model (MM5) (Grell et al., 1994). MM5 solves for the full set of atmospheric physical and thermodynamic governing equations. MCIP also processes meteorological inputs for SMOKE model.

JPROC, which is called "clear sky photolysis rate calculator", provides the temporal varying clear sky photolysis rate look-up table for the photochemical reactions in CCTM (Roselle et al., 1999). The photolysis rates at various altitudes, latitudes, and hours are calculated daily based on the chemical mechanism for every simulation day. The calculated photolysis rates are interpolated for each grid cell in the simulation domain. When there are clouds, the clear-sky photolysis rates are corrected using parameterization methods (Roselle et al., 1999).

The initial and boundary conditions are calculated by the Initial Conditions Processors (ICON) and the Boundary Conditions Processors (BCON) (Gipson, 1999). ICON produces initial concentration fields for all CMAQ chemical species from time-independent clean-atmosphere vertical concentration profiles. After a period of spin-up to eliminate the influence of the time-independent initial conditions, the model dynamics and chemistry start to take control of the simulation. The CMAQ outputs of the spin-up run are used as the initial conditions for the simulation of the research time period. To include the transport effects, the research domain can be designed to be nested into a larger domain. In this event, the boundary conditions of the large domain use the averaged concentrations provided by the CMAQ default. The inner research domain uses dynamical 3-dimensional boundary conditions processed by BCON from the large domain calculations.

3.4 Input/Output Applications Programming Interface (I/O API)

The Models-3 Input/Output Applications Programming Interface (I/O API) is designed to control data communication within and between all components in the CMAQ modeling system (Coats, 2005). I/O API provides great convenience for the CMAQ users to retrieve data directly from "multiple time steps of multiple layers of multiple variables" (CMAQ, 2007). Another two benefits of I/O API are that I/O API files are independent of computing platforms and I/O API provides a set of tools to help manipulate and analyze CMAQ data files (CMAQ, 2007).

I/O API is written in FORTRAN and C on top of the self-describing Network Common Data Format (netCDF), an interface for array-oriented standard direct data access file format developed at the National Center for Atmospheric Research (Rew et al., 2011).

The internal and external data flow of CMAQ is controlled by the I/O API library. As the CMAQ users mainly have interest in regular air quality information such concentration outputs of chemical species at a regular frequency (typically every one hour), the design of I/O API interface also has this feature.

I/O API can handle time-independent variables and restart files (Table 2: Time-independent and Circular-buffer). I/O API also deals with "time-stepped" files that contains some positive integer multiple of the time step, i.e., regular time-stepped air quality information in the model. This will limit I/O API from being applied to variable time-steps. I/O API is designed to deal with gridded 4-dimensional variables (Table 3). Using I/O API subroutines to deal with data that are not 4-dimensional causes problems.

Table 2. Possible time step structures in IO/API files. Reprint of Table 4.1 in (CMAQ, 2007).

File Type	Description
Time-independent	The file's time-step attribute is set to zero. Routines which deal with time-independent files ignore the date and time arguments
Time-stepped	The file has a starting date, a starting time, and a positive time step. Read and write requests must be for some positive integer multiple of the time step from the starting date and time.
Circular-buffer	This type of file keeps only two "records", the "even"" part and the "odd" part (useful, for example, for "restart" files where only the last data written in the file are used). The file's description has a starting date, a starting time, and a negative time step (set to the negative of the actual time step). Read and write requests must be for some positive integer multiple of the time step from the starting date and time, and they must reflect a specific time step that is in the file.

Table 3. IO/API allowed data types. Reprint from Table 4.2. Possible Data Type Structures in IO/API in (CMAQ, 2007).

File Type	Magic Number	Data Type	Description
CUSTOM3	-1	Custom	User-dimensioned array of REAL*4s that these system reads/writes reliably
DCTNRY3	0	Dictionary	Data type stores and retrieves parts of an FDESC.EXT file description
GRDDED3	1	Gridded	Dimension as REAL*4 ARRAY (NCOLS, NROWS, NLAYS, NVARS)
BNDARY3	2	Boundary	Dimension as REAL*4 ARRAY (SIZE, NLAYS, NVARS)

Chapter 4

CMAQ-ADJ and modified CMAQ-ADJ

4.1 Sensitivity methods

A sensitivity analysis studies how a system responds when one or more of its parameters change. As the atmosphere is a complex nonlinear dynamical system, the sensitivity of air pollution can be studied effectively though air quality models (AQMs). AQMs can solve the nonlinear physical and chemical processes of emissions, advection, diffusion, and photochemical reactions (Russell and Dennis, 2000) through solving the differential forms of the control fluid dynamic equations and the involving chemical processes. A complex AQM may include thousands of inputs and parameters such as chemical species in the atmosphere, emissions from various sources, variables that control the dynamics of atmosphere, parameters used by physical and chemical mechanisms. The importance of these parameters to a particular perturbation can be ranked through comparing the sensitivity coefficients (the ratio of the output change of the model to the input perturbation), which are computed by doing a sensitivity analysis using AQMs (Martien and Harley, 2006b).

4.1.1 Direct sensitivity analysis

A direct sensitivity analysis integrates a model forward in time after the perturbations are added to one or more of the model's initial parameters at a specific location (source), and hence calculates the responses of all model state variables to these perturbations at a future time throughout the modeling domain (Dunker, 1984; Dunker et al., 2002b; Hakami et al., 2003; Napelenok et al., 2008; Sandu et al., 2003; Yang et al., 1997). Such a source-oriented direct approach for sensitivity analysis is therefore efficient when studying how a small number of sources influence multiple outputs or the entire sensitivity field (Hakami et al., 2006; Martien and Harley, 2006b; Zhang et al., 2008).

One of the direct sensitivity methods that approximate the first-order sensitivity coefficient is the brute-force method (Bergin et al., 1995; Russell et al., 1995; Seigneur et al., 1981). In the brute-force method, the sensitivity is calculated by comparing the predictions of

one perturbation of model inputs each time with the model base run. Brute-force method is straightforward and easy to implement, but is not efficient when investigating a large quantity of influencing factors. Another direct sensitivity method "direct decoupled method" (DDM) solves the sensitivity coefficients by integrating the sensitivity equations decoupled from the control equations of the model (Dunker, 1981; Dunker, 1984). DDM is more efficient than the brute-force method when investigating a large number of sensitivity parameters. Dunker et al. (2002b) used a 3-D air quality model to demonstrate that the sensitivity obtained by the brute-force method can converge to the DDM sensitivity when the brute-force perturbations are small.

Most sensitivity studies using photochemical models are based on the forward source-based methods (Martien and Harley, 2006b). Yang et al. (1997) implemented a DDM sensitivity method in a 3-D air quality model and proved that this method is straightforward and computationally efficient. Dunker et al. (2002a) compared the first-order sensitivity obtained by the DDM for a 3-D simulation of an ozone episode in the Lake Michigan region with the source contributions of NOx and VOCs to ozone formation estimated by an ozone source apportionment technology. They found that the DDM first-order sensitivity can explain 70% of the ozone concentrations. Hakami et al. (2003) used a 3-D air quality model to study the ozone sensitivity with respect to NO emission in central California. They found that the DDM results show reasonable agreement with the brute-force results.

In contrast to the forward method in which the sensitivity is propagated along the model trajectories forward in time, the receptor-based adjoint analysis calculates the propagation of the perturbation given in a receptor region at a target time backward in time and space (Hakami et al., 2007).

4.1.2 Adjoint sensitivity analysis

4.1.2.1 Introduction

An adjoint sensitivity analysis is a receptor-oriented backward approach that provides the sensitivity of a pre-defined cost function (penalty function, see Section 4.1.2.3 for more details) (Hakami et al., 2007; Henze et al., 2007; Martien and Harley, 2006b; Sandu et al.,

2005; Vukicevic and Hess, 2000; Vukovich and Sherwell, 2003; Zhang et al., 2008). One adjoint model run can provide the spatial and temporal information of all sources of the changes for all times during the simulation period at a given receptor region by calculating the derivative of a cost function with respect to all the model state variables backward in time (Errico, 1997; Hakami et al., 2006). This is because the effect of the implicit diffusion is included in an adjoint solution (Vukicevic and Hess, 2000). Adjoint sensitivity studies are therefore efficient in characterizing the source-receptor relationships such as determining the locations of influencing precursor emissions on a limited number of outputs at a given receptor site and time (Errico, 1997; Hakami et al., 2006; Zhang et al., 2008). As a comparison, a back-trajectory analysis provides the single trajectory that influences the target point, but the influencing region of an adjoint method is a 3-D region that simultaneously includes all transport pathways (Vukicevic and Hess, 2000). Adjoint methods have deficiencies as well. Adjoint modeling requires large computer storage capacity, as all outputs from its high-time-resolution processes need to be recorded to generate adjoint variables for all of the model variables. The other deficiency is that the realization of the adjoint of a model requires a large amount of programming directly on the model code. The solution of the adjoint for most nonlinear atmospheric models is constructed based on the linearization of some model terms and hence it only approximates the difference solutions. The evolution of a cost function is usually assumed linear with respect to the perturbations of model fields. Le Dimet et al. (2002) stated that the first-order adjoint only provides necessary conditions for an optimal solution, but the second-order analysis can improve the convergence of the optimization methods and help estimate the impact of errors on the prediction. To go one step further, it is worthwhile to study the second-order adjoints in the future.

Adjoint models have been increasingly used in air quality studies for sensitivity analysis and data assimilation. Vukicevic and Hess (2000) used a regional chemical transport model to conduct adjoint sensitivity analysis to examine the sensitivities of chemical species over Hawaii. They analyzed the transport of modeled emissions from various regions to Hawaii, and the associated transport pathways and timescales. Vautard et al. (2000) used the adjoint of a simplified reactive transport model CHIMERE to diagnose and simulate air pollution in Paris and its surrounding areas. They found that the ozone peak is mostly sensitive to

morning solvent releases and traffic emissions. Menut (2003) investigated the sensitivity of ozone, Ox ($O_3 + NO_2$), and NOx peaks using a 3-D chemistry-transport model and its adjoint. They found that traffic, solvent surface emissions, and meteorological parameters such as temperature play the most important role in the pollutant concentrations. Mallet and Sportisse (2005) used the chemistry-transport model Polair3D to examine the time evolution and the extent of the sensitive regions of the sensitivity of ozone concentrations with respect to anthropogenic and biogenic emissions at European scale in summer 2001. They identified the chemical species to which photochemistry is the most sensitive. Muller and Stavrakou (2005) used the observed ground-based CO and GOME satellite NO_2 measurements in the adjoint of a global IMAGE model to improve CO and NOx emissions. Yumimoto and Uno (2006) used the adjoint of a chemical transport model (RAMS/CTM) to look for a missing source of CO in East Asia region. Their results showed that the missing CO emission could be from Russia or Europe. Hakami et al. (2006) applied an adjoint method to the nationwide ozone nonattainment sensitivity study using a continental scale chemical transport model (Sulfer Transport Eulerian Model) and found the inadequacy of the simple cap and trade programs. Martien and Harley (2006a) and Martien and Harley (2006b) developed the adjoint for the 3-D California Institute of Technology photochemical model and applied it to selected sites in southern California to diagnose the peak ozone sensitivity to the emissions in that area. Henze et al. (2007) presented the adjoint of the global chemical transport model GEOS-Chem and demonstrated its feasibility of exploiting gas- and aerosol-phase measurements for optimizing emission inventories of aerosol precursors. Zhang et al. (2008) investigated the sensitivity of ozone concentrations in the Dallas Fort Worth area using the adjoint approach in the Sulfer Transport Eulerian Model. Zhang et al. (2009) used GEOS-Chem and its adjoint to investigate the transport of ozone over Northern Pacific from East Asia to North American. They demonstrated the ability of GEOS-Chem to provide detailed geographical and temporal information about pollution sources. In this thesis, the CMAQ-ADJ model developed by Hakami et al. (2007) is modified to study the ozone sensitivity in southwestern Ontario and east-central Ontario.

4.1.2.2 Method

The adjoint method has both continuous and discrete approaches. In the continuous adjoint approach, the adjoint partial differential equations for calculating the desired gradients are first derived, then are linearized from the nonlinear governing equations of the forward model to generate a tangent linear model, and finally are discretised for solution (Giles and Pierce, 2000). The adjoint programming of this approach is less complex than the discrete approach but one might have difficulty to identify if a slight disagreement is due to the inexact gradient of the cost function or a code error (Giles and Pierce, 2000). In the discrete adjoint approach, the algebraic equations are derived from the discretisation of the original control equations (Giles and Pierce, 2000). The adjoint program of this approach hence can be created from the forward model code (Giles and Pierce, 2000). Due to such conceptual differences, the sensitivities calculated by the continuous and discrete adjoint approaches are different (Giles and Pierce, 2000). The discrete adjoint model results in the gradients of a cost function exactly for all cases, including nonlinear and iterative algorithms which can ensure the optimization process is fully converged. The continuous adjoint method is clearer in terms of physically interpreting the significance of the nature of the adjoint solutions (Giles and Pierce, 2000; Henze et al., 2007; Pironnea, 1974). Whether these two approaches can give a consistent results or one of them has compelling advantages over the other remains an open question because there is no proof of higher-order accuracy in multi-dimensional problems (Giles and Pierce, 2000). Vukicevic and Hess (2000) used a discrete method when developing the adjoint solution, based on the fact that some studies show that the discrete approaches are more accurate than the continuous approaches (Vukicevic, 1991; Vukicevic, 1998; Vukicevic and Errico, 1993; Zou et al., 1993). This study adopts the discrete CMAQ-ADJ rather than the continuous CMAQ-ADJ.

4.1.2.3 Cost function

The cost function has various forms for different adjoint sensitivity studies and for other applications of adjoint methods such as variational data assimilation. For example, the cost function used by Yumimoto and Uno (2006) is the discrepancy between the simulation and the observation. Errico (1997) chose the average vertical component of the relative vorticity

extending through the bottom half of the atmosphere within the target square at the target time as the cost function. Hakami et al. (2006) defined a nationwide nonattainment metric that considers both the 1-hour and 8-hour nonattainment threshold as the cost function. The cost function used in the adjoint modeling experiment by Vautard et al. (2000) is the ozone concentration in the afternoon.

In variational data assimilation, the cost function is defined to contain the information from the observations, the model predictions, and their errors. The errors in model states and in observations can never be observed directly. The error realizations can be taken to make empirical statistics by assuming that they are stationary over a time period and uniform over a domain. The error statistics can also be specified using a fraction of the climatological statistics of the field (Bouttier and Courtier, 2005).

The cost function J in variational data assimilations has two terms. The observation term J_o measures the model prediction errors. The background term J_b measures the deviation from a background (also called a priori estimates or the first guess of the model).

$$J = J_o + J_b$$

$$J_o = \frac{1}{2}(x-y)^T O^{-1}(x-y)$$

$$J_b = \frac{1}{2}(x-x^b)^T B^{-1}(x-x^b)$$

Where $(x-y)^T$ is the transpose of the vector of the discrepancy between the predicted model state vector x and the observation vector y. It is assumed that y has been interpolated to the model space.

$O^{-1} = (Var(\epsilon_o))^{-1} = (\overline{(\epsilon_o - \overline{\epsilon_o})(\epsilon_o - \overline{\epsilon_o})^T})^{-1}$ represents the inverse of the error covariance matrix for the observation errors $\epsilon_o = y - x_t$. The average $\overline{\epsilon_o}$ is the bias that represents the systematic problems in the observations. These systematic problems include instrumental errors, errors in the interpolation, and the representativeness errors such as the discretization errors which prevent the model predictions from being perfect. The state vector x_t is the best possible representation of the true solution. It is used to represent the true state at the time of the analysis (the perfect analysis). x_t can be calculated by some method used for solving nonlinear optimization problems.

$x - x^b$ represents the difference between the model state x and the background information x^b. x^b can be taken from a segment of the a priori estimate (forecast) of the true model state (before the analysis is carried out), provided by a previous forecast. When the background is a previous forecast, its errors are then a combination of the analysis and the model errors, evolved in time according to the model dynamics. x^b is the first guess (the initial point of the minimization of the cost function) when used to initiate the minimization procedure. In practice, the first guess can be taken to be equal to the background, but is not compulsory. If the minimization is satisfactory, the analysis will not depend significantly on the choice of the first guess. It will always be sensitive to the background. B is the background error covariance. It is a square symmetric matrix in a multi-dimensional system. It is usually the estimates of the error variances in the forecast that is used to produce x^b. B is only defined at the initial time. $B^{-1} = (Var(\epsilon_b))^{-1} = (\overline{(\epsilon_b - \overline{\epsilon_b})(\epsilon_b - \overline{\epsilon_b})^T})^{-1}$, where $\epsilon_b = x_b - x_t$ is the background error. The average of the background error $\overline{\epsilon_b}$ is the model drift of the assimilating system. x_t is the same as the one that is used to calculate the observation error.

4.1.2.4 The gradient of the cost function

An adjoint model can calculate the gradient of a pre-defined cost function with respect to all model fields. The gradient of the cost function is a necessary input for some optimization software to conduct 4D-Var data assimilation. Among all cost functions, those used in variational data assimilation have the most complex form. A general derivation of the gradient of the cost function used in 4D-Var is given in this section.

For a forecast model such as CMAQ, its future model state is determined by the initial values. Together with the model internal physics and chemistry, the model can therefore be assumed to have the following form:

$$x_t = M_{t-1}(x_{t-1}) = M_{t-1}M_{t-2} \ldots M_0(x_0) \qquad 4\text{-}1$$

Where x_t is the state variable. x_0 is the initial input of the model. M is the model operator, designating the model physics and chemistry.

For $x_i = M_{i-1}(x_{i-1})$,

$$dx_i \cong \frac{\partial M_{i-1}}{\partial x_{i-1}} dx_{i-1} = L_{i-1}(x_{i-1})dx_{i-1} \quad 4\text{-}2$$

Equation 4-2 is the tangent linear equation of the model. Iteratively, the relation between dx_i and dx_0 is established as:

$$dx_i = L_{i-1}(x_{i-1})L_{i-2}(x_{i-2}) \cdots L_0(x_0)dx_0 = L_i dx_0 \quad 4\text{-}3$$

L_i is the tangent linear operator, which depends on the basic state x_{i-1} and the time step $i-1$.

The optimal initial model state in variational analysis minimizes the cost function J. J therefore satisfies $\nabla J(x_0) = 0$ (Le Dimet et al., 2002). As introduced in last section, in 4D-Var, J has the following form:

$$J = J_o + J_b \quad 4\text{-}4$$

$$J_o = \frac{1}{2}(x-y)^T O^{-1}(x-y) \quad 4\text{-}5$$

$$J_b = \frac{1}{2}(x-x^b)^T B^{-1}(x-x^b) \quad 4\text{-}6$$

Equation 4-5 is the model prediction misfit from observations, weighted by the inverse of the observation error covariance O, y is the observation vector. The backround term Equation 4-6 measures the distance between the model and the background state, weighted by the inverse background error covariance B. Both O and B are symmetric matrices and satisfy:

$$(O^{-1})^T = (O^T)^{-1} = O^{-1} \quad 4\text{-}7$$

$$(B^{-1})^T = (B^T)^{-1} = B^{-1} \quad 4\text{-}8$$

The gradient of the cost function is:

$$\nabla J = \nabla J_o + \nabla J_b \quad 4\text{-}9$$

Only the background model state at initial time takes part in the calculation of the gradient of the background term of the cost function. Using the following relationship for a symmetric matrix A:

$$d(z^T Az) = z^T Adz + dz^T Az = z^T Adz + (dz^T Az)^T = z^T Adz + z^T Adz = 2z^T Adz \quad 4\text{-}10$$

Where z is a matrix, the gradient of the background term of the cost function is:

$$\nabla J_b = \frac{\partial J_b}{\partial x_0} = B_0^{-1}(x_0 - x_0^b) \quad 4\text{-}11$$

Now focus on deriving the gradient of the observation term of the cost function ∇J_o. For a vector $N = N(x_0, x_1, \cdots, x_n)$, the differential of this vector is:

$$dN = \frac{\partial N}{\partial x_0}dx_0 + \frac{\partial N}{\partial x_1}dx_1 + \cdots + \frac{\partial N}{\partial x_n}dx_n = \left[\frac{\partial N}{\partial x_0}, \frac{\partial N}{\partial x_1}, \ldots, \frac{\partial N}{\partial x_n}\right]\begin{bmatrix} dx_0 \\ dx_1 \\ \vdots \\ dx_n \end{bmatrix} = [\nabla N]^T dx \quad 4\text{-}12$$

Consider a small perturbation of the model state δx, the resulted change in the observation term of the cost function is then:

$$dJ_o = J_o(x + dx) - J_o(x) \cong \frac{\partial J_o}{\partial x}dx = [\nabla J_o(x)]^T dx \quad 4\text{-}13$$

From the definition, J_o measures the misfit between the model state and the observations:

$$J_o = \frac{1}{2}(x - y)^T O^{-1}(x - y) = \frac{1}{2}\sum_{i=0}^{N}(x_i - y_i)^T O_i^{-1}(x_i - y_i) \quad 4\text{-}14$$

Take the differential of J_o, using the relationship Equation 4-12:

$$dJ_o = \sum_{i=0}^{N}(x_i - y_i)^T O_i^{-1} dx_i \quad 4\text{-}15$$

Combine Equation 4-13 and Equation 4-15,

$$[\nabla J_o(x)]^{\mathrm{T}} dx = \sum_{i=0}^{N}(x_i - y_i)^T O_i^{-1} dx_i \quad 4\text{-}16$$

Using the relationship in Equation 4-3, for the cost function gradient at the initial state:

$$[\nabla J_o(x_0)]^{\mathrm{T}} dx_0 = \sum_{i=0}^{N}(x_i - y_i)^T O_i^{-1} dx_i \quad 4\text{-}17$$

$$[\nabla J_o(x_0)]^{\mathrm{T}} dx_0 = \sum_{i=0}^{N}(x_i - y_i)^T O_i^{-1} L_{i-1}(x_{i-1}) L_{i-2}(x_{i-2}) \cdots L_0(x_0) dx_0 \quad 4\text{-}18$$

$$[\nabla J_o(x_0)]^{\mathrm{T}} = \sum_{i=0}^{N}(x_i - y_i)^T O_i^{-1} L_{i-1}(x_{i-1}) L_{i-2}(x_{i-2}) \cdots L_0(x_0) \quad 4\text{-}19$$

Take the transpose of this equation on both sides:

$$\nabla J_o(x_0) = \sum_{i=0}^{N} {L_0}^T(x_0) \cdots {L_{i-2}}^T(x_{i-2}) {L_{i-1}}^T(x_{i-1}) O_i^{-1}(x_i - y_i) \quad 4\text{-}20$$

$$\nabla J_o(x_0) = \sum_{i=0}^{N} {L_i}^T O_i^{-1}(x_i - y_i) \quad 4\text{-}21$$

Where,

$${L_i}^T = {L_0}^T(x_0) \cdots {L_{i-2}}^T(x_{i-2}) {L_{i-1}}^T(x_{i-1}) \quad 4\text{-}22$$

is the transpose of the tangent linear operator defined in Equation 4-3. The transpose is the adjoint operator. In this equation, the integration starts from the inverse of the error-covariance-weighted difference between the observation and the model state at time i. The order of the time index of the adjoint operator is reversed. Then:

$$\nabla J_o(x_0) = O_0^{-1}(x_0 - y_0) + {L_0}^T O_1^{-1}(x_1 - y_1) + {L_1}^T O_2^{-1}(x_2 - y_2) + \cdots + {L_{i-2}}^T O_{i-1}^{-1}(x_{i-1} - y_{i-1}) + {L_{i-1}}^T O_i^{-1}(x_i - y_i)$$

4-23

$$\nabla J_o(x_0) = O_0^{-1}(x_0 - y_0) + L_0{}^T(O_1^{-1}(x_1 - y_1) + L_1{}^T(O_2^{-1}(x_2 - y_2) + \cdots + L_{i-2}{}^T(O_{i-1}^{-1}(x_{i-1} - y_{i-1}) + L_{i-1}{}^T O_i^{-1}(x_i - y_i)))$$

4-24

Equation 4-24 is the solution to the observational term of the gradient of the cost function. Together with the solution to the background term in Equation 4-11, the gradient of the cost function has been derived.

4.2 CMAQ-ADJ

The adjoint for the Community Multiscale Air Quality model (CMAQ-ADJ) was developed by Hakami et al. (2007) based on the version 4.5.1 of the CMAQ model of the U.S. EPA. CMAQ-ADJ uses the basic version of the gas-phase chemical mechanism CB4 which has 36 variables including the primary and secondary atmospheric pollutants such as ozone, nitrogen oxides and VOCs. Therefore, CMAQ-ADJ provides an efficient research tool to conduct sensitivity studies of the major pollutants in the atmosphere. CMAQ-ADJ also makes the 4-dimensional variational data assimilation of CMAQ possible by providing the gradient of a cost function with respect to all model variables. Singh and Sandu (2007) combined CMAQ-ADJ with the L-BFGS optimization package (Byrd et al., 1995; Zhu et al., 1997) to set up a 4-D variational data assimilation system for the CMAQ model. Resler et al. (2008) and Resler et al. (2009) parallelized the CMAQ-ADJ adjoint operator and applied the CMAQ 4D-Var data assimilation system to optimize the initial conditions and emission factors. They showed that the 4D-Var assimilation experiment performed well. The inverse modeling of CMAQ is also a quantitative, physically-based method for source apportionment so as to efficiently estimate the contribution of various sources to the atmospheric composition at a given location. Capps and others (2009) coupled CMAQ-ADJ with the adjoint of ISORROPIA (a package that calculates aerosol thermodynamical equilibrium) to generate a tool for source apportionment and reconciliation of emission inventories with the observed inorganic aerosol species and their gaseous precursors. The basic CB4 used by CMAQ-ADJ does not include aerosols. Zhao and others (2009) developed the adjoint for

CMAQ's aerosol modules which includes aerosol microphysics, aerosol thermodynamics, heterogeneous chemistry and cloud processes in a discrete approach. Gou et al. (2009) constructed a discrete advection adjoint for CMAQ with the aid of the automatic differential tool TAMC (Tangent linear and Adjoint Model Compiler) (Giering and Kaminski, 1998). They compared the performances of the discrete adjoint method with the continuous adjoint method. They found that the discrete adjoint sensitivity matches the finite difference results better than the continuous adjoint sensitivity.

The CMAQ-ADJ code was constructed both manually and using an automatic code generator (Hakami et al., 2007). The adjoint for the gas-phase chemical mechanism CB4 was generated using the Kinetic Pre-Processor software (KPP) version 2.2. KPP is an automatic code-generation software for adjoint sensitivity analysis of chemical kinetic systems in three-dimensional air quality models (Daescu et al., 2003; Sandu et al., 2003). Hakami et al. (2007) manually generated the discrete adjoints for the horizontal and vertical diffusions, vertical advection, and continuous adjoints for the horizontal advection. The diffusivity accounts for the stretching and shearing deformation characteristics of wind (Byun and Schere, 2006).

CMAQ-ADJ has two parts, i.e., the forward model and the backward (adjoint) model. The dynamics and chemistry of the forward model of CMAQ-ADJ are same as the CMAQ model. CMAQ generates concentration predictions every "output" time-step, i.e., the first-level time step (CMAQ has 4 levels of time-steps. The 2^{nd}-level time step is synchronization time-step. The 3^{rd}-level time step is advection time-step. The 4^{th}-level time step is chemistry time-step. More details are provided below). The "output" time-step is set by the users and is typically set to one hour. Mixing ratios at one hour intervals are mostly used for both research purposes and operational purposes. The ground-level observations of the concentration of pollution species are also usually every one hour. In CMAQ-ADJ, the state vectors and air density of CMAQ are checkpointed at each synchronization (sync) time-step. All the information calculated every sync time-step (second-level time step) in the forward model are needed for the backward (adjoint) model runs. This is because the adjoint equations are coupled to the diffusion equations that CCTM solves (Hakami et al., 2006). Predetermined fixed synchronization steps are set for checkpointing purpose in the original CMAQ-ADJ in each simulation day (Hakami et al., 2007). The checkpointed data in the

forward model will be read at the beginning of each corresponding sync time-step in the backward simulation. In the backward model, the internal chemistry time steps are recalculated by the forward integration of the concentrations for the sync time-step (Hakami et al., 2007). CMAQ-ADJ was validated for a 1 day simulation for $45 \times 46 \times 18$ grids domain with 36 km horizontal resolution (Hakami et al., 2007).

In this study, the fixed synchronization time-step algorithm was replaced. This algorithm causes problems in high resolution simulations. The model code was also modified so that the backward integration does not recalculate the internal chemistry time-steps. The recalculation reduces computational efficiency and is not necessary because the backward of the model uses the same chemistry time-steps as the forward part of CMAQ-ADJ.

4.3 Modified CMAQ-ADJ

4.3.1 New treatments to solve model resolution restrictions

In the discrete CMAQ-ADJ, a fixed time-step is used to save the concentration data, air density, and photolysis rates in the forward part of the model for the initial inputs of the adjoint model (Hakami et al., 2007). The fixed time-step is chosen as 12 minutes, which is the maximum recommended (default) sync time-step since the 2003 release of the CMAQ model (http://www.epa.gov/AMD/CMAQ/release43.html). Similar fixed time-step algorithms in adjoint models can be found in Martien and Harley (2006b) in the adjoint of California Institute of Technology model (Harley et al., 1993; Mcrae et al., 1982). They used a 3-minute output interval which is less than the minimum advective time-step in the model.

When running CMAQ-ADJ at the 12 km grid resolution over the Great Lakes region under the July 2007 weather conditions in this study, CMAQ-ADJ failed after several model-minutes of integration. The output information showed that the failure was due to a conflict between the fixed model output time and a "time" that is calculated by the model.

The CMAQ-ADJ in Hakami et al. (2007) has a horizontal resolution of 36 km. Compared with the 36 km horizontal resolution, the 12 km grid used in this study is 3 times finer. Finer resolutions make it possible to capture smaller scale intense weather phenomena

accompanying strong winds in meteorological models. In relatively coarse resolution cases, high wind speeds of sub-grid systems are usually averaged by mild winds. In addition, an intense summer weather system such as a storm usually lasts for a short time period, which implies that the highest wind speed of the different consecutive hours can be very different.

To avoid computational instabilities during the model integrations, the advective time-step Δt in CMAQ is determined by the Courant–Friedrichs–Lewy condition (Courant condition hereafter) $\Delta t \leq \frac{\Delta x}{u}$. The courant condition uses the highest horizontal wind speed (u) of a selected vertical layer during that output time-step (typically every 1 hour). The advective time-step belongs to the 3rd level of CMAQ's four time-step scales.

The first level time-step of the CMAQ modeling system is the output time-step which is defined by the user for air quality prediction at regular time intervals. The 1st level time-step is typically set to 1 hour because hourly data are most commonly used in research and prediction activities. The second level time-step of CMAQ is the sync time-step. All processes such as horizontal advection and diffusion, vertical advection and diffusion, advection adjustment in mixing ratio conservation properties, deposition, and gas-phase chemical reactions are conducted within one sync time-step and then propagated onto the next sync time-step, and so on. Sync time-steps are evenly distributed within each 1st level time-step of CMAQ. When the model resolution is set, different 1st level time-step (different hours) still might have different number of sync time-steps due to the fact that the sync time-step is determined by CMAQ's 3rd level time-step (the advective time-step). Wind speeds vary constantly. The hourly (every output time-step) highest wind speeds used by the Courant condition vary as well. As a consequence, the advective time-step might not be a constant for the whole simulation period. Therefore, the resulted sync time-step for different output time-steps can be different. If the model-calculated number of sync time-steps every output time-step is less than five, it is set to five by the CMAQ default. In this case, the sync time-step is 12 minutes, which is the same as the fixed sync time-step used in the original version CMAQ-ADJ.

As analyzed above, fine resolutions or possible strong winds should correspond to a small advective time-step $\Delta t \leq \frac{\Delta x}{u}$ to maintain computational stability. If Δt is set to a fixed

number, it must be small enough so that the model works for any fine resolutions under all weather conditions. Very small Δt is unnecessary for the coarse resolution and small wind speed cases. It consumes computation time without improving accuracy, i.e., when the mixing of the pollutants is very slow, outputs from several Δts can be very similar. Checkpointing data with such a time interval (Δt) in an adjoint model needs huge computer storage.

When the calculated sync time-step based on the Courant condition is shorter than the pre-set 12 minutes in the original version of CMAQ-ADJ, a conflict happens and the model aborts. To solve the time-step conflicts in the original version of CMAQ-ADJ and to avoid the aforementioned problems at the same time, neither the 12-minute sync time-step for data checkpointing in the whole simulation period as used in CMAQ-ADJ nor a sufficient short fixed time-step is adopted. The modified CMAQ-ADJ uses the time-varying time-steps determined by the Courant condition $\Delta t \leq \frac{\Delta x}{u}$. As such, the modified CMAQ-ADJ allows an automatic adjustment when the model resolution (Δx) changes or any weather occurs during the study period. The sensitivity runs in this study have shown that the modified CMAQ-ADJ can work for high resolution cases under different wind speeds without abnormal aborts.

Friction is larger near the Earth's surface than at high layers. Wind aloft is therefore mostly higher than wind at lower levels. The Courant-condition limited time-step for the advection at high levels therefore can be much smaller. CMAQ does not accordingly use the shortest advective time-step to determine the sync time-steps since its version released in 2003 (http://www.epa.gov/asmdnerl/CMAQ/release43.html). The planetary boundary layer (PBL) is of great research interest. Therefore, the highest horizontal wind speed on the vertical model layer that includes most of the daytime PBL in most areas is used to determine the sync time-step for all the layers. The height of this layer is about 2.5 km above ground, which is the default PBL height in CMAQ. This height can be adjusted when studying the upper atmosphere or when the PBL is expected to be higher. The layers within PBL use the same advective time-step every sync time-step. The layers above PBL allow multiple advective time-steps every sync time-step.

4.3.2 New treatments to solve model advection restrictions

In coarse resolution cases such as that reported by Hakami et al. (2007), the CMAQ sync time-steps for all output time-steps are the same as the CMAQ default value. The default 12 minute sync time-step is then the same as the fixed checkpointing time-step in the original CMAQ-ADJ, so the model does not abort like it does in high resolution runs. Every output time-step of the backward of the original CMAQ-ADJ has the same sync time-step as the corresponding output time-step in the forward model. In coarse resolution simulations, the pre-set 12 minutes sync time-step in the backward part of the model is also the same as the model default. Therefore, the backward model run will also not have problems with the time-step.

This situation will change in the high resolution cases. Every output time-step tends to have its own sync time-step which is different than other output time-steps. All the different sync time-steps can be less than 12 minutes. When the new code that solves the checkpointing problems in forward CMAQ-ADJ is applied to the backward part of the original CMAQ-ADJ, the modified backward model of CMAQ-ADJ does not automatically work for high-resolution cases, which means the modifications has intrigued other potential problems in the model.

The subroutine used so far in the backward CMAQ-ADJ to determine sync time-step is still the same as that used in the original version of the model, i.e, "ADVSTEP". "FTIME" in "ADVSTEP" is assigned the ending time of every output time-step. This is to find the maximum wind speed for Courant condition to calculate the advective time-step and hence to determine the sync time-step. In "ADVSTEP", "call NEXTIME(FDATE, FTIME, FSTEP)" will get FDATE and FTIME of the next future FSTEP (output time-step), but not the previous FSTEP that should be used in the backward CMAQ-ADJ. For example, if the 6-hour simulation time period is from hour 01 to hour 07 and the output time-step is set to 1 hour. The hour 07 is the first FTIME of the backward model, the second should be 06, the last one should be 02. However, the algorithm used in the CMAQ-ADJ model does not control the time in this reverse order, but still in the forward order, such that the maximum wind speed from 06 to 07 is used to determine advection time-step (and sync time-step) for all the six-

hour simulation period. When the number of the sync time-steps in the first several hours is different than that in the 6th hour, the backward run of the CMAQ-ADJ model aborts. CMAQ-ADJ uses the meteorology data of the last output time-step for the backward calculation of the whole simulation period. To solve this problem, a new subroutine ADVSTEP_ADJ is introduced to replace ADJVSTEP for the backward part of CMAQ-ADJ.

If the wind data of the last output time-step is used for the whole backward calculation of CMAQ-ADJ, the calculated adjoint variables will be always near the receptor region. No advections from farther sources can be captured. The modified CMAQ-ADJ must be able to simulate the advection in the whole research domain. The sensitivity simulations in later sections show this feature.

4.3.3 Suggestions on using I/O API in the model

As shown in Table 3, the gridded data in IO/API is designed to be 4-dimensional. Data will be incorrectly recorded if I/O API is used to process variables with other sizes. This problem is found in the CMAQ-ADJ code we received. The variable CHEMSTEP (chemistry integration time-step, the 4th-level time step of CMAQ) is defined to be 3-D, but is processed by IO/API. This has caused a disordered data structure of CHEMSTEP (Figure 2). The chemistry integration time-step should show different features on different underlying surfaces. There are more chemical emissions and removal processes on land than over water. Reactions are therefore expected to be faster on land than on water. The different heat capacity between water and land influences the surface air temperature, which influences the temperature-dependent atmospheric chemistry reactions. These differences in the chemical time-steps have been identified after modifying the CMAQ-ADJ (Figure 3).

To modify the problems in CMAQ-ADJ mentioned in the above paragraphs, the new FORTRAN 90 subroutines and modules added to the forward part of CMAQ-ADJ are "subroutine nc_check" (generate error messages), "subroutine nc_chk1" (open a new netCDF file for checkpointing data and create netCDF header. These data are concentrations, air density, Rosenbrock time step, and photolysis rates from tables), "subroutine nc_chk1_putvar" (write data into the new file), "subroutine nc_chk1_putvar1" (write data into

the new file), “subroutine nc_chk1_putvar2” (write data into the new file), “subroutine nc_chk1_putvar3” (write data into the new file), “subroutine nc_chk1_putvar4” (write data into the new file), and “module nc_chk1_module” (define variables) (Appendix B). The corresponding subroutines that need to be modified in the forward part of CMAQ-ADJ are “PROGRAM DRIVER” (main program), “SUBROUTINE OPCONC” (create the IO/API netCDF header and open the output CONC file), “SUBROUTINE SCIPROC” (controls all of the physical and chemical processes), and “SUBROUTINE CHEM” (KPP implementation, A. Hakami).

The new FORTRAN 90 subroutines and modules added to the backward part of CMAQ-ADJ are “subroutine nc_check” (generate error messages), “subroutine nc_chk1_bwd” (open a new netCDF file for adjoint variables and create netCDF header),, “subroutine nc_open_chk1” (open the file of checkpointed data in the forward run) , “subroutine nc_chk1_rd0” (read checkpointed data), “subroutine nc_chk1_rd1” (read checkpointed data), “subroutine nc_chk1_rd2” (read checkpointed data), “subroutine nc_chk1_rd3” (read checkpointed data), “subroutine nc_chk1_putvar” (write data into the new file), “subroutine nc_chk1_putvar1” (write adjoint variables into the new file), “subroutine nc_chk1_putvar2” (write adjoint variables into the new file), “subroutine nc_chk1_putvar3” (write adjoint variables into the new file), “module nc_adj_module” (define variables), and “SUBROUTINE ADVSTEP_ADJ” (determine sync time-steps in adjoint calculation) (Appendix C). The modified old subroutines of the backward part of CMAQ-ADJ are “PROGRAM DRIVER” (main program), “SUBROUTINE OPCONC” (create the IO/API netCDF header and open the output CONC file), “SUBROUTINE SCIPROC_ADJ” (controls all of the physical and chemical processes during the adjoint calculation), and “SUBROUTINE CHEM_ADJ” (for backward iterative solver).

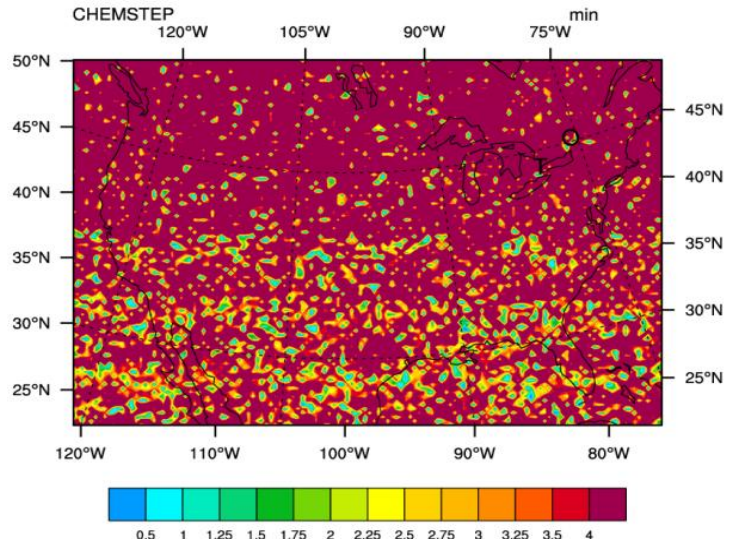

Figure 2. An example of the chemistry time step (in minutes) at 01:24 GMT 28 July 2007 in CMAQ-ADJ.

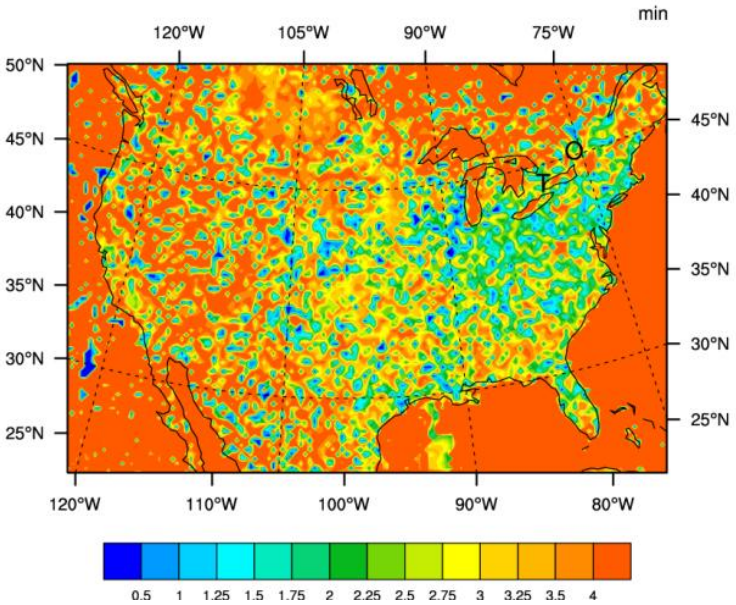

Figure 3. An example of the chemistry time step (in minutes) at 01:24 GMT 28 July 2007 in the modified CMAQ-ADJ.

Chapter 5

Ontario ozone sensitivity study

5.1 Model settings

Ozone sensitivity studies are conducted in a region (hereafter Domain 2, contained within the solid green line in Figure 4) with a spatial resolution of 12 km. Domain 2 is one-way nested within a larger region with a relatively coarse horizontal resolution of 36 km (132×90 horizontal grids, contained within the dashed green line in Figure 4, hereafter Domain 1). Domain 2 has 156×96 horizontal grids covering the Great Lakes region and the industrialized areas with significant anthropogenic emissions in the Midwest U.S. and Ohio valley region and east part of populated Canada. This study investigates the sensitivity of ozone at the ground level in a Lambert-Conformal map projection and sigma-p vertical coordinate system. Fourteen vertical sigma layers from the ground surface up to 100 hPa (about 16200 meters) are chosen for both of the model domains. Fourteen layers are adequate in this study considering that about 90% of the boundary layer O_3 is photochemically formed in this layer and the stratosphere-troposphere exchange has a minimum in summer (Lelieveld and Dentener, 2000).

The lateral boundary for CMAQ runs in the larger parent Domain 1 uses the CMAQ default, i.e., a time-invariant climatological chemical profile for ozone and other relative species. Simulated results in Domain 1 are processed by the CMAQ sub-processor BCON to generate hourly time- and space-dependent horizontal and vertical dynamic boundary conditions for model runs in Domain 2 so that mechanism species can be propagated from the parent Domain 1 to Domain 2. Any flux from the bottom and the top of the atmosphere (100 hPa) is zero.

A 3-day spin-up period is often chosen to minimize the impact of initial conditions on the ozone simulation, i.e., the simulation runs from the start of the 4th day are used in real analysis (Hogrefe et al., 2004; Sistla et al., 2001; Tao et al., 2003). In this research, at least 3-day spin-up runs are used for both of the nested regions to generate initial conditions for the later sensitivity studies. Local emissions, meteorological conditions, and model dynamics

and chemistry dominate the sensitivity simulations of the model. CMAQ simulations from July 13 to 15, 2007 are used as the spin-up data for the July 16-18 researches. The July 19-21 scenario has a 6-day spin-up period from July 13 to 18, 2007.

High levels of surface ozone mainly occur from May to September. In this study, both the typical and the unusual meteorological conditions to drive the modified CMAQ-ADJ are chosen from the simulated July 2007 conditions. The limited-area, non-hydrostatic, terrain-following Fifth-Generation National Center for Atmospheric Research/Pennsylvania State University Meso-scale Model (MM5) (Grell et al., 1994) (v3.6) is pre-calculated in advance of running CMAQ. The meteorological data calculated by MM5 provide tracer transport, precipitation, temperature, and other important features such as the boundary-layer structure for CMAQ.

Emission data from area sources, mobile sources, non-road sources, biogenic sources, and point sources are based on the national emissions inventories of 1995 and 2001. These data are processed by the SMOKE v2.3.2 to generate gridded, hourly emission data for the chemical transport model CCTM of the modified CMAQ-ADJ. The calculation of the mobile sources and biogenic sources has considered the meteorological conditions of the simulation time period.

The region contained within the solid red line in Figure 4 includes Windsor and Toronto (hereafter W-T region). It includes the areas in southwestern Ontario. The region contained within the dotted red line is located in east-central part of Ontario which has Toronto and Ottawa included (hereafter T-O region).

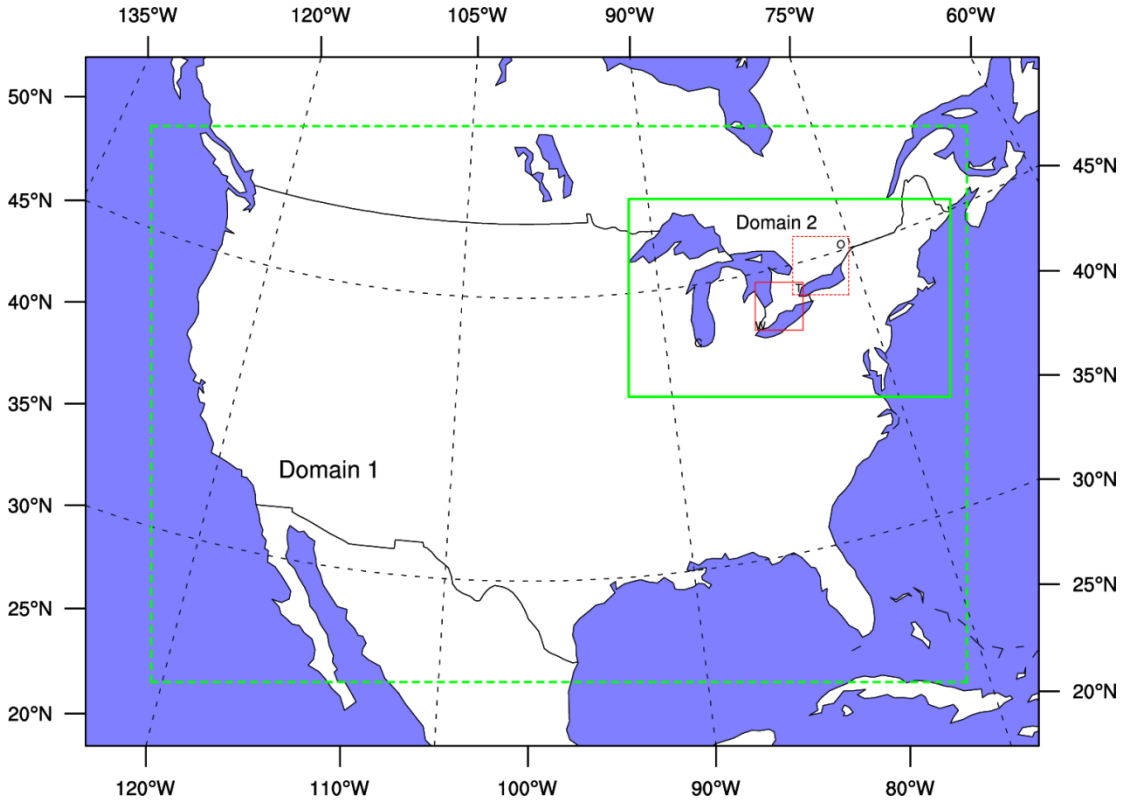

Figure 4. Double-nested research domains and receptor regions. Domain 1: the region contained within the dotted green lines. Domain 2: the region contained within solid green lines. Windsor-Toronto (W-T) region: contained within the solid red line. Toronto-Ottawa (T-O) region: contained within dotted red line. C: Chicago. W: Windsor. T: Toronto. O: Ottawa.

5.2 CMAQ simulation

5.2.1.1 CMAQ performance for ozone prediction

CMAQ's prediction ability and photochemical processing features have been extensively evaluated in various regions in the world. Among all pollutants, ozone has been given special attention because ozone is an air pollutant and is the most important oxidant of many atmospheric chemicals. It widely influences the ecosystem, humans, and climate change. Yu et al. (2007) assessed CMAQ's forecast performance for ozone and its precursor species over the eastern United States. They showed that CMAQ is able to reproduce the day-to-day variations of the observed daily maximum 8-hour O_3 and vertical distributions of O_3 on most of the days at low altitudes. Appel et al. (2007) found that the version 4.5 of CMAQ shows good overall performance for ozone predictions under the most common summer synoptic

anticyclone conditions. They also showed that ozone may be over- or under-predicted under less frequent synoptic regimes. The study of (Eder et al., 2006) revealed that CMAQ performs very well during clear sky conditions associated with anticyclones. They also found that the performance of CMAQ is poor when there is extensive cloud coverage. By comparing with observational data, Galvez (2007) demonstrated that the MM5/SMOKE/CMAQ modeling system can provide a reliable spatial and temporal distribution of ozone in southern Ontario.

Although the focus of this study is not on ozone predictions, it is still necessary to examine if the CMAQ used in this study can reproduce appropriate information on the overall spatial distributions and temporal variability of tropospheric ozone. Graphical plots of hourly time series and scatter plots of hourly ozone predictions are used to compare the model prediction with the selected monitored ozone concentrations. The hourly ozone measurements are taken from http://www.airqualityontario.ca and http://www.airnow.gov.

Figure 5 compares the CMAQ-simulated ozone concentrations (in ppb) with the observed hourly ozone concentrations at 4 stations from 0:00 GMT July 16 to 21:00 GMT July 21 in 2007. The modeled 141-hour ozone concentrations have used a 3-day period spin-up from July 13 to 16 to remove the influence of the initial conditions and let the model dynamics and chemistry take control. Of the four sites, one is in the U.S. and three are in Ontario. Figure 5 shows that CMAQ predicts characteristic diurnal cycles at all sites. In the morning hours the ozone level starts to increase due to high photochemical formations from precursors NOx and VOCs in the presence of ultraviolet radiation from the sun. By the afternoon, the ozone reaches its highest level. At night, ozone is suppressed because of low production and net deposition. In general, the CMAQ predicted variations are smaller than the observed values. Figure 6 shows the scatter plots of the simulated vs. the measured ground-level ozone values. The correlation can be quite high (e.g. in Hershey), or moderately high (eg, in Thunder Bay), or low (e.g. in London and Sarnia).

The discrepancy in the simulated ozone change with those observations can be caused by several reasons. Limitations in the dynamics and ozone formation chemistry are always an issue for any air quality model including CMAQ. Another possible reason is that the resolution chosen in this simulation is not fine enough. An average of the $12\ km \times 12\ km$

grid is used to compare against the observation at one specific site. The modeled O_3 concentration represents the average of the whole $12\ km \times 12\ km$ grid, which is not able to reproduce the sub-grid ozone fluctuations that control the ozone at observational sites. If the observation is made near the source of emissions or close to downwind direction of a power plant or an urban plume, the measurement can be expected to be especially different than the simulation (there is no such information for the 4 sites chosen here). For example, titration of NOx decreases ozone in urban and its downwind areas. The lack of including such precursor emissions in the model can cause the over-prediction of the night time ozone concentration. The precursor emission information used in the model might have changed by the year 2007, which is another possible reason for the discrepancy. These discrepancies can be smaller in the future when the physics and chemistry of CMAQ are improved and up-to-date emission data are available.

The spatial distributions of the simulated ozone concentrations in the inner Domain 2 of the double-nested domains are displayed in Figure 7. Generally, ozone concentrations are small in the whole region at night time, as shown on the 04:00 GMT (24:00 local time) plots. Ozone concentrations start to increase in the morning and reach their highest values by the late afternoon (around 20:00 GMT). During both night time and day time, the ozone over the Great Lakes and Ocean shows larger concentrations than over land area. This is because ozone is not removed efficiently by surface deposition into water. Another reason that high ozone level tends to be maintained in the lake regions is due to the effect of lake breezes. The lake breeze caused by the land-water distribution in the Great Lakes region can result in very little net transport of air (including ozone) over lakes. Ozone concentrations in urban areas are low due to high NOx emissions there. The titration of ozone by NOx is apparent in night time plots (4:00 GMT) and rush hour plots (12:00 GMT, 8:00 local time). Figure 6, Figure 5, and Figure 7 show that the overall temporal and spatial variations in the hourly simulated ozone concentrations agree reasonably well with the observations, so it is concluded that the CMAQ model used in this thesis is able to provide appropriate information on ozone for further sensitivity studies. Since the purpose of this study is not prediction, no special treatments are given to the simulated data in the later sensitivity studies.

CMAQ-simulated surface ozone for Domain 2 at 17:00 local time (21:00 GMT) on 18 July and 21 July (Figure 8) is used as the base surface ozone for later sensitivity studies. The July 18 plot in Figure 8 displays a higher ozone concentration over the southern part of the region and over the water surfaces such as Lake Erie, west Lake Superior, and near-shore Atlantic Ocean. Sea or lake breezes contribute to the build-up of the ozone over the water surfaces or coastal regions through trapping ozone and its precursors locally (Mukammal et al., 1982; Olaguer et al., 2005). Dry deposition velocities of ozone are lower over water surfaces than over forest surfaces (Brook et al., 1999; Sillman et al., 1993). Warmer temperature over the southern part of the land in Domain 2 enhances the ozone formation from its precursors than over cold northern land and over relatively cool lake and ocean surface water temperatures. Lack of NOx emissions from traffic or industry makes the ozone distribution less variable in the northern part of Canada than over the southern Canada and the U.S.. Enhanced ozone concentrations extend along the west coast of Atlantic. This is formed by the southwesterly marine tropical air flow and the elevated ozone trajectories associated with the accumulation of ozone precursors and previously formed ozone from a number of sources (Mukammal et al., 1982). High ozone concentrations over the northeastern USA are associated with the central and western parts of anticyclones (Comrie, 1990). The ozone level on the 21:00 GMT July 21 plot is lower than that on the 21:00 GMT July 18 plot because the prevailing northern wind (shown on the later sensitivity plots) has brought cold air from the north. Low temperature does not favor ozone formation, as explained in Chapter 2.

Sensitivity studies are carried out using the data simulated by MM5 and CMAQ starting from 0:00 GMT July 16 2007 to 21:00 GMT July 18 2007, and 0:00 GMT July 19 2007 to 21:00 GMT July 21 2007. During the first period, the ground level prevailing southwest flow pattern in those U.S. states in Domain 2 (shown on the later sensitivity plots) is similar to the 30-year average July wind at this region (Klink, 1999). Geddes et al. (2009) also indicated that the Greater Toronto Area in summer is often under the influence of southern and southwestern winds. Based on the above information, it is reasonable to associate the synoptic conditions in the July 16-18 case with typical summer conditions in this area. Although the weather in the July 19-21 period does not favor high ozone levels, the unusual

prevailing wind condition affords a useful opportunity to study the influences of the pollutants under such conditions.

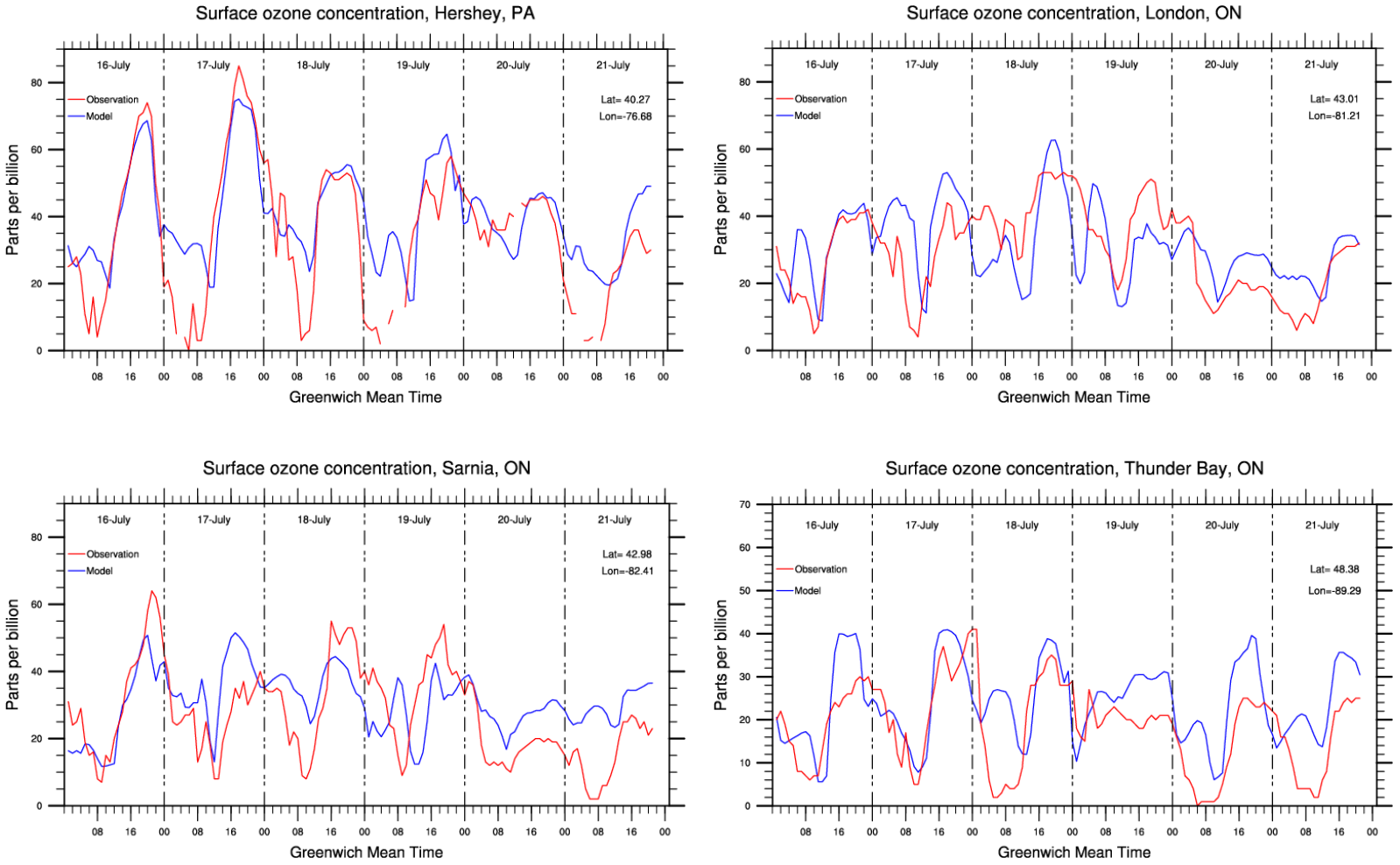

Figure 5. Measured and simulated ozone mixing ratios at selected sites from 0:00 GMT July 16 to 21:00 GMT July 21.

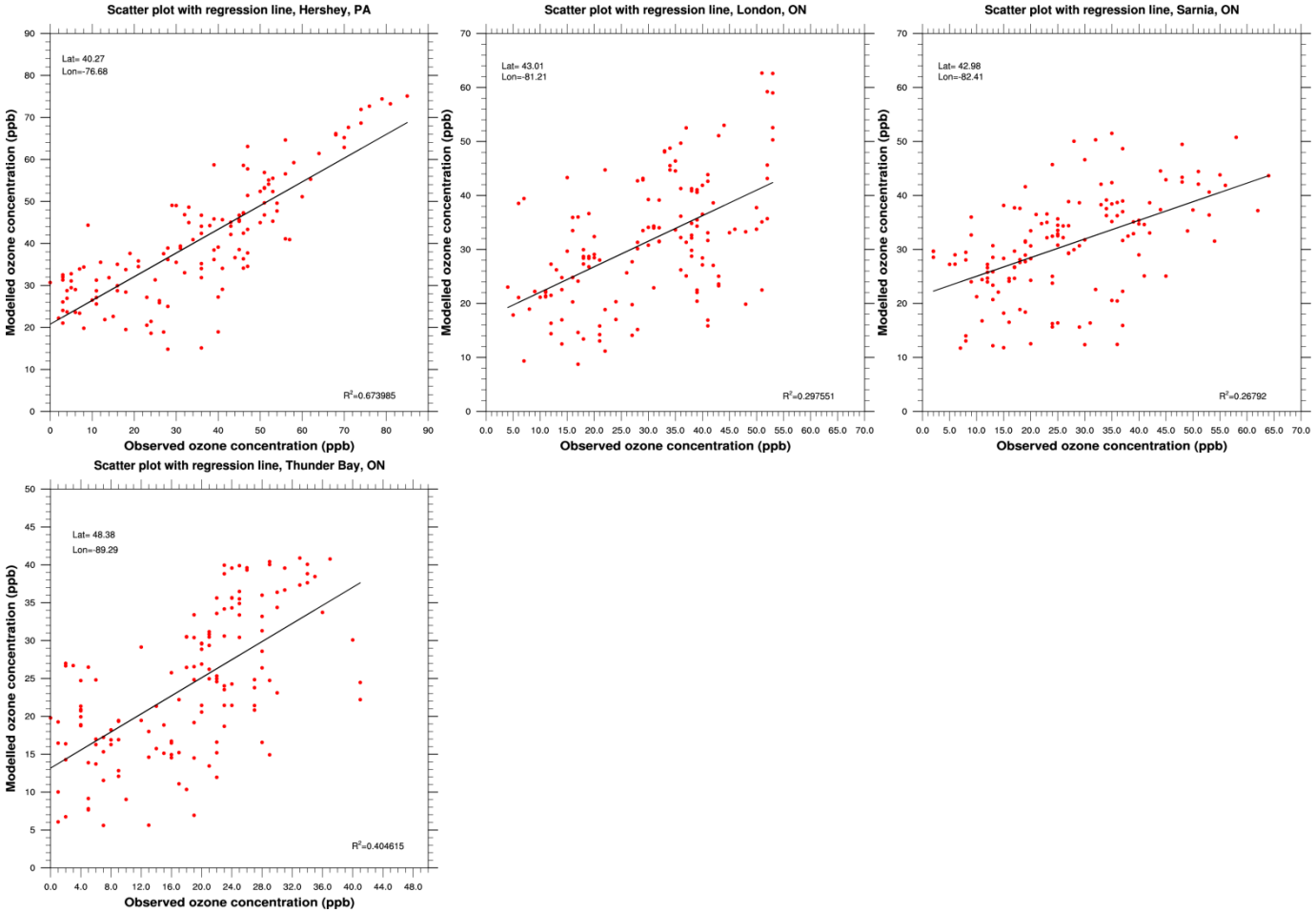

Figure 6. Measurements of surface ozone concentration against simulated surface ozone concentration by CMAQ.

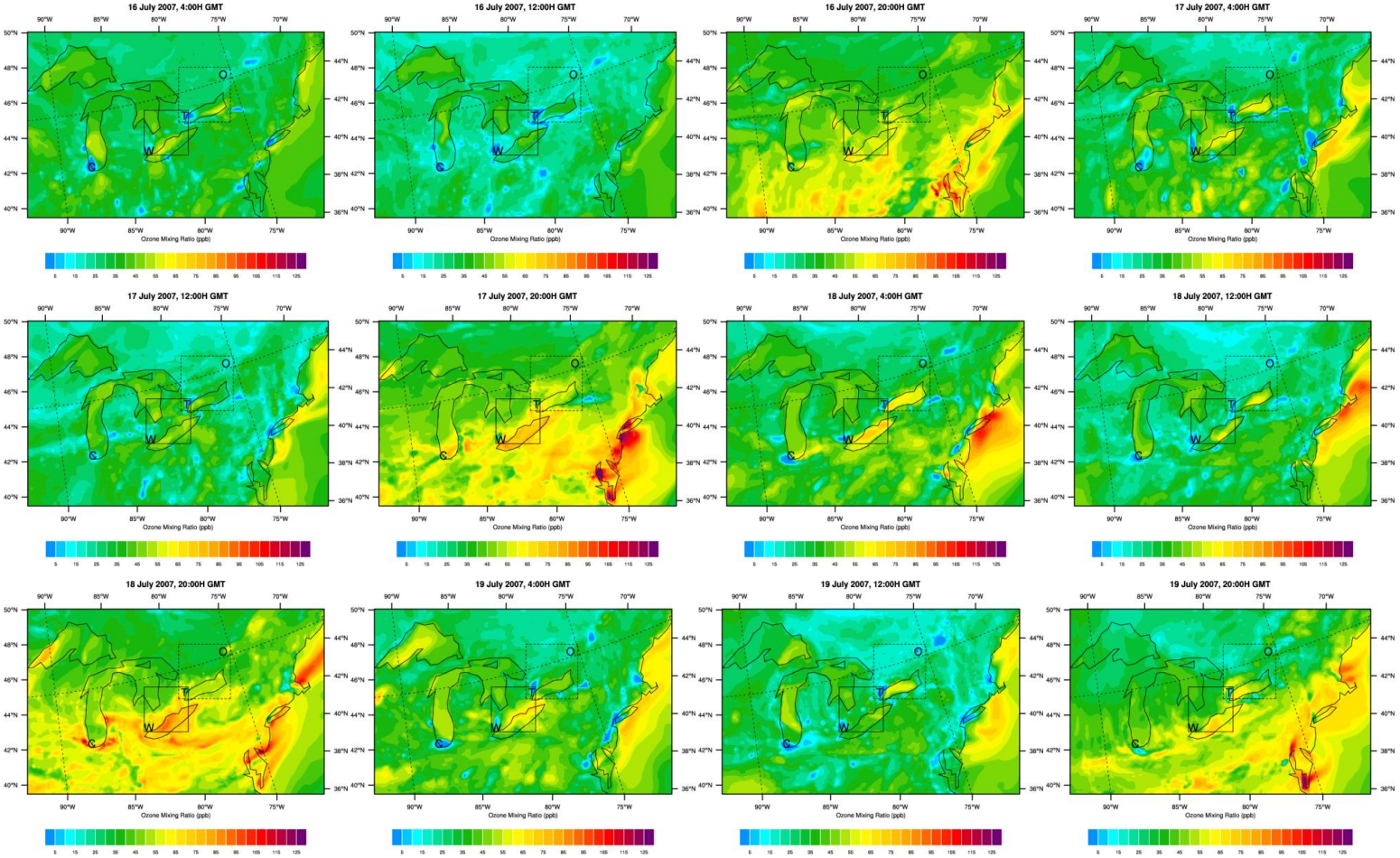
16 July 2007, 4:00H GMT
16 July 2007, 12:00H GMT
16 July 2007, 20:00H GMT
17 July 2007, 4:00H GMT
17 July 2007, 12:00H GMT
17 July 2007, 20:00H GMT
18 July 2007, 4:00H GMT
18 July 2007, 12:00H GMT
18 July 2007, 20:00H GMT
19 July 2007, 4:00H GMT
19 July 2007, 12:00H GMT
19 July 2007, 20:00H GMT
Ozone Mixing Ratio (ppb)

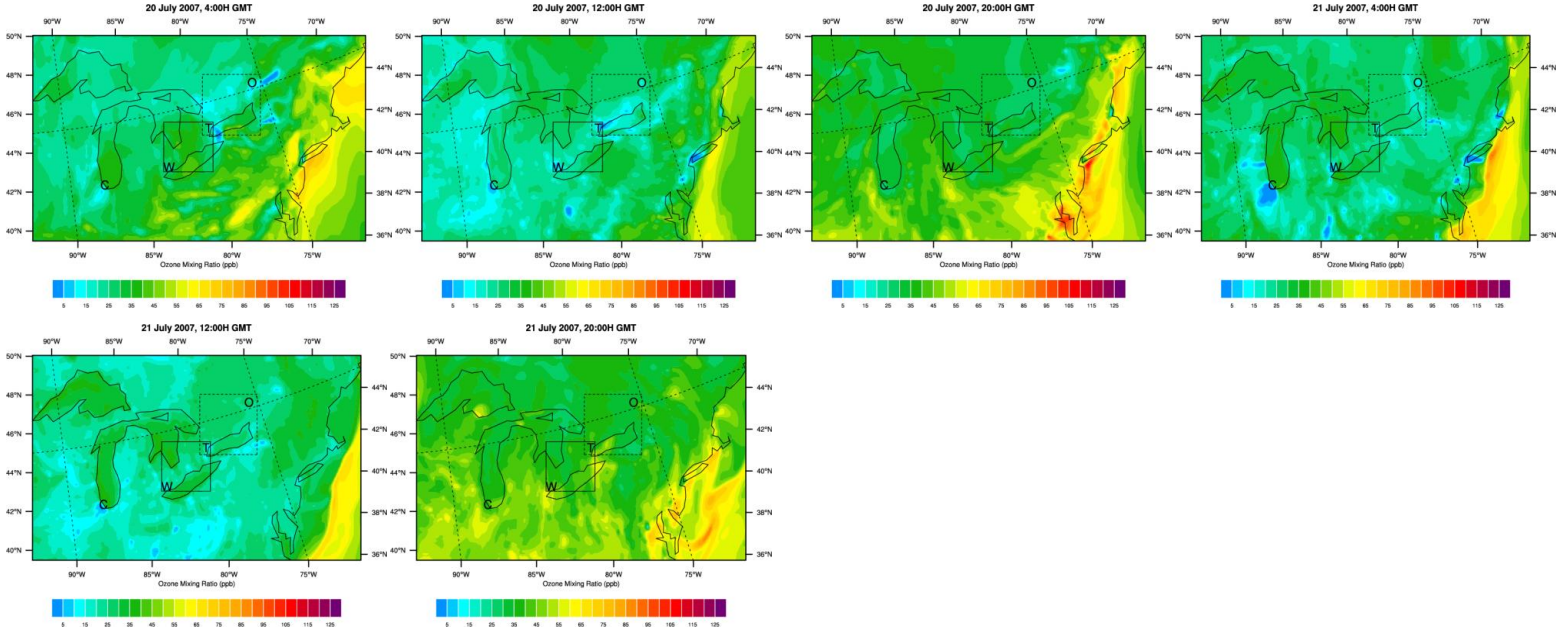

Figure 7. CMAQ simulated spatial distribution of ground-level ozone in Domain 2 for the period 04:00 GMT 18 July – 20:00 GMT 21 July. Plots are given at 8 hours intervals.

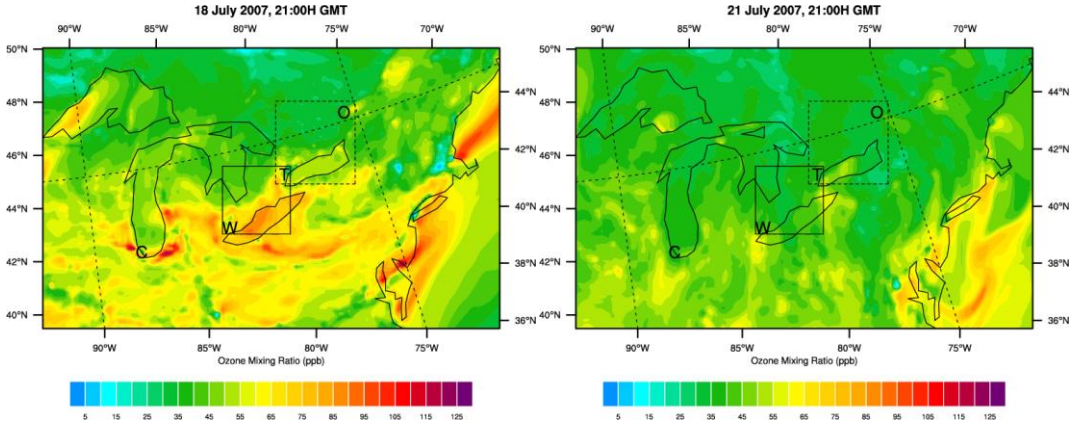

Figure 8. CMAQ simulation of ground-level ozone concentrations at 17:00 local time on July 18 and July 21.

5.2.1.2 Simulated NOx-VOC chemistry by CMAQ

The relative proportion of NOx and VOC determines the rate of the ozone production (Geddes et al., 2009c). When VOC/NOx ratio is high, ozone production is essentially independent of VOC, but NOx-limited and linearly increases with NOx concentrations (Geddes et al., 2009c). In polluted areas, VOC/NOx ratio is low. Only when sufficient NO is oxidized to NO_2 and subsequently is photolyzed to the ground-state oxygen atoms $O(^3P)$, much ozone can be formed (FinlaysonPitts and Pitts, 1997) (Equations 2-5 and 2-6). When VOC/NOx ratio is low, the OH production rate is less than the rate of NOx formation, the relative importance of $NO_2 + OH$ is increased (Ryerson et al., 2001):

$$\mathbf{NO_2 + OH + M \rightarrow HNO_3 + M} \qquad 5\text{-}1$$

The removal of ozone catalysts OH radical by NO_2 in the above reaction suppresses the production of peroxy radicals in the following reaction:

$$\mathbf{VOC + OH + O_2 \rightarrow RO_2 + H_2O} \qquad 5\text{-}2$$

Therefore, under such conditions, the oxidation of VOC is suppressed and as a consequence short-circuits ozone formation (FinlaysonPitts and Pitts, 1997). Relatively little ozone is formed in the first several hours after NOx is emitted as it is removed by oxidation to HNO_3 (Ryerson et al., 2001). Ozone production is more sensitive to VOC reactivity in this VOC-limited regime (Geddes et al., 2009c), decreasing NOx actually leads to an increase in ozone concentration (FinlaysonPitts and Pitts, 1997).

Northern Canada is not heavily populated or industrialized. There are limited NOx and VOC emissions from anthropogenic activities there. In the eastern U.S. there are large emissions of biogenic VOC isoprene from oak trees (Chameides et al., 1988; Trainer et al., 1987). The isoprene concentration is also large to the northwest and north of the Great Lake areas (Figure 9) as there are a lot of trees there.

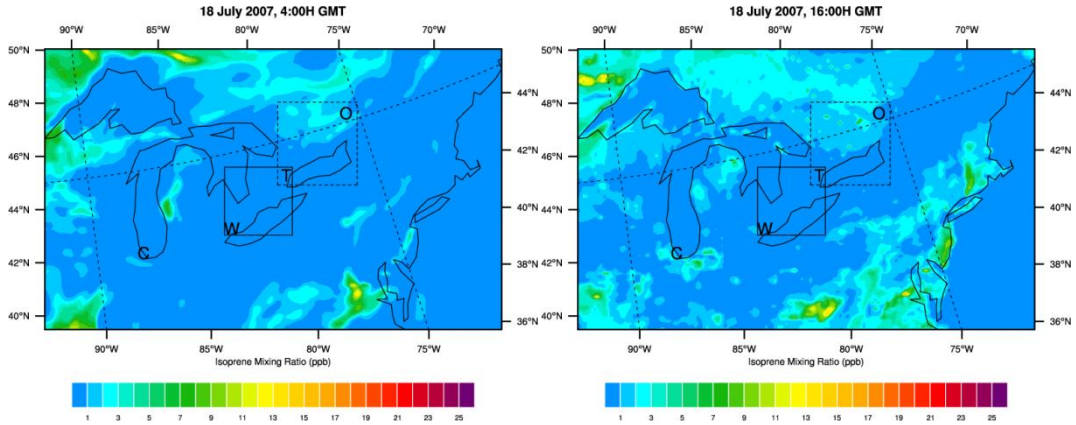

Figure 9. Selected CMAQ-simulation of isoprene concentrations at 0:00 and 12:00 local time (EST).

In Ontario, 33% of the VOC emissions are due to transport, another 33% from industrial emissions and organic solvent use, and the remainder from miscellaneous sources (Geddes et al., 2009). In 2006, transport accounted for about 68% of NOx emissions in Ontario, other industrial processes accounted for 11%, and the rest from utility and other miscellaneous sources (AQO2008, 2010). In the U.S., the major sources of VOCs are also solvent use and highway vehicles. The major sources of NOx are from electric power generation plants and motor vehicles. Therefore, large anthropogenic VOCs and NOx emissions in Domain 2 are mainly in the populated and industrial southern part of eastern Canada and the northern part of the eastern U.S..

The CMAQ simulated NOx and VOCs in Domain 2 should be able to reflect the features mentioned above. High VOC/NOx ratios in the northern part of Ontario in Domain 2 but low VOC/NOx ratios in the southern part of the research domain are anticipated. The VOC/NOx ratios should also be low in urban areas due to the large amount of NOx emissions from heavy traffic. Figure 10 shows the CMAQ simulated VOC/NOx ratios in midnight, early morning, and late afternoon from July 18 to 21. High VOC/NOx ratios can be seen in the northern part of the research domain and Atlantic Ocean. Relatively low VOC/NOx ratios are found in the southern part of the research domain where it is populated and industrialized. The VOC/NOx ratios over those lake areas near the large cities such as Chicago, Windsor (Detroit) are generally large, especially at the centers of Lake Erie and Lake Ontario by late afternoon. This is due to the accumulation of the widespread emissions of biogenic VOCs and the high solubility of NO_2 and HNO_3 removing NOx at this place. During the day time, isoprene concentrations increase with temperature as the emission rate of isoprene is temperature-dependent (Lamb et al., 1985). The complex circulation of the pollutants caused by the characteristic land/lake geography can make the chemical mix of the ozone precursors in this area very complicated. On one hand, large

amount of NOx is emitted from automobiles and power plants from the several urban areas. The oxidization of NOx to HNO_3 removes it from the air mass due to the large deposition velocity of HNO_3. Meanwhile, VOCs are supplied from biogenic sources and do not decrease as rapidly as NOx because of the less efficient deposition (FinlaysonPitts and Pitts, 1997). Therefore, in this area, the VOC-limited regime around urban areas will change to a NOx-limited regime in downwind areas. Since the wind in the model area is influenced by both large scale circulation and lake breezes, the movement of the air mass is also very complex.

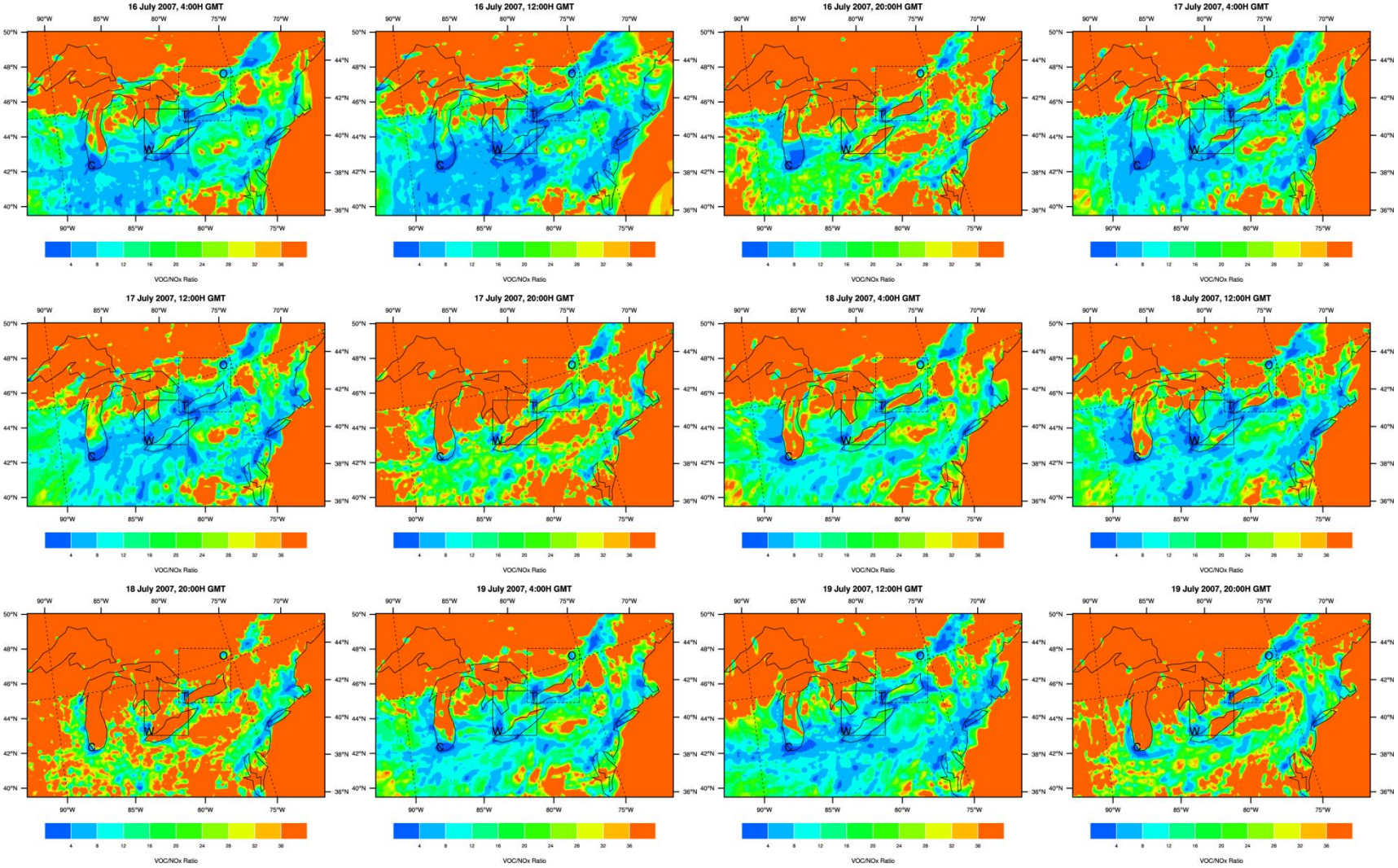
16 July 2007, 4:00H GMT
16 July 2007, 12:00H GMT
16 July 2007, 20:00H GMT
17 July 2007, 4:00H GMT
17 July 2007, 12:00H GMT
17 July 2007, 20:00H GMT
18 July 2007, 4:00H GMT
18 July 2007, 12:00H GMT
18 July 2007, 20:00H GMT
19 July 2007, 4:00H GMT
19 July 2007, 12:00H GMT
19 July 2007, 20:00H GMT
VOC/NOx Ratio

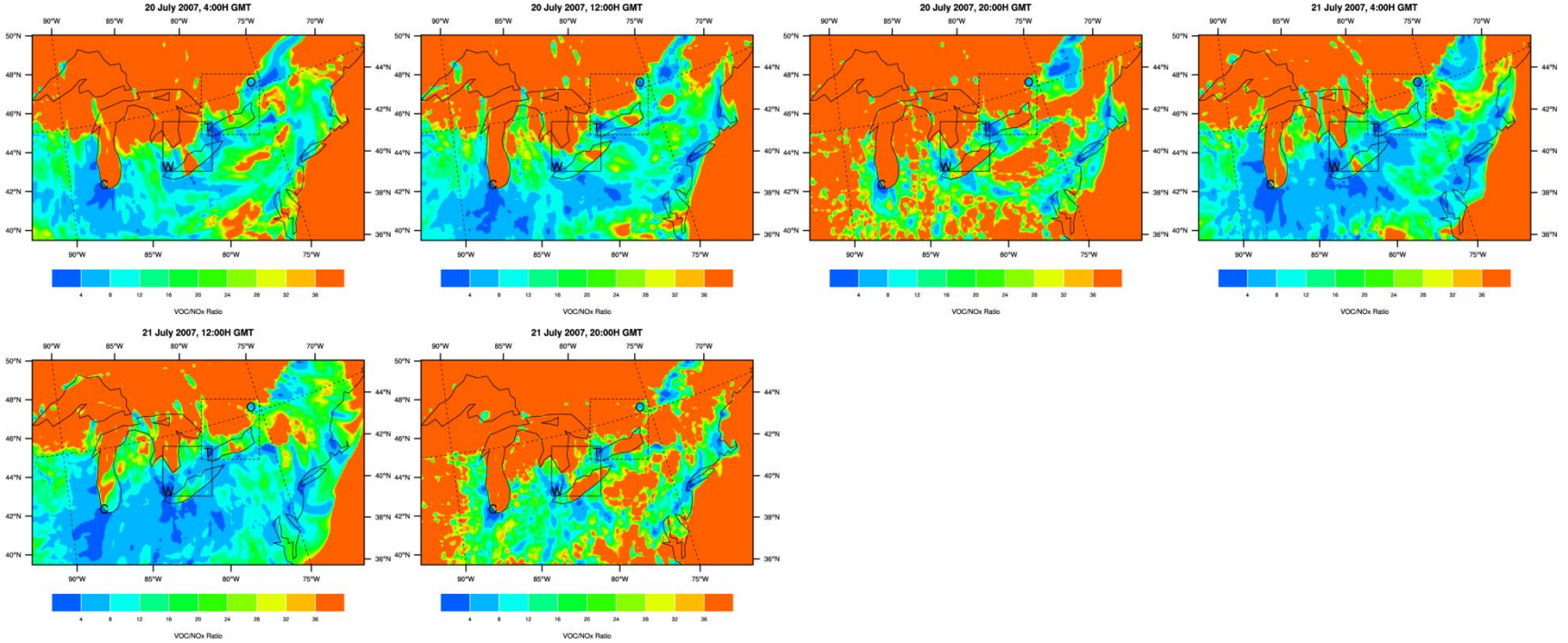

Figure 10. CMAQ simulated VOC/NOx ratios in Domain 2 for period 16-21 July, 2007. Plots are presented every 8 hours.

5.3 Sensitivity study using modified CMAQ-ADJ

5.3.1 Scenario settings

Adjoint sensitivity analysis can effectively characterize the relationships between the source and the receptor by describing the areas of influence, which contain information about the location of the factors influencing the given receptor region and time (Zhang et al., 2008). The sensitivity calculated by an adjoint model is the gradient of the cost function with respect to the control variables (Le Dimet et al., 2002). In this thesis, various sensitivity fields calculated by the modified CMAQ-ADJ are analyzed to delineate how the assumed ozone discrepancies in the target receptor regions at target time respond to the precursor changes in different regions at prior times.

The modified CMAQ-ADJ is applied to study ozone sensitivity at two regions: Windsor-Toronto (W-T) region and Toronto-Ottawa (T-O) region. The W-T region (square in solid red line in Figure 4) is used to investigate the potential influencing areas of the major influence factors for southwestern Ontario. The T-O region (square in dashed red line in Figure 4) is in east-central Ontario and is chosen as the receptor region to study which places in Domain 2 can influence the ozone in east-central Ontario. Based on the record by Ontario Smog Advisories 2007 (http://www.airqualityontario.com/press/advisories_2007.cfm), one smog advisory event can cover several cities or observation sites. Therefore, the two receptor regions in this study have reasonable areas. Three high ozone episode scenarios are assumed to happen separately in both target regions. Therefore, six separate adjoint runs were done.

In one smog episode, the daytime one-hour ozone mixing ratio at both urban and rural regions in Ontario can reach to a similar level, as observed by the BAQS 2007 experiment (BAQS, 2008). In this thesis, two scenarios (Scenarios 1 and 3) are designed based on this type of ozone event. Scenario 1 and Scenario 3 assume a high ozone event during which the ozone concentrations reach 100 ppb everywhere in the target squares. The discrepancy between 100 ppb and the simulated ozone concentrations by the CMAQ is used as the cost function to drive the modified CMAQ-ADJ integration (Figure 11). Scenario 1 uses MM5-simulated meteorological conditions of 16-18 July 2007. In comparison, Scenario 3 uses very different meteorological conditions from the MM5 simulations during 19-21 July 2007. Scenario 2 uses the same meteorological conditions as used in Scenario 1, but assumes that the ozone level in the W-T or T-O receptor regions increases by 40 ppb everywhere. In Scenarios 1 and 2, a stationary

high-pressure ridge exists to the east of the Great Lakes region. Significant anthropogenic emissions are being advected from the American Midwest and Ohio valley. These meteorological conditions favor the ozone formation in southern Ontario (Yang et al., 2003). The meteorological condition in Scenario 3 does not favor high ozone levels, but the different weather can be used to study the influence of the precursors on ozone formation in specific regions in Ontario under different conditions.

Daily ground-level ozone concentration generally rises between noon and early evening due to the high photochemical production of NOx and VOCs. Local time 17:00 (21:00 GMT) on July 18 (for Scenarios 1 and 2) and July 21 (for Scenario 3) is chosen as the outbreak time of the assumed ozone event. The CMAQ simulated surface ozone for Domain 2 (Figure 8) is used as the base surface ozone for sensitivity studies.

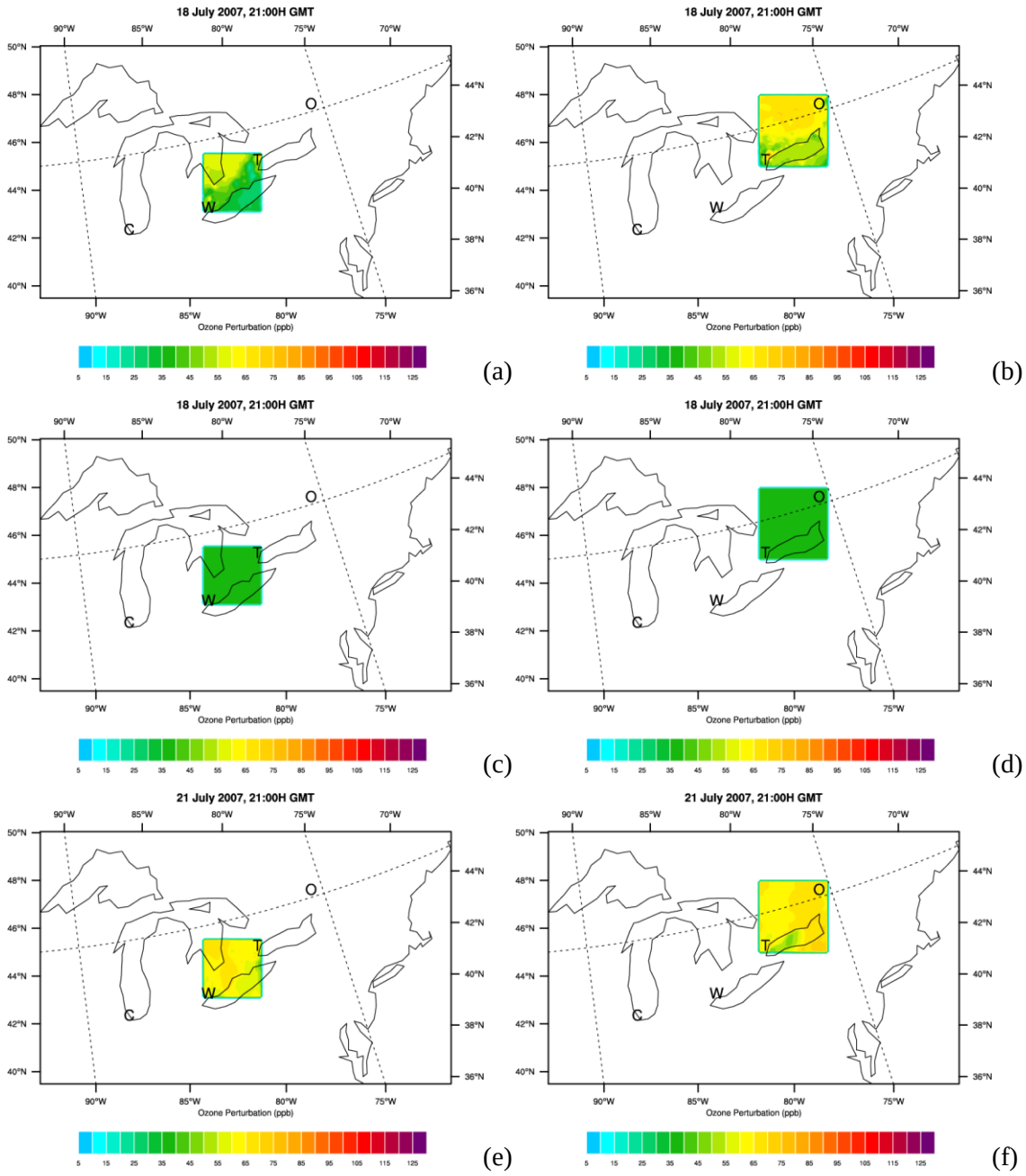

Figure 11. The assigned ozone perturbations to assume a high ozone episode in: (a) Windsor-Toronto region at 21:00 GMT July 18, 2007 for Scenario 1; (b) Toronto-Ottawa region at 21:00 GMT July 18, 2007 for Scenario 1; (c) Windsor-Toronto region at 21:00 GMT July 18, 2007 for Scenario 2; (d) Toronto-Ottawa region at 21:00 GMT July 18, 2007 for Scenario 2; (e) Windsor-Toronto region at 21:00 GMT July 21, 2007 for Scenario 3; (f) Toronto-Ottawa region at 21:00 GMT July 21, 2007 for Scenario 3.

5.3.2 Windsor-Toronto region ozone sensitivities

5.3.2.1 Influence of pre-existing ozone

Ozone has a lifetime 1-2 weeks in summer and can be transported long distance with winds (Brasseur et al., 1999; Galvez, 2007; Vukovich and Sherwell, 2003). Therefore, in addition to the photochemical formation, destruction and deposition, the transport of ozone from/to the surrounding areas is an important source/sink of ozone at a receptor. In this section, the influence of the pre-existing ozone on the ozone changes in southwestern Ontario (Windsor-Toronto region) is examined using the modified CMAQ-ADJ in three scenarios. Scenario 1 assumes that under typical summer weather conditions, the ozone concentration in the W-T region reaches up to 100 ppb. The CMAQ simulated ozone at 17:00 local time (21:00 GMT) July 18 2007 is used as the base ozone distribution. Scenario 2 assumes that under the same weather conditions, ozone concentration increases by 40 ppb everywhere in the W-T receptor region. Scenario 3 assumes the same ozone event in the W-T region as that in Scenario 1, but under very unusual weather conditions. The high ozone event is assumed to occur at 17:00 local time (21:00 GMT) 21 July 2007.

Figure 12 shows the spatial distribution of the calculated sensitivity fields of the ozone changes in the W-T region with respect to the pre-existing ozone from 0:00 GMT July 16 to 20:00 GMT July 18. The plots are given every 2 hours until one hour before the target high ozone event. The colour white represents the sensitivity between -0.00001 ppm/ppm and 0.00001 ppm/ppm. The sensitivity in this range is very small and is neglected in this study. Other colours mean that either positive or negative sensitivity is detected by the adjoint model. Sixty-nine hours prior, the influencing region of the pre-existing ozone is mainly in the upwind west side of the receptor region. Except Chicago, Detroit (Windsor), and Toronto regions, the sensitivity in a large area on the west side of the receptor region is positive. This implies that increasing ozone in these regions enhances the ozone pollution in the W-T region after 69 hours. The negative sensitivity at Chicago, Detroit (Windsor) and Toronto implies that additional ozone assigned to such urban areas suppresses the ozone formation in the W-T region 69 hours later. This phenomenon occurs through chemical interactions in that increasing ozone reacts with NO and not all of it will be re-formed by NO_2/VOC reactions later, the consumption of ozone precursors NOx causes the net result to be less ozone at the receptor. At 08:00 GMT July 16, the ozone sensitivity in Detroit (Windsor) is never negative as that in Toronto, which probably relates to the fact that the CMAQ-simulated NOx level here is much less than in Toronto (Figure 13). The magnitude of the negative influence of the pre-existing ozone of this place is therefore smaller.

When time is close to the occurrence of the high ozone event, the pre-existing ozone in Chicago is too distant to influence W-T region and hence has zero sensitivity (eg. after10:00 GMT July 18, as shown in Figure 12). The sensitivity to the pre-existing ozone in other urban areas such as Windsor (Detroit) and Toronto remains positive until the occurrence of the high ozone event.

The influencing region of the pre-existing ozone becomes closer to the W-T region with time. By 20:00 GMT July 18, only ozone in local areas are sensitive to the target ozone level changes in the next hour. Figure 12 shows clearly that the evolution of the influencing region with time has the same pace as the prevailing horizontal wind. This phenomenon can be explained by the fact that if an ozone perturbation in the simulated positive or negative sensitivity region is given to the tangent linear model (CMAQ here), a corresponding ozone increase or decrease in the receptor region will occur (Errico, 1997). The adjoint variables hence evolve along the same pathway as the evolution of a perturbation in the forward model, in which the horizontal advection plays an important role.

When the influencing region becomes closer to the target receptor region, it can also be seen that the non-zero influencing area shrinks and the magnitude increases. The shrinking of the influencing region occurs because the prevailing wind is mainly from one direction to the W-T region. Under other wind conditions the influencing region can be larger. For example, if there is a low pressure system in W-T region, the surface wind converges to the target region from the surrounding area, the influencing region will be all the places within an appropriate distance from where the pollutants can be blown to the W-T region. Therefore, a much larger area from the surrounding regions will have impacts.

During the simulation period, the ozone sensitivity to the pre-existing ozone over lakes is always likely larger than that on land areas. This can be explained by the fact that the relatively low temperature and low solubility of ozone gives it a longer lifetime over water than over land. The ozone over lakes therefore can exist longer to have more possibility to influence the ozone level at a later time. At 0:00 GMT July 16, the largest magnitude of the ozone influence is at the southern part of Lake Huron. This large sensitivity center is stagnant at the same position for almost 12 hours due to the very weak wind at this place in this period. After 12:00 GMT July 16, this large influencing area evolves to the north with wind, but still remains on Lake Huron. At the same time, another large sensitivity center appears on Lake Erie and evolves to the east following the easterly wind on Lake Erie. When the pre-existing ozone over Georgian Bay area starts to show its influence on the target ozone pollution, the sensitivity over water is still larger than that on land. The large ozone sensitivity over Lake Huron and over Georgian Bay never shifts far away from the major water areas. It starts to shift back to the center of Lake Huron and

Georgian Bay from 08:00 GMT to 16:00 GMT July 17. By this time the wind on the northeastern side of Georgian Bay is blowing from the land to the water. This is because the air temperature on land drops faster than on water bodies at night time since water has a larger heat capacity than land. Air sinks over land and rises over the water body. The surface wind therefore blows from land to Georgian Bay. By 16:00 GMT July 17, the non-zero sensitivity over Lake Ontario shows that the pre-existing ozone here influences the ozone level in the W-T region one day later. A large ozone sensitivity center can be found over the lake surface. Similarly, the magnitude of the negative sensitivity associated with high NOx concentrations in Toronto is also larger over the nearby lake surface than the magnitude of the negative values on nearby land. Six hours before the high ozone event, all the three lake areas in (or near) W-T region show larger ozone sensitivity than almost all land areas except in the locations near Windsor. The emission or the temperature condition in the large sensitivity area near Windsor is not very different from that in Toronto, but similar large sensitivity cannot be found near Toronto. This can be because the light wind near Windsor makes the ozone stagnant and increases its likelihood of influencing the ozone level in the W-T region 6 hours later. In the same period, the wind direction near Toronto changes from northeast to southeast directing to the outside of the W-T region. The pre-existing ozone here tends to be blown out and therefore contributes less to the later high ozone episode.

Four sub-regions are used to investigate local ozone's influence on the ozone level in southwestern Ontario: Toronto, Windsor, southern part of Lake Huron, central part of Lake Erie (Figure 17). The time series of the average ozone sensitivity the pre-existing ozone over these 4 locations is shown in Figure 18 (a). The pre-existing ozone at Lake Huron and Toronto can influence the ozone level in southwestern Ontario in the next 69 hours due to the recycling of the circulation in this region. When time approaches the outbreak of the high ozone event, the largest influence occurs over lake areas. The urban area has a smaller influence due to the titration effect of NOx. Any additional ozone in the same day (from morning) of the target time is able to enhance the local ozone. In all sub-regions, more and more portion of pre-existing ozone can remain to enhance the ozone level as the target time approaches.

The sensitivity fields of the pre-existing ozone in Scenario 2 are shown in Figure 14. Similar to Scenario 1, the negative ozone sensitivity always corresponds to places with large NOx emissions one half day before the high ozone episode. During this period, Toronto area always maintains negative ozone sensitivity. The sensitivity decreases and finally becomes zero in Windsor – air mass here is transported to places other than the W-T region. The disappearance of the negative values around Chicago by 08:00 GMT July 16 is because sixty hours is not long enough to enable the air from here to be transported to the receptor area. Similar to Scenario 1,

the positive sensitivity in urban areas from about one half day (-11H) earlier implies that increasing ozone in such places can enhance the local ozone event in the late afternoon of the same day.

By use of the notion presented in Errico (1997) and Vukicevic and Hess (2000), the spatial pattern of the adjoint variables calculated by the modified CMAQ-ADJ reflects the pathway of the transport of the pre-existing ozone. As seen in Figure 14, two days prior to the target time, the ozone changes in the northwest corner of the research domain have influence on the assumed high ozone episode in the W-T region. Similar to Scenario 1, positive ozone sensitivity in the southwest direction of the W-T region shows that enhanced ozone concentration in the Midwest and Ohio valley region of the U.S. can enhance the ozone level in southwestern Ontario. As discussed in former sections, the wind fields used in this scenario and Scenario 1 are close to the climate average in the southern part of the Domain 2. The simulated ozone sensitivity in Scenarios 1 and 2 therefore implies that the transport of ozone from the U.S. is an important source of ozone pollution in southwestern Ontario. When time approaches the assumed high ozone episode, the pre-existing ozone's contribution to the W-T ozone becomes local. The magnitude becomes larger with time. The largest sensitivity to the pre-existing ozone is mainly over water bodies.

The ozone sensitivity in Scenario 2 has a very similar spatial pattern to that in Scenario 1 during the whole simulation period. This suggests that the effect of the location and magnitude of the pre-existing ozone on future ozone depends significantly on the meteorological conditions, the underlying surface types, and the emissions in the transport pathway. The pre-existing ozone's local influence in the four sub-regions (Figure 18 (b)) shows that the time series of ozone at Lake Huron, Toronto, and Windsor is very close to that in Scenario 1. The magnitude of the average ozone sensitivity over Lake Erie is a little different, which could be because the difference in the magnitude of the assumed smog strength over this region in the two scenarios is large. In this thesis, the W-T square is studied as an integrated receptor region. If Lake Erie is investigated separately, the mechanisms that cause this difference will be verified more clearly. For the small Lake Erie area, a higher resolution simulation by the modified CMAQ-ADJ is more appropriate.

Scenario 3 uses the same ozone perturbation in the W-T region as Scenario 1, but different meteorological conditions. Meteorological data from July 19 to July 21 are used for this scenario. The modified CMAQ-ADJ is run for 69 hours from 0:00 GMT July 19 to 21:00 GMT July 21. Local time 17:00 (21:00 GMT) on July 21 is set as the target time. During this 69-hour time period, a cold front accompanying strong wind from the north crosses the research Domain 2.

The cold front starts to influence the target W-T region from 16:00 GMT July 19 (53 hours before the target time). The wind in most land regions is from the northwest or northeast from 13:00 GMT July 20 until the end of the simulation.

The strong wind in Scenario 3 makes it impossible for the pre-existing ozone at anywhere in Domain 2 to influence the ozone level in the target W-T region 39 hours later. Thirty-nine hours is a sufficiently long period for ozone added anywhere in Domain 2 to be blown out of the target region. The calculated sensitivity to pre-existing ozone is therefore zero. From 39 hours prior to the high ozone event, positive ozone sensitivity to the pre-existing ozone can be observed in Domain 2. The region with positive sensitivity evolves closer to the Windsor-Toronto region along the wind direction. As previously stated, if an ozone perturbation is given to the positive sensitivity region, an ozone increase in the receptor regions can be simulated by the forward part of the model (Errico, 1997). Therefore, Scenario 3 has shown that the pre-existing ozone from the distant upwind northern regions can be transported to southwestern Ontario and increase the ozone level in this area.

In Scenario 3 (Figure 15), the pre-existing ozone in urban areas starts to influence the ozone in the receptor region at target time from 06:00 GMT July 21. Similar to the cases in Scenarios 1 and 2, the influence of the pre-existing ozone about 15 hours before the target time is always to enhance the ozone level of the receptor region by the late afternoon. The largest ozone sensitivity simulated in Scenario 3 is over lake regions (the northern part of Lake Erie and south Lake Huron). The ozone on land can be taken up by vegetation and other materials. Therefore for the same amount of ozone, less on land than that over lakes is left to make contributions to the ozone level changes in later hours. Figure 18 (c) shows that the pre-existing ozone in local W-T regions always increases the ozone level at the target square, with the largest contribution over lakes, smaller in city areas. Non-zero sensitivities at Lake Erie and Windsor appear later than those at the other two locations. This is because under the strong transport conditions, the pre-existing ozone in the southern part of the W-T region at an earlier time will be blown out of this region by the occurrence of the high ozone event. It can not make any contributions to the assumed high ozone event in the late afternoon on July 21.

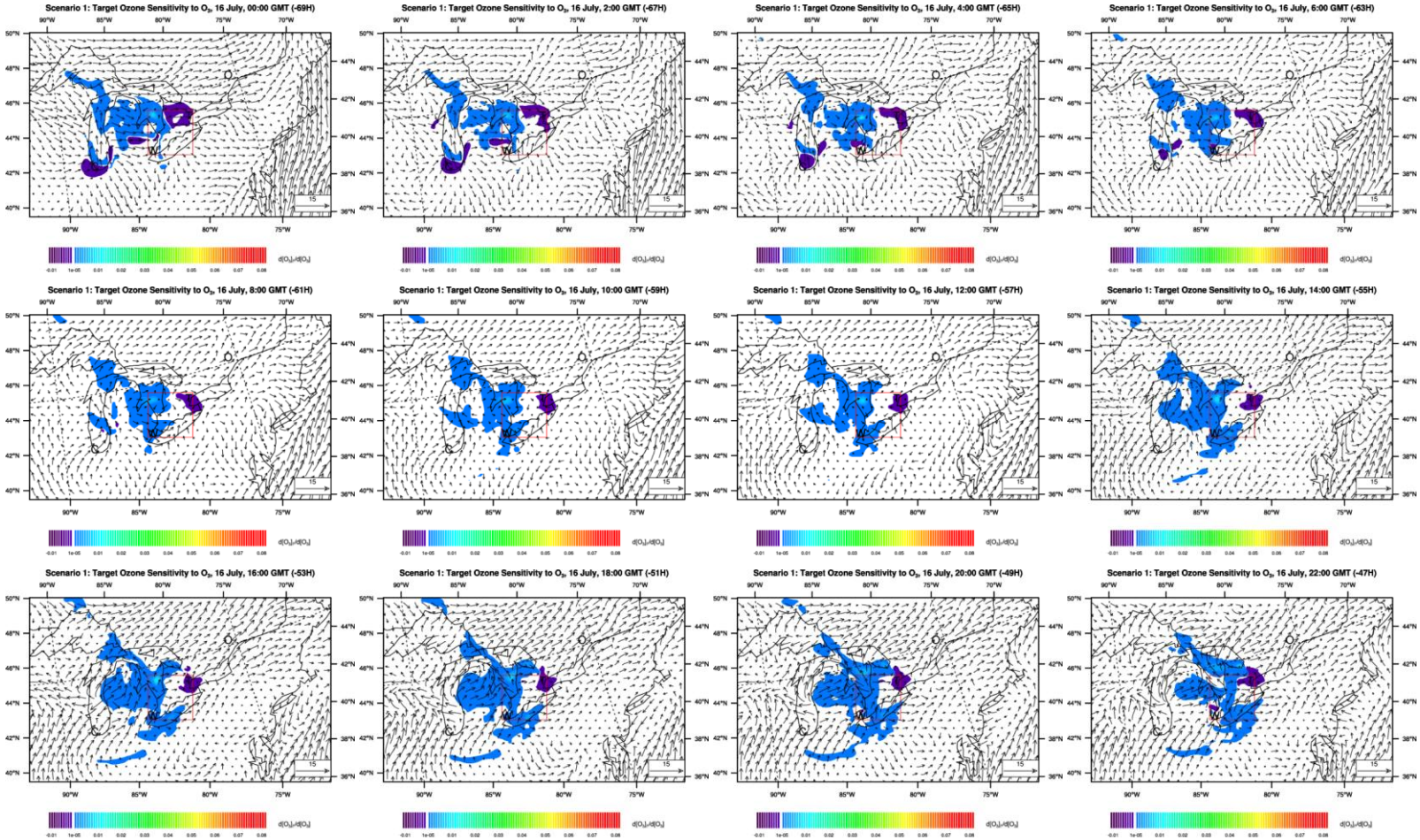
Scenario 1: Target Ozone Sensitivity to O_3, 16 July, 00:00 GMT (-69H)
Scenario 1: Target Ozone Sensitivity to O_3, 16 July, 2:00 GMT (-67H)
Scenario 1: Target Ozone Sensitivity to O_3, 16 July, 4:00 GMT (-65H)
Scenario 1: Target Ozone Sensitivity to O_3, 16 July, 6:00 GMT (-63H)
Scenario 1: Target Ozone Sensitivity to O_3, 16 July, 8:00 GMT (-61H)
Scenario 1: Target Ozone Sensitivity to O_3, 16 July, 10:00 GMT (-59H)
Scenario 1: Target Ozone Sensitivity to O_3, 16 July, 12:00 GMT (-57H)
Scenario 1: Target Ozone Sensitivity to O_3, 16 July, 14:00 GMT (-55H)
Scenario 1: Target Ozone Sensitivity to O_3, 16 July, 16:00 GMT (-53H)
Scenario 1: Target Ozone Sensitivity to O_3, 16 July, 18:00 GMT (-51H)
Scenario 1: Target Ozone Sensitivity to O_3, 16 July, 20:00 GMT (-49H)
Scenario 1: Target Ozone Sensitivity to O_3, 16 July, 22:00 GMT (-47H)

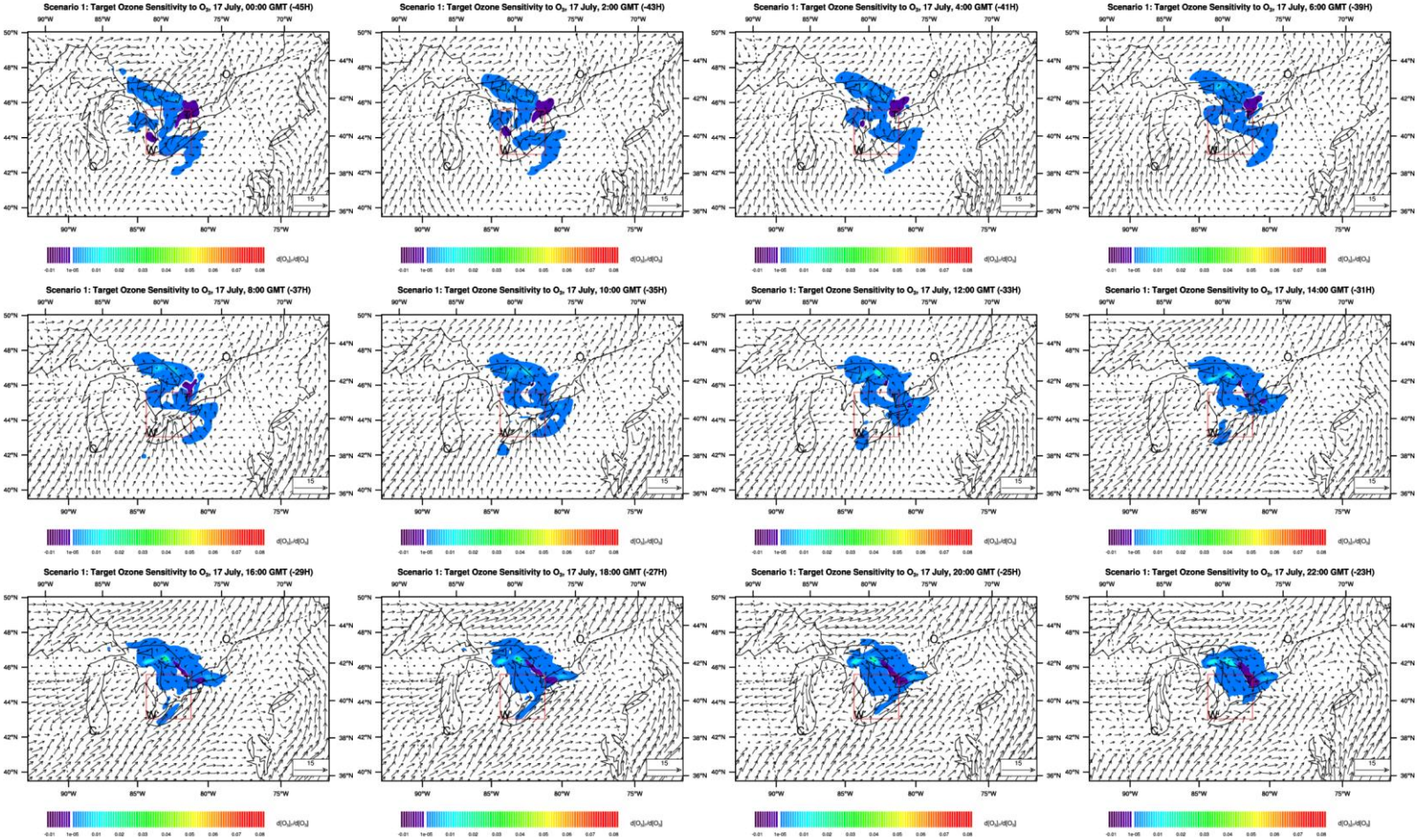
Scenario 1: Target Ozone Sensitivity to O3, 17 July, 00:00 GMT (-45H)
Scenario 1: Target Ozone Sensitivity to O3, 17 July, 2:00 GMT (-43H)
Scenario 1: Target Ozone Sensitivity to O3, 17 July, 4:00 GMT (-41H)
Scenario 1: Target Ozone Sensitivity to O3, 17 July, 6:00 GMT (-39H)
Scenario 1: Target Ozone Sensitivity to O3, 17 July, 8:00 GMT (-37H)
Scenario 1: Target Ozone Sensitivity to O3, 17 July, 10:00 GMT (-35H)
Scenario 1: Target Ozone Sensitivity to O3, 17 July, 12:00 GMT (-33H)
Scenario 1: Target Ozone Sensitivity to O3, 17 July, 14:00 GMT (-31H)
Scenario 1: Target Ozone Sensitivity to O3, 17 July, 16:00 GMT (-29H)
Scenario 1: Target Ozone Sensitivity to O3, 17 July, 18:00 GMT (-27H)
Scenario 1: Target Ozone Sensitivity to O3, 17 July, 20:00 GMT (-25H)
Scenario 1: Target Ozone Sensitivity to O3, 17 July, 22:00 GMT (-23H)

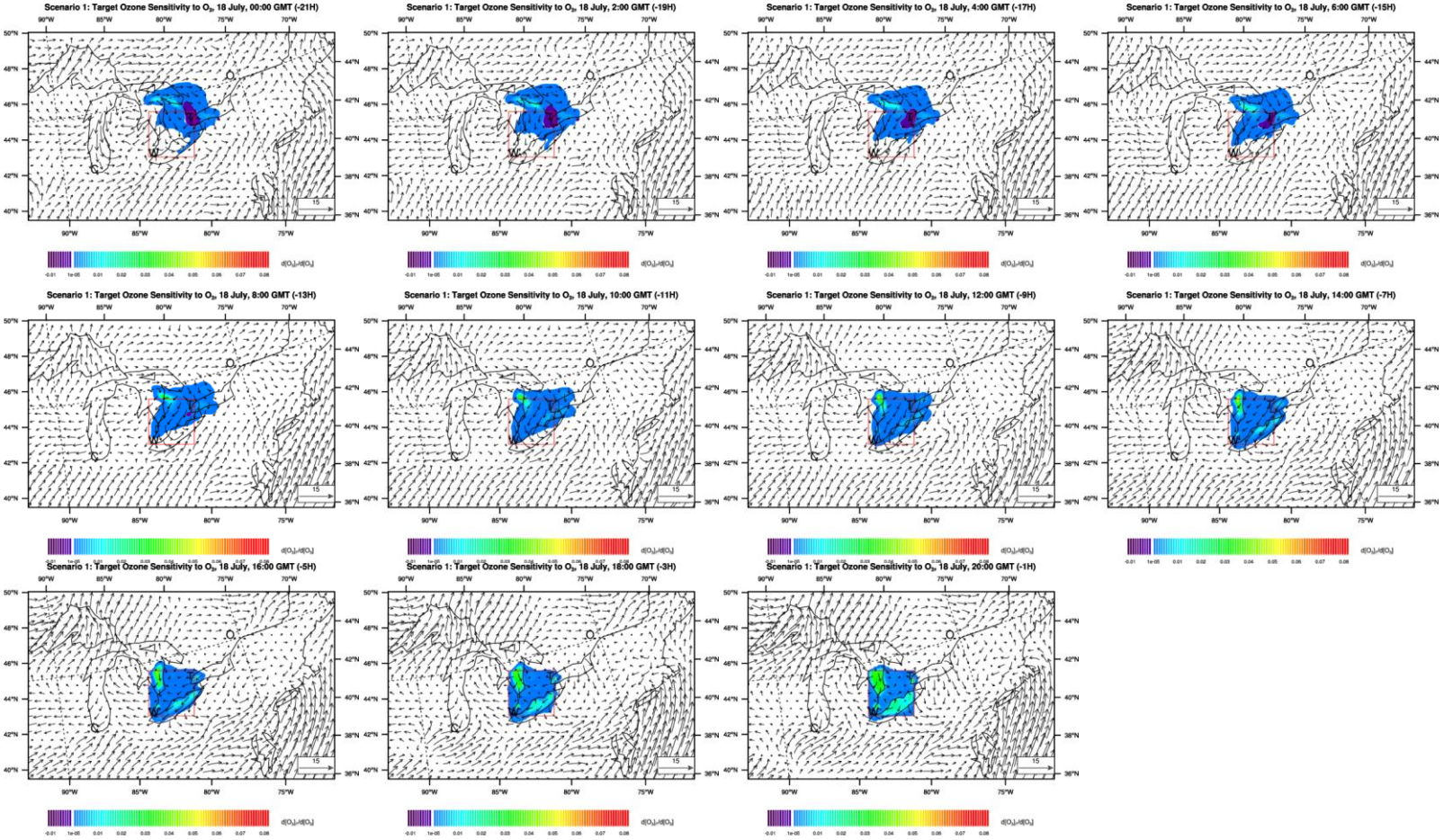

Figure 12. Scenario 1: target ozone sensitivity to pre-existing ozone changes in the 69 hours before the assumed high ozone episode in the W-T region at 21:00 GMT July 18. Plots are presented every 2 hours. White colour represents sensitivity values between -0.00001 ppm/ppm and +0.00001 ppm/ppm. The vectors are horizontal winds calculated by MM5, in m/s.

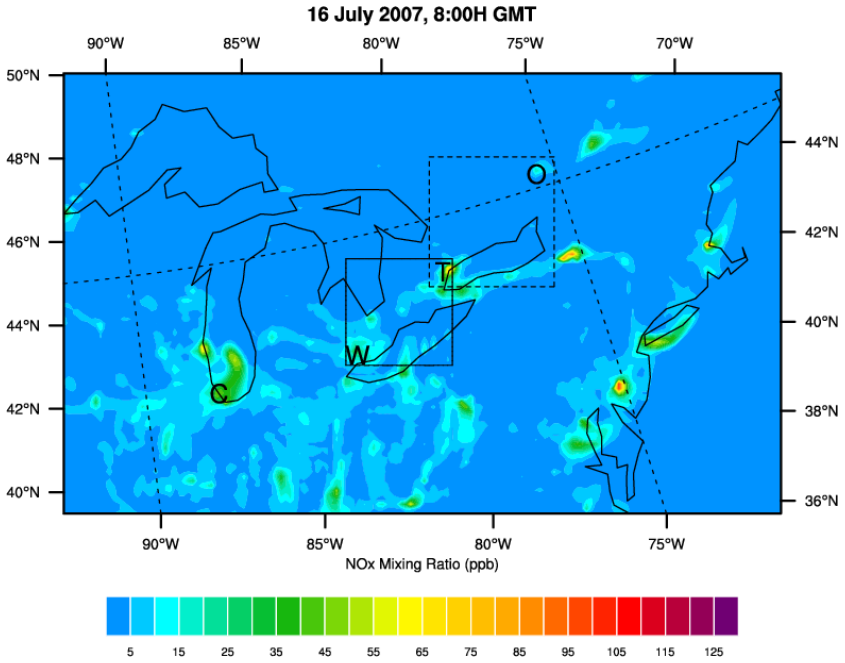

Figure 13. CMAQ simulated NOx mixing ratio at 08:00 GMT July 16, 2007. Unit: ppb.

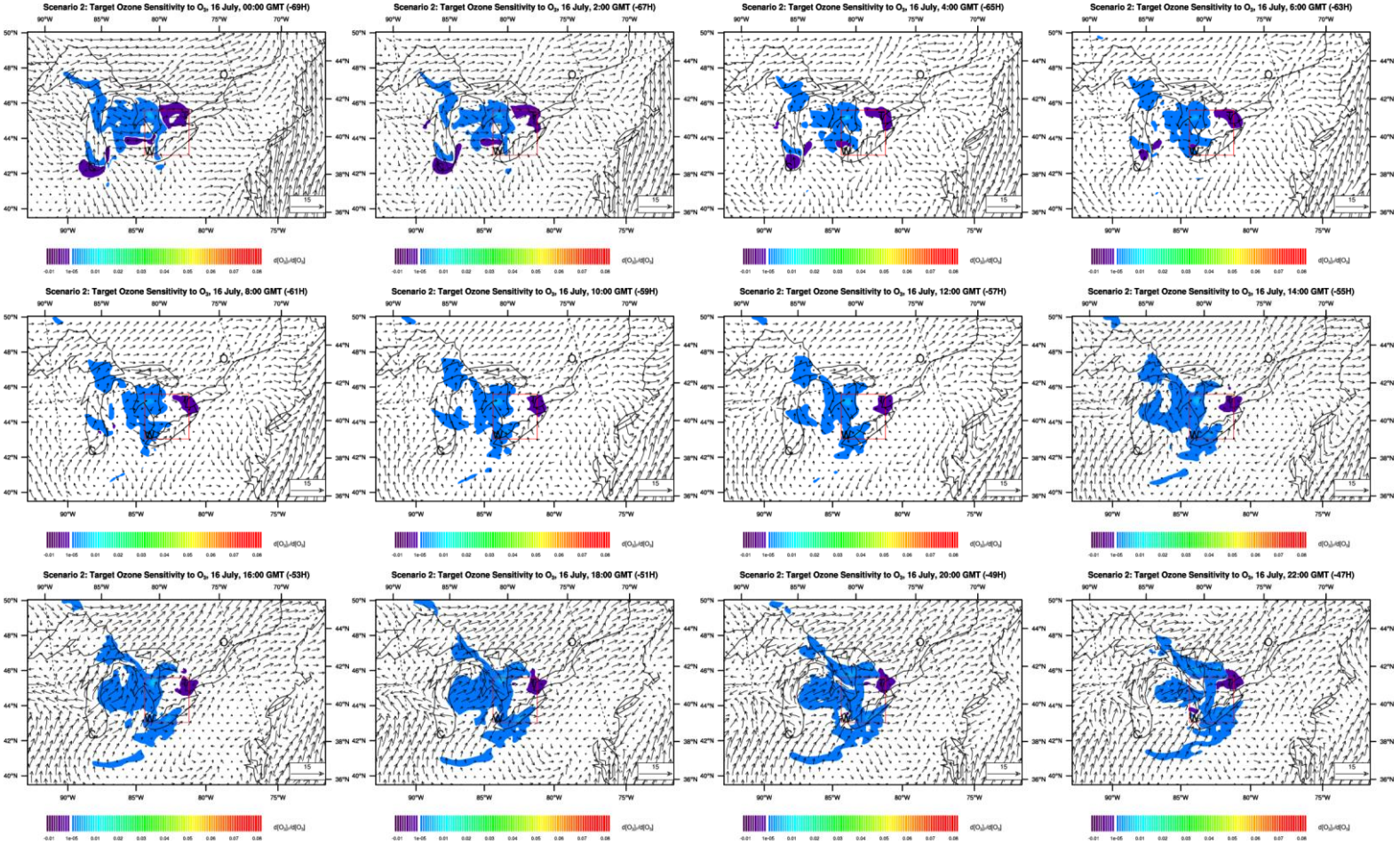
Scenario 2: Target Ozone Sensitivity to O3, 16 July, 00:00 GMT (-69H)
Scenario 2: Target Ozone Sensitivity to O3, 16 July, 2:00 GMT (-67H)
Scenario 2: Target Ozone Sensitivity to O3, 16 July, 4:00 GMT (-65H)
Scenario 2: Target Ozone Sensitivity to O3, 16 July, 6:00 GMT (-63H)
Scenario 2: Target Ozone Sensitivity to O3, 16 July, 8:00 GMT (-61H)
Scenario 2: Target Ozone Sensitivity to O3, 16 July, 10:00 GMT (-59H)
Scenario 2: Target Ozone Sensitivity to O3, 16 July, 12:00 GMT (-57H)
Scenario 2: Target Ozone Sensitivity to O3, 16 July, 14:00 GMT (-55H)
Scenario 2: Target Ozone Sensitivity to O3, 16 July, 16:00 GMT (-53H)
Scenario 2: Target Ozone Sensitivity to O3, 16 July, 18:00 GMT (-51H)
Scenario 2: Target Ozone Sensitivity to O3, 16 July, 20:00 GMT (-49H)
Scenario 2: Target Ozone Sensitivity to O3, 16 July, 22:00 GMT (-47H)

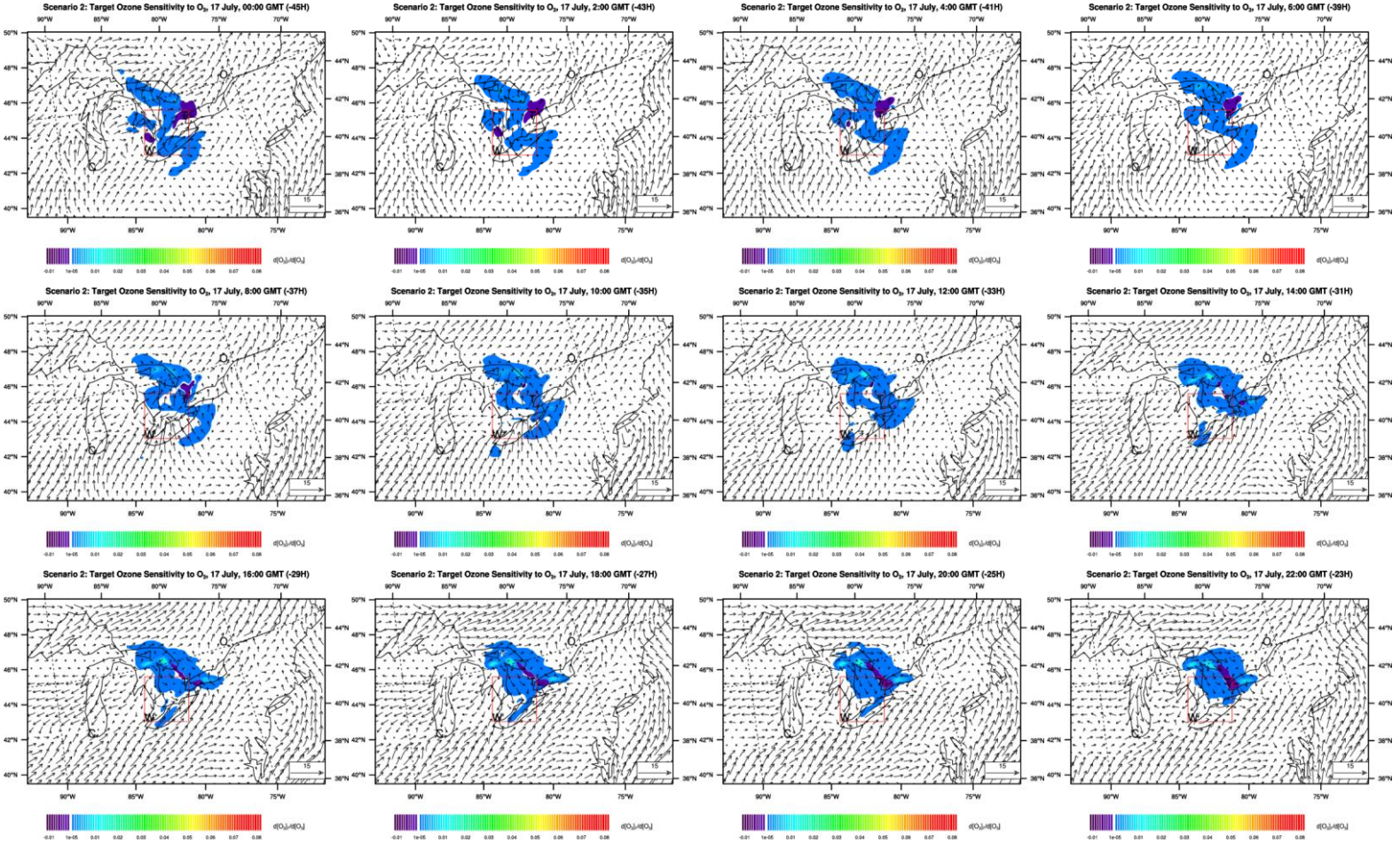
Scenario 2: Target Ozone Sensitivity to O_3, 17 July, 00:00 GMT (-45H)
Scenario 2: Target Ozone Sensitivity to O_3, 17 July, 2:00 GMT (-43H)
Scenario 2: Target Ozone Sensitivity to O_3, 17 July, 4:00 GMT (-41H)
Scenario 2: Target Ozone Sensitivity to O_3, 17 July, 6:00 GMT (-39H)
Scenario 2: Target Ozone Sensitivity to O_3, 17 July, 8:00 GMT (-37H)
Scenario 2: Target Ozone Sensitivity to O_3, 17 July, 10:00 GMT (-35H)
Scenario 2: Target Ozone Sensitivity to O_3, 17 July, 12:00 GMT (-33H)
Scenario 2: Target Ozone Sensitivity to O_3, 17 July, 14:00 GMT (-31H)
Scenario 2: Target Ozone Sensitivity to O_3, 17 July, 16:00 GMT (-29H)
Scenario 2: Target Ozone Sensitivity to O_3, 17 July, 18:00 GMT (-27H)
Scenario 2: Target Ozone Sensitivity to O_3, 17 July, 20:00 GMT (-25H)
Scenario 2: Target Ozone Sensitivity to O_3, 17 July, 22:00 GMT (-23H)

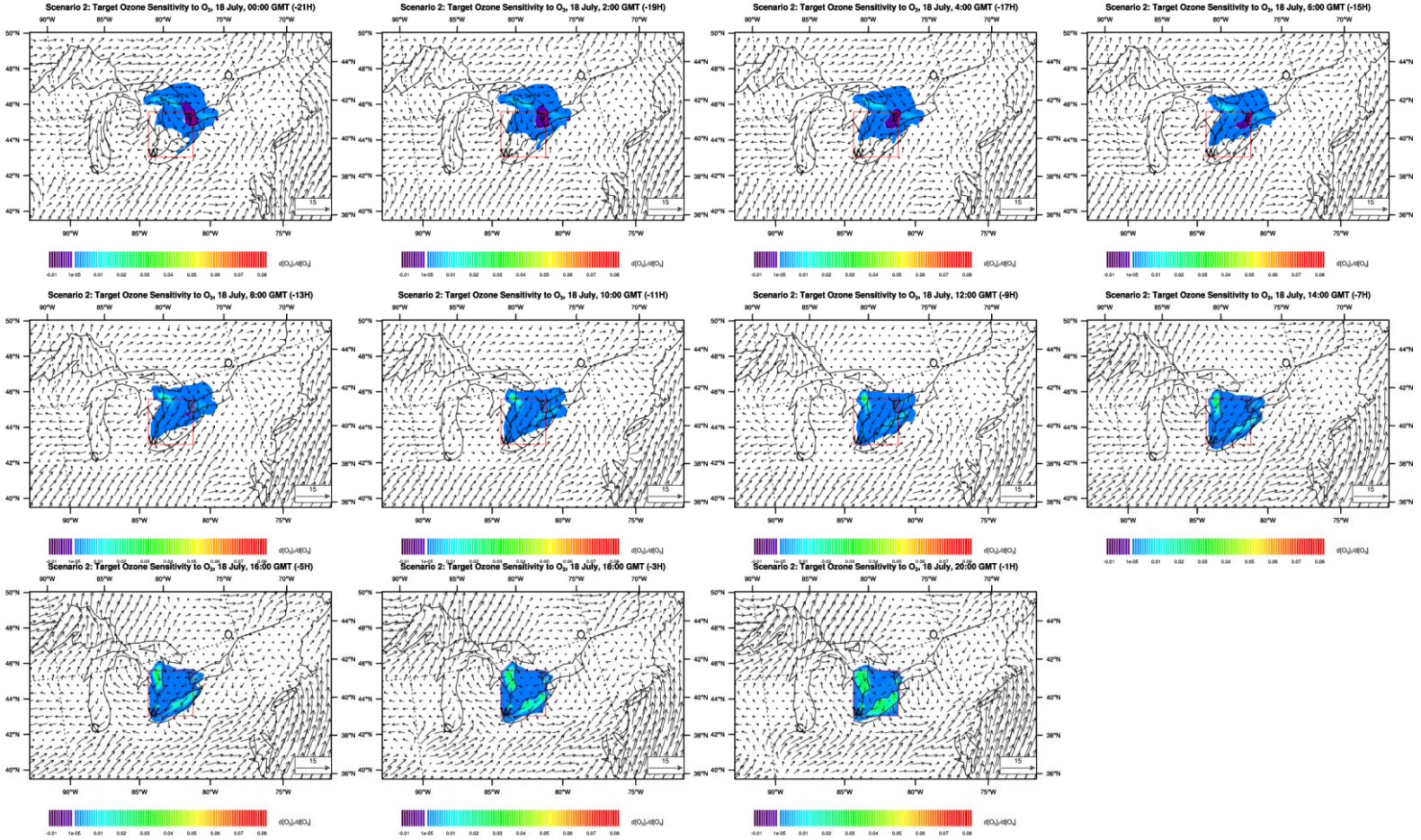

Figure 14. Scenario 2: target ozone sensitivity to pre-existing ozone changes in the 69 hours before the assumed high ozone episode in the W-T region at 21:00 GMT July 18, in ppm/ppm. Plots are presented every 2 hours. White colour represents sensitivity values between -0.00001 ppm/ppm and +0.00001 ppm/ppm. The vectors are horizontal winds calculated by MM5, in m/s.

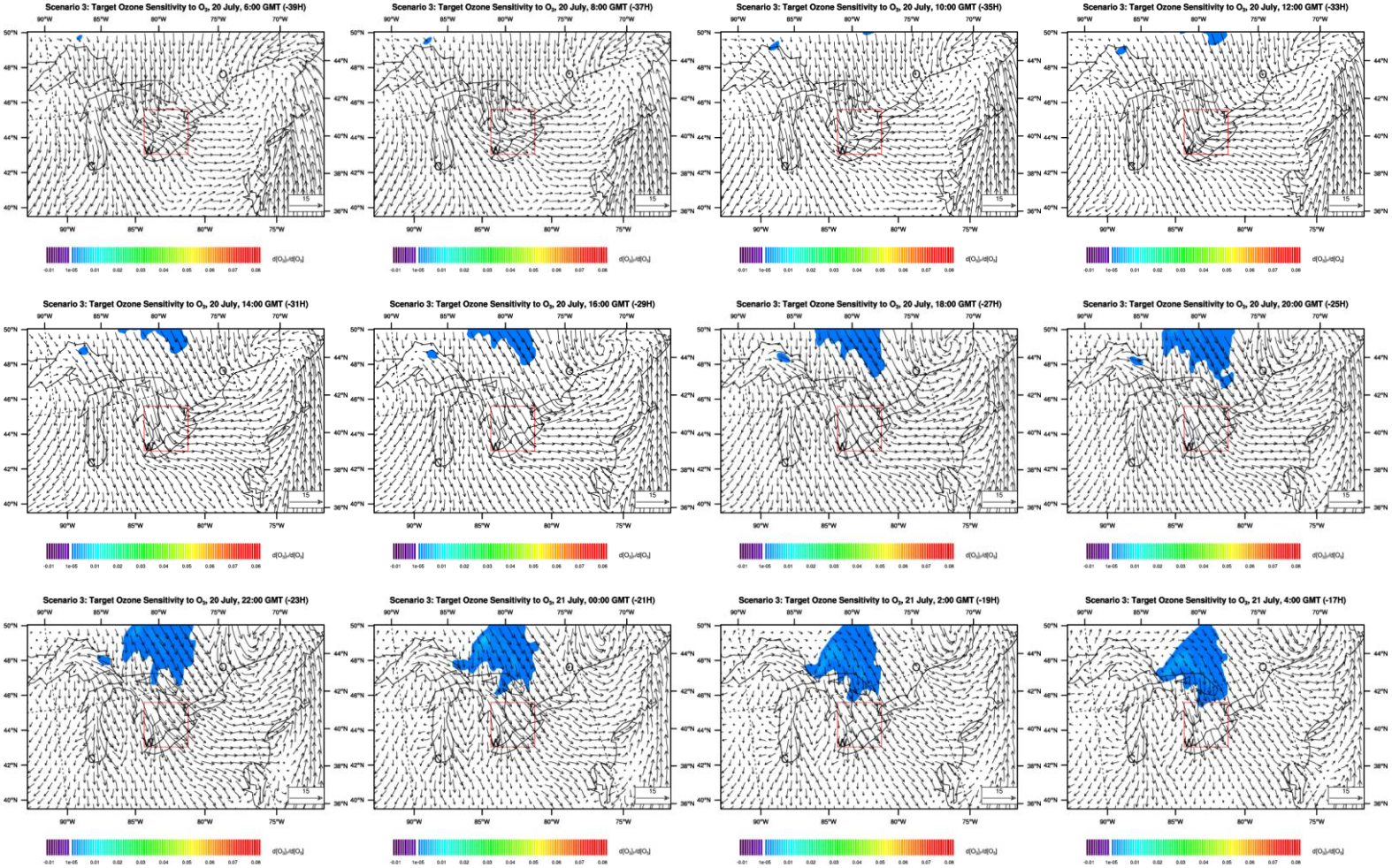
Scenario 3: Target Ozone Sensitivity to O_3, 20 July, 6:00 GMT (-39H)
Scenario 3: Target Ozone Sensitivity to O_3, 20 July, 8:00 GMT (-37H)
Scenario 3: Target Ozone Sensitivity to O_3, 20 July, 10:00 GMT (-35H)
Scenario 3: Target Ozone Sensitivity to O_3, 20 July, 12:00 GMT (-33H)
Scenario 3: Target Ozone Sensitivity to O_3, 20 July, 14:00 GMT (-31H)
Scenario 3: Target Ozone Sensitivity to O_3, 20 July, 16:00 GMT (-29H)
Scenario 3: Target Ozone Sensitivity to O_3, 20 July, 18:00 GMT (-27H)
Scenario 3: Target Ozone Sensitivity to O_3, 20 July, 20:00 GMT (-25H)
Scenario 3: Target Ozone Sensitivity to O_3, 20 July, 22:00 GMT (-23H)
Scenario 3: Target Ozone Sensitivity to O_3, 21 July, 00:00 GMT (-21H)
Scenario 3: Target Ozone Sensitivity to O_3, 21 July, 2:00 GMT (-19H)
Scenario 3: Target Ozone Sensitivity to O_3, 21 July, 4:00 GMT (-17H)

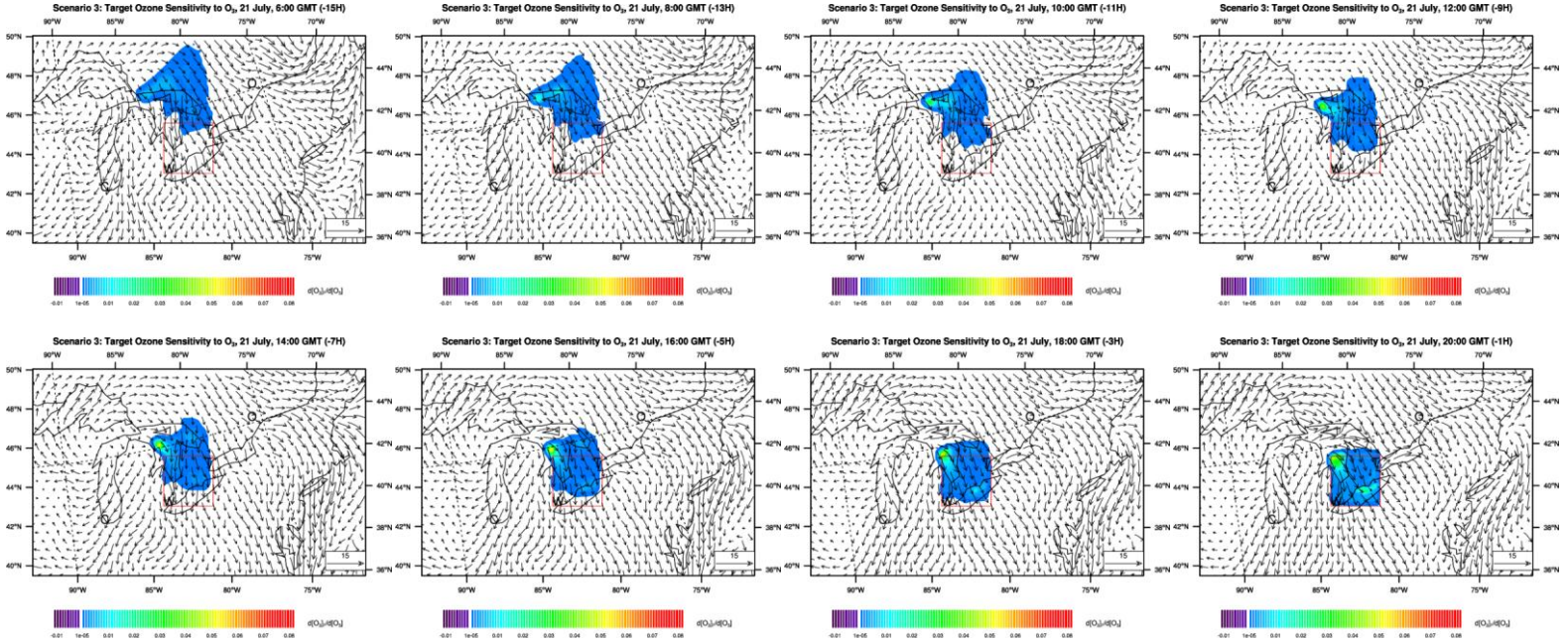

Figure 15. Scenario 3: target ozone sensitivity to pre-existing ozone changes in the 69 hours before the assumed high ozone episode in the W-T region at 21:00 GMT July 21, in ppm/ppm. Plots are presented every 2 hours. White colour represents sensitivity values between -0.00001 ppm/ppm and +0.00001 ppm/ppm. The vectors are horizontal winds calculated by MM5, in m/s. The sensitivity 39 hours before the assumed high ozone episode is zero everywhere and is not plotted.

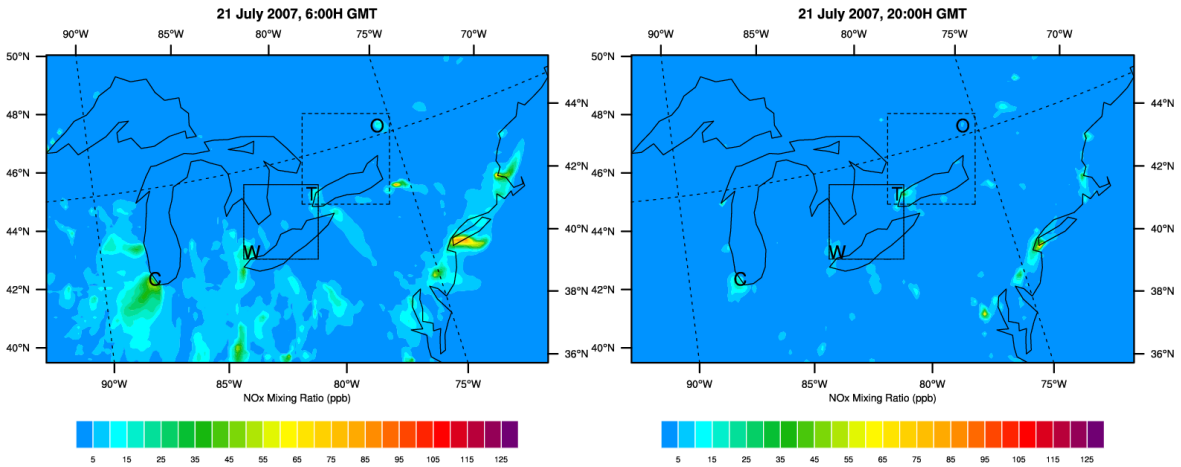

Figure 16. CMAQ simulated NOx mixing ratio at 06:00 GMT July 18 (a) and 20:00 GMT July 21 (b), 2007. Unit: ppb.

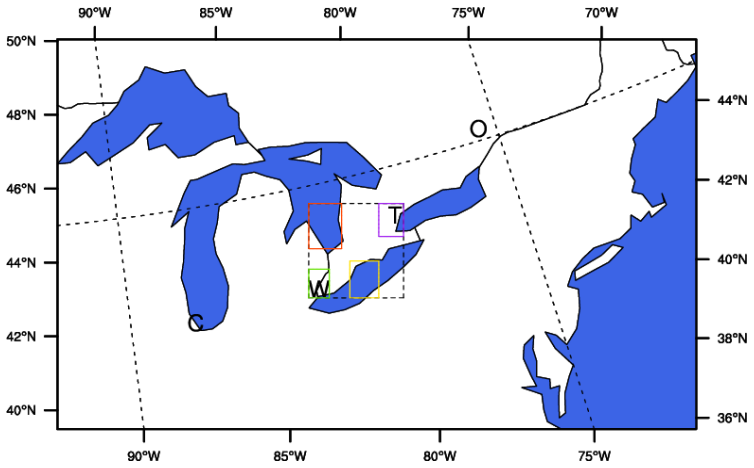

Figure 17. Four sub-regions in Windsor-Toronto region. Southern Lake Huron: in red square; Windsor: in green square; central Lake Erie: in yellow square; Toronto: in purple square.

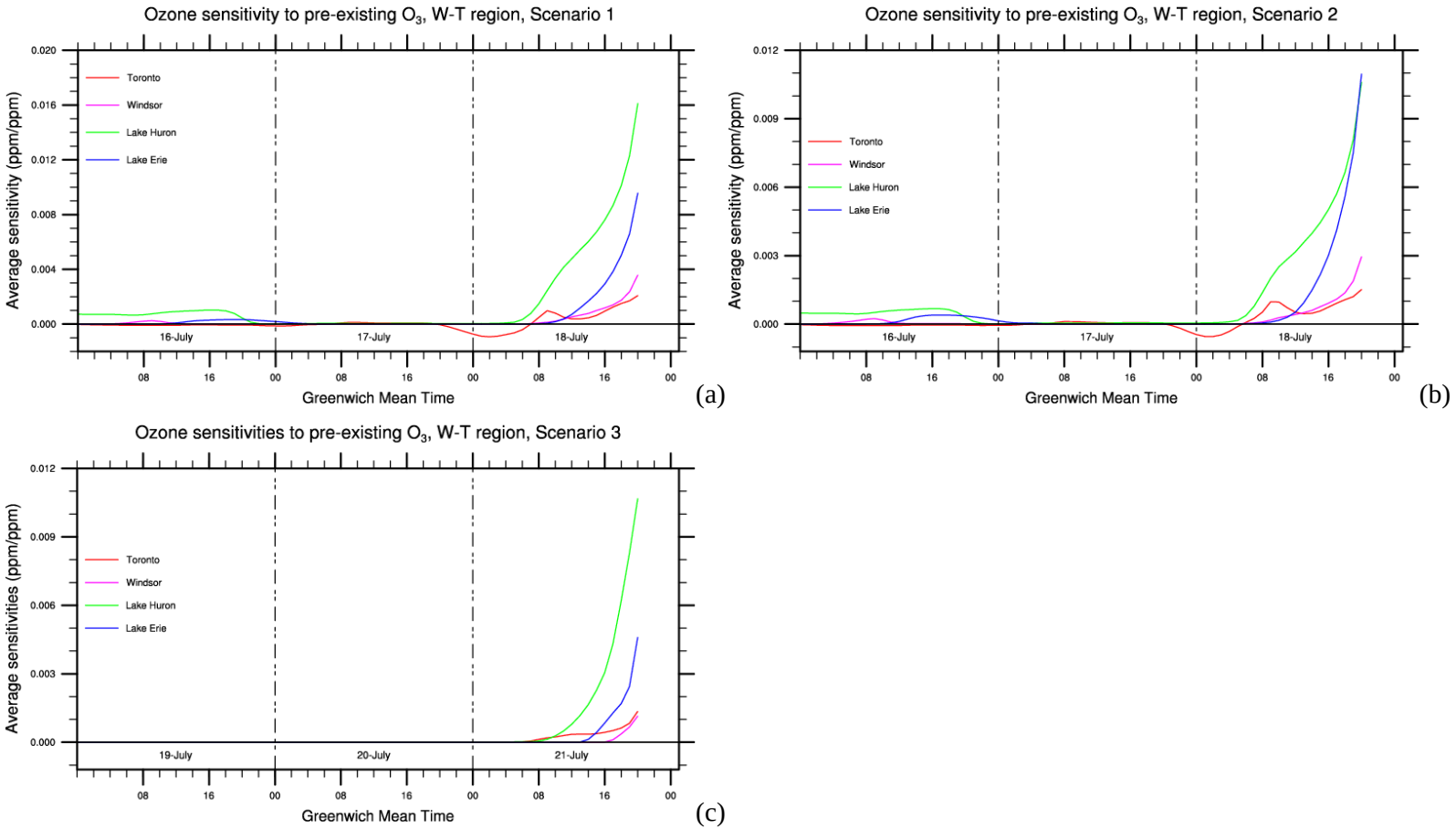

Figure 18. Time series of the average ozone sensitivity to the pre-existing ozone changes in 4 sub-regions of the Windsor-Toronto region for Scenario 1 (a), Scenario 2 (b), and Scenario 3 (c). The 4 local regions are Toronto, Windsor, southern part of Lake Huron, and middle Lake Erie.

5.3.2.2 Influence of NO

Ozone formation from its precursor species NOx and VOCs is nonlinear (Liu et al., 1987). Both the formation and the destruction of ozone happen in the presence of NOx emissions (http://www.epa.gov/air/ozonepollution/actions.html#standard). The rate of ozone production is determined by the relative proportions of NOx and VOCs (Geddes et al., 2009c). When VOC/NOx ratio is low, the oxidation of VOC is suppressed so that the ozone formation is short-circuited (FinlaysonPitts and Pitts, 1997) (Chemical reactions 5-1 and 5-2). Decreasing NOx in regions having low VOC/NOx ratio therefore can lead to an increase in the ozone concentration (FinlaysonPitts and Pitts, 1997). This case associates the negative ozone sensitivity with respect to NOx. When VOC/NOx ratio is high, ozone is formed when the peroxy radical RO_2 reacts with NO (Ryerson et al., 2001). Enhancing NOx emission will enhance the ozone formation. Trainer et al. (1987) showed that a reduction of NOx emission may be more effective than anthropogenic VOC reductions to reduce the ozone formation in rural area. Ryerson et al. (2001) showed that more ozone tends to form when NOx is emitted into the forested, isoprene-rich areas in the eastern United States where the VOC/NOx ratio is large.

In this section, the influence of NO on the changes in the ozone levels in southwestern Ontario is studied using the modified CMAQ-ADJ. The three scenarios used here are the same as those used in Section 5.3.2.1. Figure 19 shows the gradient (sensitivity) of the assumed ozone increase in the Windsor-Toronto receptor region with respect to NO for Scenario 1. In Scenario 1, the high ozone event is assumed to occur at 21:00 GMT July 18. By then, the ozone mixing ratio in southwestern Ontario (W-T region) is assumed to be 100 ppb everywhere. At the beginning of the 69-hour simulation period, a large area of positive sensitivity values can be observed extending from the northwest corner of Domain 2 and west of Lake Michigan to the northwest part of the W-T region (Figure 19). If the same amount of NO is allocated to all the 156×96 grids in Domain 2 on the -69H plot ("-69H" in the title of the plot means this plot is the sensitivity 69 hours before the assumed high ozone episode), a portion of the assigned NO in the non-zero sensitivity regions is then converted to ozone to enhance the ozone level in the W-T receptor square at target time (21:00 GMT July 18). The large influencing area of NO in the northern regions of the research domain exists because the high VOC/NOx ratio there makes these regions NOx-limited (except Toronto). The large area of the positive sensitivity does not mean that these places do have a large amount of NO. The NO concentrations in Northern Canada are always very low due to the lack of industry or heavy traffic. At -69H, the ozone sensitivity to NO near

urban areas (Chicago, Detroit (Windsor), and Toronto) is positive. Reducing NO emission in such places reduces the overall ozone level in southwestern Ontario after 69 hours.

In the remote northern Pennsylvania and northeast Ohio, increasing NO between 22:00 GMT July 16 and 04:00 GMT July 17 slightly reduces the ozone level in the receptor region by the target time. The nighttime titration of ozone by NO will be enhanced if NO in this area further increases. Hence, less ozone can be transported to the downwind target region. Except the local night time between 23:00 GMT July 16 and 04:00 GMT July 17, and before 04:00 GMT July 16, negative ozone sensitivity with respect to NO evolves from the upwind region of Toronto to the Toronto area. From 22 hours before the high ozone event, the prevailing wind in the W-T region is northerly. The negative sensitivity in the upwind direction of Windsor starts to evolve along the wind vectors. Detroit (Windsor) and Toronto maintain negative sensitivity since 9 hours (morning) prior to the high ozone event at 17:00 local time. The negative sensitivity corresponds to the urban areas where the VOC/NOx ratio is low (below 4). When the non-zero sensitivity fields evolve with the prevailing southerly wind from the northwestern U.S and Ohio Valley, the sensitivity is always positive, including those at Windsor. This suggests that once NO is emitted to such region, it enhances the ozone level in southwestern Ontario.

During the 69-hour simulation period, the gradient of the ozone perturbation in the target W-T square at target time with respect to NO over lakes (sometimes along lake shore) is always larger than that over the adjacent land areas. If the same amount of NO is released to lakes and to land at the same time, a greater portion of that to lakes is transformed to ozone in the southwestern Ontario than that released to land areas. At 0:00 GMT July 16, the largest sensitivity is on the southern part of Lake Huron. Lake Superior and Lake Michigan are too far from the receptor region to have as large an influence as Lake Huron. The reason that the largest sensitivity is on the major water body is because the ozone formed over waters remains longer than that formed on land area due to fewer removal mechanisms and low solubility of ozone. Ozone formed on land has more removal mechanism such as being taken up by vegetation. By 12:00 GMT 16 July, the location of the NO influencing region on Lake Huron does not change much, although its area expands and its magnitude intensifies. This influencing region evolves with wind and is always near the lake shore or over the lake body. The influence of the lake breezes on the northern shore of Georgian Bay is especially clear in the simulations from 08:00 GMT July 17 to 16:00 GMT July 17. Once NO is released to this location, lake breezes can prevent it and its production from being blown away to farther land regions. With the time approaching the high ozone event, NO in Georgian Bay and the Lake Erie region become close enough to influence the ozone in the

target W-T square. The ozone sensitivity to NO over these major water bodies is also larger than that on land.

By morning of the high ozone episode day, the region having non-zero sensitivity to NO almost coincides with the target region. Therefore, only local NO takes part in the ozone formation during the later several hours. The area of the large NO influencing region increases. The magnitude does not further increase, especially in the southern part of the W-T region where the VOC/NOx ratio is low. An increase in NO emission in area with low VOC/NOx ratio suppresses the oxidation of VOCs and hence the ozone formation is suppressed, the reason is as analyzed in Section 5.2.1.2. Generally, relatively little ozone is formed in the first several hours after NO is emitted as it is removed by oxidation to HNO_3 (Ryerson et al., 2001). Reflected in the time series of the average ozone sensitivity to NO in the four sub-regions in the W-T region in Figure 22 (a), the largest average ozone sensitivity over the sub-regions to NO happens several hours before the outbreak of the high ozone episode in all the selected local regions. The difference in the magnitude of the average sensitivity on different sub-regions has reflected the phenomenon found in Figure 19, i.e., NO emitted to lake regions has a large influence to the later high ozone event, especially when the VOC/NOx in the lake region is large. The negative sensitivity values associated with Windsor and Toronto in Figure 19 is averaged out in Figure 22 (a).

Scenario 2 uses the same meteorological conditions as Scenario 1, but a uniform perturbation when assuming a high ozone episode. It is assumed that the ozone level everywhere in the W-T region is enhanced by 40 ppb at 21:00 GMT July 18. Different VOC-NOx regimes have an apparent influence on ozone formation. NOx-rich regions such as Toronto have negative ozone sensitivity with respect to NO. Suppressing NO at such places enhances the ozone production. This relationship in Windsor and Toronto is especially apparent when time approaches to the high ozone episode. This phenomenon is not apparent at the earlier hours of the research period when the overall influence in the research domain is small. In earlier hours, the negative effect of NO on ozone is only clear in Toronto where the VOC/NOx ratio is very small. Figure 20 shows that the sensitivity in almost all the non-urban upwind influencing regions is positive in the beginning of the research period. If NO is emitted to these regions, a portion of it will enhance the ozone formation in southwestern Ontario in 69 hours. NO released to lake regions tends to have a larger influence than that released in land areas. Lakes in northern Ontario such as Lake Huron have a larger influence than Lakes in the south. The reason is because VOC/NOx ratio in the north is much larger than in the south, which is more industrialized and populated.

The ozone sensitivity to NO in Scenario 2 is very similar to that in Scenario 1. Scenarios 1 and 2 use different cost functions. The reason for this similarity therefore should be attributed to other conditions as analyzed in Section 5.3.2.1, i.e., the same meteorology and underlying surfaces, and the same emission feature in the pollutant's transport pathway. These features play a determining role in the spatial pattern and temporal variability of the sensitivity fields. The average sensitivity in the four local sub-regions also shows a similarity between Scenario 1 and Scenario 2. The time series of the average ozone sensitivity to NO over the four sub-regions in Figure 22 (b) evolves in a very similar manner as those in Figure 22 (a). The magnitude of the NO over Lake Huron in Scenario 1 is larger than that in Scenario 2, which is due to the fact that the introduced ozone perturbation there in Scenario 1 is much larger than that in Scenario 2 (Figure 11). This small region should be investigated in a higher resolution simulation.

Scenario 3 uses the same ozone perturbation as used in Scenario 1, but different meteorological conditions. The ozone sensitivity with respect to NO calculated by the modified CMAQ-ADJ is shown in Figure 21. In this scenario, most land regions of the research domain are controlled by strong northeast or northwest wind. The cold air blown from the north causes the temperature in Domain 2 to be lower than in Scenario 1. During the 69-hour simulation period, the sensitivity is zero everywhere in the research domain until 45 hours before the occurrence of the high ozone episode. Forty-five hours is a sufficient interval to blow any NO before 0:00 GMT 20 July and ozone produced by it later out of the W-T region by the target time. The calculated ozone sensitivity is therefore zero. From 0:00 GMT 20 July, the non-zero sensitivity fields evolve quickly toward the W-T region. The largest positive sensitivity is in lake regions. The sensitivity is smaller in most land areas. Nine hours before the assumed high ozone episode, NO in Toronto starts to make contributions to the high ozone episode with a negative sensitivity. One hour before the outbreak of the high ozone event, NO in Windsor can influence the ozone level in the target region with negative sensitivity values. NO in such places that have low VOC/NOx ratio suppresses the ozone formation in southwestern Ontario in the next several hours. Local ozone's response to NO in Scenario 3 shows some similar features as in Scenarios 1 and 2. Under the strong transport conditions, the largest impact of NO on the ozone formation in southwestern Ontario is also over the southern part of Lake Huron (Figure 22 (c)). The largest average ozone sensitivity to NO happens several hours before the outbreak of the high ozone episode in all the selected local regions. The negative sensitivity in these two urban areas in Figure 21 is averaged out and cannot be seen in Figure 22 (c). Due to the rapid movement of the air mass in this Scenario, earlier emitted NO cannot influence the W-T region as in Scenarios 1

and 2. The average non-zero ozone sensitivity to NO mainly occurs in the same day as the assumed ozone non-attainment.

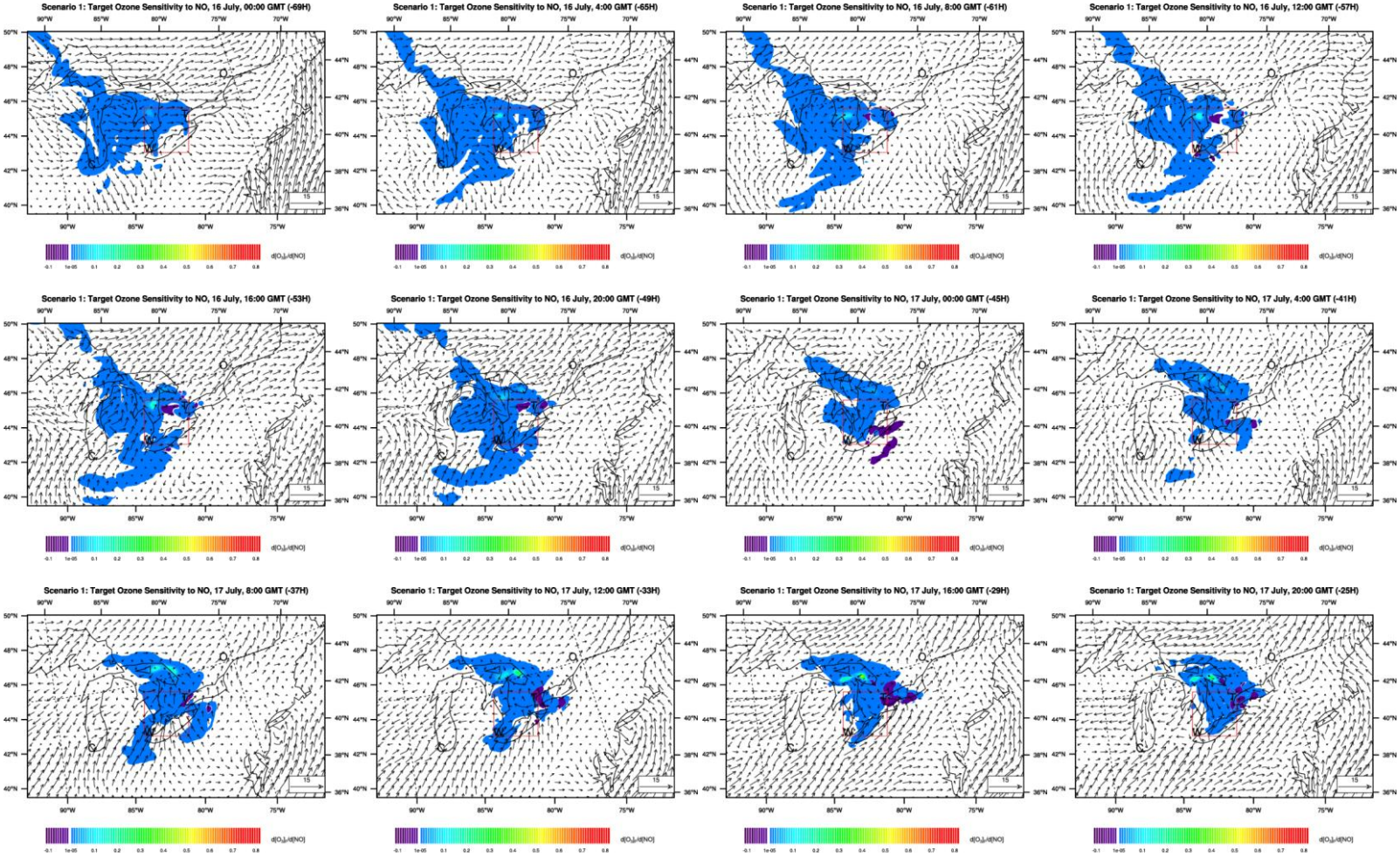
Scenario 1: Target Ozone Sensitivity to NO, 16 July, 00:00 GMT (-69H)
Scenario 1: Target Ozone Sensitivity to NO, 16 July, 4:00 GMT (-65H)
Scenario 1: Target Ozone Sensitivity to NO, 16 July, 8:00 GMT (-61H)
Scenario 1: Target Ozone Sensitivity to NO, 16 July, 12:00 GMT (-57H)
Scenario 1: Target Ozone Sensitivity to NO, 16 July, 16:00 GMT (-53H)
Scenario 1: Target Ozone Sensitivity to NO, 16 July, 20:00 GMT (-49H)
Scenario 1: Target Ozone Sensitivity to NO, 17 July, 00:00 GMT (-45H)
Scenario 1: Target Ozone Sensitivity to NO, 17 July, 4:00 GMT (-41H)
Scenario 1: Target Ozone Sensitivity to NO, 17 July, 8:00 GMT (-37H)
Scenario 1: Target Ozone Sensitivity to NO, 17 July, 12:00 GMT (-33H)
Scenario 1: Target Ozone Sensitivity to NO, 17 July, 16:00 GMT (-29H)
Scenario 1: Target Ozone Sensitivity to NO, 17 July, 20:00 GMT (-25H)

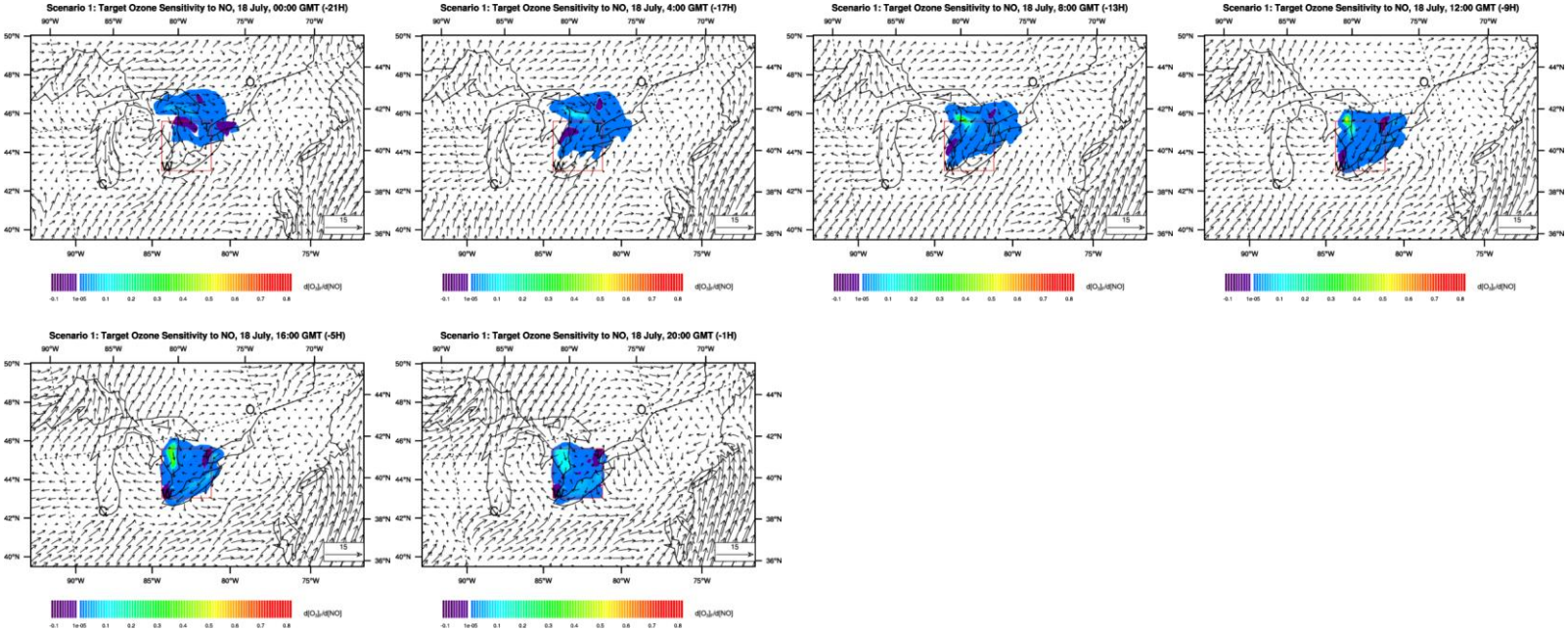

Figure 19. Scenario 1: target ozone sensitivity to NO changes in the 69 hours before the assumed high ozone episode in the W-T region at 21:00 GMT July 18, in ppm/ppm. Plots are presented every 4 hours. White colour represents sensitivity values between -0.00001 ppm/ppm and +0.00001 ppm/ppm. The vectors are horizontal winds calculated by MM5, in m/s.

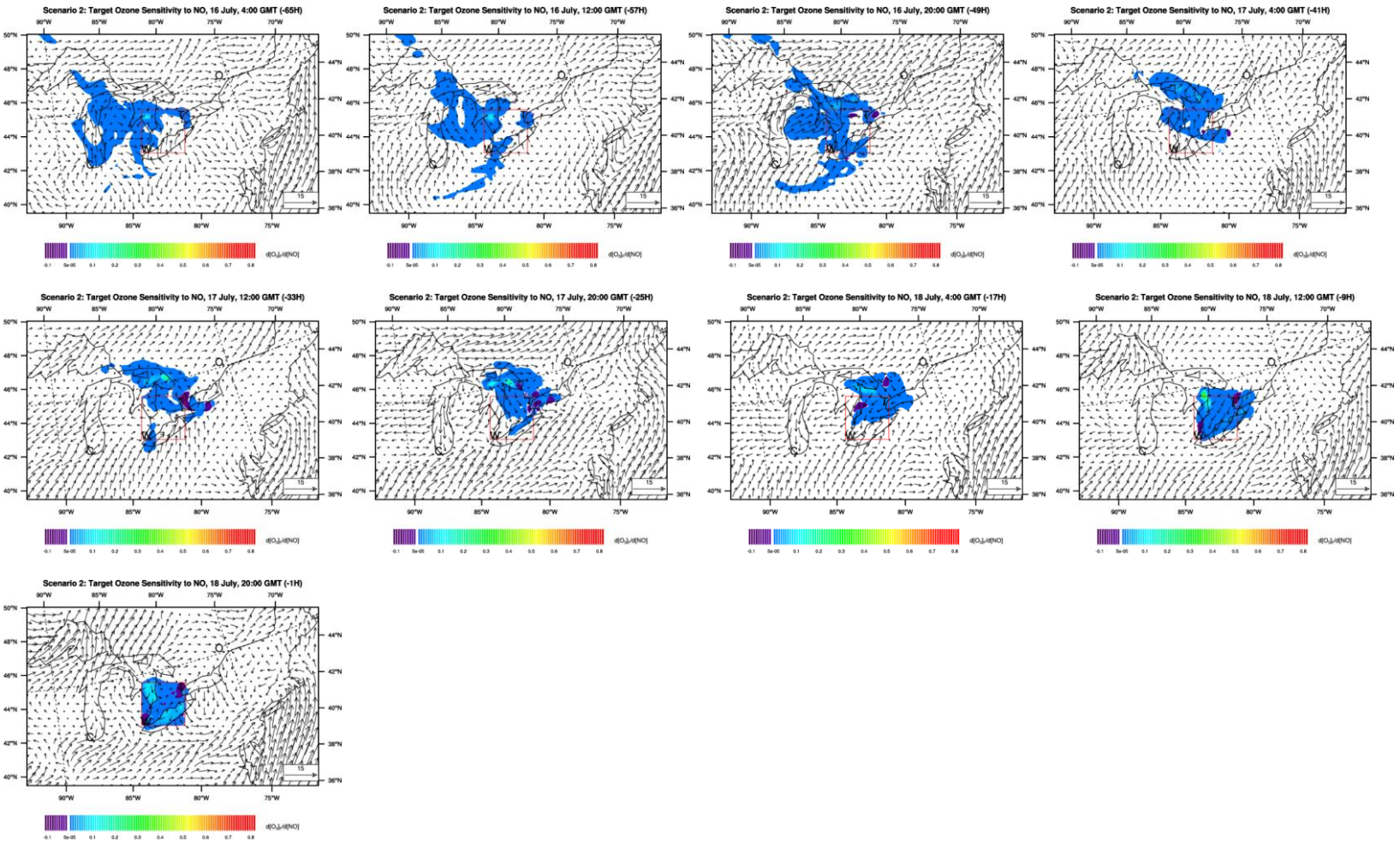

Figure 20. Scenario 2: target ozone sensitivity to NO changes in the 69 hours before the assumed high ozone episode in the W-T region at 21:00 GMT July 18, in ppm/ppm. Plots are presented every 8 hours. White colour represents sensitivity values between -0.00001 ppm/ppm and +0.00001 ppm/ppm. The vectors are horizontal winds calculated by MM5, in m/s.

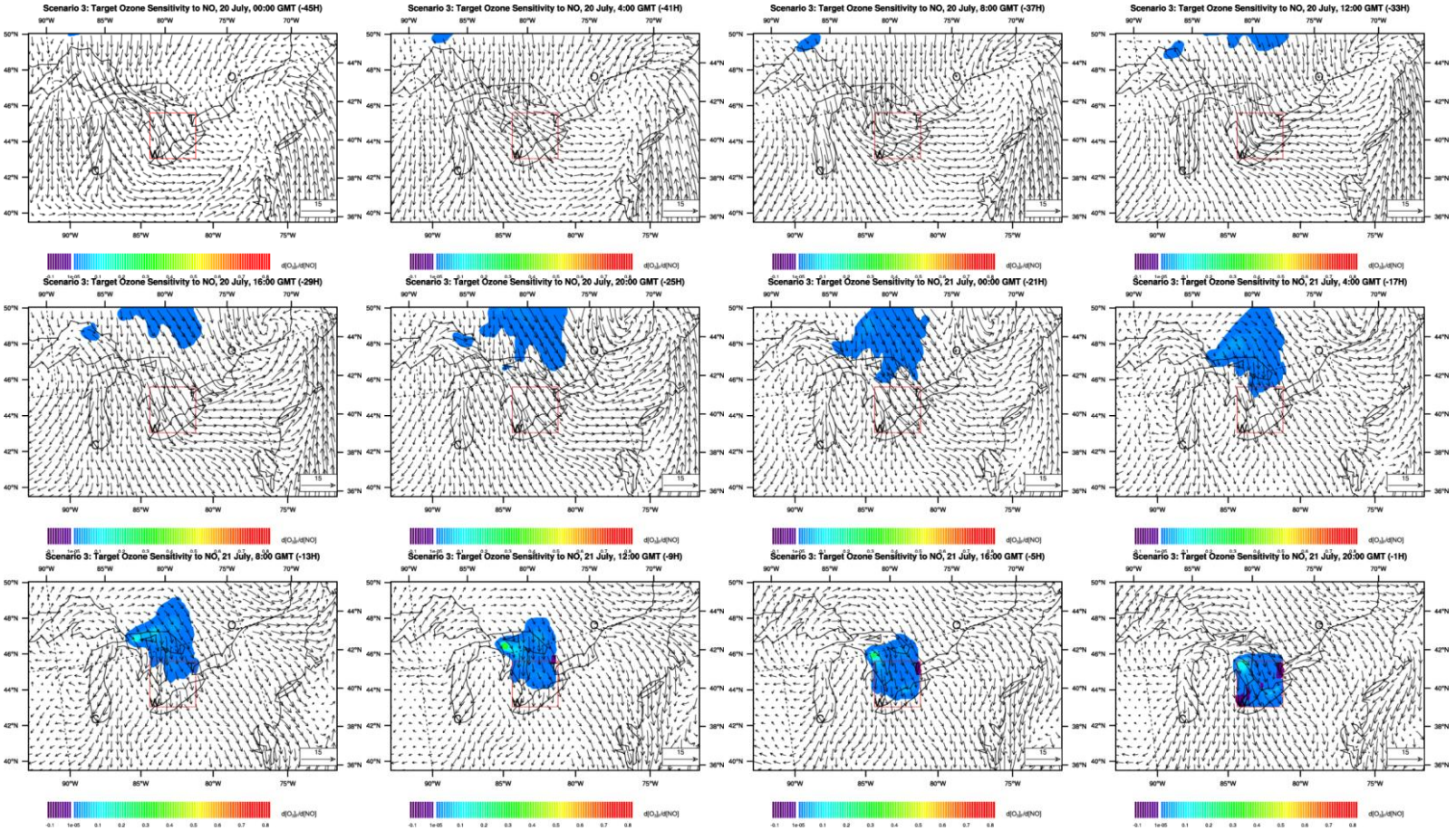

Figure 21. Scenario 3: target ozone sensitivity to NO changes in the 69 hours before the assumed high ozone episode in the W-T region at 21:00 GMT July 21, in ppm/ppm. Plots are presented every 4 hours. White colour represents sensitivity values between -0.00001 ppm/ppm and +0.00001 ppm/ppm. The vectors are horizontal winds calculated by MM5, in m/s. Sensitivities 45 hours before the assumed high ozone episode are zero everywhere and are not plotted.

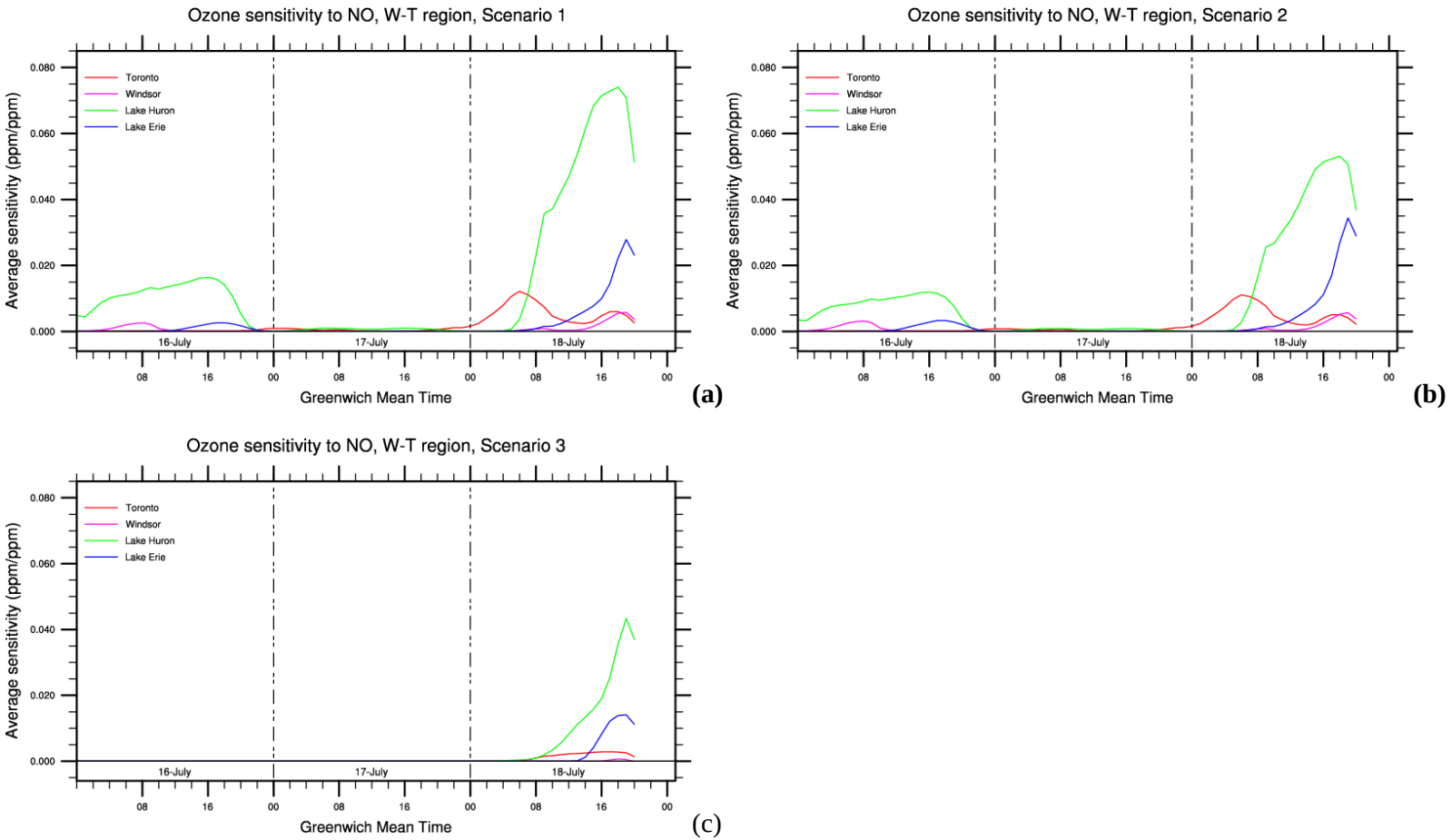

Figure 22. Time series of the average ozone sensitivity to NO changes in 4 sub-regions of the Windsor-Toronto region for Scenario 1 (a), Scenario 2 (b), and Scenario 3 (c). The 4 local regions are Toronto, Windsor, southern part of Lake Huron, and middle Lake Erie.

5.3.2.3 Influence of CO and VOCs

In traditional ozone control strategies, all of the organic species tend to be treated in a similar way by regulations aimed at reducing ozone levels through reducing the emission of ozone precursors (Bergin et al., 1995). Considering the fact that different organic compounds react at different rates and with different reaction mechanisms when taking part in ozone production (Atkinson, 1990), the ozone formation potentials, or reactivity, of an individual VOC should be treated differently.

The relative importance of each organic compound in ozone production have been investigated for long time using environmental chamber experiments and air quality models of different complexity (Derwent et al., 1996; Derwent et al., 1998; Khattatov et al., 1999; Lewis et al., 2000). Carter (1994) ranked the photochemical ozone formation reactivity of 118 VOCs in box model scenarios for 39 different urban areas. Russell et al. (1995) used both a box model and a 3-D airshed model to quantify the reactivities and found that ozone formation from some organic species such as alkanes and alcohols is an order of magnitude less than from other species such as alkenes and aldehydes. Hakami (2003) applied a regional 3-D sensitivity study to assess the behavior of different organic reactivity scales and evaluated the robustness of those scales under different environmental conditions. Compared with box models, 3-D air quality models can capture very detailed temporal and spatial variability of the ozone formation potential.

CMAQ-ADJ (as well as the modified CMAQ-ADJ) can calculate the sensitivity of ozone with respect to 36 model variables. The basic CB4 chemical mechanism used in the model explicitly includes the biogenic VOC isoprene, anthropogenic VOCs formaldehyde and ethylene, and the lumped anthropogenic VOCs paraffins, olefins, toluene, xylene, and aldehydes (details in Section 3.2.2). CMAQ-ADJ can calculate the geographic distribution and temporal evolution of the potential contribution of all these explicit and lumped VOC species to future ozone changes in a receptor region through only one model run. CMAQ-ADJ can therefore be used to effectively compare the individual VOC's importance to future ozone production.

Biogenic emissions of non-methane organic compounds from vegetation include isoprene, monoterprenes, etc. All biogenic VOCs react with hydroxyl radicals (OH), many of them also react with nitrate radicals (NO_3) and ozone (Atkinson and Arey, 2003). Isoprene is the only biogenic VOC in the basic CB4 gas-phase chemistry mechanism, which reacts with OH, NO_3, O_3, NO_2, and atomic oxygen (O) to take part in complex nonlinear reactions in tropospheric chemistry in CMAQ-ADJ. In addition to an explicitly included direct ozonolysis of isoprene by ozone associated with depletion of OH concentrations, the oxidation of isoprene by OH (at

daytime) and NO_3 (at nighttime) leads to the production of isoprene nitrates ($RONO_2$), which contains a double bond and is highly reactive with ozone (Horowitz et al., 2007). NO is consumed during the oxidation pathway of isoprene at day time (Horowitz et al., 2007) which implies that further ozone formation can be suppressed due to the lack of NO, especially in regions of low NOx emissions (Fiore et al., 2005; Horowitz et al., 2007; Kang et al., 2003). The productions during the isoprene oxidation at night can further form stable organic nitrates or decompose to release NOx (Horowitz et al., 2007), NOx is a necessary precursor of ozone. Therefore, both negative and positive ozone sensitivity to isoprene can be expected. Due to the complex nonlinearity between the 93 chemical reactions in the model, both positive and negative ozone sensitivities with respect to anthropogenic VOCs are possible as well. Former studies have found that increasing VOCs in places having a high VOC/NOx ratio can suppress ozone formation by suppressing the formation of peroxyl radical RO_2 (FinlaysonPitts and Pitts, 1997). It was also found that reducing the emission of anthropogenic hydrocarbons may not always substantially reduce the ozone formation in rural areas where VOC/NOx is high (Trainer et al., 1987). Reducing anthropogenic VOC emissions in large cities, where VOCs are mainly anthropogenic in origin, can reduce peak ozone concentrations (Fiore et al., 1998).

A study of the U.S. natural hydrocarbon emission showed that natural VOCs are significant compared to the emission of anthropogenic non-methane hydrocarbons (Lamb et al., 1987). Chameides et al. (1988) used CB-4 to check the role of isoprene on photochemical smog in Atlanta and found natural hydrocarbons can significantly affect urban ozone levels. In this section, the importance of isoprene and the other 7 primary anthropogenic VOCs to the changes in the ozone levels in southwestern Ontario is studied. The influence of CO on ozone level is also analyzed. In Canada, automobile emissions and forest fires can generate a large amount of CO, which controls OH concentration and hence the oxidation of most atmospheric trace gases in adjacent regions (Lelieveld and Dentener, 2000; Wotawa and Trainer, 2000; Forster and others, 2001).

The three scenarios that are investigated here are the same as those used in Section 5.3.2.1 and Section 5.3.2.2. Similar to those two sections, the results of Scenario 2 are very close to those of Scenario 1. Only results from Scenario 1 and Scenario 3 are analyzed in detail in this section. The close relationship between the horizontal wind and the distribution of the sensitivity fields of all organic compounds is very similar to that of pre-existing ozone and NO. This section does not focus on the hourly spatial evolution feature of the sensitivity fields. Only those sensitivity fields at local time 0:00 local time (04:00 GMT), 8:00 local time (12:00 GMT), and 16:00 local time (20:00 GMT) of the past 69 hours before the high ozone episode are presented.

The sensitivities of ozone in Windsor-Toronto region to CO and VOCs for Scenarios 1 and 3 are shown in Figure 23 and Figure 24. The sensitivity with a magnitude less than 0.00001 ppm/ppm is neglected (in white colour). Figure 23 and Figure 24 show that the sensitivity of CO is positive in its influencing region throughout the modeling period. Both the area of the influencing region and the magnitude are very small compared to all the other carbon compounds. This implies that only a very small portion of the CO emission takes part in the process of enhancing the ozone in the receptor region within the next 69 hours, but it hardly makes significant contributions to the assumed high ozone episode in southwestern Ontario due to its secondary effects in ozone formation through reacting with OH.

The carbon compounds formaldehyde and paraffins also have a small influence on the ozone level changes in the late afternoon on July 18. Before 20:00 GMT July 17, the negative sensitivity evolving around Toronto shows that increasing formaldehyde there can slightly decrease the ozone level in the W-T region in 25 hours. Formaldehyde emitted later than 4:00 GMT July 18 always increases the ozone formation by the target time. Larger sensitivity is always found over lake regions than the nearby land areas due to the fact that once ozone is formed, it remains longer over water due to its low solubility, but ozone over land area is readily taken up by vegetation. Nine hours before the high ozone episode, positive sensitivity near Detroit (Windsor) amplifies due to the large NOx emissions there. The calculated ozone sensitivity to paraffins has shown that 1 hour before the high ozone episode, increasing paraffins slightly enhances the local ozone formation at the W-T receptor region. Nine hours before the high ozone episode, in the regions with high VOC/NOx ratio, increasing paraffins is likely to suppress the ozone formation in the W-T region at the target time. The largest positive ozone sensitivity to paraffins is also near lake regions, or near urban areas where the VOC/NOx is small.

The area of the regions where aldehydes, ethylene, isoprene, olefins, toluene, and xylene can influence ozone level in the W-T region is large in the beginning of the simulation period. With the exception of toluene, all of the VOCs have positive ozone sensitivity in the Midwest U.S. and Ohio Valley from 69 hours prior to the assumed high ozone episode until around 12:00 GMT July 17. This suggests that these VOCs in this U.S. region can enhance the ozone formation in southwestern Ontario in 1.5 to 69 hours. The influences of these VOCs in the northern part of the model domain with very large VOC/NOx ratios (above 36) are either zero or negative. The non-zero ozone sensitivity field to toluene is mostly negative for all the 69 hours until about 1 day (the -25H plot of Figure 23) before the assumed high ozone episode. Positive sensitivity to toluene in two areas in the upwind direction region of Windsor and Toronto starts to develop and evolves toward these two urban areas where there are the large NOx emissions and small VOC/NOx ratio.

By one hour before the high ozone episode, aldehydes and xylene also show negative sensitivity in large VOC/NOx region and positive sensitivity in regions with small VOC/NOx ratio. The ozone sensitivity to ethylene, olefins, and isoprene are all positive by one hour before the assumed ozone episode, with a larger magnitude in the regions with small VOC/NOx ratios.

To further investigate the ozone response to CO and VOC emissions in local regions, the same four sub-regions are selected in the Windsor-Toronto receptor region as those in Section 5.3.2.1 and Section 5.3.2.2: Windsor and Toronto where there are abundant anthropogenic emissions, the southern part of Lake Huron where the VOC/NOx ratio is high, and the central region of Lake Erie where VOC/NOx is larger than urban areas. The time series of the average ozone sensitivity to CO and VOCs in these 4 locations are displayed in Figure 25. Based on Figure 23, the ozone changes in the target square in the late afternoon are mostly influenced by air in local area since the morning of the same day. The air mass at earlier times of the simulation period is influenced by the prevailing wind, which becomes an influencing factor of the fluctuation of the average sensitivity in Figure 25. When the air mass is blown out of the sub-regions, the average sensitivity is then very small. Therefore, the average ozone sensitivity several hours before the target time (21:00 GMT Jul 18) is representative when studying the influence of local air on ozone level changes. From the morning of the day, the average ozone sensitivity in urban areas to all VOCs is positive (positive sensitivity to aldehydes in Toronto and Windsor of this period can be seen in Figure 23, it is averaged out in Figure 25). This means VOC emissions in Toronto and Windsor always enhances the ozone formation in the next several hours. Enhanced ozone in city area titrates NOx, as a consequence, later ozone formation will be suppressed. This process is consistent with those results shown in Figure 12, i.e., the negative sensitivity of pre-existing ozone in Toronto at earlier hours of the simulation period. Such negative ozone sensitivity to VOCs is also reflected by the average negative ozone sensitivity in Toronto in Figure 25 in the beginning of the simulation period. Negative ozone sensitivity to VOCs in the Windsor area in the beginning of the simulation period does not occur because the air in Windsor is not as stagnant as in Toronto (the wind can be observed in Figure 23). In regions with high VOC/NOx ratio such as the southern part of Lake Huron, a morning increase of all VOCs except ethylene and formaldehyde causes the ozone level to decrease in the late afternoon. This negative sensitivity is not apparent over Erie because the area of negative sensitivity there is small (can be seen in Figure 23) and is averaged out in Figure 25.

Based on Figure 25, the magnitude of the ozone sensitivity to CO is much smaller during the whole simulation period than that to most VOCs. Paraffin has the smallest magnitude among all VOCs. In CB4 (Appendix A), both the reaction of CO and paraffins initiates from the reaction

with OH with a rate constant of $2.4 \times 10^{-13} cm^3 s^{-1}$ and $8.1 \times 10^{-13} cm^3 s^{-1}$ (these numbers are calculated for 298 K and one atmosphere), respectively. Such slow reactions is the possible reason that increasing these carbon compounds will not cause as large changes of ozone concentrations as increasing other VOCs. Although different VOCs has different structure and different chemical reaction pathways of ozone formation and loss, when adding different VOCs in the atmosphere, the ozone response to them such as the shape of the time series can still show great similarity at specific locations and time period (Figure 25). Great difference in their ozone formation responses also exist, especially the magnitude of the ozone sensitivities, which is due to different rate constants and different productions used in CB4. Similar to NO, the largest influence of these carbon compounds to ozone level in the late afternoon on July 18 at all locations occurs several hours before the high ozone episode, i.e., from early morning to noon, implying that it takes several hours for them to form ozone. The influence of a morning increase in different VOCs in different sub-regions on ozone level by late afternoon is summarized in Table 4.

Under the strong northerly wind conditions in Scenario 3, CO and VOCs at anywhere of the model domain before 12:00 GMT July 20 are blown out of the W-T region and cannot take part in the ozone formation or destruction there. The model-calculated sensitivity to these carbon compounds is then zero. Non-zero sensitivity to some species starts to appear at the edge of Domain 2 at the upwind direction of W-T square from one and a half day before the high ozone episode at 21:00 GMT July 21 (Figure 24). The sensitivity fields evolve quickly with the wind. If the carbon compound is emitted to the region with non-zero sensitivity to this carbon compound, a portion of it (and/or its productions after reacting with other species) is transported quickly to the target W-T region to influence the ozone level there. By one hour before the high ozone episode, the ozone response in the W-T region to all the 8 carbon compounds tends to be local.

Similar to Scenario 1, the ozone sensitivity to CO and paraffins has a similar magnitude, which is almost one order of magnitude smaller than to formaldehyde and almost two orders of magnitude smaller than to the rest of the VOCs. At 12:00 GMT July 20, the sensitivity to CO, formaldehyde and paraffins in the whole domain is zero, but changing the other 6 VOCs near the upwind border of the research domain can enhance (due to the positive sensitivity) or suppress (due to the negative sensitivity) the ozone level in the W-T region. When the sensitivity fields evolve from the northern regions to the southwestern Ontario, if increasing CO in the non-zero sensitivity covered region, the ozone formation in the target W-T region in the next day can always be enhanced, although the magnitude is very small. By 8:00 local time, in regions other

than those upwind of Windsor and Toronto, the non-zero sensitivity to paraffins is negative. By one hour before the high ozone episode, the influence of paraffins is local and mostly slightly enhances the ozone level one hour later. The ozone sensitivity to formaldehyde is mainly positive by one hour before the occurence of the high ozone event, with the largest near Windsor and Toronto where there is the largest NOx emission.

Among the other 6 VOCs, increasing ethylene in the non-zero sensitivity regions can always enhance the ozone level in the W-T region in the next 1.5 days. By 20:00 GMT July 21 (one hour before the high ozone event), ozone sensitivity to ethylene, isoprene, and olefins is all positive, i.e., increasing such VOCs can enhance the ozone formation in one hour. Xylene in most of the W-T region has positive sensitivity by 20:00 GMT July 21, except over southern part of Lake Huron and Lake Erie where the VOC/NOx ratio is large. At this time, the ozone sensitivity to toluene is also positive in places with low VOC/NOx ratio such as Windsor, Toronto, and the land area between these two urban centres, increasing toluene can enhance the ozone formation in the next hour. As a contrast, ozone formation will be decreased if the increased toluene is in lake areas. One hour before the high ozone event, positive ozone sensitivity to aldehydes only appears at Windsor and Toronto where the VOC/NOx ratio is very small. Increasing aldehydes locally and in the upwind northern directions 1.5 days before the high ozone event can decrease the ozone level in southwestern Ontario by the occurrence of the high ozone event. During the 1.5 days period before the high ozone event in the W-T region (especially at earlier hours), the behavior of the ozone sensitivity to isoprene, olefins, toluene, and xylene is similar to that of aldehydes. Increasing these VOCs in the upwind regions of the W-T square very likely decreases the ozone formation in southwestern Ontario in 1.5 days. This relates to the fact that almost all the upwind north area of the research Domain 2 has very large VOC/NOx ratios (greater than 27). Regions in the upwind direction of Windsor and Toronto that are characterized by small VOC/NOx ratio tend to have positive ozone sensitivity, especially to isoprene and olefins. The reason that different VOCs show different sensitivity to ozone formation should relate to their own intrinsic properties.

The average ozone responses to individual carbon compounds under strong transport conditions are also investigated for the same four sub-regions as used in Scenario 1. Since air moves very quickly in Scenario 3, the ozone changes in the receptor region are mainly influenced by those precursors transported from distant regions, while not locally. A detailed analysis is not meaningful, but it is worthwhile to mention that the magnitude of the average ozone sensitivity to the same carbon compound under different meteorological conditions is different. For the same species, the average sensitivity in Scenario 1 can be one order of magnitude larger than that in

Scenario 3. At high temperature conditions, a larger portion of VOCs can be transformed to ozone in the next several hours than at low temperature conditions. This is because the reaction rates for VOC reactions in CB4 are temperature-dependent.

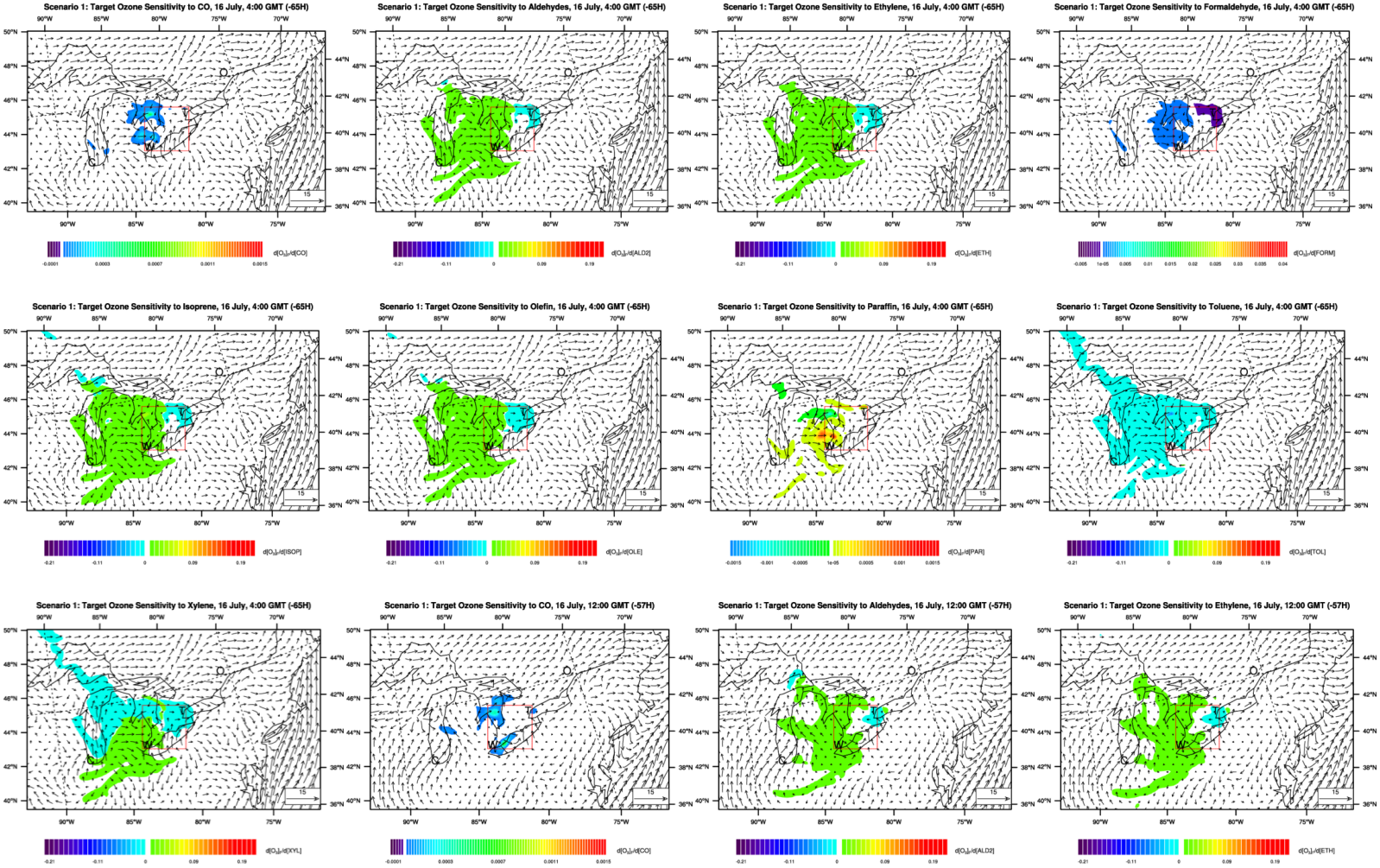
Scenario 1: Target Ozone Sensitivity to CO, 16 July, 4:00 GMT (-65H)
Scenario 1: Target Ozone Sensitivity to Aldehydes, 16 July, 4:00 GMT (-65H)
Scenario 1: Target Ozone Sensitivity to Ethylene, 16 July, 4:00 GMT (-65H)
Scenario 1: Target Ozone Sensitivity to Formaldehyde, 16 July, 4:00 GMT (-65H)
Scenario 1: Target Ozone Sensitivity to Isoprene, 16 July, 4:00 GMT (-65H)
Scenario 1: Target Ozone Sensitivity to Olefin, 16 July, 4:00 GMT (-65H)
Scenario 1: Target Ozone Sensitivity to Paraffin, 16 July, 4:00 GMT (-65H)
Scenario 1: Target Ozone Sensitivity to Toluene, 16 July, 4:00 GMT (-65H)
Scenario 1: Target Ozone Sensitivity to Xylene, 16 July, 4:00 GMT (-65H)
Scenario 1: Target Ozone Sensitivity to CO, 16 July, 12:00 GMT (-57H)
Scenario 1: Target Ozone Sensitivity to Aldehydes, 16 July, 12:00 GMT (-57H)
Scenario 1: Target Ozone Sensitivity to Ethylene, 16 July, 12:00 GMT (-57H)

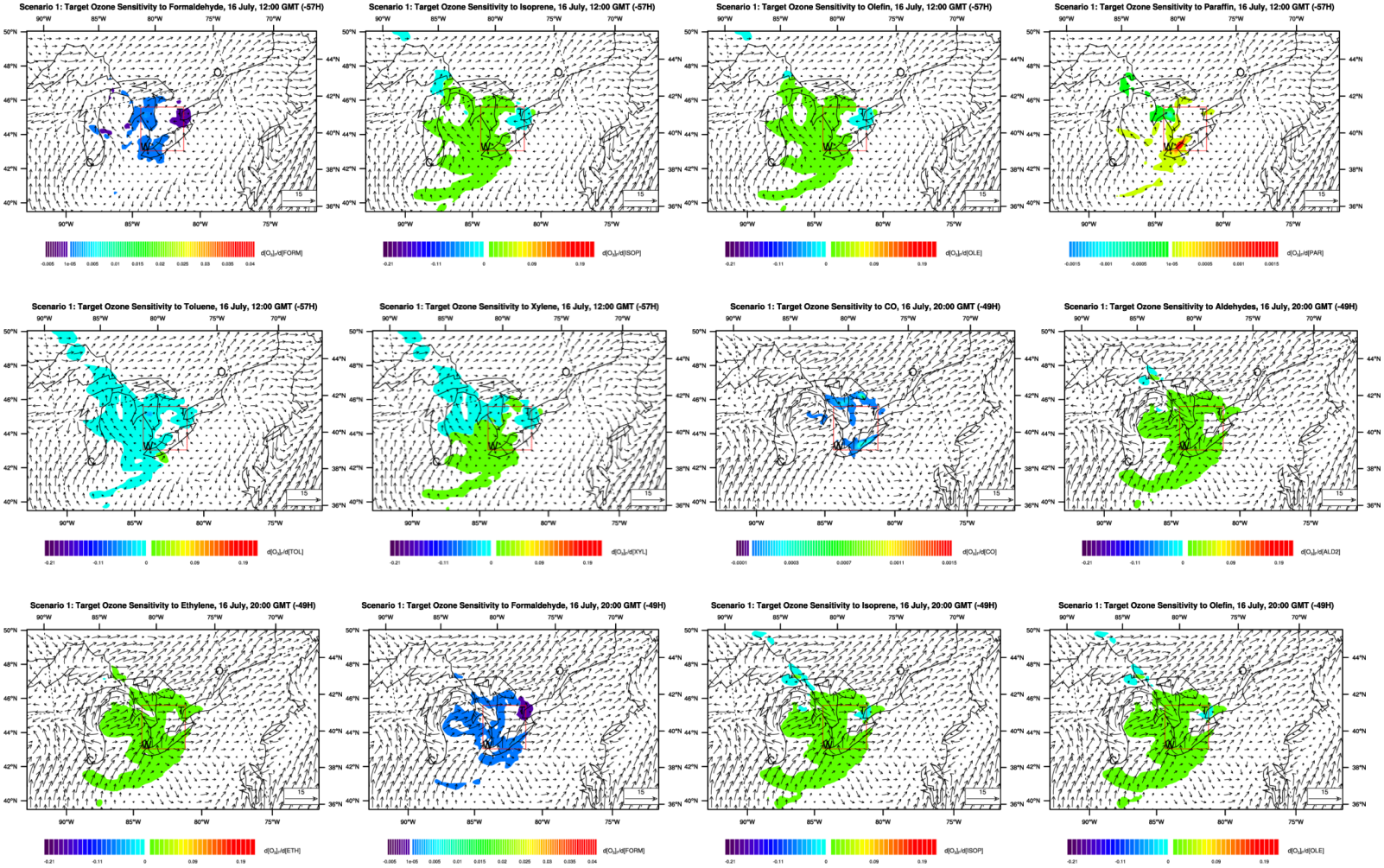
Scenario 1: Target Ozone Sensitivity to Formaldehyde, 16 July, 12:00 GMT (-57H)
Scenario 1: Target Ozone Sensitivity to Isoprene, 16 July, 12:00 GMT (-57H)
Scenario 1: Target Ozone Sensitivity to Olefin, 16 July, 12:00 GMT (-57H)
Scenario 1: Target Ozone Sensitivity to Paraffin, 16 July, 12:00 GMT (-57H)
Scenario 1: Target Ozone Sensitivity to Toluene, 16 July, 12:00 GMT (-57H)
Scenario 1: Target Ozone Sensitivity to Xylene, 16 July, 12:00 GMT (-57H)
Scenario 1: Target Ozone Sensitivity to CO, 16 July, 20:00 GMT (-49H)
Scenario 1: Target Ozone Sensitivity to Aldehydes, 16 July, 20:00 GMT (-49H)
Scenario 1: Target Ozone Sensitivity to Ethylene, 16 July, 20:00 GMT (-49H)
Scenario 1: Target Ozone Sensitivity to Formaldehyde, 16 July, 20:00 GMT (-49H)
Scenario 1: Target Ozone Sensitivity to Isoprene, 16 July, 20:00 GMT (-49H)
Scenario 1: Target Ozone Sensitivity to Olefin, 16 July, 20:00 GMT (-49H)

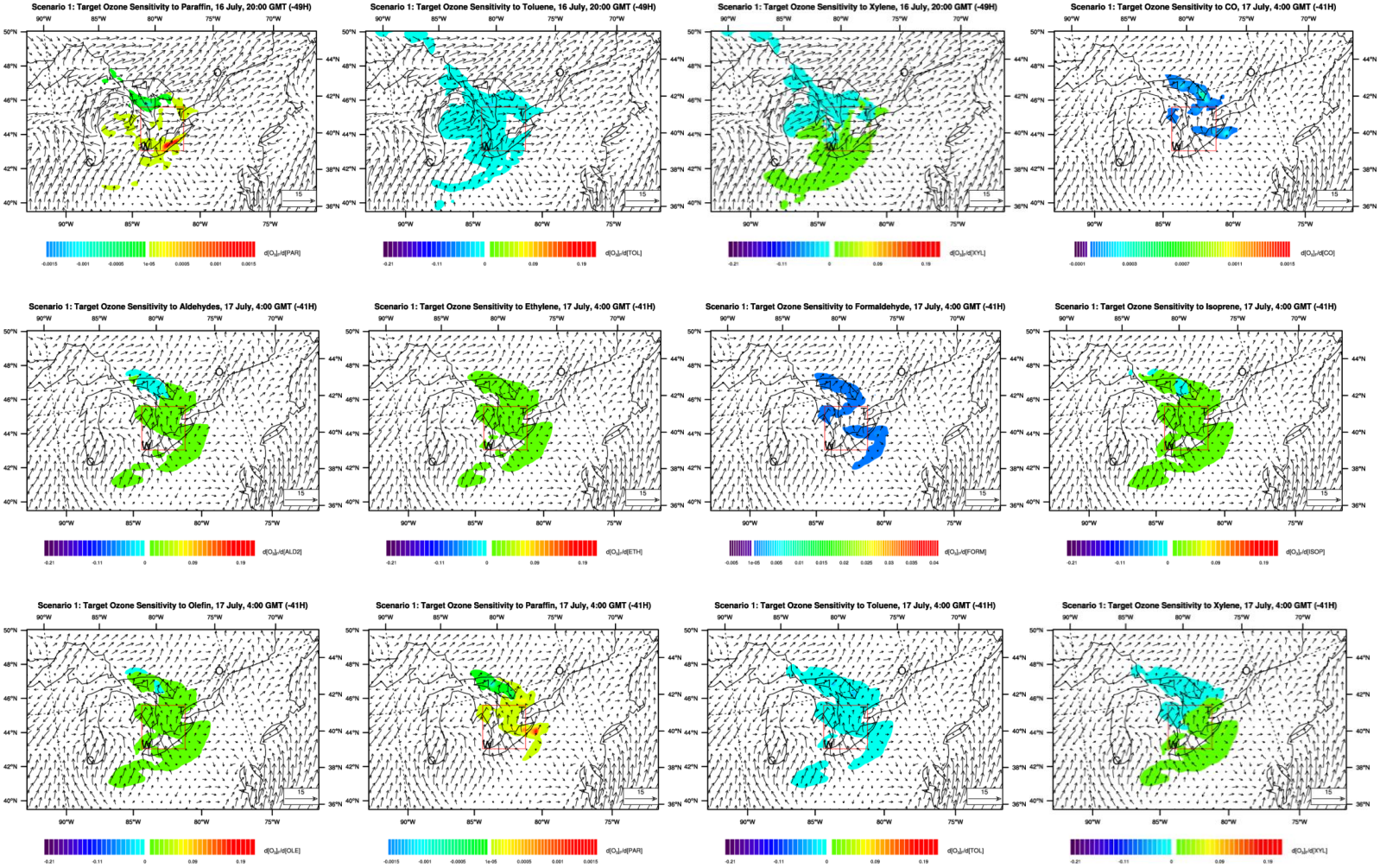
Scenario 1: Target Ozone Sensitivity to Paraffin, 16 July, 20:00 GMT (-49H)
Scenario 1: Target Ozone Sensitivity to Toluene, 16 July, 20:00 GMT (-49H)
Scenario 1: Target Ozone Sensitivity to Xylene, 16 July, 20:00 GMT (-49H)
Scenario 1: Target Ozone Sensitivity to CO, 17 July, 4:00 GMT (-41H)
Scenario 1: Target Ozone Sensitivity to Aldehydes, 17 July, 4:00 GMT (-41H)
Scenario 1: Target Ozone Sensitivity to Ethylene, 17 July, 4:00 GMT (-41H)
Scenario 1: Target Ozone Sensitivity to Formaldehyde, 17 July, 4:00 GMT (-41H)
Scenario 1: Target Ozone Sensitivity to Isoprene, 17 July, 4:00 GMT (-41H)
Scenario 1: Target Ozone Sensitivity to Olefin, 17 July, 4:00 GMT (-41H)
Scenario 1: Target Ozone Sensitivity to Paraffin, 17 July, 4:00 GMT (-41H)
Scenario 1: Target Ozone Sensitivity to Toluene, 17 July, 4:00 GMT (-41H)
Scenario 1: Target Ozone Sensitivity to Xylene, 17 July, 4:00 GMT (-41H)

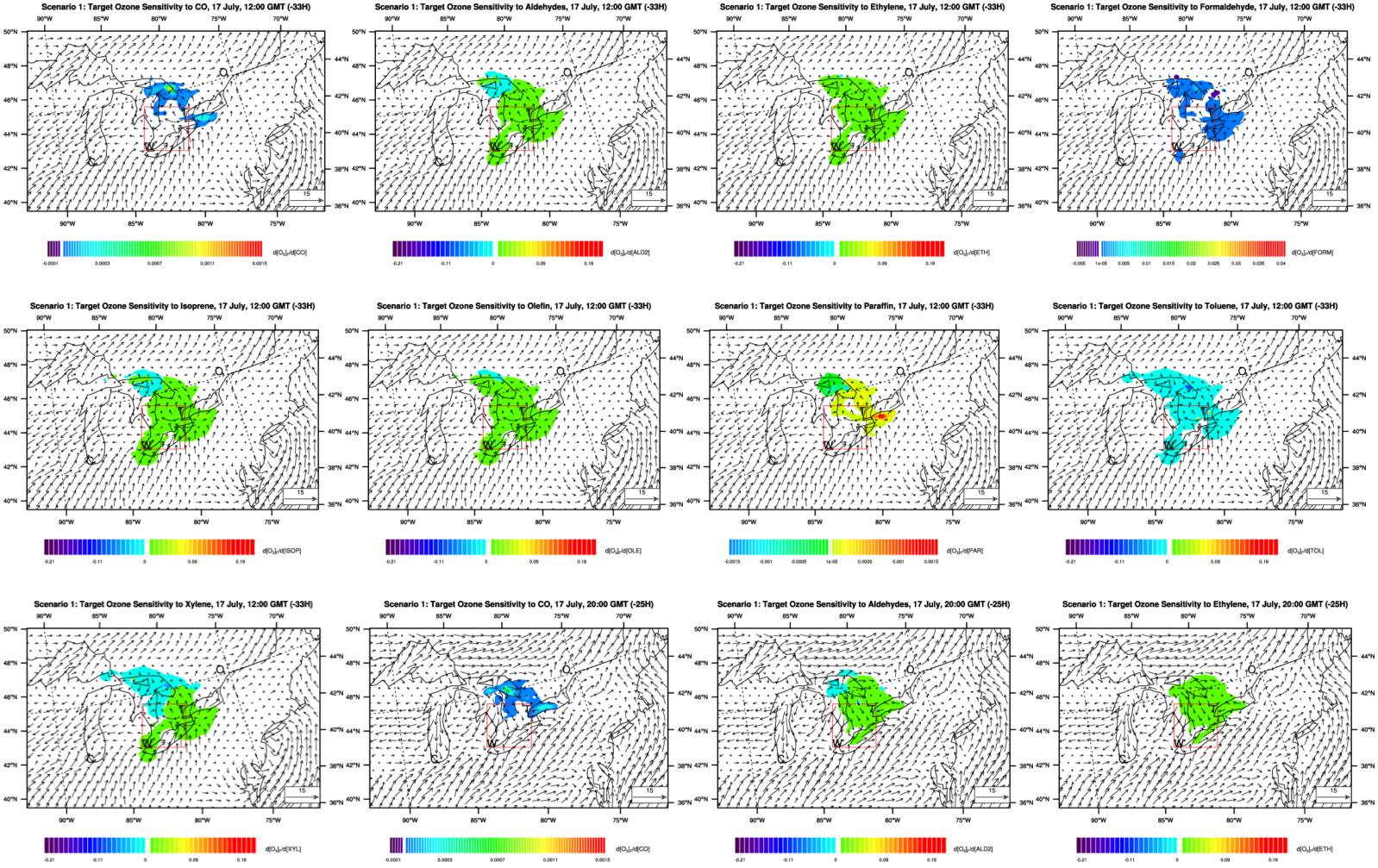
Scenario 1: Target Ozone Sensitivity to CO, 17 July, 12:00 GMT (-33H)
Scenario 1: Target Ozone Sensitivity to Aldehydes, 17 July, 12:00 GMT (-33H)
Scenario 1: Target Ozone Sensitivity to Ethylene, 17 July, 12:00 GMT (-33H)
Scenario 1: Target Ozone Sensitivity to Formaldehyde, 17 July, 12:00 GMT (-33H)
Scenario 1: Target Ozone Sensitivity to Isoprene, 17 July, 12:00 GMT (-33H)
Scenario 1: Target Ozone Sensitivity to Olefin, 17 July, 12:00 GMT (-33H)
Scenario 1: Target Ozone Sensitivity to Paraffin, 17 July, 12:00 GMT (-33H)
Scenario 1: Target Ozone Sensitivity to Toluene, 17 July, 12:00 GMT (-33H)
Scenario 1: Target Ozone Sensitivity to Xylene, 17 July, 12:00 GMT (-33H)
Scenario 1: Target Ozone Sensitivity to CO, 17 July, 20:00 GMT (-25H)
Scenario 1: Target Ozone Sensitivity to Aldehydes, 17 July, 20:00 GMT (-25H)
Scenario 1: Target Ozone Sensitivity to Ethylene, 17 July, 20:00 GMT (-25H)

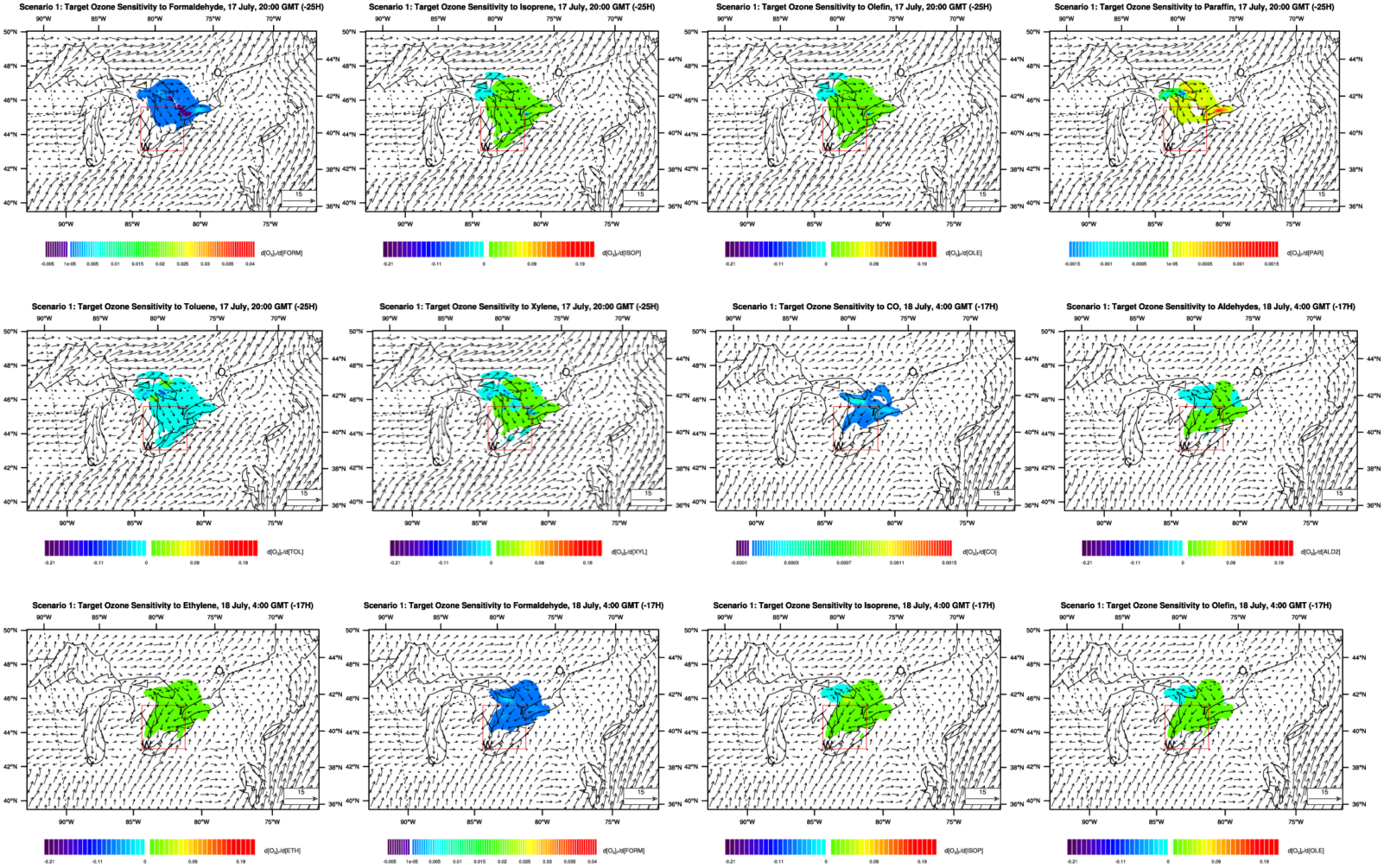
Scenario 1: Target Ozone Sensitivity to Formaldehyde, 17 July, 20:00 GMT (-25H)
Scenario 1: Target Ozone Sensitivity to Isoprene, 17 July, 20:00 GMT (-25H)
Scenario 1: Target Ozone Sensitivity to Olefin, 17 July, 20:00 GMT (-25H)
Scenario 1: Target Ozone Sensitivity to Paraffin, 17 July, 20:00 GMT (-25H)
Scenario 1: Target Ozone Sensitivity to Toluene, 17 July, 20:00 GMT (-25H)
Scenario 1: Target Ozone Sensitivity to Xylene, 17 July, 20:00 GMT (-25H)
Scenario 1: Target Ozone Sensitivity to CO, 18 July, 4:00 GMT (-17H)
Scenario 1: Target Ozone Sensitivity to Aldehydes, 18 July, 4:00 GMT (-17H)
Scenario 1: Target Ozone Sensitivity to Ethylene, 18 July, 4:00 GMT (-17H)
Scenario 1: Target Ozone Sensitivity to Formaldehyde, 18 July, 4:00 GMT (-17H)
Scenario 1: Target Ozone Sensitivity to Isoprene, 18 July, 4:00 GMT (-17H)
Scenario 1: Target Ozone Sensitivity to Olefin, 18 July, 4:00 GMT (-17H)

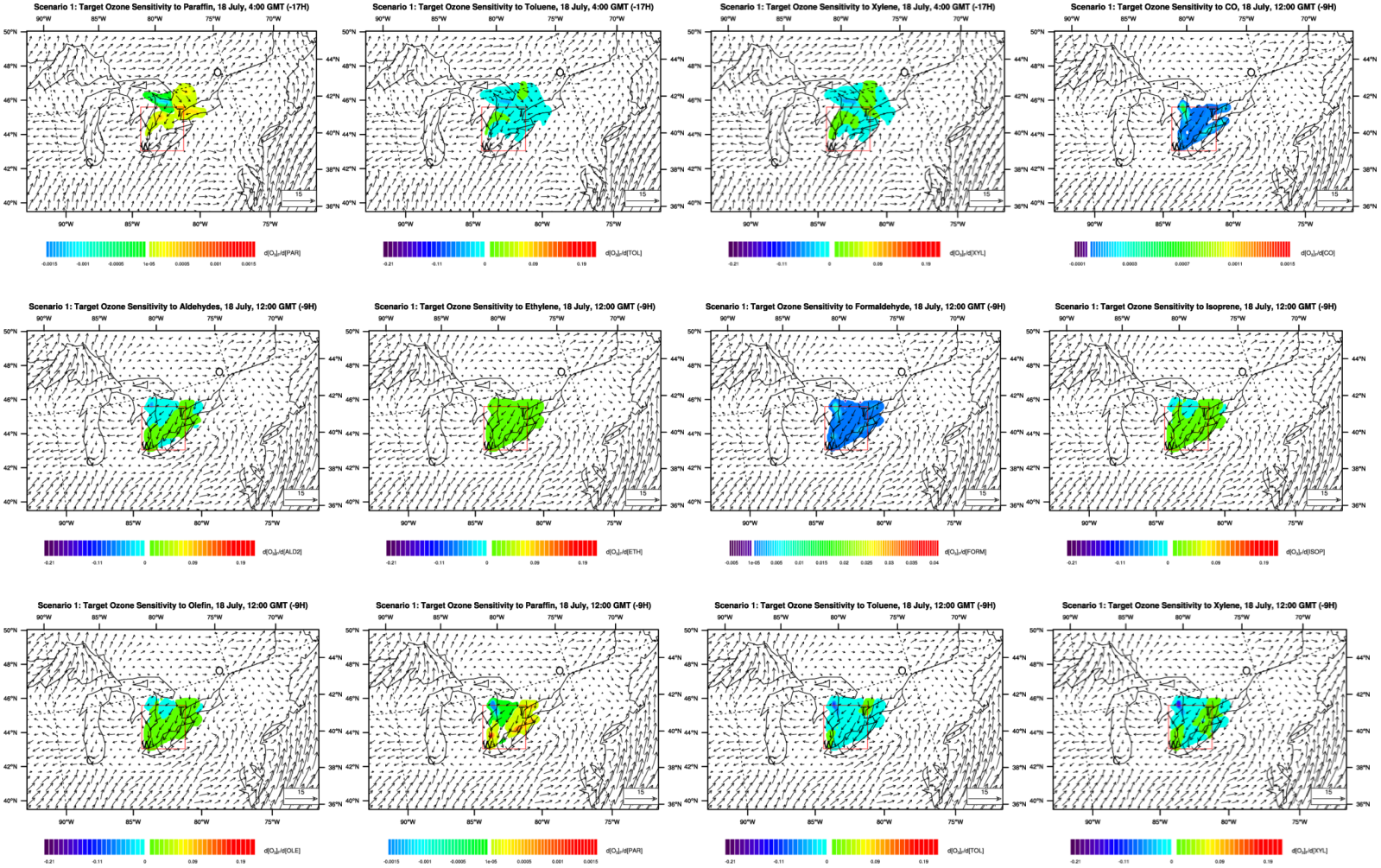
Scenario 1: Target Ozone Sensitivity to Paraffin, 18 July, 4:00 GMT (-17H)
Scenario 1: Target Ozone Sensitivity to Toluene, 18 July, 4:00 GMT (-17H)
Scenario 1: Target Ozone Sensitivity to Xylene, 18 July, 4:00 GMT (-17H)
Scenario 1: Target Ozone Sensitivity to CO, 18 July, 12:00 GMT (-9H)
Scenario 1: Target Ozone Sensitivity to Aldehydes, 18 July, 12:00 GMT (-9H)
Scenario 1: Target Ozone Sensitivity to Ethylene, 18 July, 12:00 GMT (-9H)
Scenario 1: Target Ozone Sensitivity to Formaldehyde, 18 July, 12:00 GMT (-9H)
Scenario 1: Target Ozone Sensitivity to Isoprene, 18 July, 12:00 GMT (-9H)
Scenario 1: Target Ozone Sensitivity to Olefin, 18 July, 12:00 GMT (-9H)
Scenario 1: Target Ozone Sensitivity to Paraffin, 18 July, 12:00 GMT (-9H)
Scenario 1: Target Ozone Sensitivity to Toluene, 18 July, 12:00 GMT (-9H)
Scenario 1: Target Ozone Sensitivity to Xylene, 18 July, 12:00 GMT (-9H)

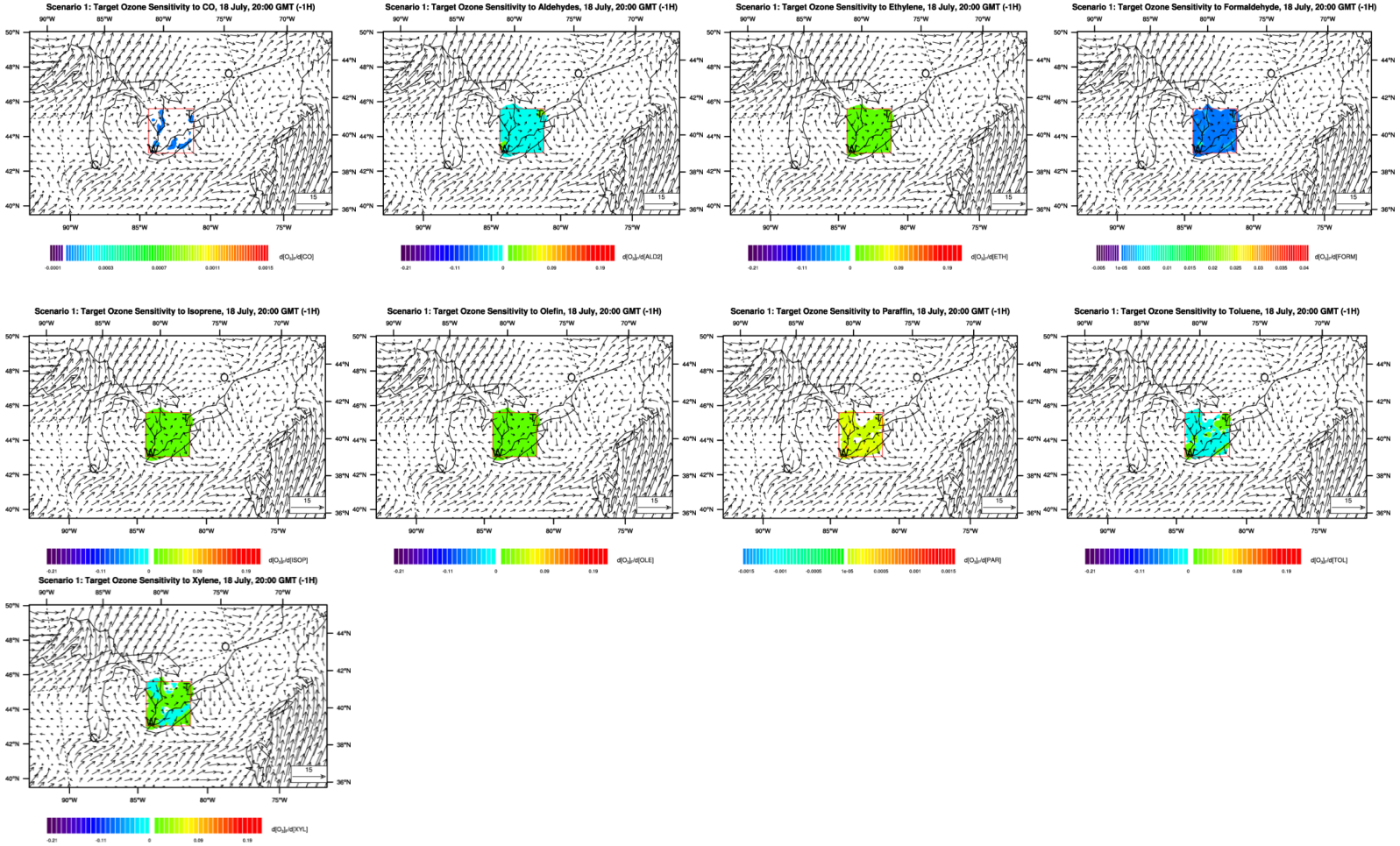

Figure 23. Scenario 1: target ozone sensitivity to CO and 8 kinds VOCs in the 69 hours before the assumed high ozone episode in the W-T region at 21:00 GMT July 18. Plots are presented every 8 hours. The 8 VOCs are aldehyde, formaldehyde, ethylene, isoprene, oflefin, paraffins, toluene, and ethylene. White colour represents sensitivity values between -0.00001 ppm/ppm and +0.00001 ppm/ppm. The vectors are horizontal winds calculated by MM5, in m/s.

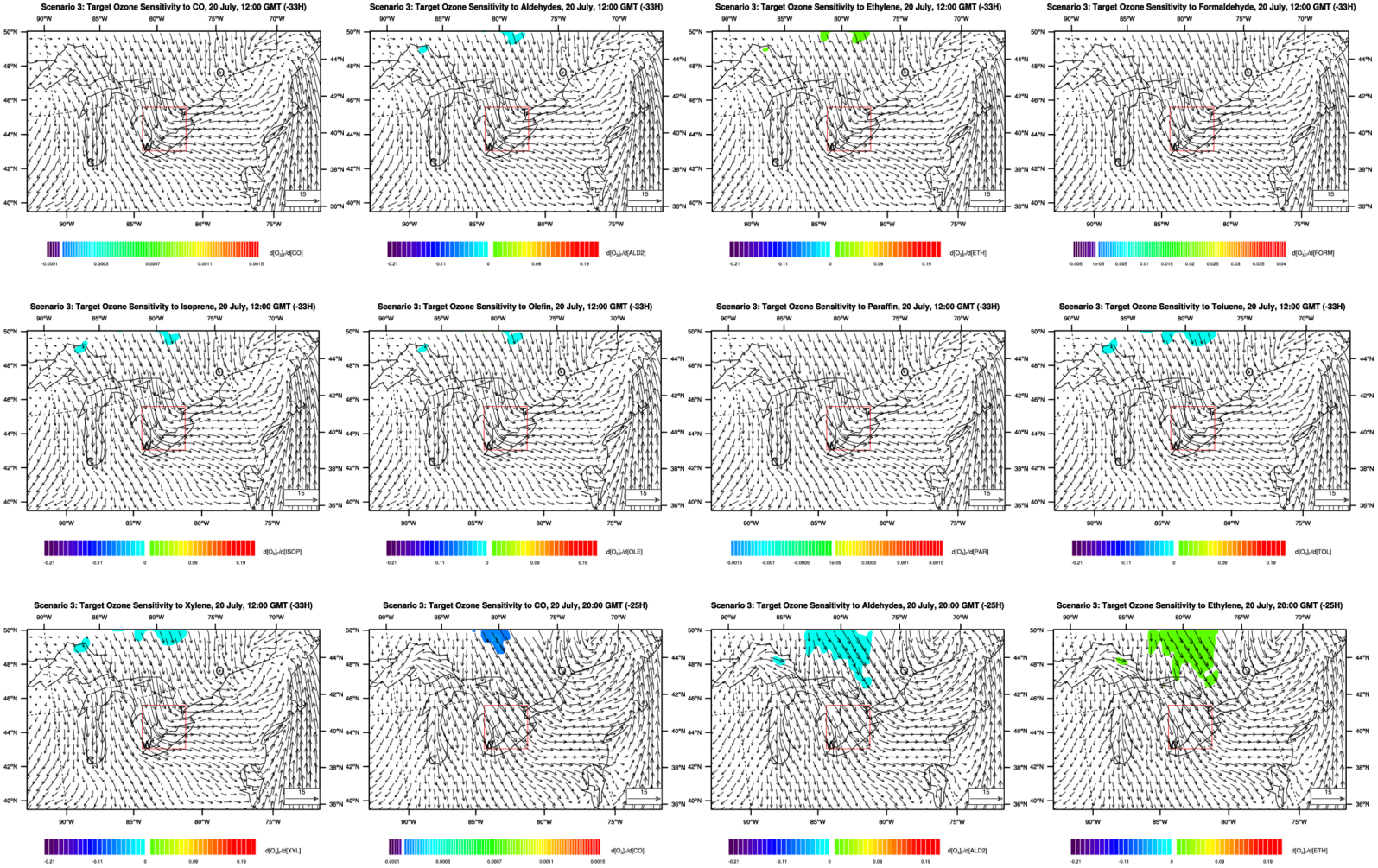
Scenario 3: Target Ozone Sensitivity to CO, 20 July, 12:00 GMT (-33H)
Scenario 3: Target Ozone Sensitivity to Aldehydes, 20 July, 12:00 GMT (-33H)
Scenario 3: Target Ozone Sensitivity to Ethylene, 20 July, 12:00 GMT (-33H)
Scenario 3: Target Ozone Sensitivity to Formaldehyde, 20 July, 12:00 GMT (-33H)
Scenario 3: Target Ozone Sensitivity to Isoprene, 20 July, 12:00 GMT (-33H)
Scenario 3: Target Ozone Sensitivity to Olefin, 20 July, 12:00 GMT (-33H)
Scenario 3: Target Ozone Sensitivity to Paraffin, 20 July, 12:00 GMT (-33H)
Scenario 3: Target Ozone Sensitivity to Toluene, 20 July, 12:00 GMT (-33H)
Scenario 3: Target Ozone Sensitivity to Xylene, 20 July, 12:00 GMT (-33H)
Scenario 3: Target Ozone Sensitivity to CO, 20 July, 20:00 GMT (-25H)
Scenario 3: Target Ozone Sensitivity to Aldehydes, 20 July, 20:00 GMT (-25H)
Scenario 3: Target Ozone Sensitivity to Ethylene, 20 July, 20:00 GMT (-25H)

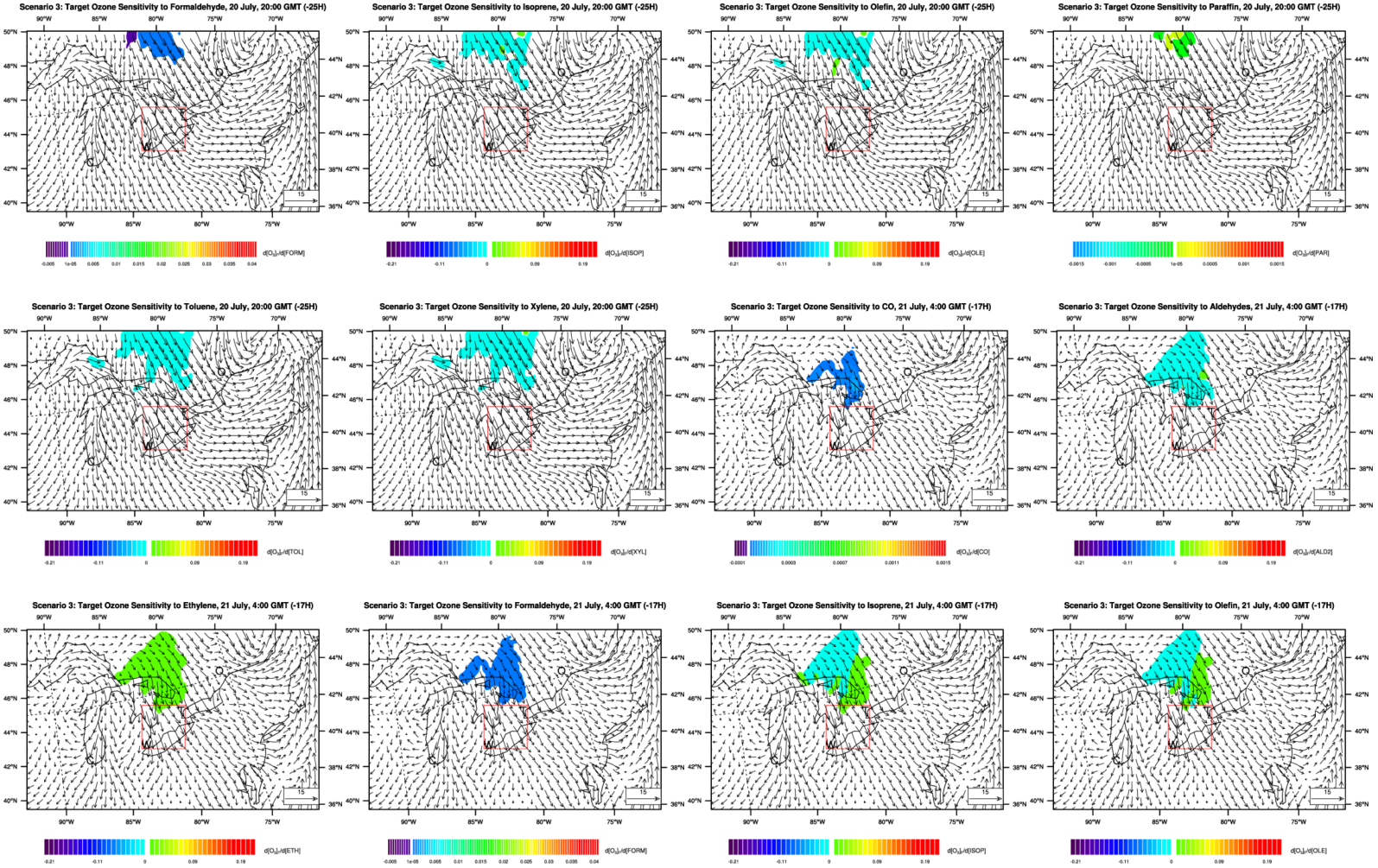
Scenario 3: Target Ozone Sensitivity to Formaldehyde, 20 July, 20:00 GMT (-25H)
Scenario 3: Target Ozone Sensitivity to Isoprene, 20 July, 20:00 GMT (-25H)
Scenario 3: Target Ozone Sensitivity to Olefin, 20 July, 20:00 GMT (-25H)
Scenario 3: Target Ozone Sensitivity to Paraffin, 20 July, 20:00 GMT (-25H)
Scenario 3: Target Ozone Sensitivity to Toluene, 20 July, 20:00 GMT (-25H)
Scenario 3: Target Ozone Sensitivity to Xylene, 20 July, 20:00 GMT (-25H)
Scenario 3: Target Ozone Sensitivity to CO, 21 July, 4:00 GMT (-17H)
Scenario 3: Target Ozone Sensitivity to Aldehydes, 21 July, 4:00 GMT (-17H)
Scenario 3: Target Ozone Sensitivity to Ethylene, 21 July, 4:00 GMT (-17H)
Scenario 3: Target Ozone Sensitivity to Formaldehyde, 21 July, 4:00 GMT (-17H)
Scenario 3: Target Ozone Sensitivity to Isoprene, 21 July, 4:00 GMT (-17H)
Scenario 3: Target Ozone Sensitivity to Olefin, 21 July, 4:00 GMT (-17H)

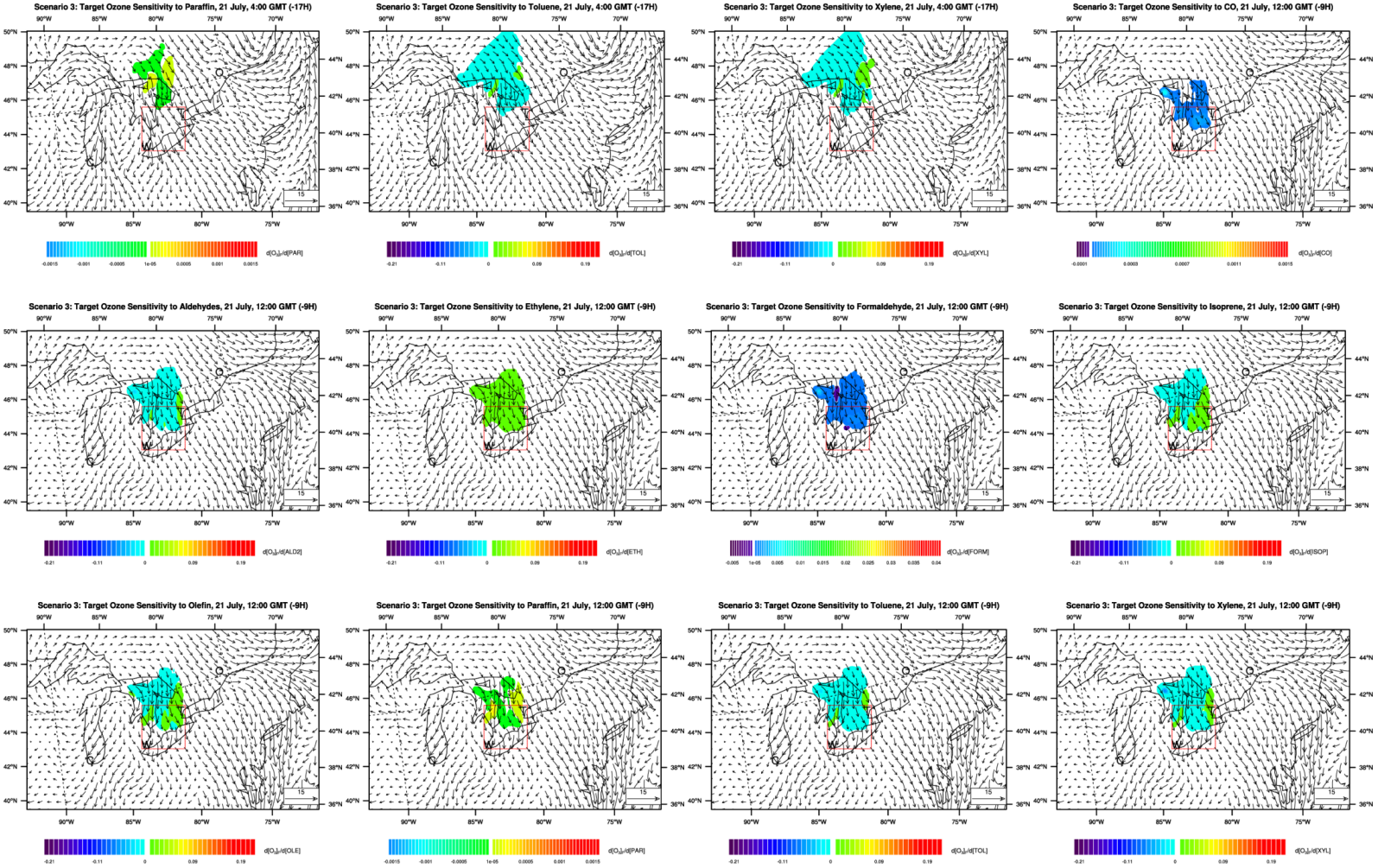
Scenario 3: Target Ozone Sensitivity to Paraffin, 21 July, 4:00 GMT (-17H)
Scenario 3: Target Ozone Sensitivity to Toluene, 21 July, 4:00 GMT (-17H)
Scenario 3: Target Ozone Sensitivity to Xylene, 21 July, 4:00 GMT (-17H)
Scenario 3: Target Ozone Sensitivity to CO, 21 July, 12:00 GMT (-9H)
Scenario 3: Target Ozone Sensitivity to Aldehydes, 21 July, 12:00 GMT (-9H)
Scenario 3: Target Ozone Sensitivity to Ethylene, 21 July, 12:00 GMT (-9H)
Scenario 3: Target Ozone Sensitivity to Formaldehyde, 21 July, 12:00 GMT (-9H)
Scenario 3: Target Ozone Sensitivity to Isoprene, 21 July, 12:00 GMT (-9H)
Scenario 3: Target Ozone Sensitivity to Olefin, 21 July, 12:00 GMT (-9H)
Scenario 3: Target Ozone Sensitivity to Paraffin, 21 July, 12:00 GMT (-9H)
Scenario 3: Target Ozone Sensitivity to Toluene, 21 July, 12:00 GMT (-9H)
Scenario 3: Target Ozone Sensitivity to Xylene, 21 July, 12:00 GMT (-9H)

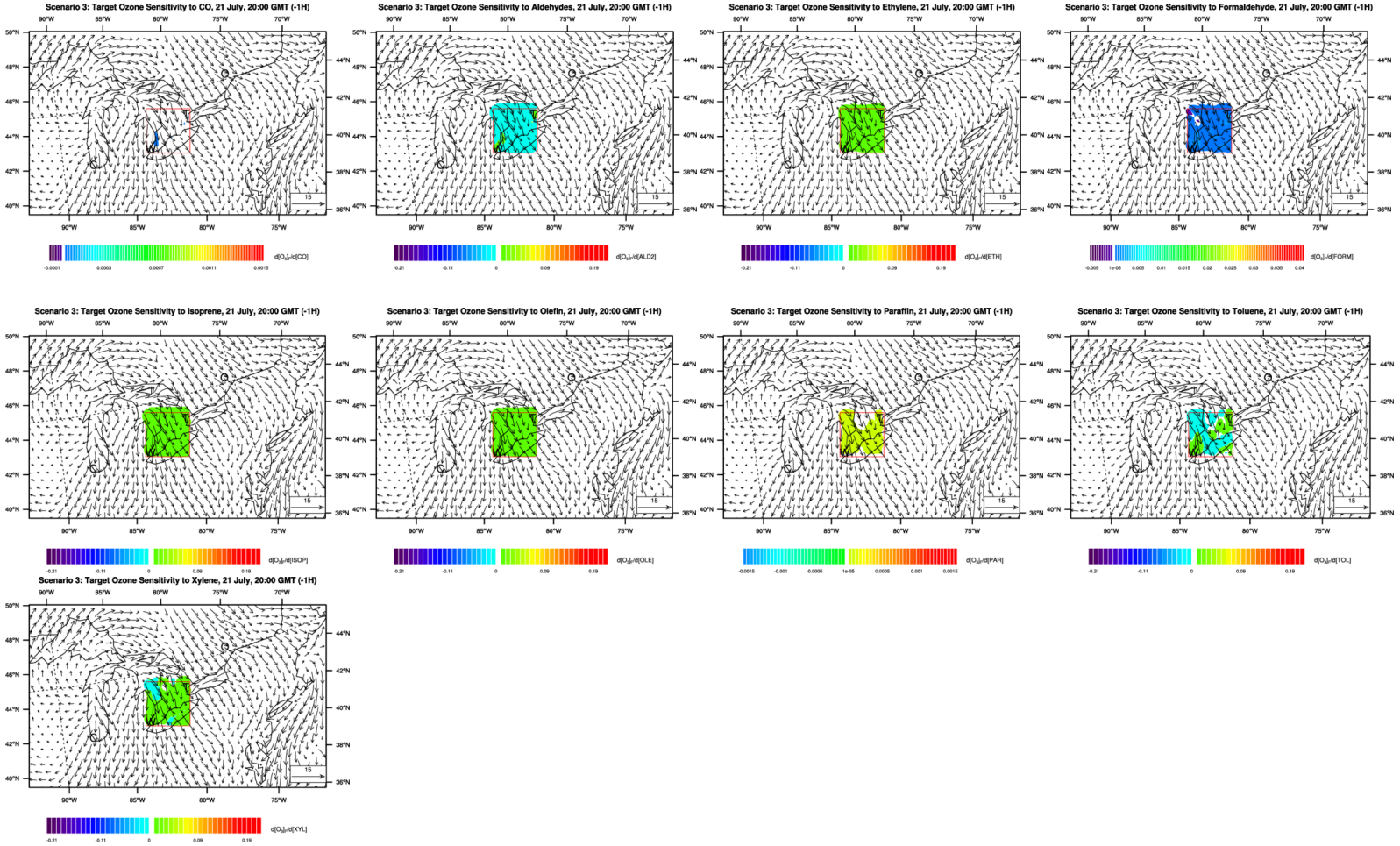

Figure 24. Scenario 3: target ozone sensitivity to CO and 8 kinds VOCs in the 69 hours before the assumed high ozone episode in the W-T region at 21:00 GMT July 21. Plots are presented every 8 hours. The 8 VOCs are aldehyde, formaldehyde, ethylene, isoprene, oflefin, paraffins, toluene, and ethylene. White colour represents sensitivity values between -0.00001 ppm/ppm and +0.00001 ppm/ppm. The vectors are horizontal winds calculated by MM5, in m/s.

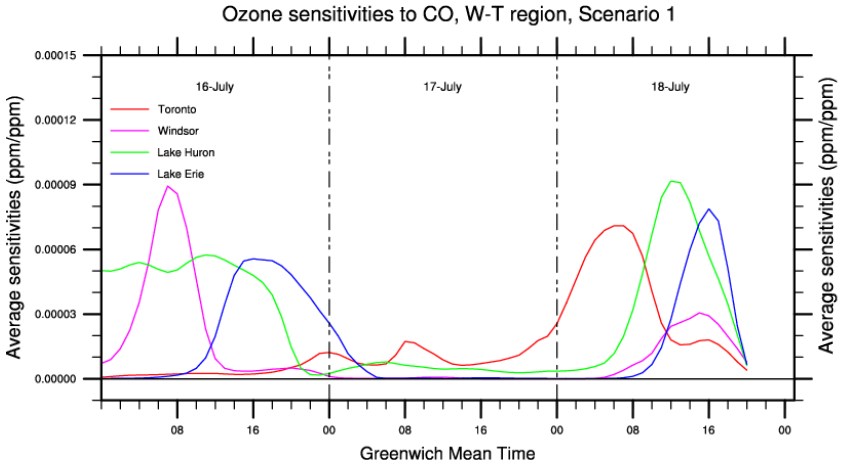
Ozone sensitivities to CO, W-T region, Scenario 1
Average sensitivities (ppm/ppm)
0.00015
0.00012
0.00009
0.00006
0.00003
0.00000
16-July
17-July
18-July
Toronto
Windsor
Lake Huron
Lake Erie
08
16
00
Greenwich Mean Time

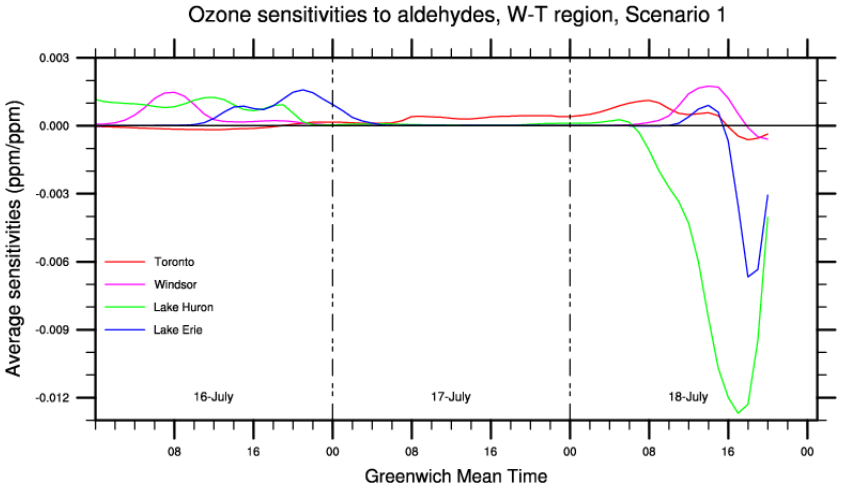
Ozone sensitivities to aldehydes, W-T region, Scenario 1
Average sensitivities (ppm/ppm)
0.003
0.000
-0.003
-0.006
-0.009
-0.012
Toronto
Windsor
Lake Huron
Lake Erie
16-July
17-July
18-July
08
16
00
Greenwich Mean Time

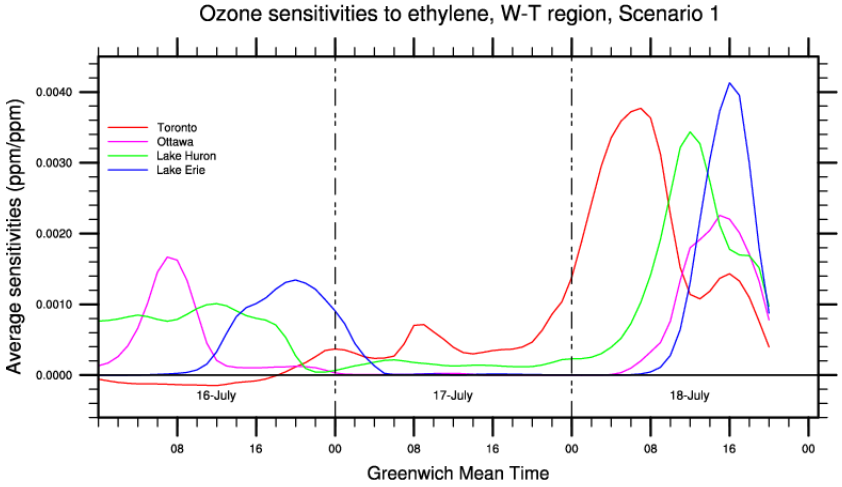
Ozone sensitivities to ethylene, W-T region, Scenario 1
Average sensitivities (ppm/ppm)
0.0040
0.0030
0.0020
0.0010
0.0000
Toronto
Ottawa
Lake Huron
Lake Erie
16-July
17-July
18-July
08
16
00
Greenwich Mean Time

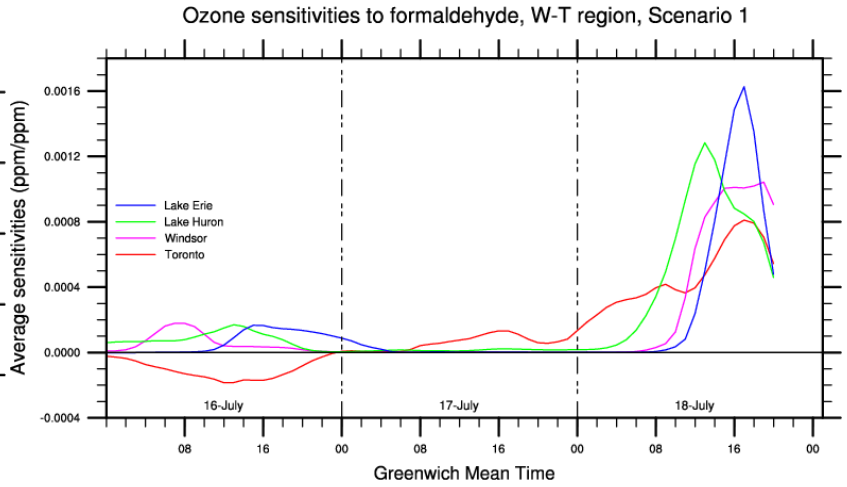
Ozone sensitivities to formaldehyde, W-T region, Scenario 1
Average sensitivities (ppm/ppm)
0.0016
0.0012
0.0008
0.0004
0.0000
-0.0004
Lake Erie
Lake Huron
Windsor
Toronto
16-July
17-July
18-July
08
16
00
Greenwich Mean Time

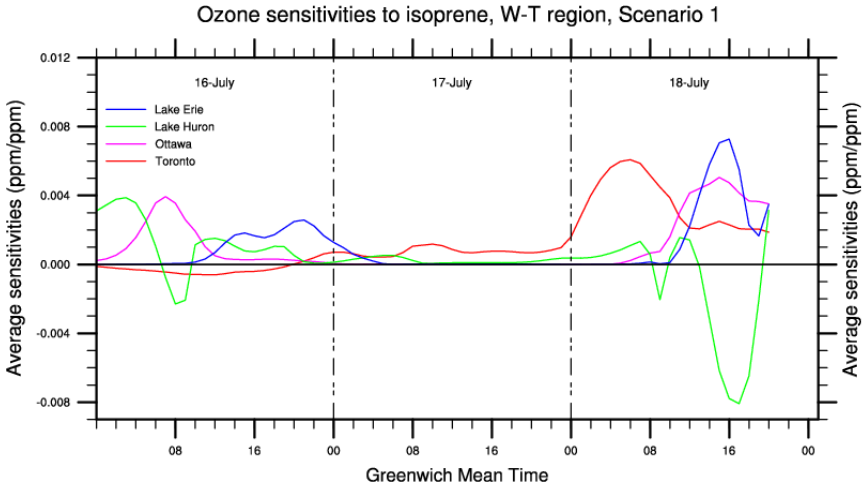
Ozone sensitivities to isoprene, W-T region, Scenario 1
Average sensitivities (ppm/ppm)
0.012
0.008
0.004
0.000
-0.004
-0.008
16-July
17-July
18-July
Lake Erie
Lake Huron
Ottawa
Toronto
08
16
00
Greenwich Mean Time

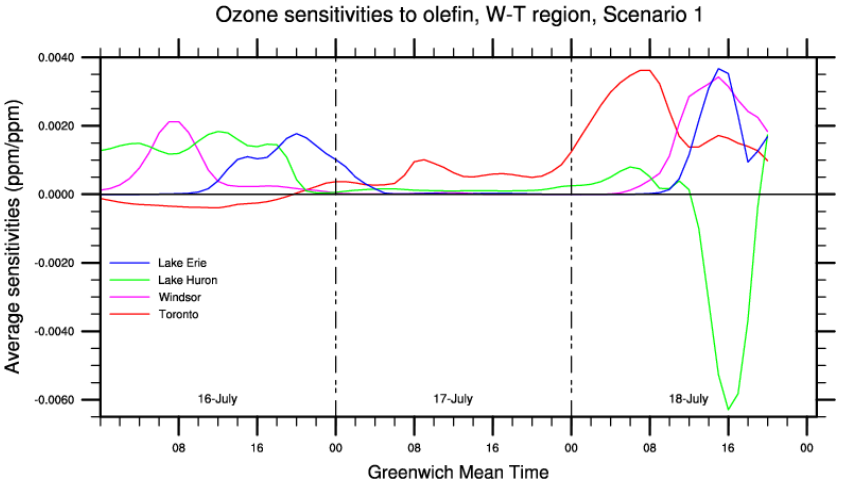
Ozone sensitivities to olefin, W-T region, Scenario 1
Average sensitivities (ppm/ppm)
0.0040
0.0020
0.0000
-0.0020
-0.0040
-0.0060
Lake Erie
Lake Huron
Windsor
Toronto
16-July
17-July
18-July
08
16
00
Greenwich Mean Time

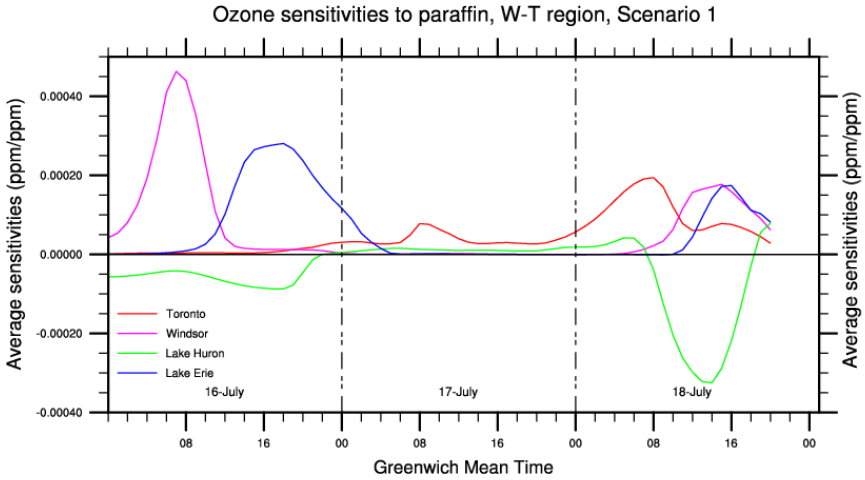
Ozone sensitivities to paraffin, W-T region, Scenario 1
Average sensitivities (ppm/ppm)
0.00040
0.00020
0.00000
-0.00020
-0.00040
Toronto
Windsor
Lake Huron
Lake Erie
16-July
17-July
18-July
08
16
00
Greenwich Mean Time

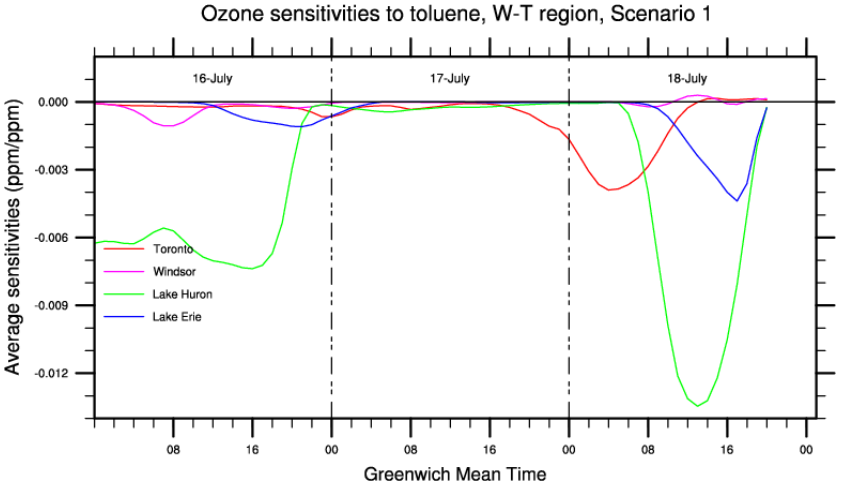
Ozone sensitivities to toluene, W-T region, Scenario 1
Average sensitivities (ppm/ppm)
0.000
-0.003
-0.006
-0.009
-0.012
16-July
17-July
18-July
Toronto
Windsor
Lake Huron
Lake Erie
08
16
00
Greenwich Mean Time

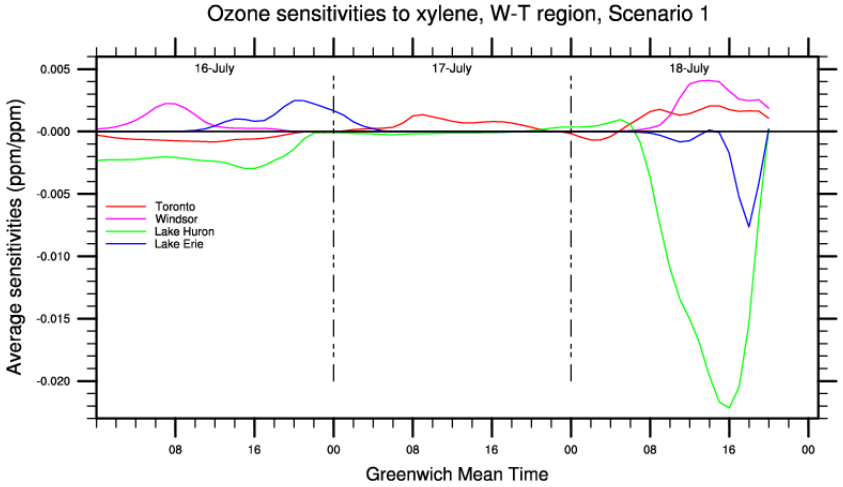

Figure 25. Time series of the average ozone sensitivity to CO and 8 VOC changes in 4 sub-regions of the Windsor-Toronto region for Scenario 1. The 4 local regions are Toronto, Windsor, southern part of Lake Huron, and middle Lake Erie.

Table 4. How a morning release of CO or VOCs enhances (+) or suppresses (-) local ozone formation at 17:00 local time in the 4 sub-regions of southwestern Ontario in Scenario 1.

	CO	Aldehyde	Ethylene	Formaldehyde	Isoprene	Olefins	Paraffins	Toluene	Xylene
Toronto	+	+	+	+	+	+	+	+	+
Windsor	+	+	+	+	+	+	+	+	+
Lake Huron	+	-	+	+	-	-	-	-	-
Lake Erie	+	+	+	+	+	+	+	-	-

5.3.2.4 Summary

The modified CMAQ-ADJ works effectively in the double-nested research domain. No manual interference is needed for the communication of the checkpointed data with the sub-processes of the model in high resolution simulations. This shows that replacing the fixed sync time-step in the original CMAQ-ADJ with the time-varying sync time-step that is determined by the model's algorithm has been successfully implemented. The evolution of the sensitivity fields with large-scale horizontal winds and lake breezes has a close relationship with the underlying surface features such as land, lakes, and large cities. This suggests that the horizontal winds in the current meteorological interface are correct. The transport processes of the modified CMAQ-ADJ are able to determine the locations of all the sensitivity values. The fact that the model captures the strong contrast between ozone sensitivity on land, major water bodies, and urban areas shows that the chemistry time-step has been treated correctly in the modified CMAQ-ADJ.

The modified CMAQ-ADJ is used to study the sensitivity of ozone in southern Ontario with respect to the pre-existing ozone and its major precursor species. The sensitivity runs show that compared with former studies (reviewed in Section 2.1), one sensitivity run of the modified CMAQ-ADJ can obtain some results from several separate forward sensitivity researches conducted in this region (Brankov et al., 2003; Fast and Heilman, 2005; Galvez, 2007; Geddes et al., 2009; Johnson et al., 2007; Yap et al., 1988). More important issues can be revealed by further analysis of the simulated results by the modified CMAQ-ADJ.

Under the typical meteorological conditions in southern Ontario in Scenario 1 and Scenario 2, large influencing region of NOx and VOCs are detected in the upwind direction from the W-T receptor. The influencing area can extend from the northern side to the southern side of the research Domain in the beginning of the simulation period. Although the northern areas have influence on the ozone level in southwestern Ontario, the lack of anthropogenic emissions in these regions leaves the biogenic VOCs (isoprene in this model) an important source of ozone depletion in southwestern Ontario. The negative ozone sensitivity to isoprene shows that increased isoprene in the north decreases the ozone level in southwestern Ontario in the next 2 days to 69 hours. The non-zero sensitivity in the upwind southern area make the transport of pollutants from the Midwest U.S. and Ohio Valley an important issue for the ozone pollution in southwestern Ontario. An increase in the emission of all the VOCs except toluene in the Midwest U.S. and Ohio Valley enhances the ozone formation in southwestern Ontario during the next 24 to 69 hours. Ozone concentrations in southwestern Ontario can also be enhanced by the increased ozone concentration in this industrialized U.S. area (except in urban areas). An increase in the

ozone level in large urban areas such as Chicago and Detroit (Windsor) leads to decreased ozone level in the W-T region due to the titration of the ozone precursor NOx. The lake breezes caused by the characteristic land/water geography in Great Lakes region makes the pollutant recycle near lakes. Pollutants in the W-T region influence the ozone level in the same region after 69 hours owing to the local circulation. An increase in the ozone concentration over southern Lake Huron enhances the ozone level in southwestern Ontario after 69 hours, while increased ozone in Toronto can suppress the ozone level in southwestern Ontario in 69 hours. Increased NO in both of these areas enhances the local ozone formation in 69 hours.

As time approaches the outbreak of the assumed high ozone episode, the influencing region becomes closer to the receptor region and becomes local at the end of the simulation period. The average magnitude of the local sensitivity with respect to pre-existing ozone increases with time. NOx emission around noon has the largest impact on the ozone formation in the late afternoon of the same day. Morning release of CO and VOCs to urban areas where the VOC/NOx ratio is low always enhances the local ozone formation in the afternoon, with the largest magnitude appearing in the morning to noon, i.e., several hours before the assumed high ozone episode by late afternoon. Over southern Lake Huron area where the VOC/NOx ratio is large, increasing the emissions of the carbon compounds in the morning tends to suppress the local ozone formation in the afternoon, with the exceptions of CO, ethylene, and formaldehyde. A morning increase in CO, ethylene, and formaldehyde emissions always enhances the ozone formation over central Lake Erie by the late afternoon.

In Scenarios 1 and 2, pollutants over lakes have larger contributions to the ozone level change in the W-T region than those over the surrounding land areas at almost all times. This conclusion can also be drawn based on results in Scenario 3. Among all species, NO has the largest impact on the ozone in the W-T receptor, which is several times larger than the impact of the pre-existing ozone and most VOCs. Among all the species examined, CO has the smallest contribution to ozone pollution in southern Ontario, but its sensitivity is always positive. The influence of paraffins on the southwestern Ontario ozone is also small. The emitted CO in the non-zero sensitivity areas of CO always enhances the ozone formation in southwestern Ontario, but the small sensitivity makes CO very unlikely to become the main reason for ozone increase in southwestern Ontario. The average ozone sensitivity to different species over the four sub-regions has shown that more VOCs is transformed to ozone in higher temperature conditions than in lower temperature conditions, which is due to the reactions of these VOCs is temperature-dependent. The magnitude of the ozone sensitivity to pre-existing ozone and NOx does not change under different air temperature conditions.

5.3.3 Toronto-Ottawa region ozone sensitivities

5.3.3.1 Influence of pre-existing ozone

The Toronto-Ottawa (T-O) region is located in east-central Ontario. It is downwind of the Great Lakes region. In this section, three scenario runs are done using the modified CMAQ-ADJ to investigate how the pre-existing ozone influences the ozone levels in the T-O region at the target time.

In Scenario 1, a high ozone event is assumed to happen at 17:00 local afternoon of July 18. The ozone level in the T-O region is enhanced to 100 ppb everywhere in this receptor square. The CMAQ simulated ozone distributions at 21:00 GMT July 18 are used as the base ozone case. The difference between 100 ppb and the simulated ozone concentrations in the target T-O square is used as the input cost function of the modified CMAQ-ADJ. The gradients (sensitivities) of the cost function (ozone perturbation) with respect to model variables are calculated by only one model run.

Figure 26 shows the influence of the pre-existing ozone on the target ozone perturbation for every 2 hours in the simulation period. The sensitivity plotted in white colour are values from -10e-5 to +10e-5, which are so small that they are neglected in this study. The 0:00 GMT July 16 plot shows that 69 hours before the assumed high ozone episode, ozone from the northwest side of Lake Superior can eventually influence the ozone level in the T-O receptor region. As indicated by Errico (1997), a portion of the ozone in this non-zero sensitivity region will evolve with time in a similar pathway as the sensitivity fields and finally reach to the receptor region. The horizontal advection of this portion of ozone is due to the prevailing wind as shown by the wind vectors in Figure 26. Westerly wind can bring ozone from upwind regions to east-central Ontario along the northern side of the Great Lake Basin.

Until about two days before the outbreak of the assumed high ozone episode, the ozone sensitivity with respect to the pre-existing ozone in most areas of the T-O region is zero. This implies that if the ozone in this place is increased, the increased ozone does not remain for more than two days to influence the ozone level by then, but is transported to other places or is transformed into other species. The sensitivity at Toronto shows that increasing ozone in Toronto at earlier hours of the simulation time period suppresses the ozone level of the target square. The first four graphs in Figure 26 also show that large urban areas such as Chicago and Detroit (Windsor) have negative ozone sensitivity to the pre-existing ozone. In the NOx-rich urban areas, increased ozone can react with NO and only a part of it will be re-formed by NO_2/VOC reactions

later. As a consequence, the ozone precursor NO is reduced and hence less ozone will be produced than the case without those increased ozone. Similar to the results in Section 5.3.2.1, it is shown that under typical summer weather conditions, pre-existing ozone suppresses the ozone formation in 36 to 69 hours in the NOx-rich urban areas Toronto. When time approaches 21:00 GMT July 18, as shown in Figure 26, increasing ozone in the influencing regions can increase the ozone level in the T-O region by the target time.

From the beginning of the simulation period, the pre-existing ozone over Lake Superior shows a large influence on the target ozone perturbation due to low solubility of ozone, which is larger than that on the adjacent land area. The large ozone sensitivity center over the lake shifts to the east, in the same direction as the prevailing wind. It returns when reaching the eastern shore of the lake after 16:00 GMT July 16 with the wind blowing from the shore to the inner lake area. A larger portion of the pre-existing ozone that is trapped over the lake areas can be eventually transported to the target square than the ozone over the adjacent land areas of the same time. By 14:00 GMT July 17, the lake breeze effect is replaced by a strong southwest wind. The large positive ozone sensitivity center moves to the land. There are also more ozone scavenging mechanisms such as the uptake of ozone by vegetation or other materials over land area. As a consequence, the magnitude of the ozone sensitivity gradually decreases. It disappears by 0:00 GMT July 18.

During the first two days of the research period, another large ozone sensitivity center develops over southern part of Lake Huron and evolves over Lake Huron and Georgian Bay followed the wind vectors (Figure 26). Later, the largest sensitivity in the northern part of non-zero sensitivity fields moves to land and enters the T-O region. During this process, the magnitude of the sensitivity decreases. The sensitivity has also shown larger values over water bodies than over land.

The plots in Figure 26 show that there is a large positive sensitivity center associated with Lake Erie evolving from the northeast of Windsor. It enters Lake Erie by 12:00 GMT July 16 and gets enhanced over the water body. This center weakens when moving away from Lake Erie by 05:00 GMT July 17, but strengthens again when moving towards Lake Ontario. A combination of the effects of both lake breeze and large weather system causes this center to circulate around Lake Ontario. During the process it moves from the inner T-O region back to Lake Ontario, the magnitude is enhanced to its largest value about 4 hours before the high ozone event. The largest value then decreases, but the overall magnitude of sensitivity in the area increases. Observational data have shown that in southern Ontario, very rapid increases in ozone, NO, and hydrocarbons can occur simultaneously with the arrival of a Lake Ontario lake breeze

(Hastie et al., 1999). During the last 4 hours before the target time, the area of the large sensitivity values over Lake Ontario enlarges. The magnitude of the sensitivity over land also increases. By one hour before the assumed high ozone episode in the T-O region at 21:00 GMT July 18, it can be seen from the last graph (-1H) of Figure 26 that ozone sensitivity at several places on land have become much larger than the sensitivity of the same place one hour earlier. The reason for this relates to the relatively large emissions of VOCs (Figure 27 (a)) at these places in the large VOC/NOx ratio region (Figure 10). Increasing ozone in the research region around one hour before the high ozone episode, the following reactions happen everywhere:

$$\mathbf{O_3 + h\gamma \xrightarrow{\lambda<330\,nm} O + O_2} \quad 5\text{-}3$$

$$\mathbf{H_2O + O \rightarrow OH + OH} \quad 5\text{-}4$$

In those places with more VOCs, more peroxy radical RO_2 can be generated to cause the formation of more ozone through reactions 5-7 to 5-10.

$$\mathbf{VOC + OH \xrightarrow{O_2} RO_2 + H_2O} \quad 5\text{-}5$$

$$\mathbf{RO_2 + NO \xrightarrow{O_2} secondary\ VOC + HO_2 + NO_2} \quad 5\text{-}6$$

$$\mathbf{NO_2 + h\gamma \rightarrow NO + O} \quad 5\text{-}7$$

$$\mathbf{O + O_2 + M \rightarrow O_3 + M} \quad 5\text{-}8$$

The T-O receptor region is divided into four sub-regions to examine the influence of the pre-existing ozone in the local areas. The four sub-regions are Toronto, Ottawa, north land area (North Land), and Lake Ontario (Figure 30). Figure 31 (a) shows the evolution of the average ozone sensitivity in these four sub-regions during the simulation period. The lake region shows the largest positive sensitivity at all times due to a low solubility of ozone over waters. The ozone influence in the north land area where there is large VOC/NOx ratio is also large. Increasing ozone in urban areas can decrease the ozone level in the T-O receptor in 69 hours. The recent increase in ozone can enhance the local ozone level of the same day. As time approaches the outbreak time of the assumed high ozone episode, any newly added ozone has larger contribution than that added earlier to the assumed high ozone episode in the late afternoon of July 18 because more of it ends in the target square.

In Scenario 2, a uniform ozone perturbation of 40 ppb is assigned to the CMAQ-simulated ozone distribution in all grid cells in the Toronto-Ottawa region (east-central Ontario) at 21:00 GMT July 18 to assume a high ozone event. The modified CMAQ-ADJ is run between 0:00

GMT July 16 2007 and 21:00 GMT July 18 to calculate the gradient of the ozone perturbation with respect to all model variables. The ozone sensitivity with respect to the pre-existing ozone is shown in

Figure 28. The overall evolution of the sensitivity fields with time is very similar to that in Scenario 1. The pre-existing ozone at the northwest corner of the research domain can influence the ozone level in east-central Ontario from 2 days to 69 hours prior to target time. Aportion of the increased ozone in this region can be transported to the T-O receptor region to enhance the ozone level there. During the entire simulation period, the sensitivity over lakes is always larger than that in the surrounding land area, which suggests that if the same amount of ozone is assigned to multiple places, those over a major water body will have a larger potential to enhance the ozone level in the T-O region.

As time approaches the outbreak of the assumed high ozone episode, distant regions become too far away to influence the T-O region. Ozone there does not have enough time to be transported to the T-O region and take part in the high ozone event by 21:00 GMT on July 18. Meanwhile, the magnitude of the sensitivity in the influencing region becomes larger over both land and water bodies. The largest values are over Lake Ontario around noon, 4 to 6 hours before the occurrence of the high ozone event at 17:00 local time on July 18.

About one and a half days before the assumed high ozone event, as shown by the plots before the -37H graph in

Figure 28, the urban areas that have very large NOx emission such as Toronto have negative influence on the ozone level in the T-O receptor. Sandu et al. (2005) interpreted that such a phenomenon is caused by the reduction of NO_2 and/or peroxyl radicals by increased ozone and therefore future ozone production is decreased. This process is initiated by the reaction of NO and the increased ozone. As time approaches the target time, increasing ozone in the large cities Toronto and Ottawa will take part in enhancing the ozone level in the T-O region within the next one and a half days.

The plots for 16:00 GMT to 20:00 GMT July 18 (

Figure 28) show that the influence of the pre-existing ozone at several locations above land become larger and larger. These locations correspond with the relatively high VOC concentrations. Same as Scenario 1, increasing ozone in regions with large VOC/NOx ratio, more peroxyl radical RO_2 can form to produce more ozone than increasing ozone in those places with smaller VOC/NOx ratio. Time series of the average sensitivity in various local areas (Figure 31 (b)) show a very similar evolution for all locations as in Scenario 1.

The similarity between the calculated target ozone sensitivity to pre-existing ozone in Scenarios 2 and 1 can be attributed to the fact that the meteorological conditions and the underlying conditions on the pollutant transport pathways used are the same. The slight difference between Scenario 1 and 2 is because of using different cost functions (ozone perturbations here). To examine the difference in the sensitivity for various meteorological conditions, while holding the cost function consistent, Scenario 3 is run with weather conditions from July 19 to 21, 2007. In Scenario 3, the ozone level everywhere in the T-O region is assumed to reach 100 ppb by 17:00 local (21:00 GMT) on July 21. The CMAQ-ADJ calculated gradients of this target ozone perturbation with respect to pre-existing ozone are shown in Figure 29. Before 12:00 GMT July 20 (33 hours before the assumed high ozone episode), any assigned ozone anywhere in the research domain has been blown out of the T-O square and cannot influence the ozone level changes there at the target time. The influencing region evolves quickly toward the T-O receptor square, in the same direction as the horizontal wind vectors. Ozone in such regions can transport along the same pathway as the sensitivity fields to the T-O receptor and increase the ozone level there. The large sensitivity above Lake Ontario 4 hours before the target high ozone episode time is established on land and gradually shifts to the lake area. The magnitude increases as time approaches the target time. The closer the time is to the assumed high ozone episode, the greater the sensitivity is. More of the allocated ozone at an earlier time is likely to be blown out of the receptor region than that at a later time. Earlier sensitivity are therefore smaller than that close to the target time. At places with relatively large VOC concentrations on land area in the target T-O region (Figure 27 (b)), the ozone sensitivity at -1H is clearly larger than the surrounding area (Figure 29). As analyzed in Scenarios 1 and 2, high VOCs favor the formation of more peroxyl radical RO_2 through chemical reactions. If the ozone level is increased here, RO_2 further enhances later ozone formation. When dividing the T-O receptor into four sub-regions as in Scenarios 1 and 2, the average ozone sensitivity in these four sub-regions (Figure 31 (c)) shows that under the condition of strong transport and low temperature, ozone above Lake Ontario also has an overall larger impact on later high ozone episode than that in other regions. The non-zero sensitivity over northern land area appears earlier than other sub-regions because the prevailing wind reaches this area earlier than in other sub-regions. The smallest influence of the pre-existing ozone is in the NOx-rich urban areas in Toronto and Ottawa.

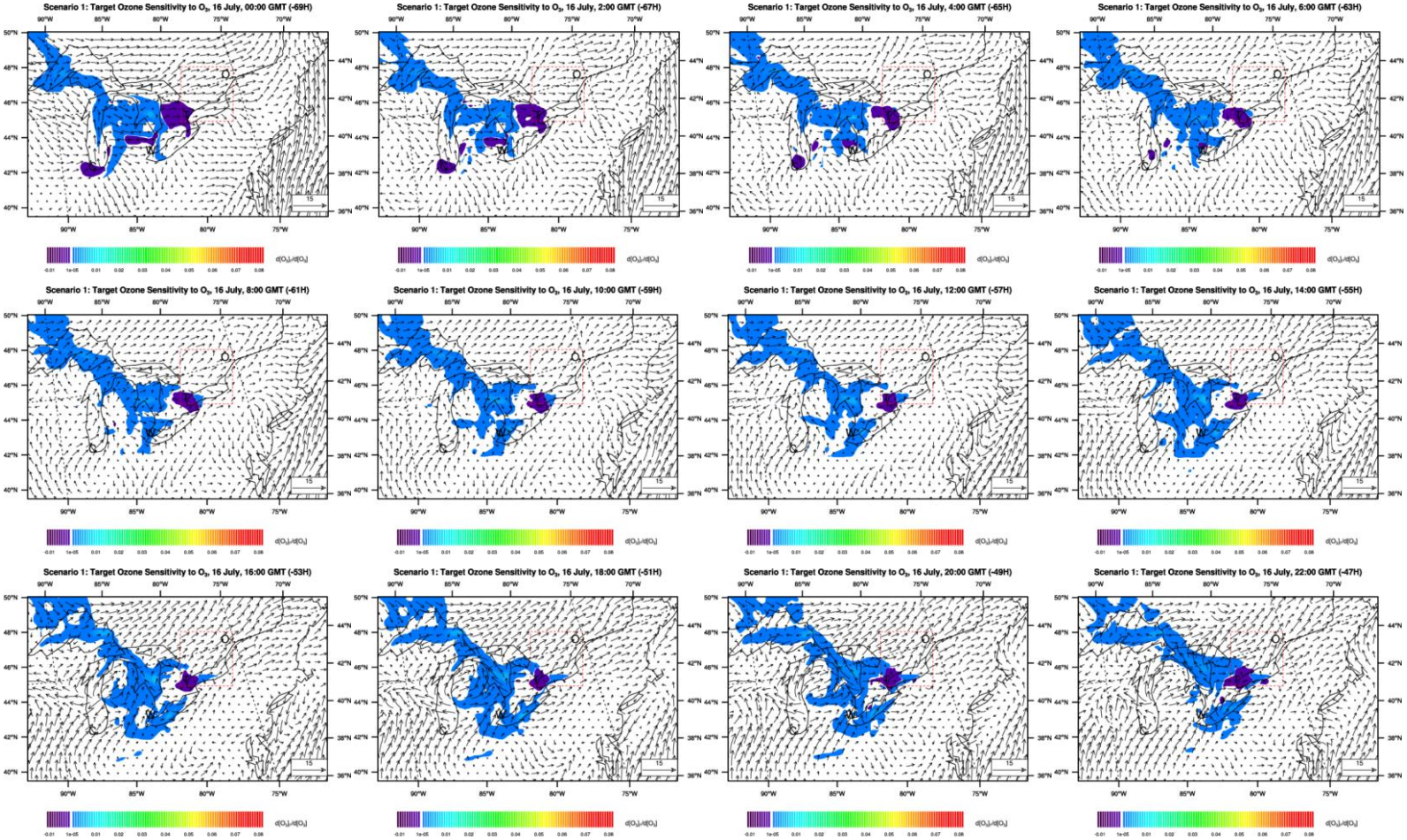
Scenario 1: Target Ozone Sensitivity to O_3, 16 July, 00:00 GMT (-69H)
Scenario 1: Target Ozone Sensitivity to O_3, 16 July, 2:00 GMT (-67H)
Scenario 1: Target Ozone Sensitivity to O_3, 16 July, 4:00 GMT (-65H)
Scenario 1: Target Ozone Sensitivity to O_3, 16 July, 6:00 GMT (-63H)
Scenario 1: Target Ozone Sensitivity to O_3, 16 July, 8:00 GMT (-61H)
Scenario 1: Target Ozone Sensitivity to O_3, 16 July, 10:00 GMT (-59H)
Scenario 1: Target Ozone Sensitivity to O_3, 16 July, 12:00 GMT (-57H)
Scenario 1: Target Ozone Sensitivity to O_3, 16 July, 14:00 GMT (-55H)
Scenario 1: Target Ozone Sensitivity to O_3, 16 July, 16:00 GMT (-53H)
Scenario 1: Target Ozone Sensitivity to O_3, 16 July, 18:00 GMT (-51H)
Scenario 1: Target Ozone Sensitivity to O_3, 16 July, 20:00 GMT (-49H)
Scenario 1: Target Ozone Sensitivity to O_3, 16 July, 22:00 GMT (-47H)

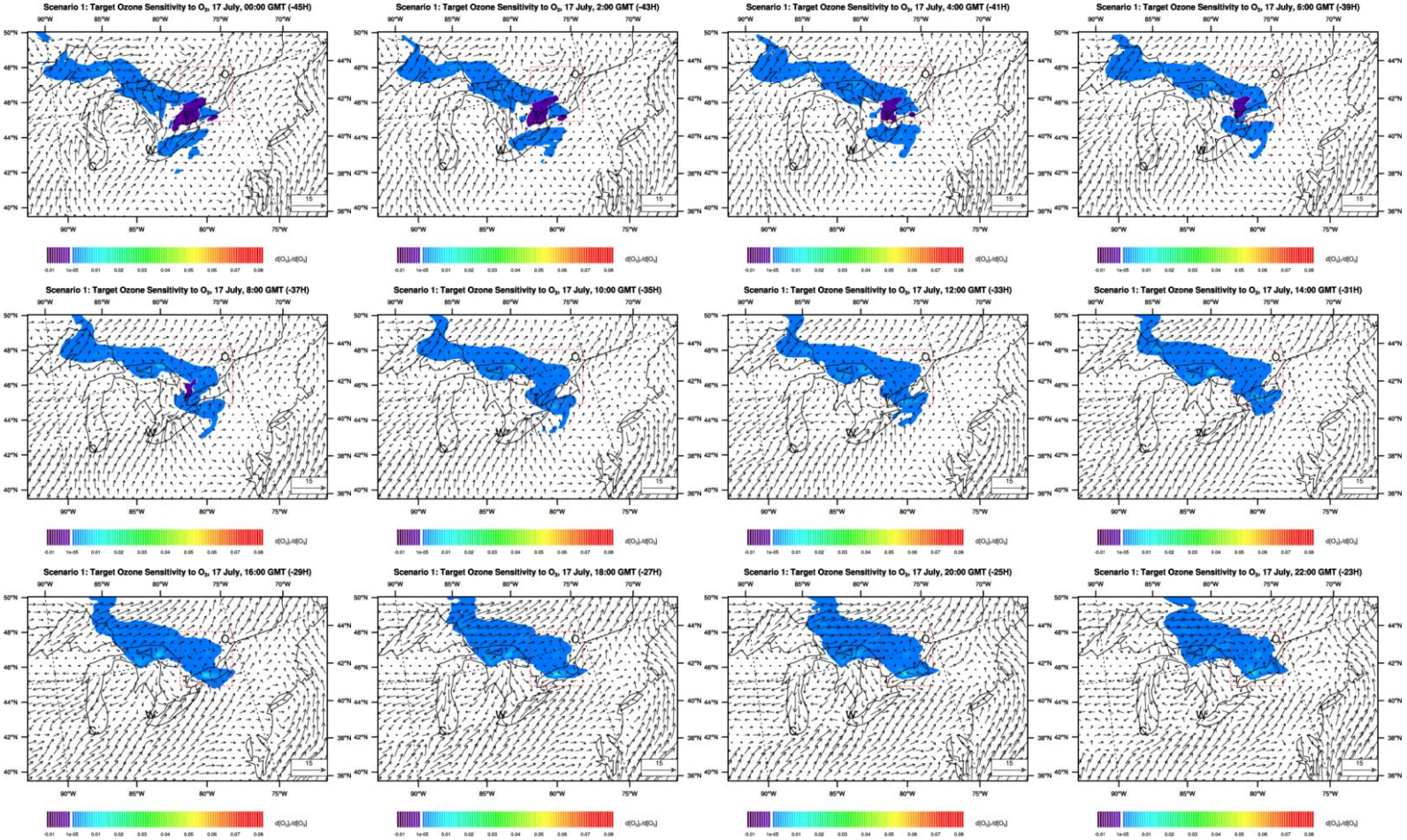
Scenario 1: Target Ozone Sensitivity to O_3, 17 July, 00:00 GMT (-45H)
Scenario 1: Target Ozone Sensitivity to O_3, 17 July, 2:00 GMT (-43H)
Scenario 1: Target Ozone Sensitivity to O_3, 17 July, 4:00 GMT (-41H)
Scenario 1: Target Ozone Sensitivity to O_3, 17 July, 6:00 GMT (-39H)
Scenario 1: Target Ozone Sensitivity to O_3, 17 July, 8:00 GMT (-37H)
Scenario 1: Target Ozone Sensitivity to O_3, 17 July, 10:00 GMT (-35H)
Scenario 1: Target Ozone Sensitivity to O_3, 17 July, 12:00 GMT (-33H)
Scenario 1: Target Ozone Sensitivity to O_3, 17 July, 14:00 GMT (-31H)
Scenario 1: Target Ozone Sensitivity to O_3, 17 July, 16:00 GMT (-29H)
Scenario 1: Target Ozone Sensitivity to O_3, 17 July, 18:00 GMT (-27H)
Scenario 1: Target Ozone Sensitivity to O_3, 17 July, 20:00 GMT (-25H)
Scenario 1: Target Ozone Sensitivity to O_3, 17 July, 22:00 GMT (-23H)

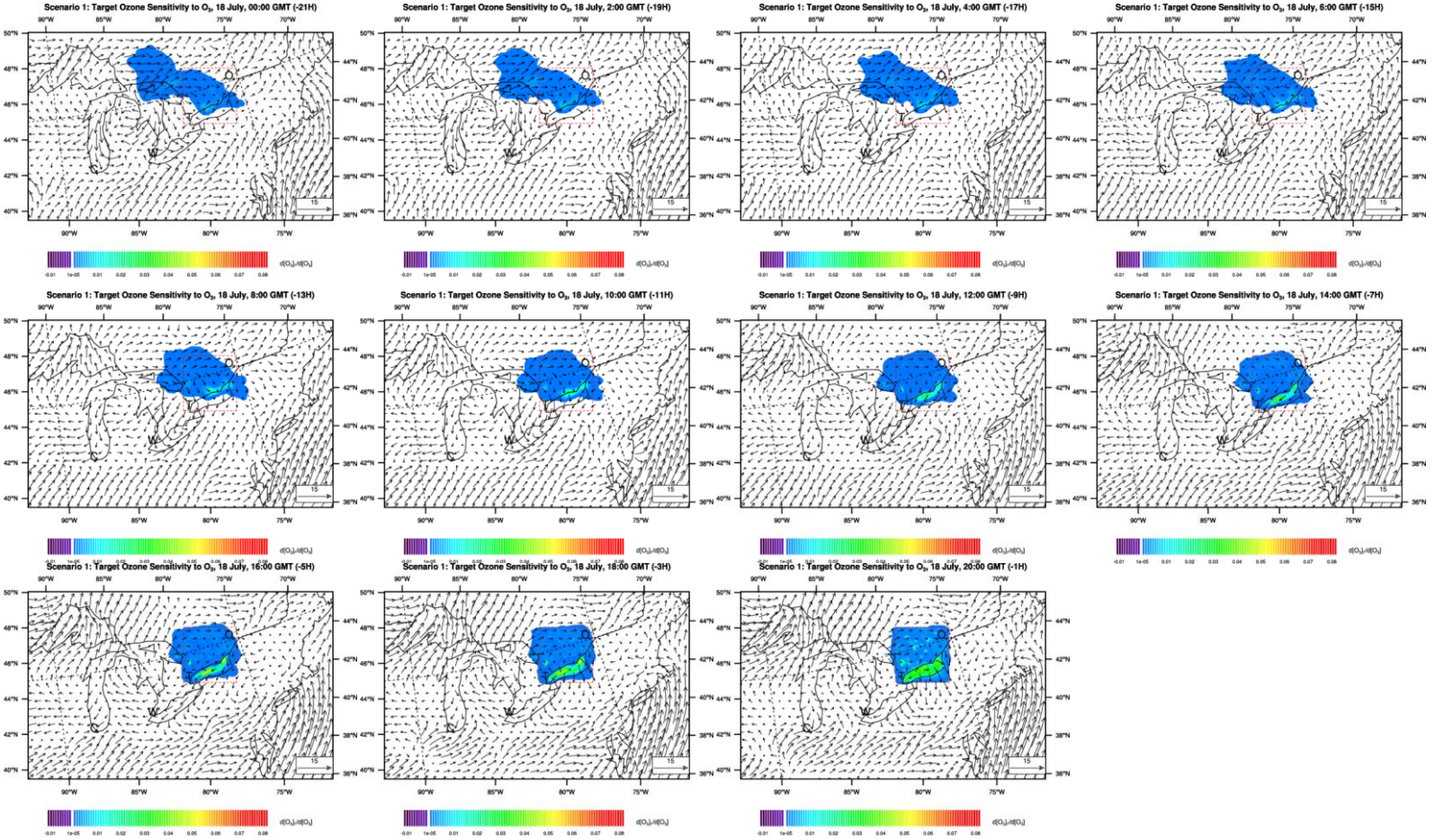

Figure 26. Scenario 1: target ozone sensitivity to pre-existing ozone changes in the 69 hours before the assumed high ozone episode in the W-T region at 21:00 GMT July 18, in ppm/ppm. Plots are presented every 2 hours. White colour represents sensitivity values between -0.00001 ppm/ppm and +0.00001 ppm/ppm. The vectors are horizontal winds calculated by MM5, in m/s.

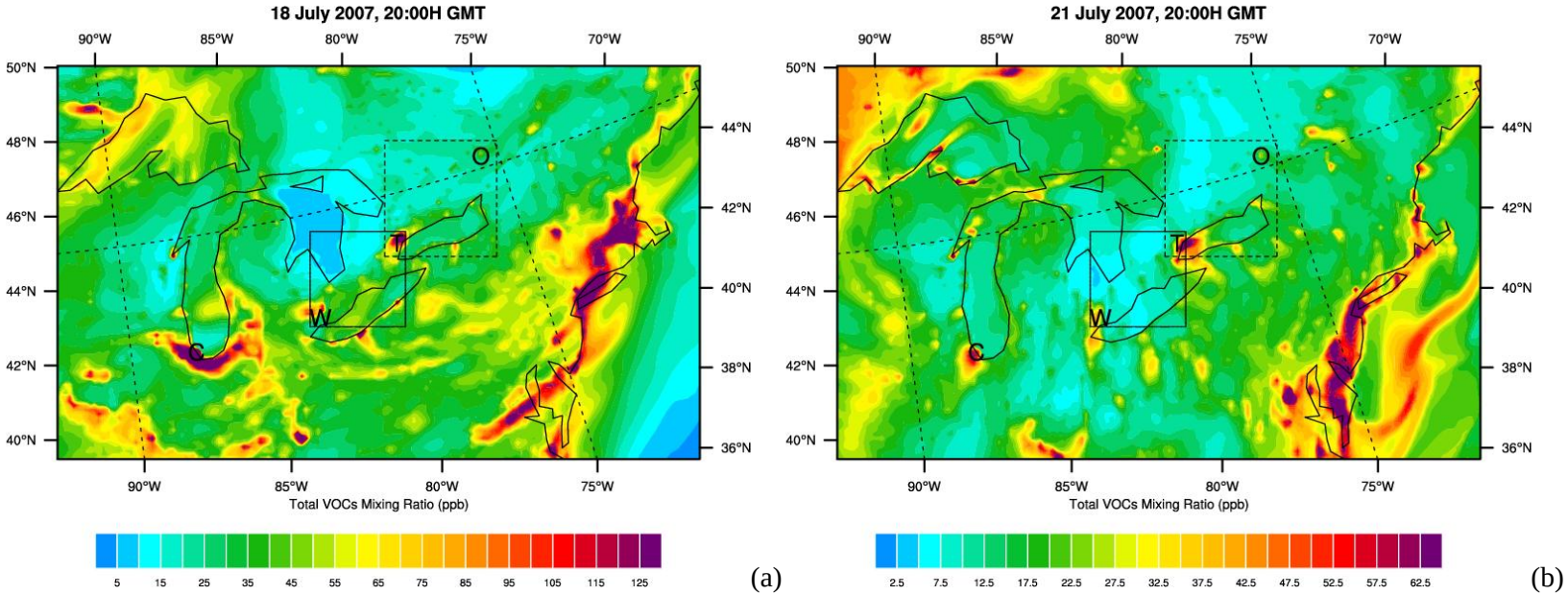

Figure 27. CMAQ simulated total VOC concentrations on July 18 (a) and July 21 (b), 2007. Unit: ppb.

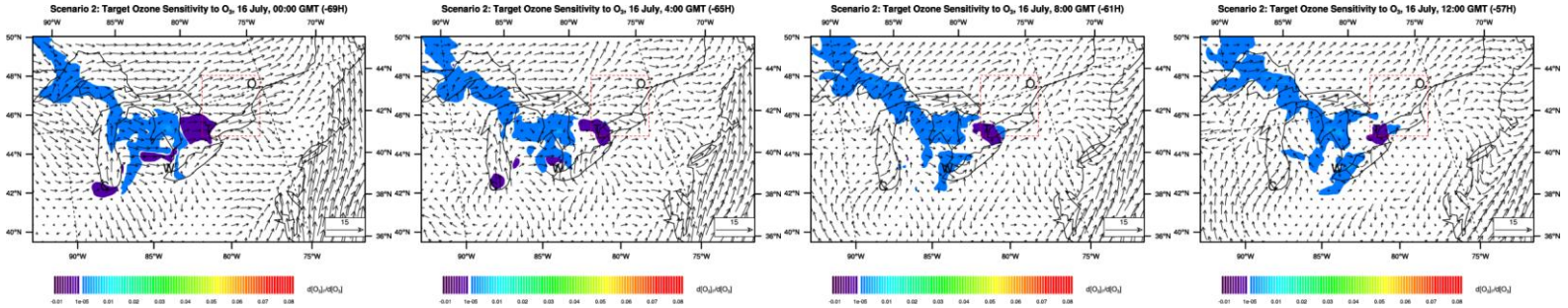

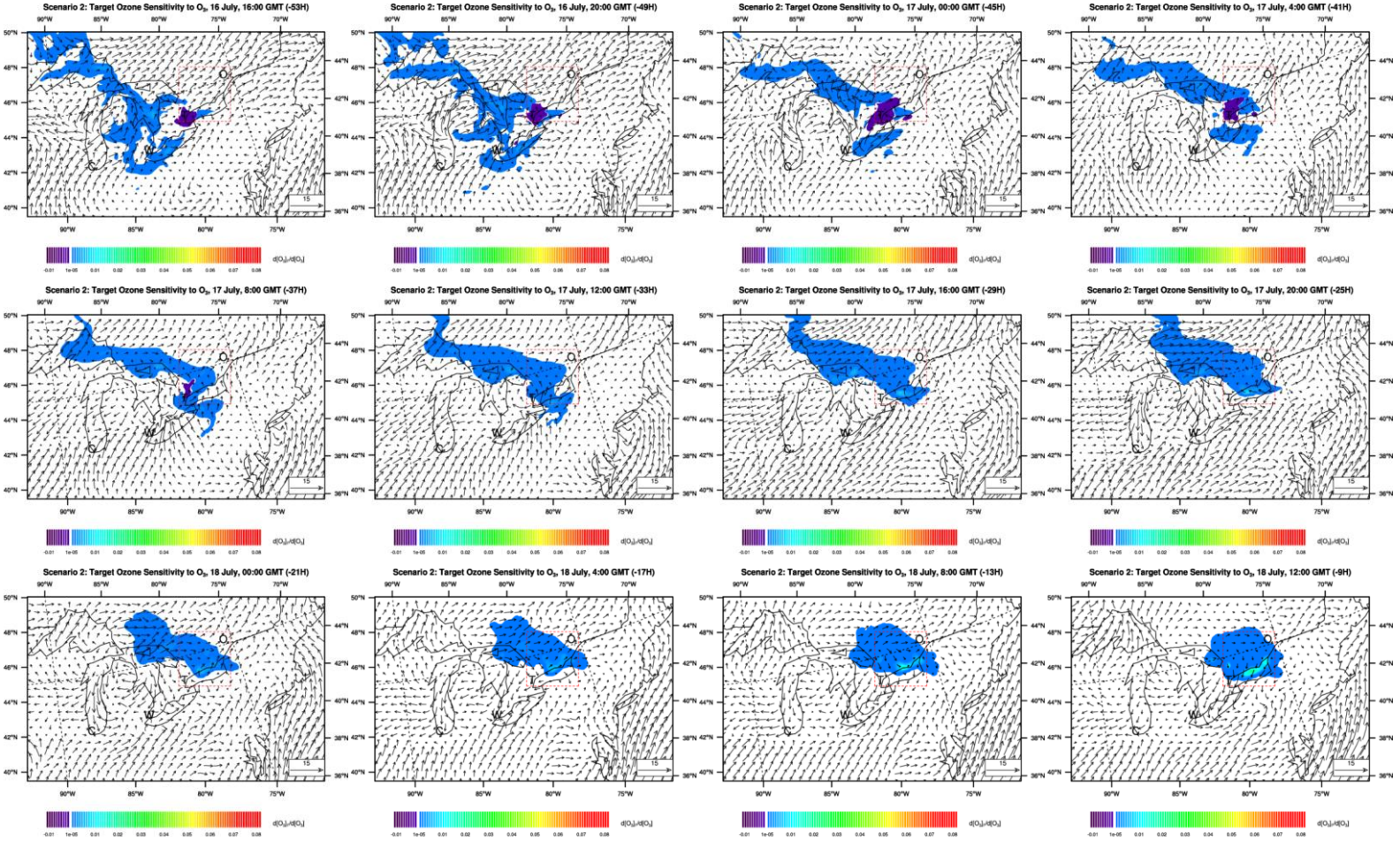
Scenario 2: Target Ozone Sensitivity to O3, 16 July, 16:00 GMT (-53H)
Scenario 2: Target Ozone Sensitivity to O3, 16 July, 20:00 GMT (-49H)
Scenario 2: Target Ozone Sensitivity to O3, 17 July, 00:00 GMT (-45H)
Scenario 2: Target Ozone Sensitivity to O3, 17 July, 4:00 GMT (-41H)
Scenario 2: Target Ozone Sensitivity to O3, 17 July, 8:00 GMT (-37H)
Scenario 2: Target Ozone Sensitivity to O3, 17 July, 12:00 GMT (-33H)
Scenario 2: Target Ozone Sensitivity to O3, 17 July, 16:00 GMT (-29H)
Scenario 2: Target Ozone Sensitivity to O3, 17 July, 20:00 GMT (-25H)
Scenario 2: Target Ozone Sensitivity to O3, 18 July, 00:00 GMT (-21H)
Scenario 2: Target Ozone Sensitivity to O3, 18 July, 4:00 GMT (-17H)
Scenario 2: Target Ozone Sensitivity to O3, 18 July, 8:00 GMT (-13H)
Scenario 2: Target Ozone Sensitivity to O3, 18 July, 12:00 GMT (-9H)

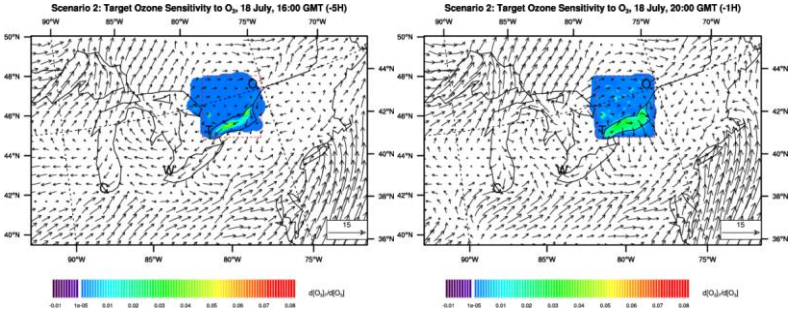

Figure 28. Scenario 2: target ozone sensitivity to pre-existing ozone changes in the 69 hours before the assumed high ozone episode in the W-T region at 21:00 GMT July 18, in ppm/ppm. Plots are presented every 4 hours. White colour represents sensitivity values between -0.00001 ppm/ppm and +0.00001 ppm/ppm. The vectors are horizontal winds calculated by MM5, in m/s.

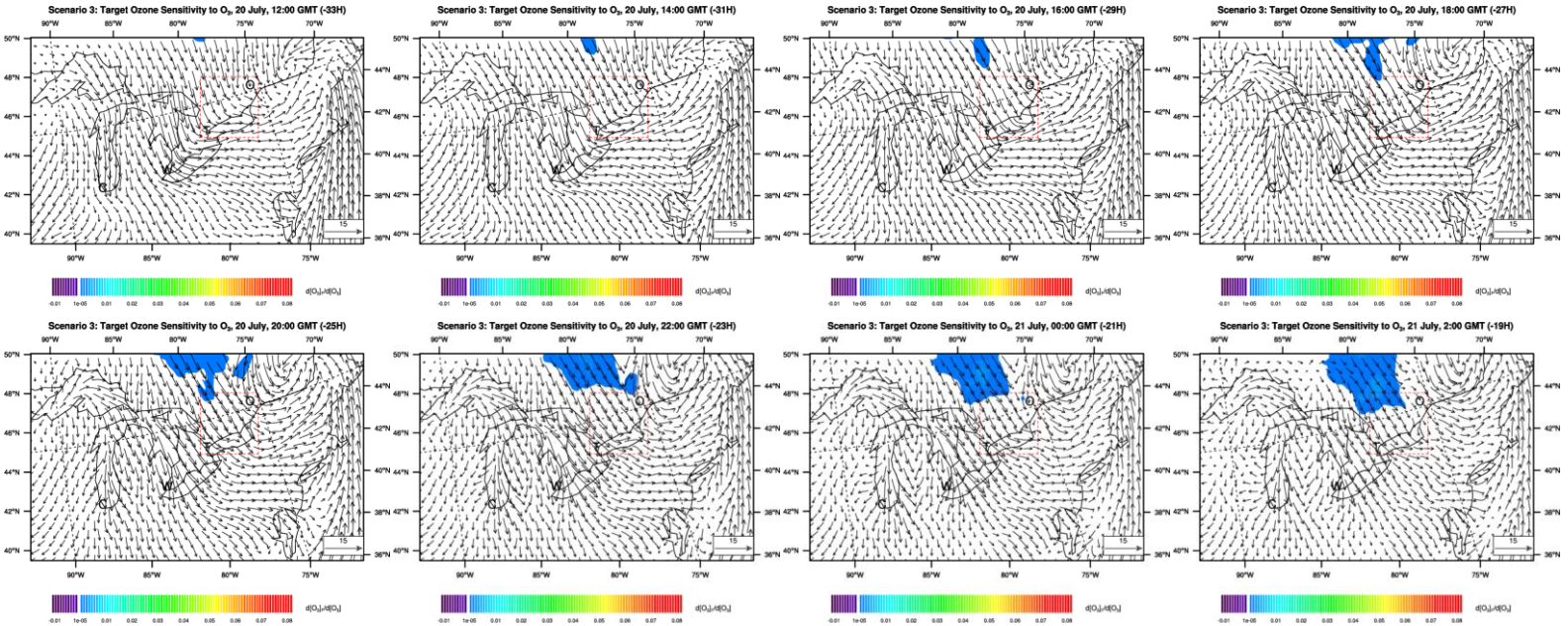

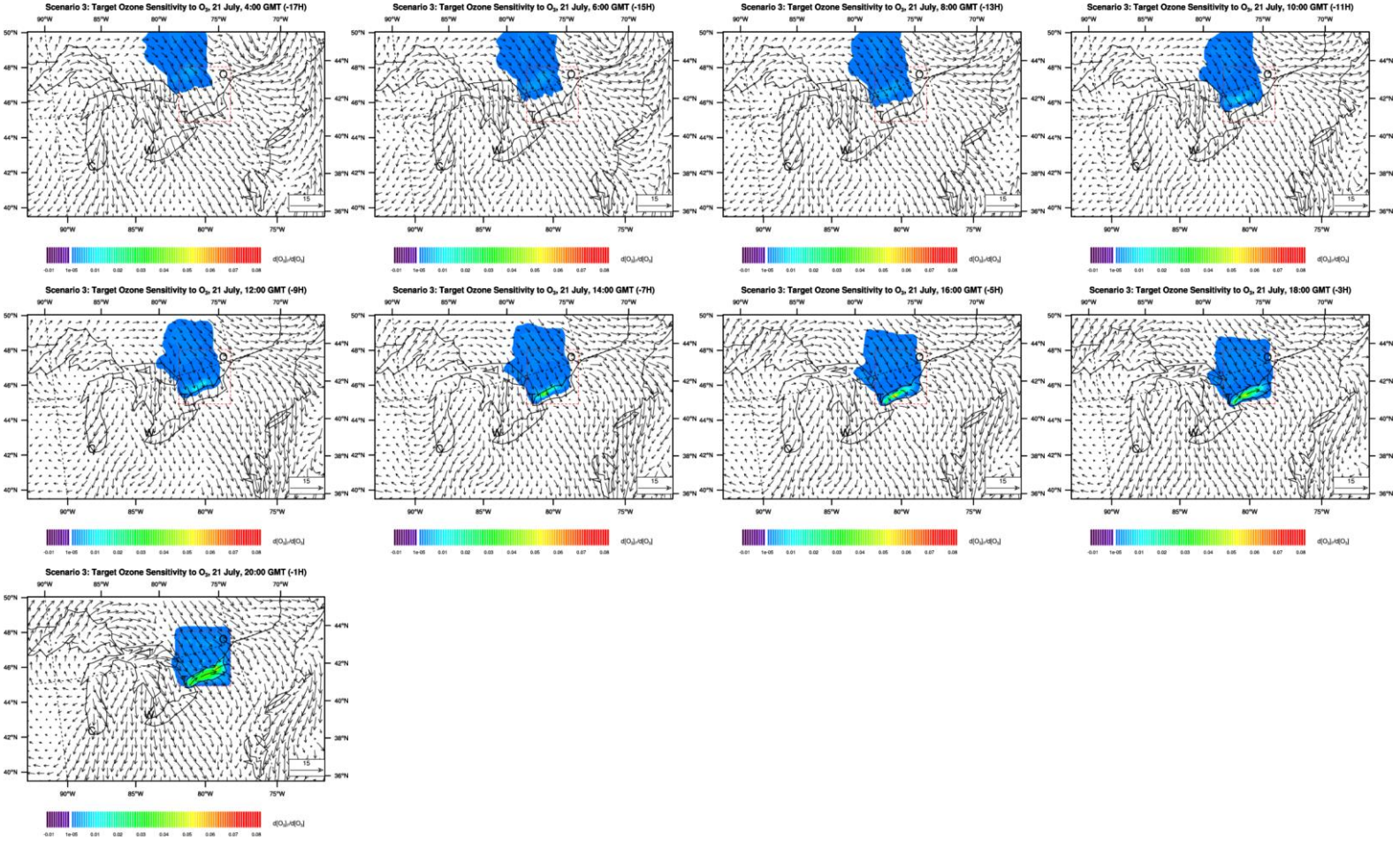

Figure 29. Scenario 3: target ozone sensitivity to pre-existing ozone changes in the 69 hours before the assumed high ozone episode in the W-T region at 21:00 GMT July 21, in ppm/ppm. Plots are presented every 2 hours. White colour represents sensitivity values between -0.00001 ppm/ppm and +0.00001 ppm/ppm. The vectors are horizontal winds calculated by MM5, in m/s. Sensitivity 31 hours before the high ozone episode are zero everywhere and are not plotted.

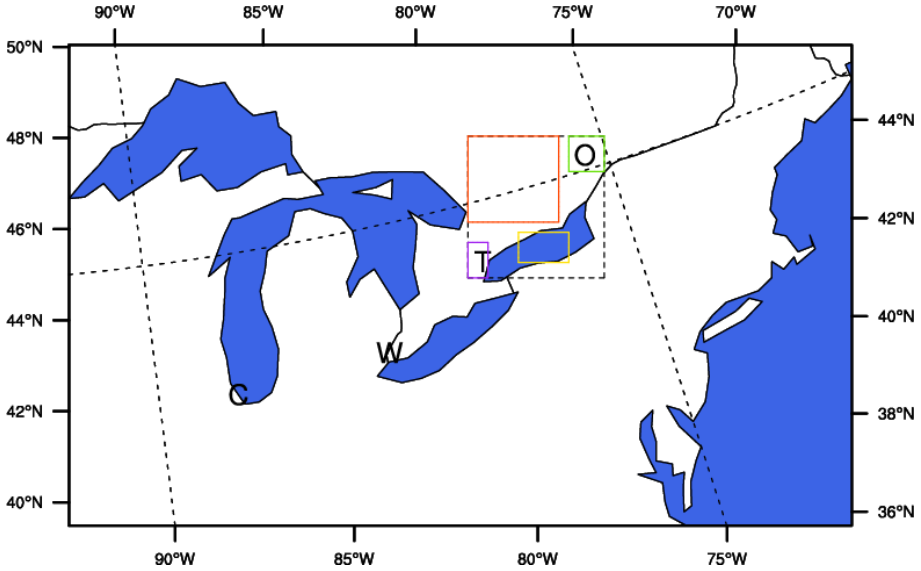

Figure 30. Four sub-regions in Toronto-Ottawa region. Northern land area: in red square; Ottawa: in green square; central part of Lake Ontario: in yellow square; Toronto: in purple square.

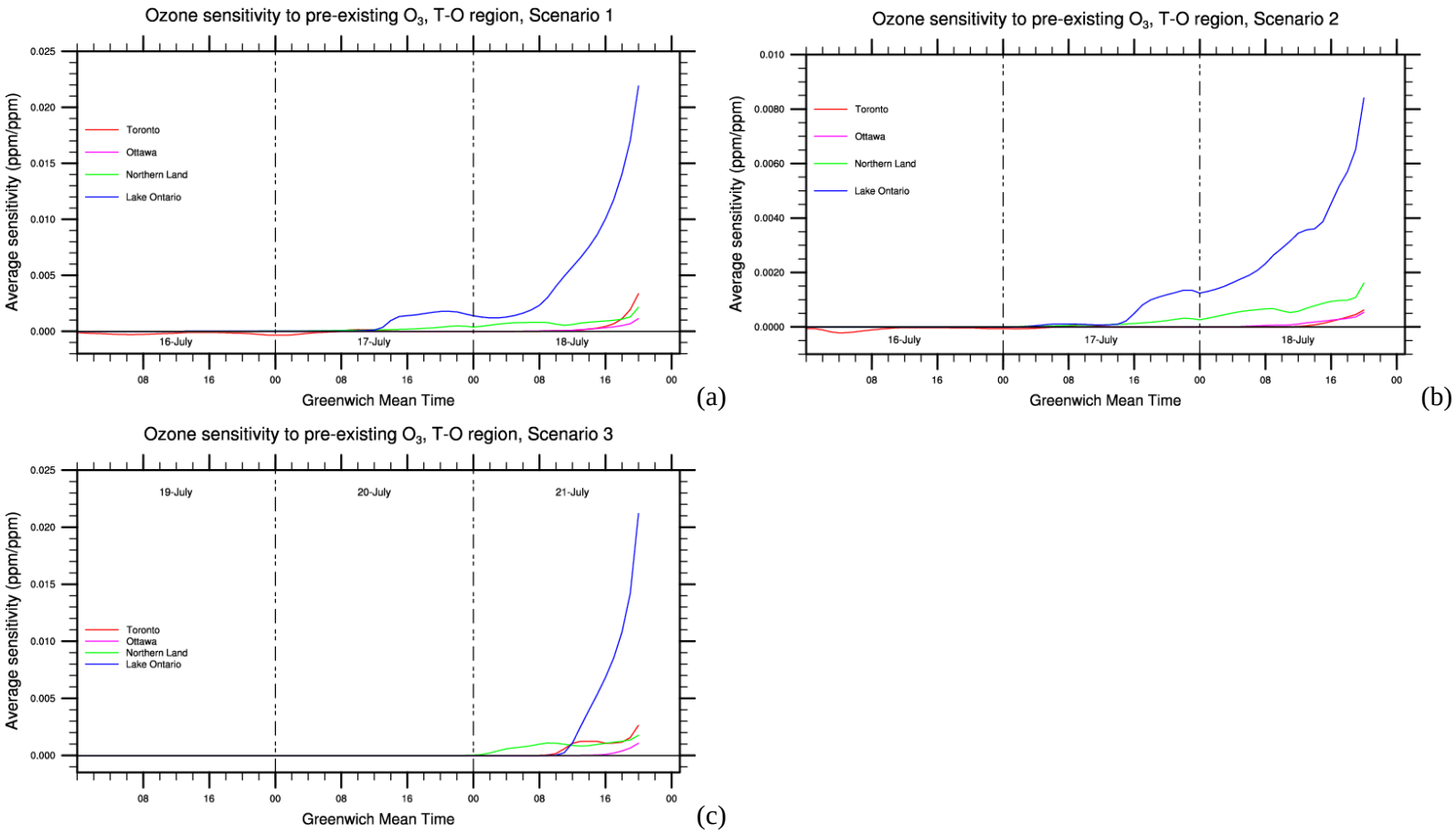

Figure 31. Time series of the average ozone sensitivity to pre-existing ozone changes in 4 sub-regions of the Toronto-Ottawa region for Scenario 1 (a), Scenario 2 (b), and Scenario 3 (c). The 4 local regions are Toronto, Ottawa, northern land area, central part of Lake Ontario

5.3.3.2 Influence of NO

As analyzed in Section 5.2.1.2, increasing NOx can enhance the ozone formation in regions with high VOC/NOx ratio. The CMAQ-simulated VOC/NOx ratio in most places north of 45 degrees latitude is larger than 27 (Figure 10). Figure 32 shows that 69 hours before the assumed high ozone event in the target T-O region, the non-zero ozone sensitivity to NO as simulated by the modified CMAQ-ADJ using conditions in Scenario 1 is mostly positive. The influencing area extends to the northwestern corner of the research region. Increasing NO emission in northern Ontario enhances the ozone level in east-central Ontario after 69 hours. The VOC/NOx ratio in the Midwest U.S. and Ohio Valley is much smaller than those in the northern unpopulated regions, but most of the ozone sensitivity with respect to NO is also positive in the beginning of the modeling period. This suggests that NO emissions in this region increase the ozone concentration in east-central Ontario in the next 69 hours. The plots after -33H in Figure 32 show that an increase in NO emission in very small VOC/NOx urban area and its upwind areas suppresses the ozone formation in the target T-O region during the occurrence of the high ozone event.

Comparing the magnitude of all the positive sensitivity in the upwind direction of the receptor square, the magnitude over lakes is much larger than that over land. At 0:00 GMT July 16, there is a large NO sensitivity center over the southern part of Lake Superior. This large center stays over the lake area for about 42 hours until 18:00 GMT on July 17. The local wind circulation plays an important role in the recycling of this center on Lake Superior, as can be derived from the change of the wind vectors during this period. When this sensitivity center moves away from the lake area and enters the eastern inland area after 16:00 GMT July 17, the magnitude keeps decreasing to almost the same as that of the surrounding regions by 23:00 GMT July 17.

On the -69H plot in Figure 32, the Lake Michigan area does not show a larger sensitivity than the surrounding influencing land area. The reason for this is that the southerly wind is strong, which causes any NO emitted here to be blown to the north or east very soon. As a comparison, the relatively weak wind in the southern part of Lake Huron has helped maintain a large NO sensitivity center until 17:00 GMT July 16. The center then evolves to the north above Lake Huron and the magnitude decreases. When it arrives at the eastern shore of Georgian Bay at 04:00 GMT on July 17, the night time lake breeze moves it back toward the lake area and it gets enhanced again, according to the 08:00 GMT and 12:00 GMT July 17 plots. These atmospheric conditions around the lakes and the low solubility of NO together with those already-formed ozone help maintain larger ozone sensitivity to NO over water. By 20:00 GMT July 17, the large sensitivity center moves to the eastern side of Georgian Bay and finally reaches the in-land area

by about 17 hours before the high ozone event in the T-O region. During the time when this inland large sensitivity region moves slowly to the target receptor region, another large sensitivity center appears at the northern shore of Lake Ontario. This large sensitivity center moves to the center of Lake Ontario following the northerly wind. By 12:00 local time (5 hours before the high ozone event), the largest sensitivity appears above Lake Ontario.

As time approaches the target time, the influencing region of NO becomes local from the upwind north direction. The northern part of the T-O region is mostly land. The sensitivity in this land region becomes larger when time is close to the outbreak of the assumed high ozone event at 21:00 GMT on July 18. The sensitivity is especially large near those locations with larger VOC concentrations (Figure 27 (a)). In regions having high VOC/NOx ratio, increasing NO emission enhances the ozone formation by enhancing the oxidation of VOCs.

On the -1H sensitivity plot, negative sensitivity regions are near Toronto, Rochester, and southeast corner of the T-O region (Figure 32). All these three places have large NOx emissions and low VOC/NOx ratio at -1H (Figure 33). The negative sensitivity region near Toronto is evolved from the upwind direction starting around 0:00 GMT July 18. The reason that NO emitted to such upwind region also has a negative sensitivity relates to the fact that it is transported to Toronto within an appropriate time period (about 21 hours in this case). Increasing NO in the high NOx mixing ratio regions such as Toronto further titrates ozone and causes negative ozone sensitivity. Negative ozone sensitivity associated with large NO concentrations is also detected at earlier times, i.e., negative sensitivity values are always found associated with either Toronto, Cleveland, or Rochester from 16:00 GMT July 16 until the outbreak of the assumed high ozone event.

The average ozone sensitivity to NO in the east-central Ontario is further analyzed by dividing the Toronto-Ottawa region into the same four sub-regions (Figure 30) as those used in Section 5.3.3.1. The time series of the average sensitivity for the four local locations is shown in Figure 36 (a). At most times, NO over Lake Ontario has the largest influence on ozone formation, which is due to both the large VOC/NOx ratio here and low solubility of NO and the ozone formed from NO. NO over the northern land region has the second largest influence. NO release in the area with the smallest VOC/NOx ratio (Toronto) has the smallest contribution to local ozone formation. Release of NO to Toronto area 69 hours before the assumed high ozone episode has been shown to enhance the ozone level at the target time in the T-O region. Such an early released ozone precursor is trapped in east-central Ontario by the wind circulation there. The largest average ozone response to NO over Lake Ontario occurs several hours before the high ozone event, implying that the NO released then need several hours to produce ozone. This

relationship is not apparent in other sub-regions. An even higher spatial resolution adjoint model than that used in this study should be used to study small-area regions in case some details are averaged out.

Scenario 2 is designed to test how the influence of NO changes for a different type of ozone perturbation in the Toronto-Ottawa region. It is assumed in this high ozone episode that the ozone concentrations are enhanced by 40 ppb everywhere in the T-O region. This uniform ozone perturbation is given to the CMAQ-ADJ to calculate its gradient with respect to all model variables. The sensitivity (gradient) with respect to NO is displayed in Figure 34. The time series of the average sensitivity for four sub-regions is shown in Figure 36(b). Both the spatial distribution and temporal variability of the sensitivity fields evolve in a very similar manner as those in Scenario 1, implying that the same meteorological conditions, surface types, and emission in the pollutant pathway used in both scenarios play the most important role. A portion of the NO emission in anywhere of the non-zero sensitivity region produces ozone on the way to the target region and enhances the ozone in the T-O area.

Both Scenarios 1 and 2 have shown that NO released to major water bodies has a larger influence on downwind ozone in the T-O region than that released to land area. The same conclusion is drawn when the prevailing winds are not from the Great Lakes regions, as in Scenario 3. In Scenario 3, the prevailing wind from the north begins to control the regions to the north of the T-O region from about 2 days before the time of the assumed high ozone episode (target time) (Figure 35). Based on Figure 35, the largest NO sensitivity appears over Lake Ontario about 5 hours before the target time, which is evolved from the upwind northern land area. After then, the NO influencing area becomes larger over Lake Ontario, but the overall magnitude decreases. Meanwhile, the influence over land becomes larger. The negative sensitivity near Toronto and Rochester associates with high NO emissions (low VOC/NOx ratio). The negative sensitivity associated with Toronto evolves with the wind from 0:00 GMT July 21. NO at this time is transported to Toronto quickly by strong northerly wind and suppresses the future ozone formation by suppressing the oxidation of VOCs. Figure 36 (c) show the time series of the average ozone sensitivity to NO in the same four sub-regions in east-central Ontario as in Scenario 1. Ozone increases in the target region almost always respond strongest to NO released to local lake regions where the VOC/NOx ratio is largest, then the northern land area where the VOC/NOx is also large. The smallest VOC/NOx corresponds to the smallest (sometimes even negative) ozone response, such as those in Toronto area in Figure 34 and in Figure 35. The average sensitivity in Toronto in Figure 36 (c) shows both negative and positive values, which is because this result is the average of all of the values in the selected sub-region that represents

Toronto. In typical weather conditions in Scenario 1, local circulation allows NO in some sub-regions such as in Toronto to influence the ozone level of east-central Ontario for several days. When the wind is strong, only recently released NO in local areas influences local ozone level within the next several hours. Similar to the cases in Scenario 1, the largest average ozone sensitivity to NO over the central part of Lake Ontario occurs several hours before the target time. An even higher resolution simulation should be used to discover how clear this relationship is in other small sub-regions.

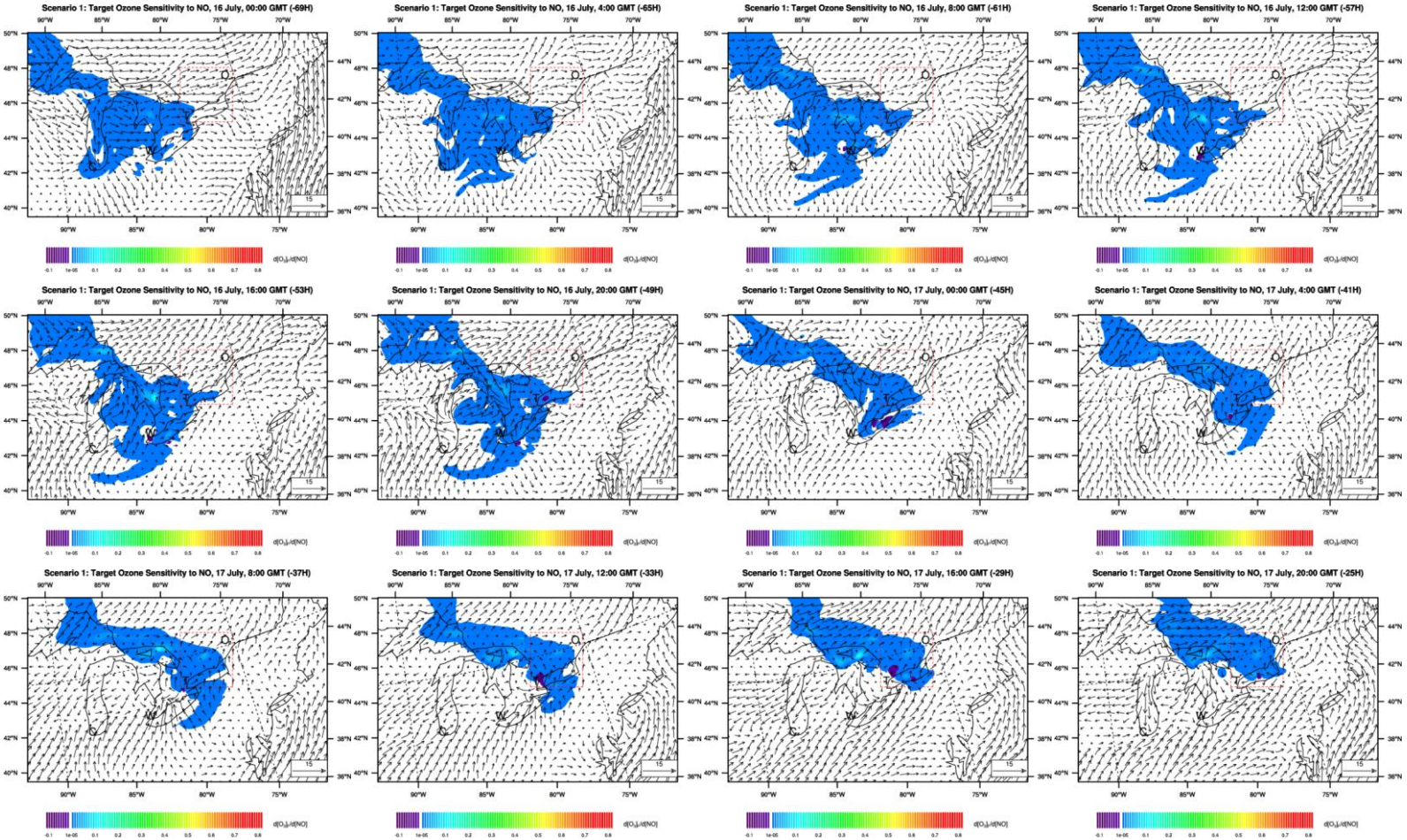
Scenario 1: Target Ozone Sensitivity to NO, 16 July, 00:00 GMT (-69H)
Scenario 1: Target Ozone Sensitivity to NO, 16 July, 4:00 GMT (-65H)
Scenario 1: Target Ozone Sensitivity to NO, 16 July, 8:00 GMT (-61H)
Scenario 1: Target Ozone Sensitivity to NO, 16 July, 12:00 GMT (-57H)
Scenario 1: Target Ozone Sensitivity to NO, 16 July, 16:00 GMT (-53H)
Scenario 1: Target Ozone Sensitivity to NO, 16 July, 20:00 GMT (-49H)
Scenario 1: Target Ozone Sensitivity to NO, 17 July, 00:00 GMT (-45H)
Scenario 1: Target Ozone Sensitivity to NO, 17 July, 4:00 GMT (-41H)
Scenario 1: Target Ozone Sensitivity to NO, 17 July, 8:00 GMT (-37H)
Scenario 1: Target Ozone Sensitivity to NO, 17 July, 12:00 GMT (-33H)
Scenario 1: Target Ozone Sensitivity to NO, 17 July, 16:00 GMT (-29H)
Scenario 1: Target Ozone Sensitivity to NO, 17 July, 20:00 GMT (-25H)

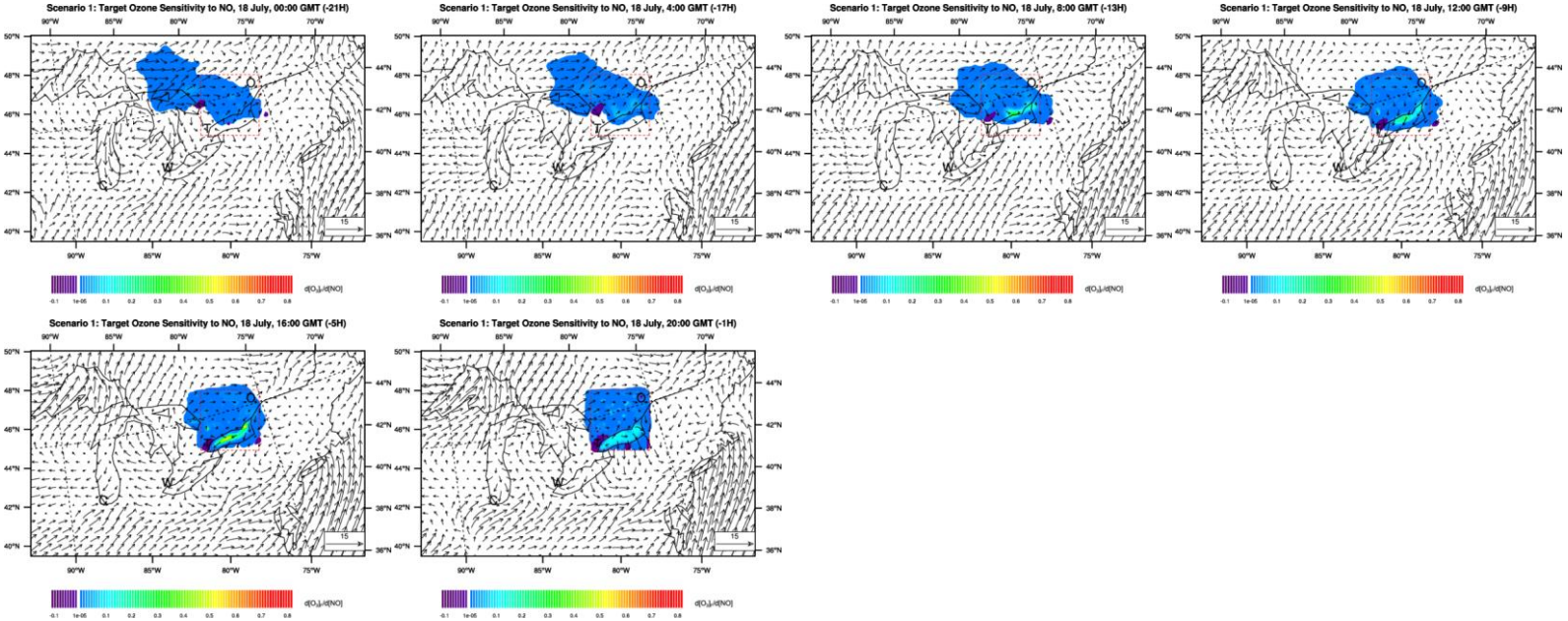

Figure 32. Scenario 1: target ozone sensitivity to NO changes in the 69 hours before the assumed high ozone episode in the T-O region at 21:00 GMT July 18, in ppm/ppm. Plots are presented every 4 hours. White colour represents sensitivity values between -0.00001 ppm/ppm and +0.00001 ppm/ppm. The vectors are horizontal winds calculated by MM5, in m/s.

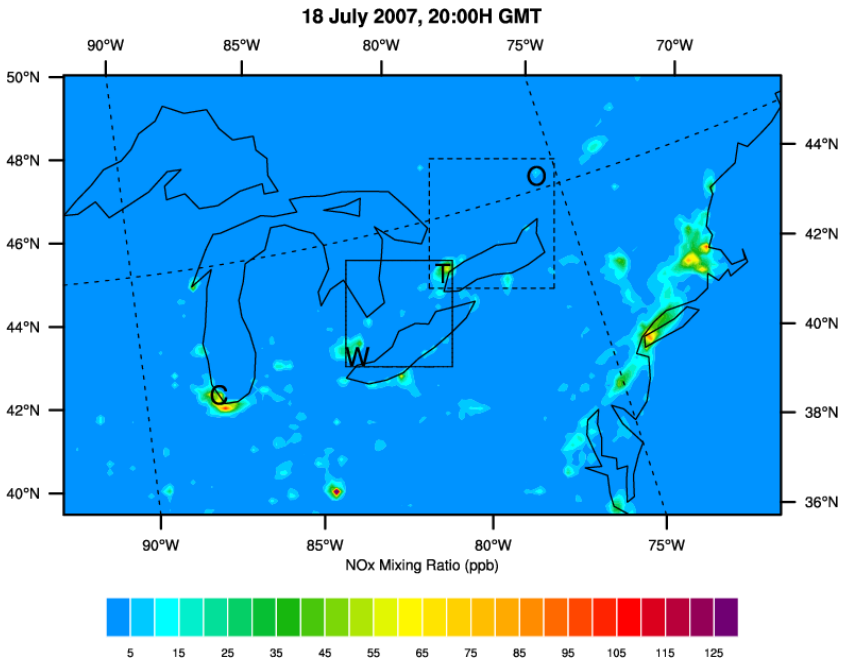

Figure 33. CMAQ simulated NOx mixing ratio at 20:00 GMT July 18, 2007. Unit: ppb.

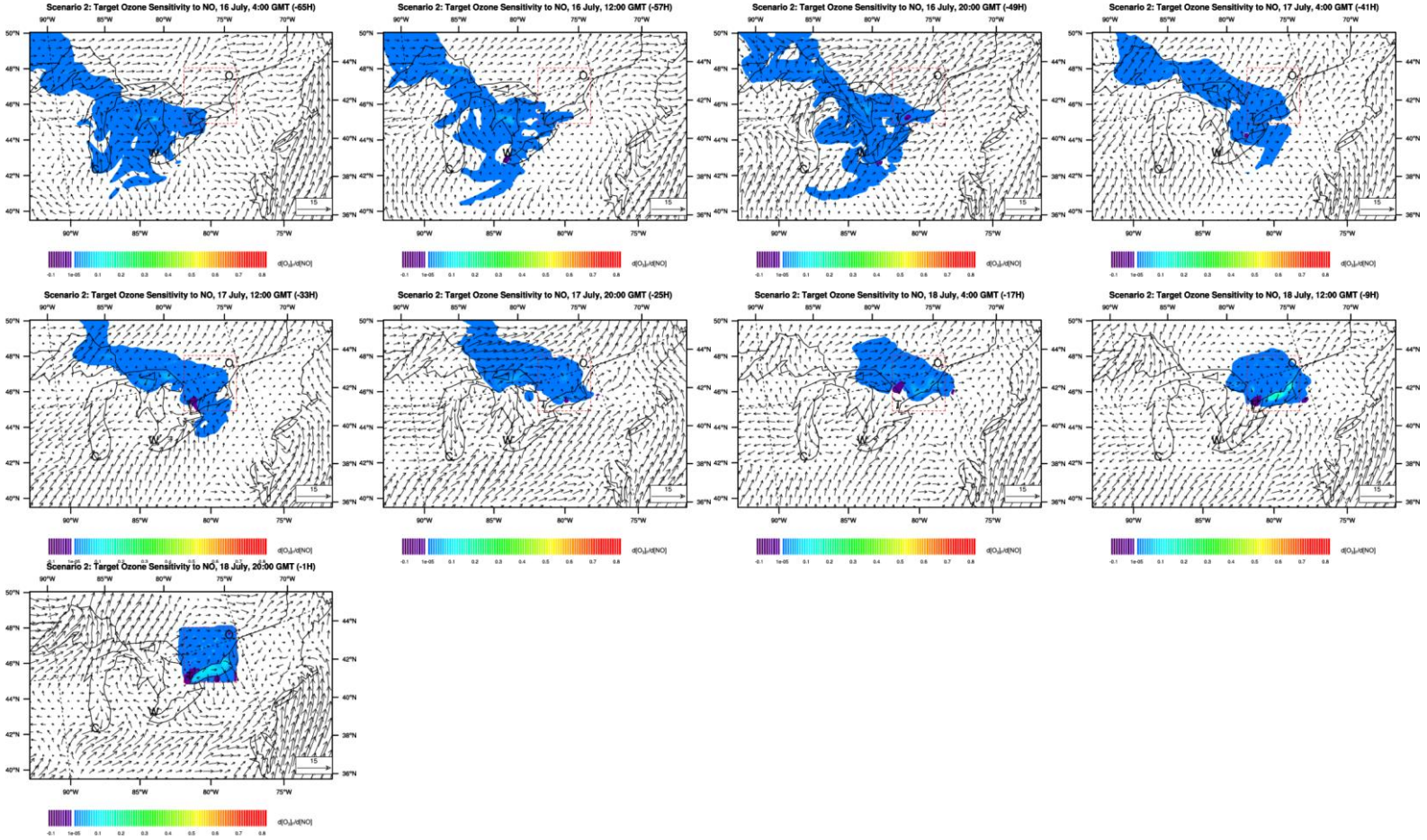

Figure 34. Scenario 2: target ozone sensitivity to NO changes in the 69 hours before the assumed high ozone episode in the W-T region at 21:00 GMT July 18, in ppm/ppm. Plots are presented every 8 hours. White colour represents sensitivity values between -0.00001 ppm/ppm and +0.00001 ppm/ppm. The vectors are horizontal winds calculated by MM5, in m/s.

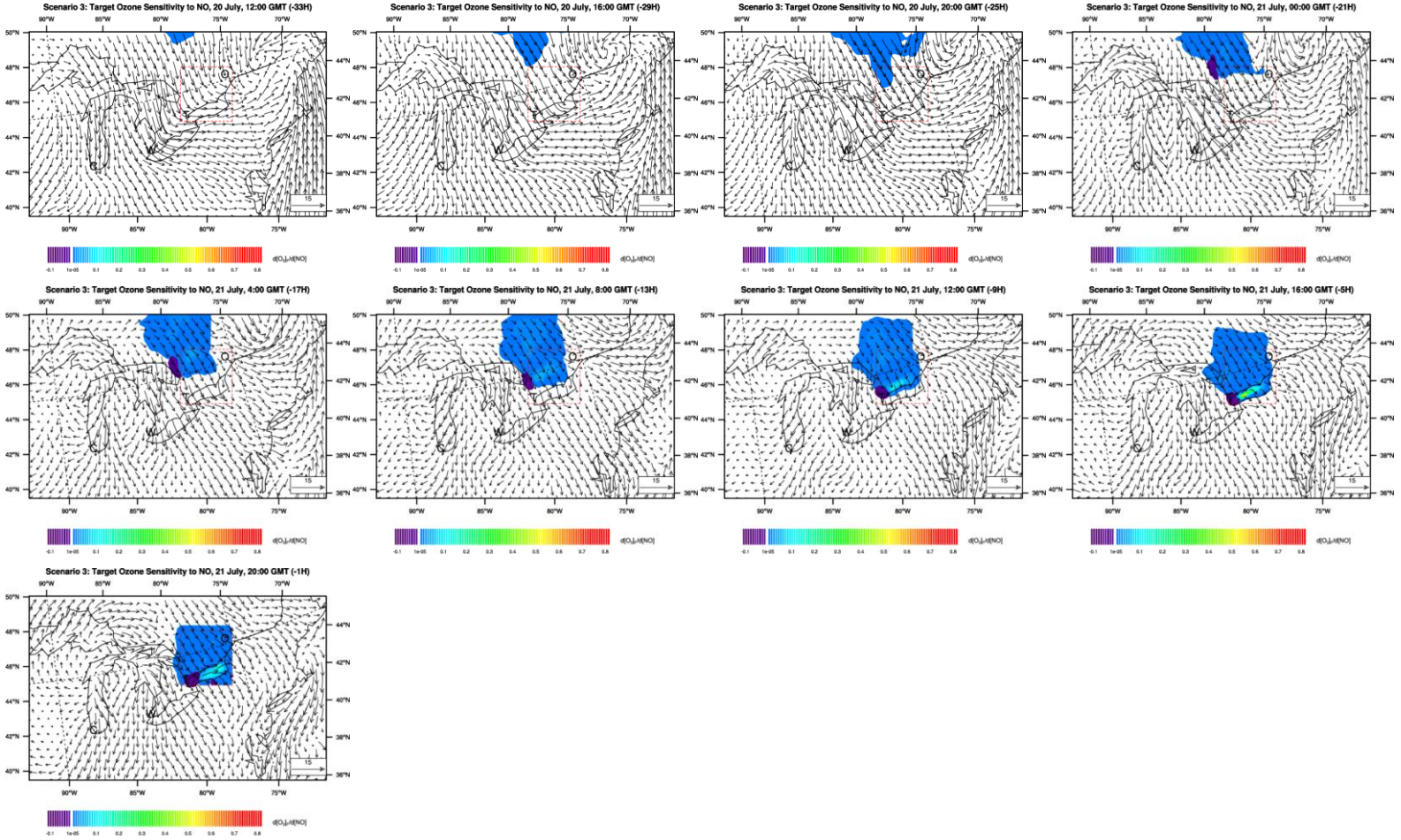

Figure 35. Scenario 3: target ozone sensitivity to NO changes in the 69 hours before the assumed high ozone episode in the T-O region at 21:00 GMT July 21, in ppm/ppm. Plots are presented every 4 hours. White colour represents sensitivity values between -0.00001 ppm/ppm and +0.00001 ppm/ppm. The vectors are horizontal winds calculated by MM5, in m/s. The sensitivity 33 hours before the high ozone episode is zero everywhere and is not plotted.

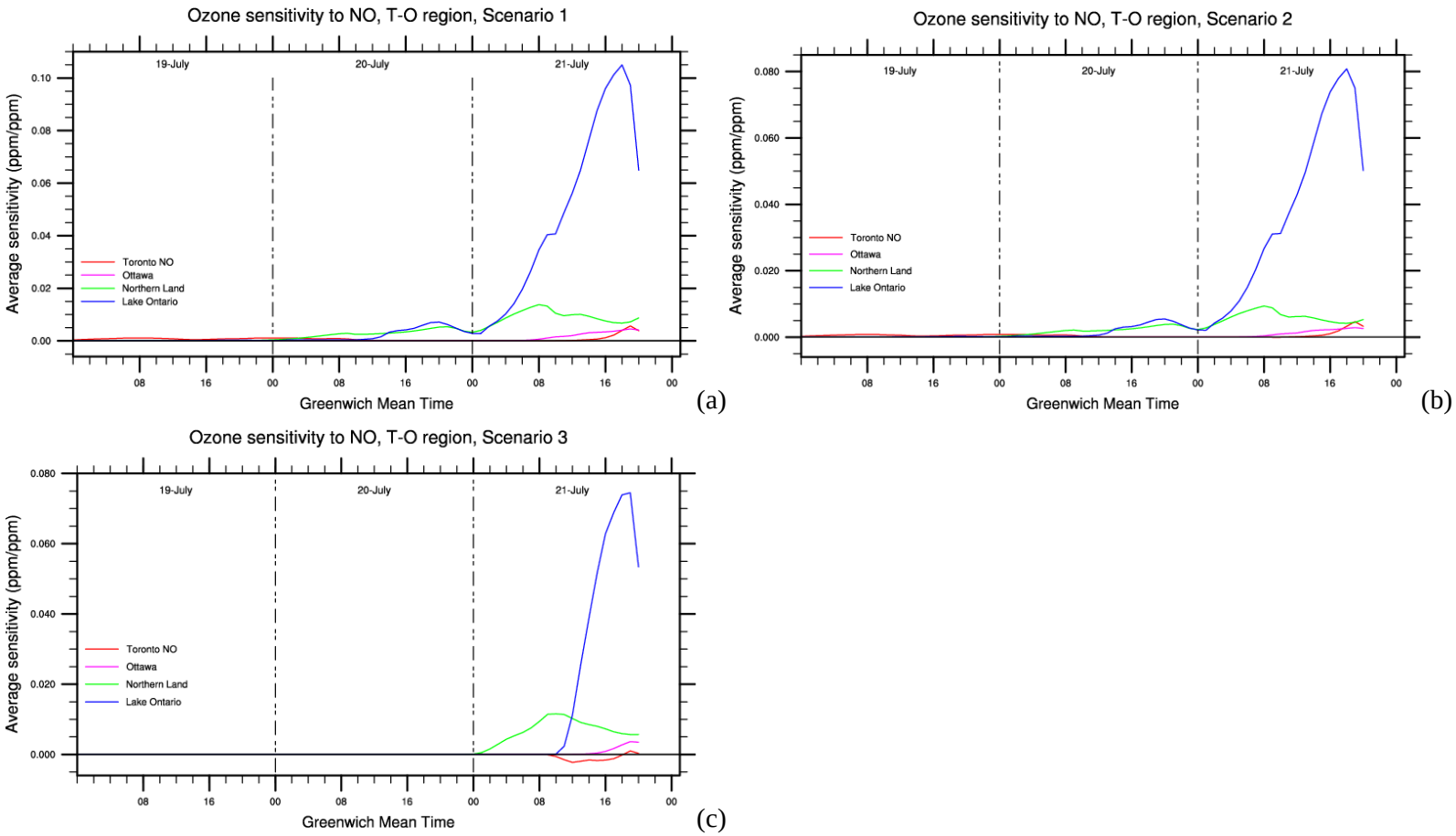

Figure 36. Time series of the average ozone sensitivity to NO changes in 4 sub-regions of the Toronto-Ottawa region for Scenario 1: (a), Scenario 2: (b), and Scenario 3: (c). The 4 local regions are Toronto, Ottawa, northern land area, and central part of Lake Ontario.

5.3.3.3 Influence of CO and VOCs

An area is considered to be NOx limited when the VOC to NOx ratio is larger than 15 to 1 (http://capita.wustl.edu/nescaum/reports/pams94/nepams4.html). The Toronto-Ottawa region is located in the east-central Ontario, with the exception of Ottawa, Toronto, and southern shore of Lake Ontario near Rochester where the VOC/NOx ratios are small, the VOC/NOx ratios in most T-O region are larger than 27. Therefore, ozone production is mostly NOx-limited and typically independent of VOC in this region. When NOx is in short supply, the ozone production can increase linearly with NOx concentrations (Geddes et al., 2009c). In small VOC/NOx ratio urban areas, the ozone formation chemistry is in a VOC-sensitive chemical regime where additional VOCs have a large influence.

This section examines the sensitivity of ozone in Toronto-Ottawa region to carbon compounds in the research domain under the conditions in Scenario 1 and Scenario 3. The results of Scenario 2 are very close to those of Scenario 1 and therefore not presented here. The meteorological conditions used in Scenario 1 are typical summer weather conditions in the Northern U.S. and southern Ontario. The southern land area in the research domain has southerly or south-westerly winds blowing from the U.S. This is similar to the 30-year average July wind in this region (Klink, 1999). As shown in Figure 38, the ozone sensitivity fields to CO and VOCs evolve with the wind from the upwind west directions. The close relationship between the sensitivity and the wind vectors is similar to that found in the results in last two sections. Therefore, this section does not focus on analyzing the features associated with horizontal advection. Figure 38 gives the ozone sensitivity fields every 8 hours from 65 to one hour prior to the assumed high ozone episode in the target Toronto-Ottawa square at 17:00 local time (21:00 GMT) July 18.

The sensitivity to carbon monoxide CO is always positive during the whole simulation peiod, but the magnitude is very small. Enhancing CO in the non-zero sensitivity regions slightly leads to enhanced ozone concentration in the T-O region. The influencing region evolves slowly to the T-O area by about 9 hours prior to the occurance of the assumed high ozone event, with the largest sensitivity always associated with lake regions – once ozone is formed due to an increase in CO, ozone over waters remain longer due to low solubility of ozone. Ozone over land is easy to be taken up by materials such as vegetation. In Scenario 1, CO perturbations in distant regions hardly influence ozone levels in east-central Ontario as the calculated sensitivity is almost zero over there. Similar to CO, paraffins in distant locations can not influence the ozone in the T-O region during the simulation period as the sensitivity there is so small as to be neglected. Both

CO and paraffins only reacts with OH with a rate constant of $2.4 \times 10^{-13} cm^3 s^{-1}$ and $8.1 \times 10^{-13} cm^3 s^{-1}$ (these numbers are calculated for 298 K and one atmosphere). Such low reactivity is the reason that CO and paraffins have a small influence on the ozone level changes.

Almost in the whole simulation period, the ozone sensitivity to all VOCs evolving from the upwind northwestern region of the research domain is mainly negative. The area of the non-zero sensitivity region of different VOCs differs due to their different structure and ozone formation pathways. The VOC/NOx ratio in such negative ozone sensitivity regions are large, increasing VOCs in such region can suppress the ozone formation in the pollutant pathways at later times, in this case, the ozone level in east-central Ontario at 17:00 local time July 18 is suppressed. The VOC emissions from anthropogenic activities in northern Ontario is small, therefore the biogenic VOC isoprene emission from vegetation and forest is a possible sink for ozone in east-central Ontario.

The fields of positive ozone sensitivity to all carbon compounds except toluene are found to evolve from the regions in the Midwest U.S. and Ohio Valley to the T-O region. Increasing VOC emissions except toluene in these areas enhances the ozone level in the receptor region by 17:00 local time July 18. Increasing toluene in the polluted U.S. regions mainly causes the ozone level in the T-O region decrease. By one day before the assumed high ozone event, positive sensitivity to toluene starts to appear in the upwind of Toronto and Rochester. The positive sensitivity fields evolve closer to these city areas with time. By 20:00 GMT July 18, increasing toluene near Toronto, Rochester, or Ottawa enhances the ozone formation in the T-O region.

The evolution of the average ozone sensitivity to CO and VOCs in the four sub-regions of the Toronto-Ottawa receptor region is illustrated in Figure 39. The four sub-regions are North Land, Toronto, Ottawa, and the central part of Lake Ontario (Figure 30). Due to the special local circulation around the Great Lakes, the local influence maintains for at least 69 hours, as shown in Figure 39, non-zero sensitivity in some regions can be observed at the start of July 16. The magnitude of the average sensitivity in some sub-regions is zero or small in the beginning of the simulation period such as Ottawa region. The reason is that a portion of the air there at that time might have been blown out of T-O region and never influences the high ozone event. The wind vectors in in Figure 38 show that air around Toronto area is relatively stagnant. Emissions of almost all the selected carbon compounds in Toronto in the morning of July 18 enhance the ozone formation by the late afternoon. Increasing VOCs in highly polluted Toronto enhances ozone formation over the next several hours. The negative ozone sensitivity in Toronto area in first several hours of the simulation period shows that the VOC emissions at that time suppresses the ozone level in the late afternoon in July 18. Increasing VOC in Toronto first enhance the ozone

formation, the enhanced ozone can remove NO through titration process so as to suppress further ozone formation (the negative effect of such newly formed ozone in Toronto area can be seen in Figure 26). The -9H plots in Figure 38 show that by around nine hours before the high ozone event, the air mass that can influence the ozone level in the T-O receptor is mainly over this region. Therefore, increasing carbon compounds locally from around nine hours before the high ozone event will cause local ozone level changes. During this period, increasing all carbon compounds in Ottawa (or upwind Ottawa) can enhance the ozone level here (the positive sensitivity to aldehyde, xylene, and toluene can be seen in Figure 37. Their positive values are averaged out in Figure 39). Increasing VOCs except ethylene and formaldehyde over areas such as the central part of Lake Ontario having large VOC/NOx ratio from morning to one hour before the high ozone event suppresses ozone formation. During this period, such VOC emissions in the northern land area where the VOC/NOx also tends to suppress ozone formation. Although the ozone formation/destruction pathway and the reaction rates of all the carbon compounds are different, the time evolution of the influence of some of them shows similarity in some sub-regions during some period. The reaction list of the chemical mechanism CB4 in Appendix A can tell what reactions are started when adding a specific carbon compound, but further details about more involved reactions and products can only be captured by the modified CMAQ-ADJ. The way in which these 10 selected carbon compounds make contributions to ozone formation in the late afternoon in the 4 locations is summarized in Table 5.

Scenario 3 simulates how the ozone formation in Toronto-Ottawa area responds to CO and VOCs changes in the research area under unusual meteorological conditions. As shown in Figure 38, before 12:00 GMT July 20 these carbon compounds at any place in the research domain cannot influence the high ozone event in the T-O region. The sensitivity of the perturbed ozone change with respect to these variables is then zero. Under such strong wind background, if increasing CO or VOCs 33 hours before the target time, they are likely be blown out of the T-O region, or cannot reach T-O region by the target time. One day before the high ozone event (20:00 GMT July 20), non-zero ozone sensitivity to all the carbon compounds in northern Ontario appears. If changing CO or VOCs emissions in these regions, the ozone level in east-central Ontario will either be enhanced or suppressed a little as a response. The sensitivity fields evolve quickly to the downwind direction toward the target T-O square. By 04:00 GMT July 21, almost all the regions in the upwind direction of the T-O region in the northern Ontario are covered by non-zero sensitivity. Compared with the others, the influencing area of CO and paraffins is small due to the low reactivity of their reactions. The ozone sensitivity to formaldehyde is also small. The magnitude of the influence of these three chemicals on the T-O ozone level is smaller than

the others at all times, similar to the results in Scenario 1. CO emissions in the upwind direction always slightly enhance the ozone level in the downwind T-O region. The increase in formaldehyde emission in the northwest part of the non-zero sensitivity regions slightly suppresses the ozone formation in the receptor square. The largest positive sensitivity values correspond to Lake Ontario. Based on the plots in Figure 38, by one hour before the assumed high ozone event, these three carbon compounds emitted to the lake area near Toronto have the largest influence (enhance) to the ozone level in the next hour than those emitted to other places. This area has the smallest VOC/NOx ratio, increasing VOCs and CO in such place causes enhanced ozone formation.

Of the other 6 VOCs that have larger impacts on the assumed high ozone event in the receptor region, the -17H to -9H sensitivity fields in Figure 38 show that increasing these VOCs (ethylene) in the upwind regions in northern Ontario at -17H and -9H is likely to suppress the ozone formation in the T-O region. One hour before the target time, in the southern area of the T-O region (where the VOC/NOx ratios are large), the ozone sensitivity to ethylene, isoprene, olefins, and xylene, and toluene is mostly positive (except to toluene over central Lake Ontario), which means that increasing the emission of these VOCs causes local ozone level to increase in one hour. For aldehydes, only near the very small VOC/NOx ratio locations Toronto and Rochester, enhanced aldehydes cab cause enhanced ozone formation in the next hour. For most places where the VOC/NOx ratio is larger than 6, increased aldehydes emission will cause a slight decrease of local ozone concentrations.

The average ozone sensitivity in the same four sub-regions as those used in Scenario 1 to individual carbon compounds are also calculated for Scenario 3. A detailed analysis is not made because the wind in Scenario 3 is so strong that any pollutants in the receptor region are blown out of the region very quickly. For the same species, the average sensitivity in Scenario 1 is about one order of magnitude larger than that in Scenario 3. Since the reactions rates for VOC reactions in CB4 are temperature-dependent, a larger portion of VOCs is transformed to ozone in the next several hours at high tempeture conditions than at lower temperature conditions.

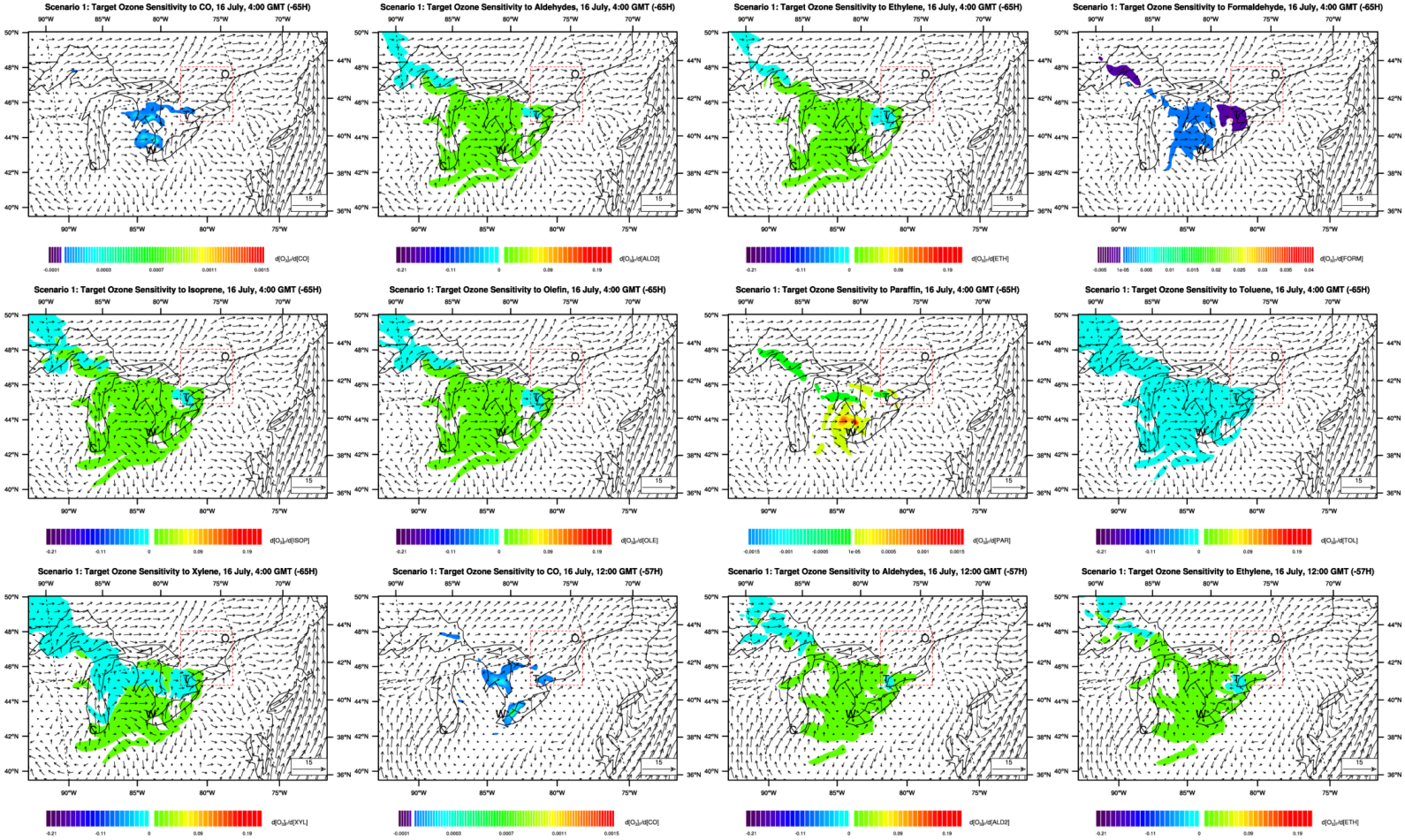
Scenario 1: Target Ozone Sensitivity to CO, 16 July, 4:00 GMT (-65H)
Scenario 1: Target Ozone Sensitivity to Aldehydes, 16 July, 4:00 GMT (-65H)
Scenario 1: Target Ozone Sensitivity to Ethylene, 16 July, 4:00 GMT (-65H)
Scenario 1: Target Ozone Sensitivity to Formaldehyde, 16 July, 4:00 GMT (-65H)
Scenario 1: Target Ozone Sensitivity to Isoprene, 16 July, 4:00 GMT (-65H)
Scenario 1: Target Ozone Sensitivity to Olefin, 16 July, 4:00 GMT (-65H)
Scenario 1: Target Ozone Sensitivity to Paraffin, 16 July, 4:00 GMT (-65H)
Scenario 1: Target Ozone Sensitivity to Toluene, 16 July, 4:00 GMT (-65H)
Scenario 1: Target Ozone Sensitivity to Xylene, 16 July, 4:00 GMT (-65H)
Scenario 1: Target Ozone Sensitivity to CO, 16 July, 12:00 GMT (-57H)
Scenario 1: Target Ozone Sensitivity to Aldehydes, 16 July, 12:00 GMT (-57H)
Scenario 1: Target Ozone Sensitivity to Ethylene, 16 July, 12:00 GMT (-57H)

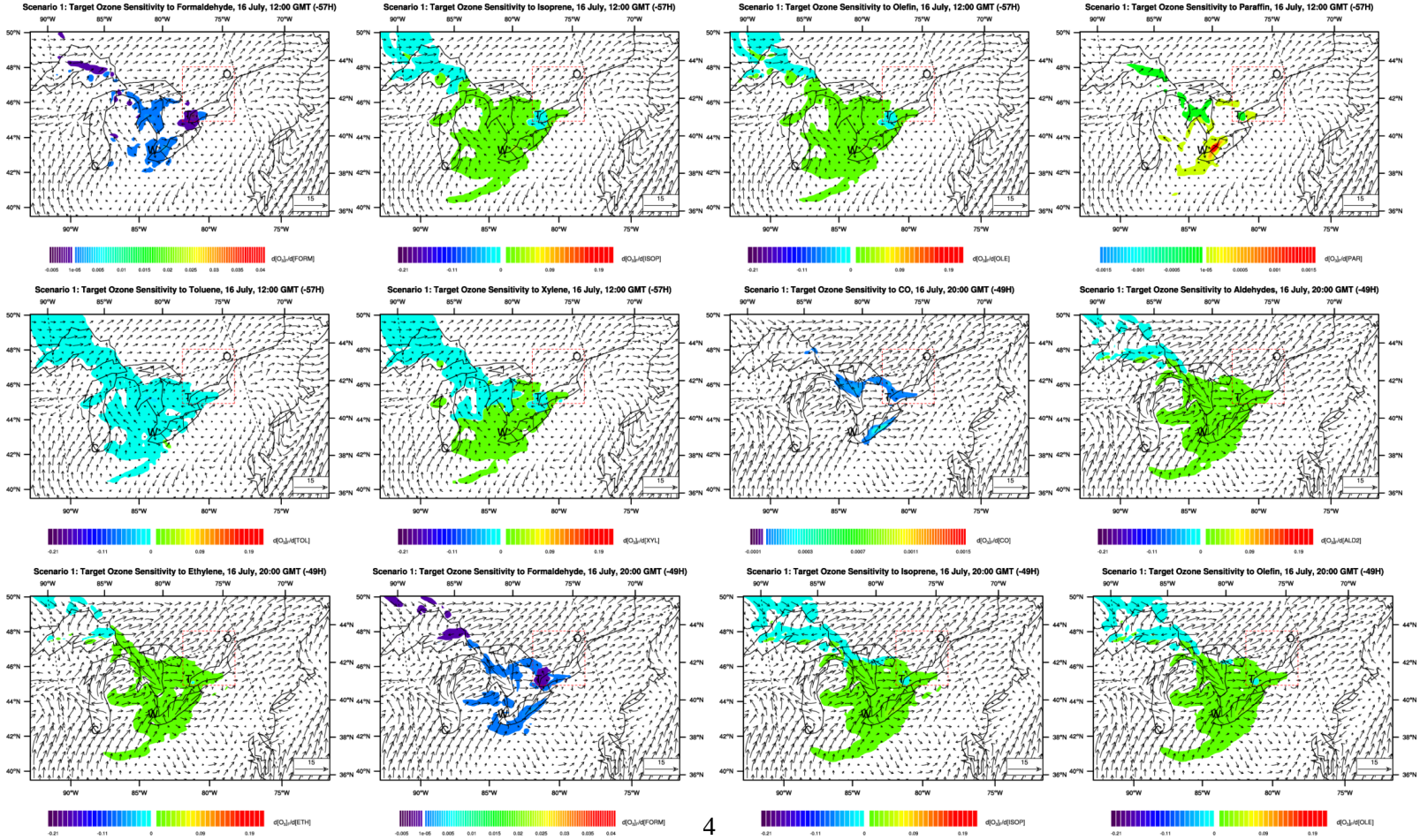
Scenario 1: Target Ozone Sensitivity to Formaldehyde, 16 July, 12:00 GMT (-57H)
Scenario 1: Target Ozone Sensitivity to Isoprene, 16 July, 12:00 GMT (-57H)
Scenario 1: Target Ozone Sensitivity to Olefin, 16 July, 12:00 GMT (-57H)
Scenario 1: Target Ozone Sensitivity to Paraffin, 16 July, 12:00 GMT (-57H)
Scenario 1: Target Ozone Sensitivity to Toluene, 16 July, 12:00 GMT (-57H)
Scenario 1: Target Ozone Sensitivity to Xylene, 16 July, 12:00 GMT (-57H)
Scenario 1: Target Ozone Sensitivity to CO, 16 July, 20:00 GMT (-49H)
Scenario 1: Target Ozone Sensitivity to Aldehydes, 16 July, 20:00 GMT (-49H)
Scenario 1: Target Ozone Sensitivity to Ethylene, 16 July, 20:00 GMT (-49H)
Scenario 1: Target Ozone Sensitivity to Formaldehyde, 16 July, 20:00 GMT (-49H)
Scenario 1: Target Ozone Sensitivity to Isoprene, 16 July, 20:00 GMT (-49H)
Scenario 1: Target Ozone Sensitivity to Olefin, 16 July, 20:00 GMT (-49H)

4

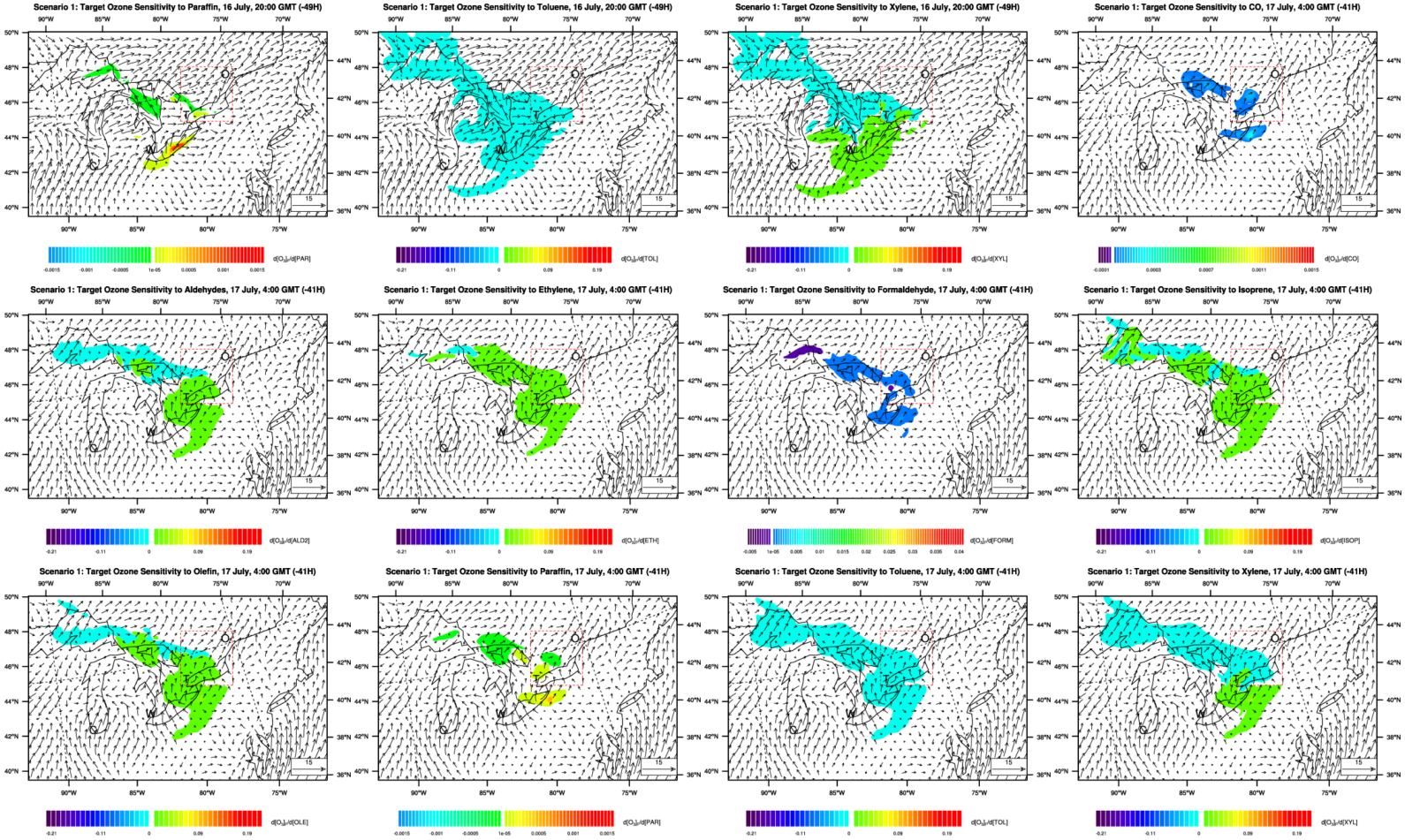
Scenario 1: Target Ozone Sensitivity to Paraffin, 16 July, 20:00 GMT (-49H)
Scenario 1: Target Ozone Sensitivity to Toluene, 16 July, 20:00 GMT (-49H)
Scenario 1: Target Ozone Sensitivity to Xylene, 16 July, 20:00 GMT (-49H)
Scenario 1: Target Ozone Sensitivity to CO, 17 July, 4:00 GMT (-41H)
Scenario 1: Target Ozone Sensitivity to Aldehydes, 17 July, 4:00 GMT (-41H)
Scenario 1: Target Ozone Sensitivity to Ethylene, 17 July, 4:00 GMT (-41H)
Scenario 1: Target Ozone Sensitivity to Formaldehyde, 17 July, 4:00 GMT (-41H)
Scenario 1: Target Ozone Sensitivity to Isoprene, 17 July, 4:00 GMT (-41H)
Scenario 1: Target Ozone Sensitivity to Olefin, 17 July, 4:00 GMT (-41H)
Scenario 1: Target Ozone Sensitivity to Paraffin, 17 July, 4:00 GMT (-41H)
Scenario 1: Target Ozone Sensitivity to Toluene, 17 July, 4:00 GMT (-41H)
Scenario 1: Target Ozone Sensitivity to Xylene, 17 July, 4:00 GMT (-41H)

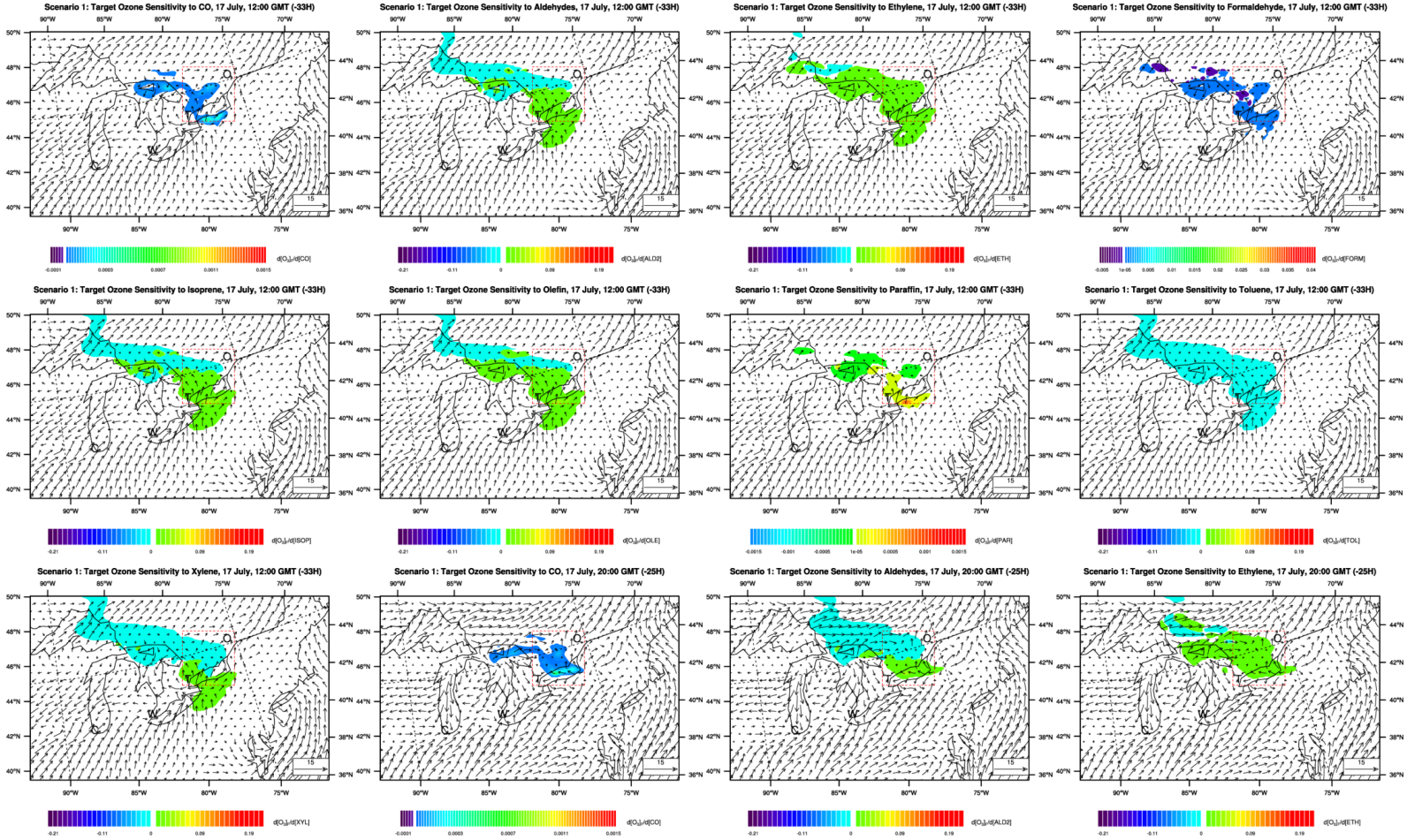
Scenario 1: Target Ozone Sensitivity to CO, 17 July, 12:00 GMT (-33H)
Scenario 1: Target Ozone Sensitivity to Aldehydes, 17 July, 12:00 GMT (-33H)
Scenario 1: Target Ozone Sensitivity to Ethylene, 17 July, 12:00 GMT (-33H)
Scenario 1: Target Ozone Sensitivity to Formaldehyde, 17 July, 12:00 GMT (-33H)
Scenario 1: Target Ozone Sensitivity to Isoprene, 17 July, 12:00 GMT (-33H)
Scenario 1: Target Ozone Sensitivity to Olefin, 17 July, 12:00 GMT (-33H)
Scenario 1: Target Ozone Sensitivity to Paraffin, 17 July, 12:00 GMT (-33H)
Scenario 1: Target Ozone Sensitivity to Toluene, 17 July, 12:00 GMT (-33H)
Scenario 1: Target Ozone Sensitivity to Xylene, 17 July, 12:00 GMT (-33H)
Scenario 1: Target Ozone Sensitivity to CO, 17 July, 20:00 GMT (-25H)
Scenario 1: Target Ozone Sensitivity to Aldehydes, 17 July, 20:00 GMT (-25H)
Scenario 1: Target Ozone Sensitivity to Ethylene, 17 July, 20:00 GMT (-25H)

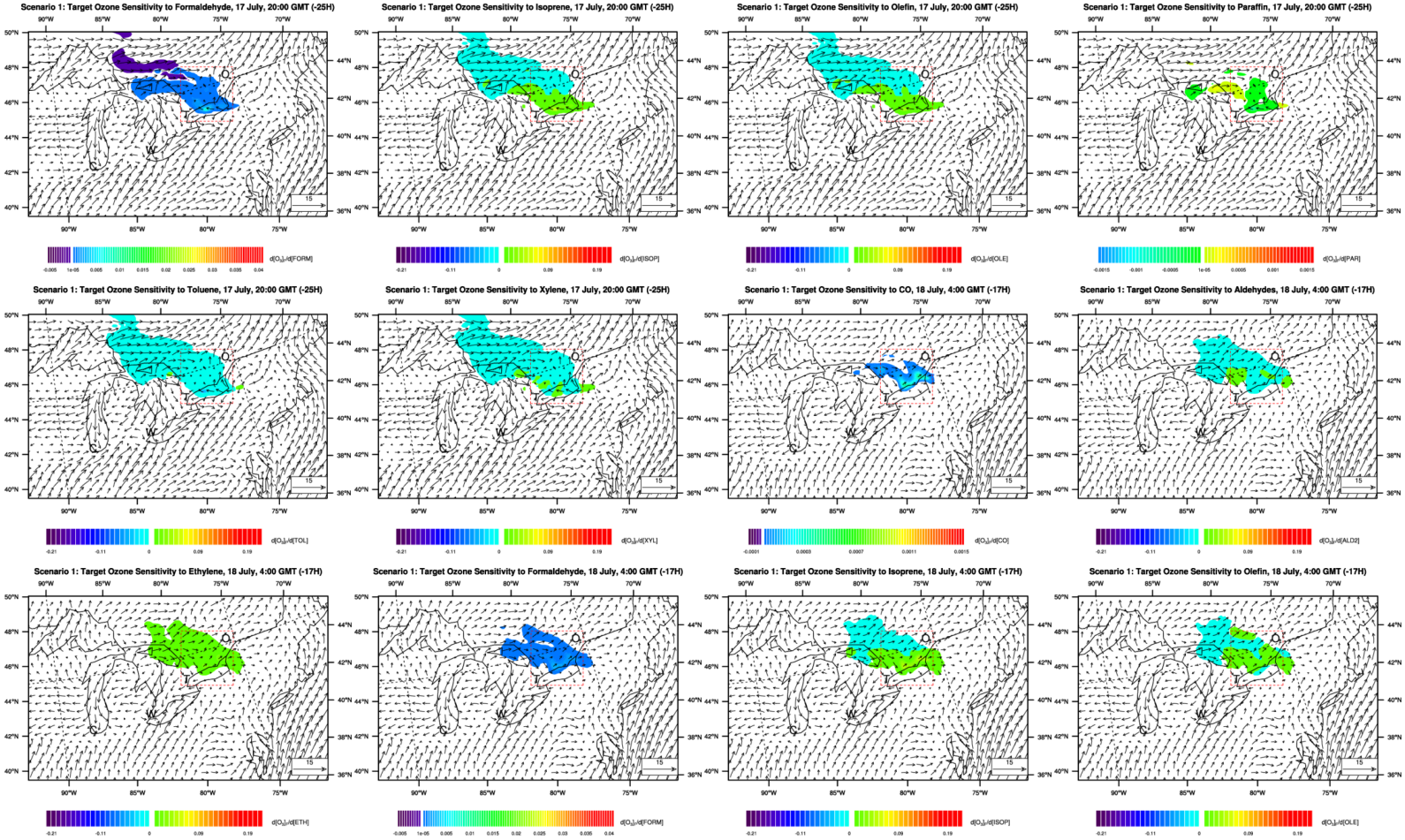
Scenario 1: Target Ozone Sensitivity to Formaldehyde, 17 July, 20:00 GMT (-25H)
Scenario 1: Target Ozone Sensitivity to Isoprene, 17 July, 20:00 GMT (-25H)
Scenario 1: Target Ozone Sensitivity to Olefin, 17 July, 20:00 GMT (-25H)
Scenario 1: Target Ozone Sensitivity to Paraffin, 17 July, 20:00 GMT (-25H)
Scenario 1: Target Ozone Sensitivity to Toluene, 17 July, 20:00 GMT (-25H)
Scenario 1: Target Ozone Sensitivity to Xylene, 17 July, 20:00 GMT (-25H)
Scenario 1: Target Ozone Sensitivity to CO, 18 July, 4:00 GMT (-17H)
Scenario 1: Target Ozone Sensitivity to Aldehydes, 18 July, 4:00 GMT (-17H)
Scenario 1: Target Ozone Sensitivity to Ethylene, 18 July, 4:00 GMT (-17H)
Scenario 1: Target Ozone Sensitivity to Formaldehyde, 18 July, 4:00 GMT (-17H)
Scenario 1: Target Ozone Sensitivity to Isoprene, 18 July, 4:00 GMT (-17H)
Scenario 1: Target Ozone Sensitivity to Olefin, 18 July, 4:00 GMT (-17H)

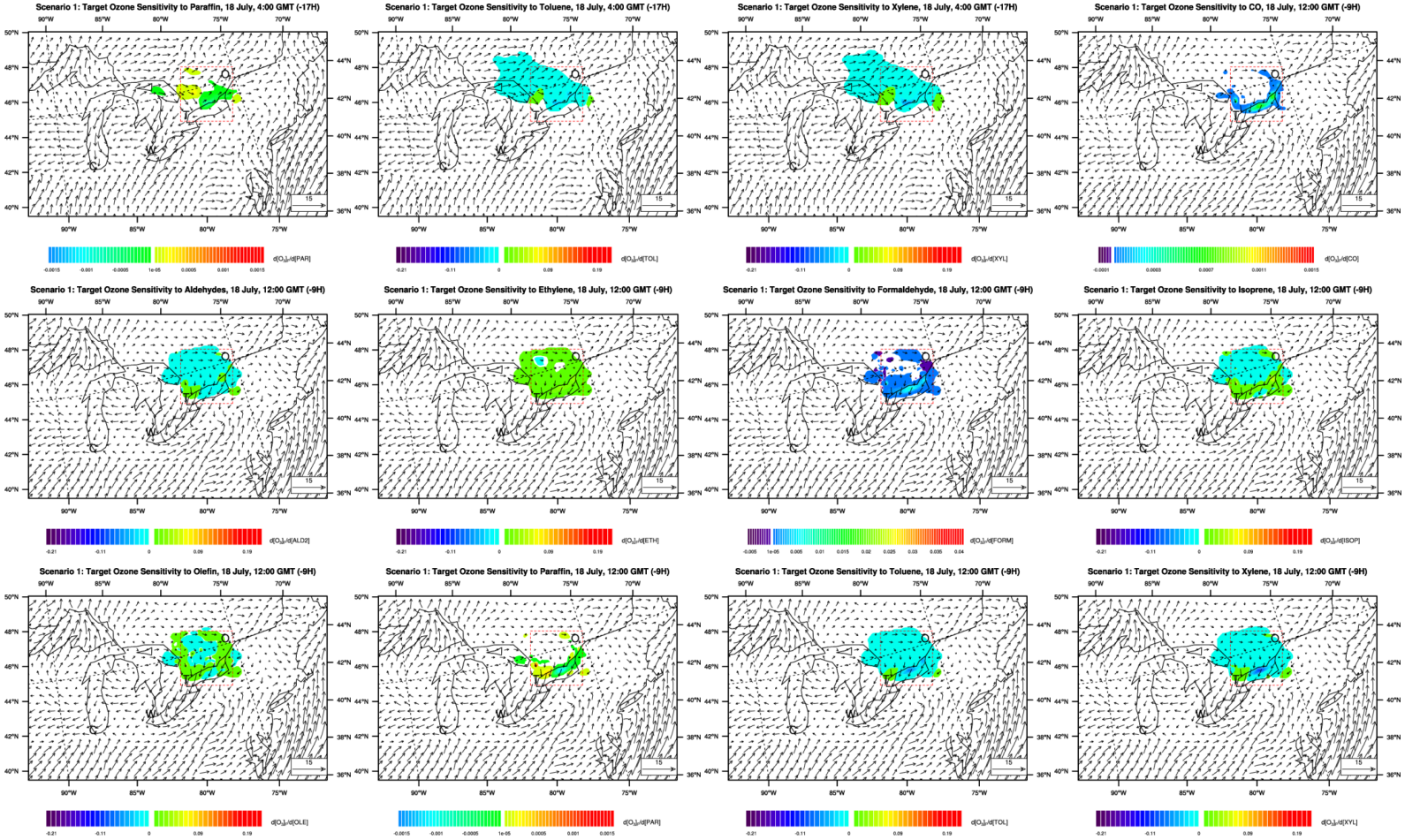
Scenario 1: Target Ozone Sensitivity to Paraffin, 18 July, 4:00 GMT (-17H)
Scenario 1: Target Ozone Sensitivity to Toluene, 18 July, 4:00 GMT (-17H)
Scenario 1: Target Ozone Sensitivity to Xylene, 18 July, 4:00 GMT (-17H)
Scenario 1: Target Ozone Sensitivity to CO, 18 July, 12:00 GMT (-9H)
Scenario 1: Target Ozone Sensitivity to Aldehydes, 18 July, 12:00 GMT (-9H)
Scenario 1: Target Ozone Sensitivity to Ethylene, 18 July, 12:00 GMT (-9H)
Scenario 1: Target Ozone Sensitivity to Formaldehyde, 18 July, 12:00 GMT (-9H)
Scenario 1: Target Ozone Sensitivity to Isoprene, 18 July, 12:00 GMT (-9H)
Scenario 1: Target Ozone Sensitivity to Olefin, 18 July, 12:00 GMT (-9H)
Scenario 1: Target Ozone Sensitivity to Paraffin, 18 July, 12:00 GMT (-9H)
Scenario 1: Target Ozone Sensitivity to Toluene, 18 July, 12:00 GMT (-9H)
Scenario 1: Target Ozone Sensitivity to Xylene, 18 July, 12:00 GMT (-9H)

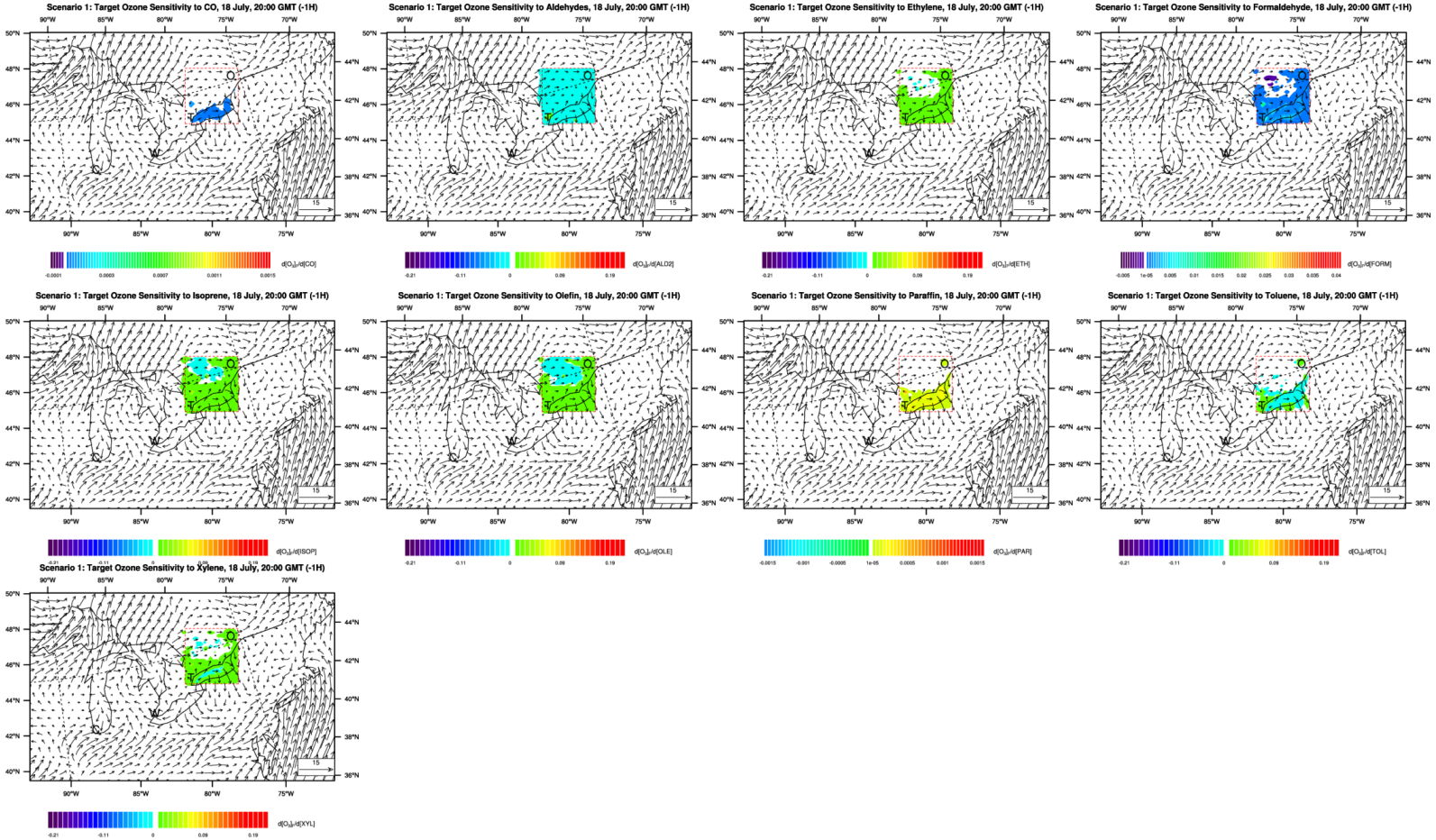

Figure 37. Scenario 1: target ozone sensitivity to CO and 8 kinds VOCs in the 69 hours before the assumed high ozone episode in the T-O region at 21:00 GMT July 18. Plots are presented every 8 hours. The 8 VOCs are aldehyde, formaldehyde, ethylene, isoprene, oflefin, paraffins, toluene, and ethylene. White colour represents sensitivity values between -0.00001 ppm/ppm and +0.00001 ppm/ppm. The vectors are horizontal winds calculated by MM5, in m/s.

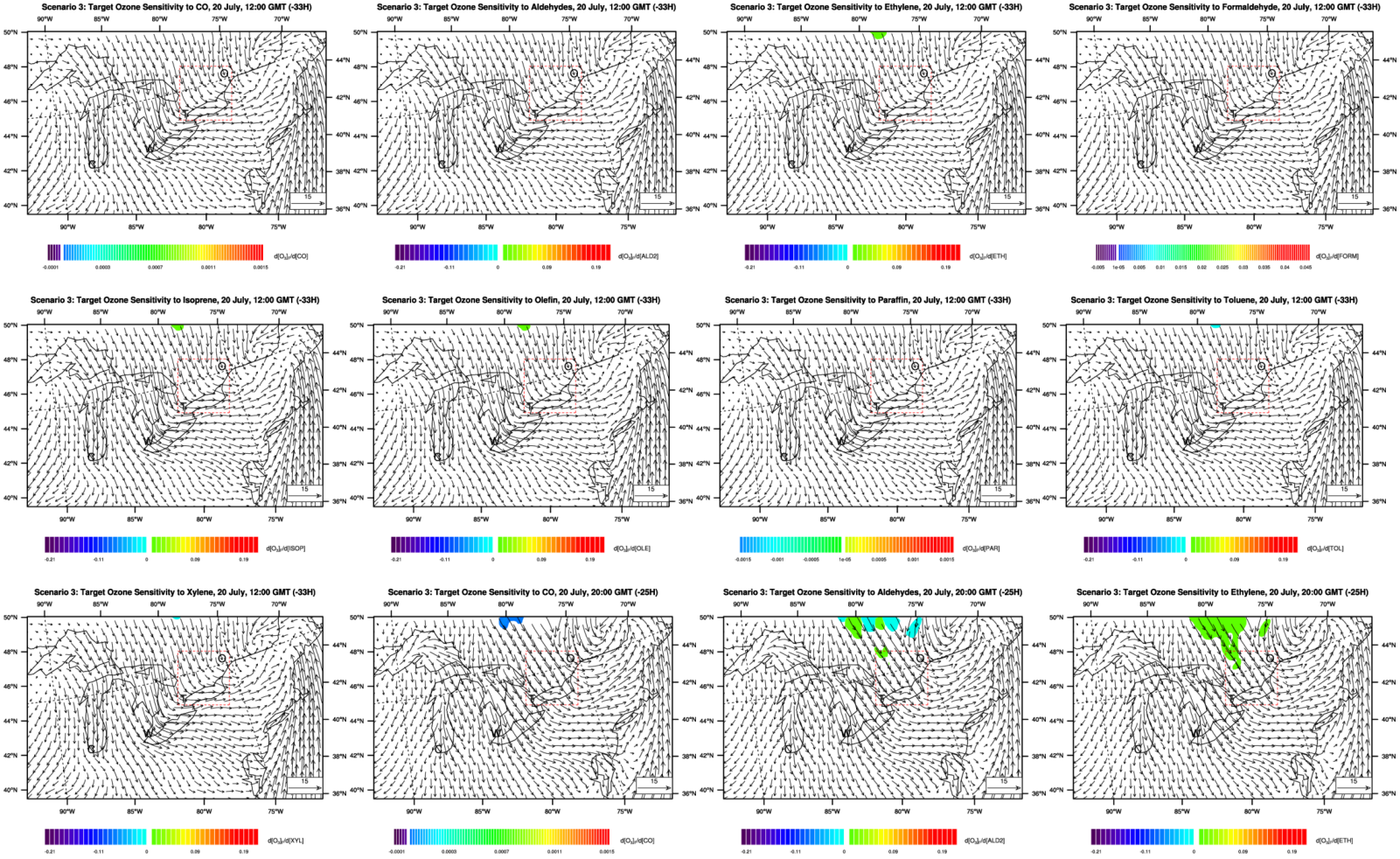
Scenario 3: Target Ozone Sensitivity to CO, 20 July, 12:00 GMT (-33H)
Scenario 3: Target Ozone Sensitivity to Aldehydes, 20 July, 12:00 GMT (-33H)
Scenario 3: Target Ozone Sensitivity to Ethylene, 20 July, 12:00 GMT (-33H)
Scenario 3: Target Ozone Sensitivity to Formaldehyde, 20 July, 12:00 GMT (-33H)
Scenario 3: Target Ozone Sensitivity to Isoprene, 20 July, 12:00 GMT (-33H)
Scenario 3: Target Ozone Sensitivity to Olefin, 20 July, 12:00 GMT (-33H)
Scenario 3: Target Ozone Sensitivity to Paraffin, 20 July, 12:00 GMT (-33H)
Scenario 3: Target Ozone Sensitivity to Toluene, 20 July, 12:00 GMT (-33H)
Scenario 3: Target Ozone Sensitivity to Xylene, 20 July, 12:00 GMT (-33H)
Scenario 3: Target Ozone Sensitivity to CO, 20 July, 20:00 GMT (-25H)
Scenario 3: Target Ozone Sensitivity to Aldehydes, 20 July, 20:00 GMT (-25H)
Scenario 3: Target Ozone Sensitivity to Ethylene, 20 July, 20:00 GMT (-25H)

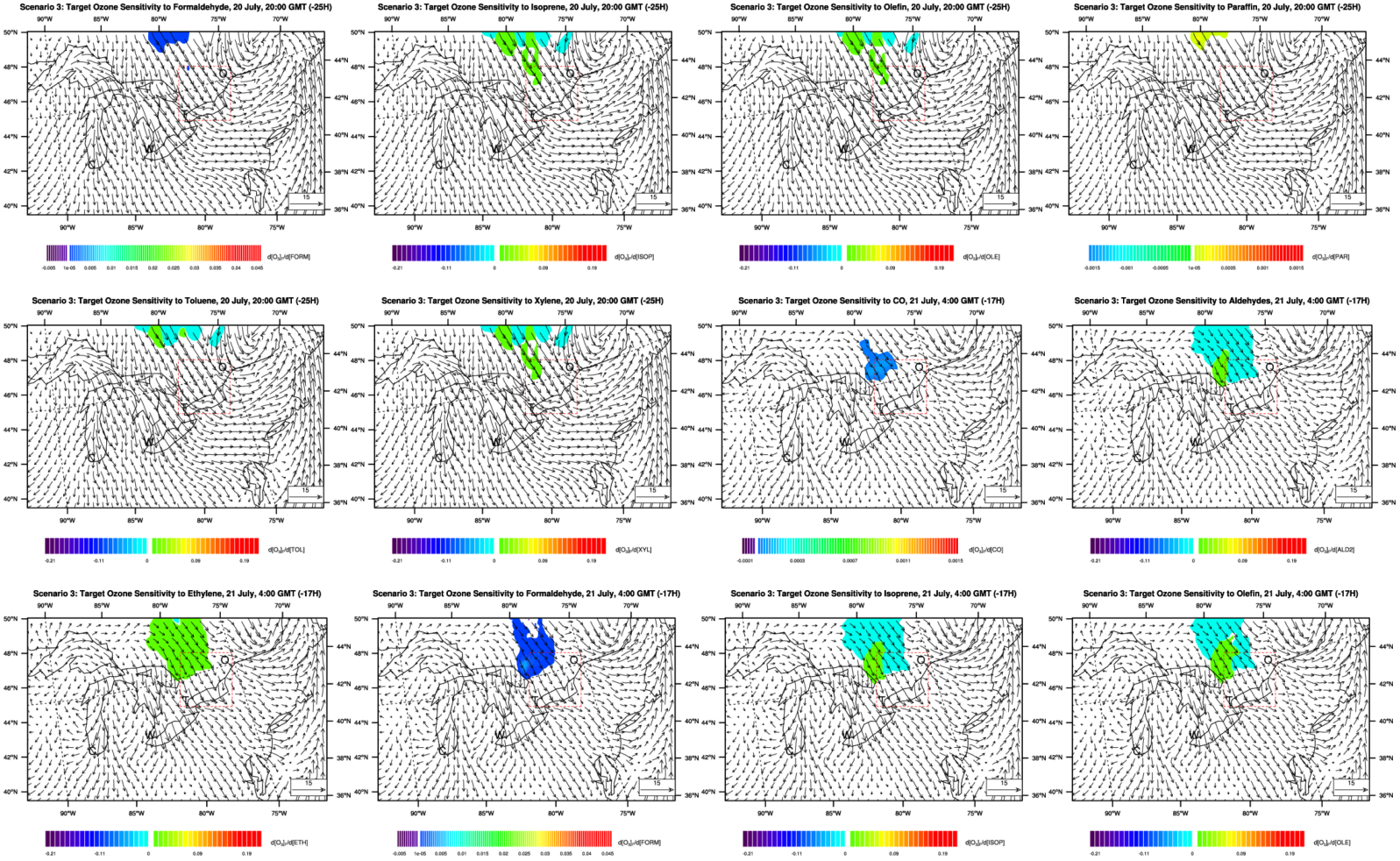
Scenario 3: Target Ozone Sensitivity to Formaldehyde, 20 July, 20:00 GMT (-25H)
Scenario 3: Target Ozone Sensitivity to Isoprene, 20 July, 20:00 GMT (-25H)
Scenario 3: Target Ozone Sensitivity to Olefin, 20 July, 20:00 GMT (-25H)
Scenario 3: Target Ozone Sensitivity to Paraffin, 20 July, 20:00 GMT (-25H)
Scenario 3: Target Ozone Sensitivity to Toluene, 20 July, 20:00 GMT (-25H)
Scenario 3: Target Ozone Sensitivity to Xylene, 20 July, 20:00 GMT (-25H)
Scenario 3: Target Ozone Sensitivity to CO, 21 July, 4:00 GMT (-17H)
Scenario 3: Target Ozone Sensitivity to Aldehydes, 21 July, 4:00 GMT (-17H)
Scenario 3: Target Ozone Sensitivity to Ethylene, 21 July, 4:00 GMT (-17H)
Scenario 3: Target Ozone Sensitivity to Formaldehyde, 21 July, 4:00 GMT (-17H)
Scenario 3: Target Ozone Sensitivity to Isoprene, 21 July, 4:00 GMT (-17H)
Scenario 3: Target Ozone Sensitivity to Olefin, 21 July, 4:00 GMT (-17H)

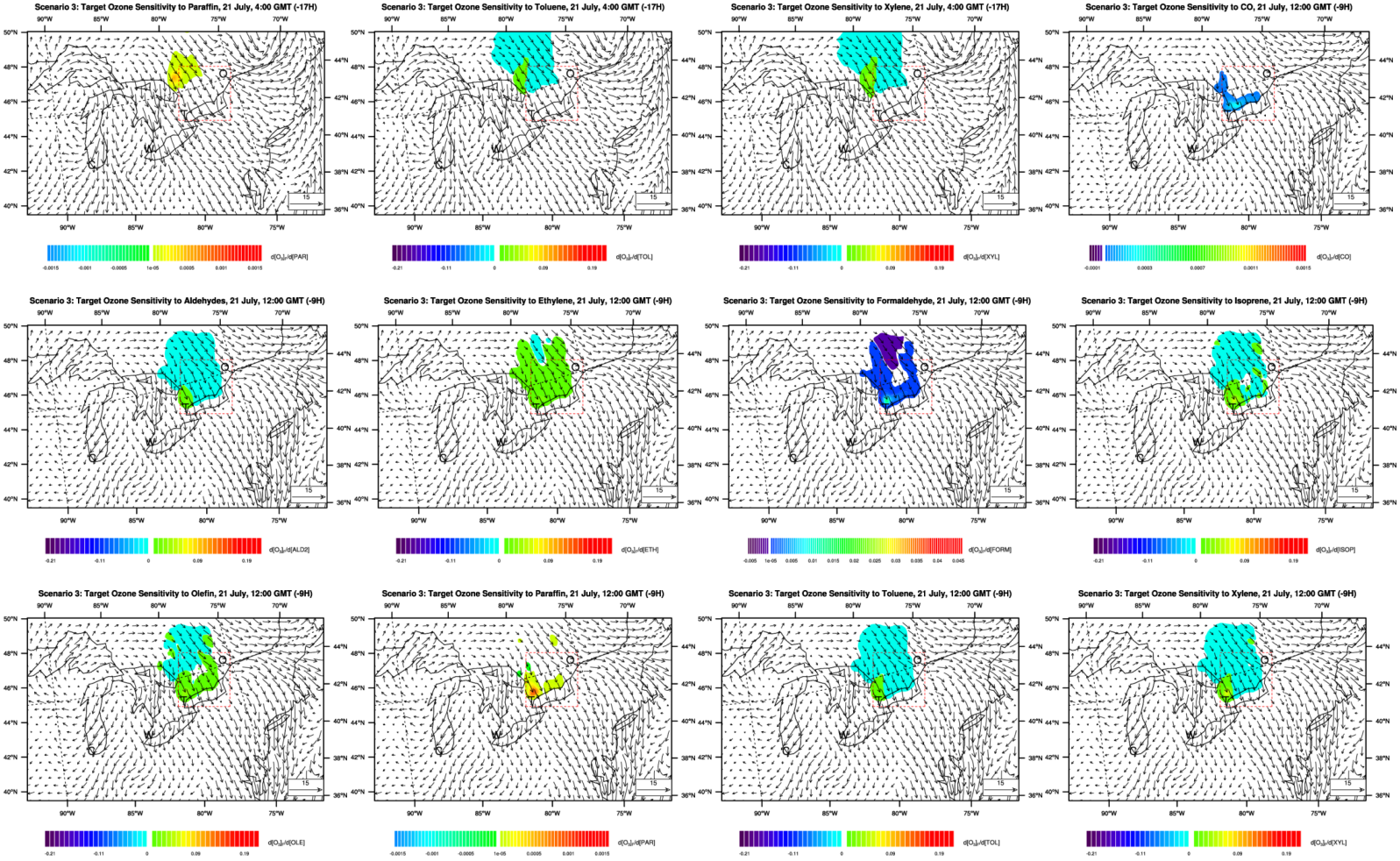
Scenario 3: Target Ozone Sensitivity to Paraffin, 21 July, 4:00 GMT (-17H)
Scenario 3: Target Ozone Sensitivity to Toluene, 21 July, 4:00 GMT (-17H)
Scenario 3: Target Ozone Sensitivity to Xylene, 21 July, 4:00 GMT (-17H)
Scenario 3: Target Ozone Sensitivity to CO, 21 July, 12:00 GMT (-9H)
Scenario 3: Target Ozone Sensitivity to Aldehydes, 21 July, 12:00 GMT (-9H)
Scenario 3: Target Ozone Sensitivity to Ethylene, 21 July, 12:00 GMT (-9H)
Scenario 3: Target Ozone Sensitivity to Formaldehyde, 21 July, 12:00 GMT (-9H)
Scenario 3: Target Ozone Sensitivity to Isoprene, 21 July, 12:00 GMT (-9H)
Scenario 3: Target Ozone Sensitivity to Olefin, 21 July, 12:00 GMT (-9H)
Scenario 3: Target Ozone Sensitivity to Paraffin, 21 July, 12:00 GMT (-9H)
Scenario 3: Target Ozone Sensitivity to Toluene, 21 July, 12:00 GMT (-9H)
Scenario 3: Target Ozone Sensitivity to Xylene, 21 July, 12:00 GMT (-9H)

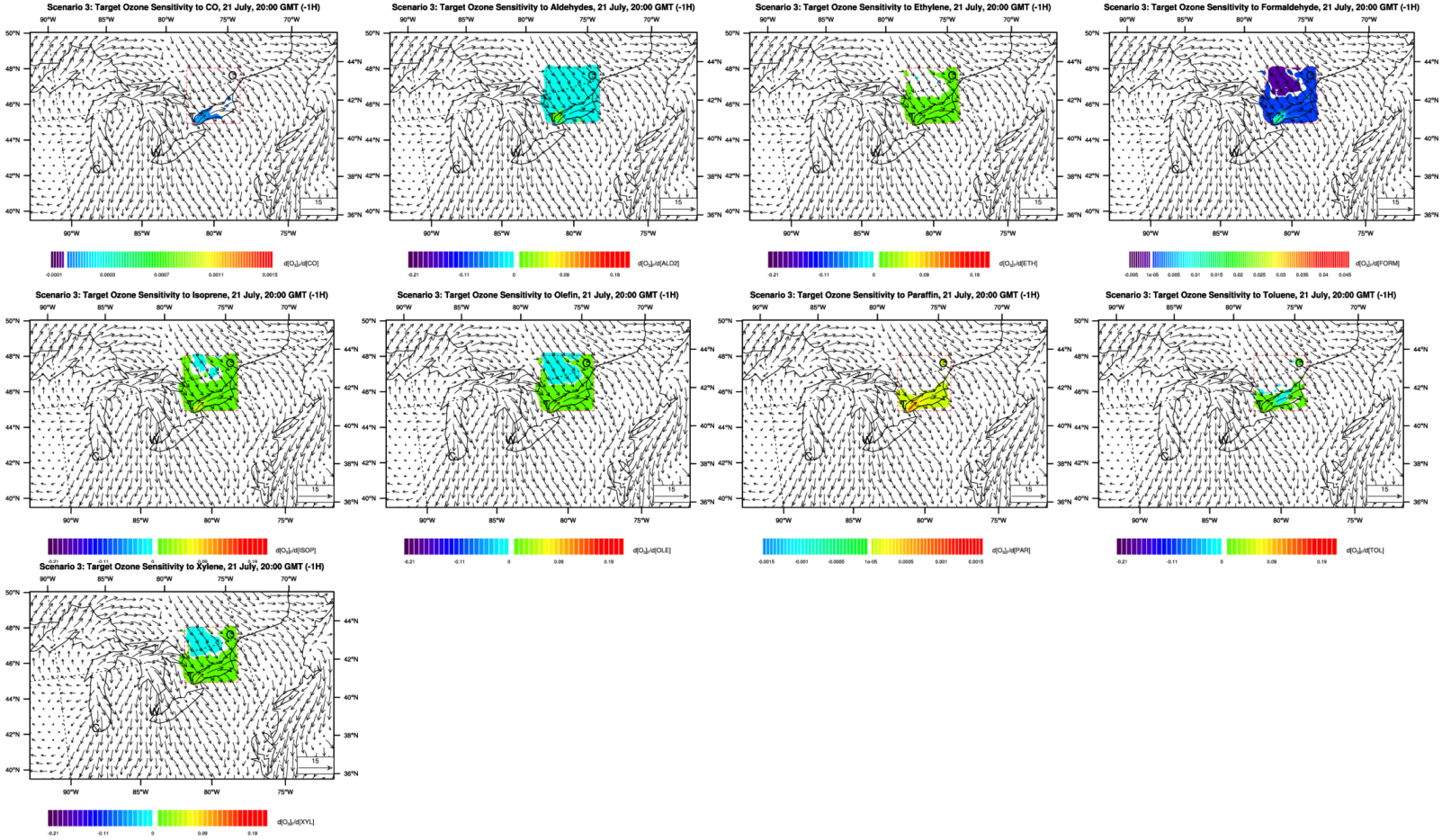

Figure 38. Scenario 3: target ozone sensitivity to CO and 8 kinds VOCs in the 69 hours before the assumed high ozone episode in the W-T region at 21:00 GMT July 21. Plots are presented every 8 hours. The 8 VOCs are aldehyde, formaldehyde, ethylene, isoprene, oflefin, paraffins, toluene, and ethylene. White colour represents sensitivity values between -0.00001 ppm/ppm and +0.00001 ppm/ppm. The vectors are horizontal winds calculated by MM5, in m/s.

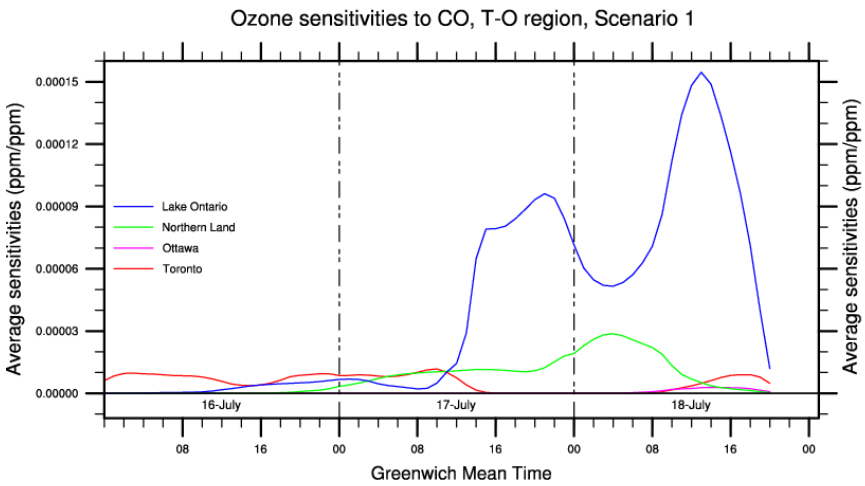
Ozone sensitivities to CO, T-O region, Scenario 1
Average sensitivities (ppm/ppm)
0.00015
0.00012
0.00009
0.00006
0.00003
0.00000
Lake Ontario
Northern Land
Ottawa
Toronto
16-July
17-July
18-July
08
16
00
Greenwich Mean Time

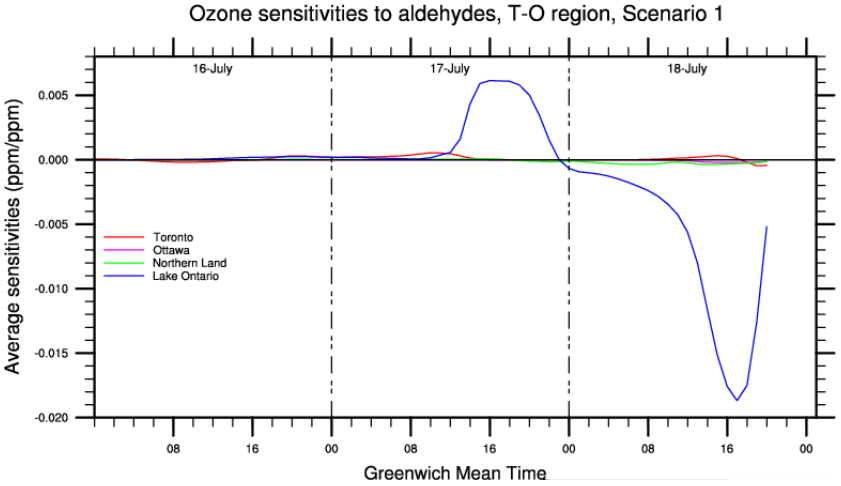
Ozone sensitivities to aldehydes, T-O region, Scenario 1
Average sensitivities (ppm/ppm)
0.005
0.000
-0.005
-0.010
-0.015
-0.020
16-July
17-July
18-July
Toronto
Ottawa
Northern Land
Lake Ontario
08
16
00
Greenwich Mean Time

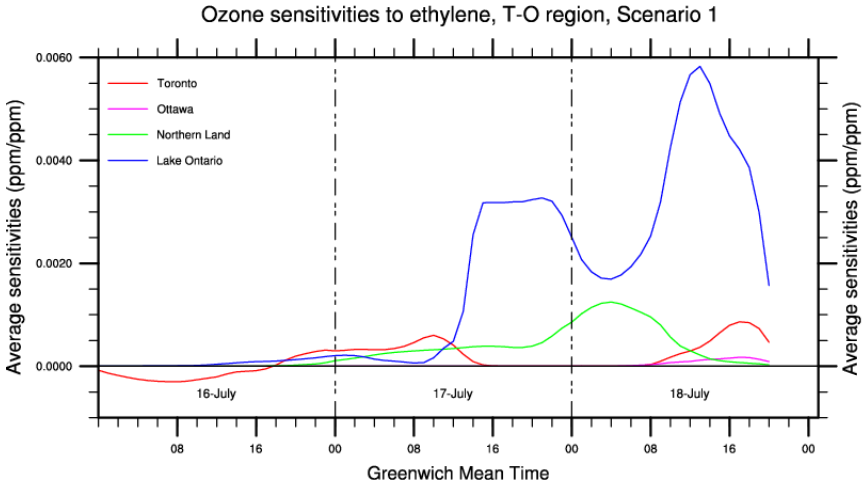
Ozone sensitivities to ethylene, T-O region, Scenario 1
Average sensitivities (ppm/ppm)
0.0060
0.0040
0.0020
0.0000
Toronto
Ottawa
Northern Land
Lake Ontario
16-July
17-July
18-July
08
16
00
Greenwich Mean Time

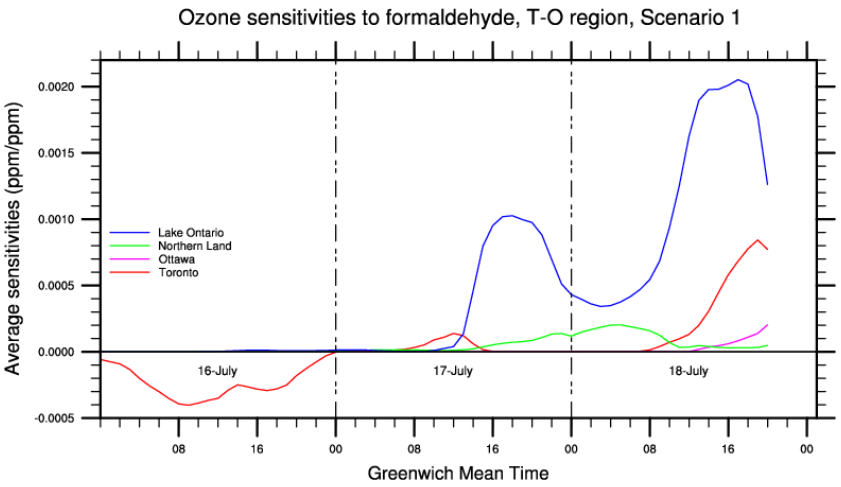
Ozone sensitivities to formaldehyde, T-O region, Scenario 1
Average sensitivities (ppm/ppm)
0.0020
0.0015
0.0010
0.0005
0.0000
-0.0005
Lake Ontario
Northern Land
Ottawa
Toronto
16-July
17-July
18-July
08
16
00
Greenwich Mean Time

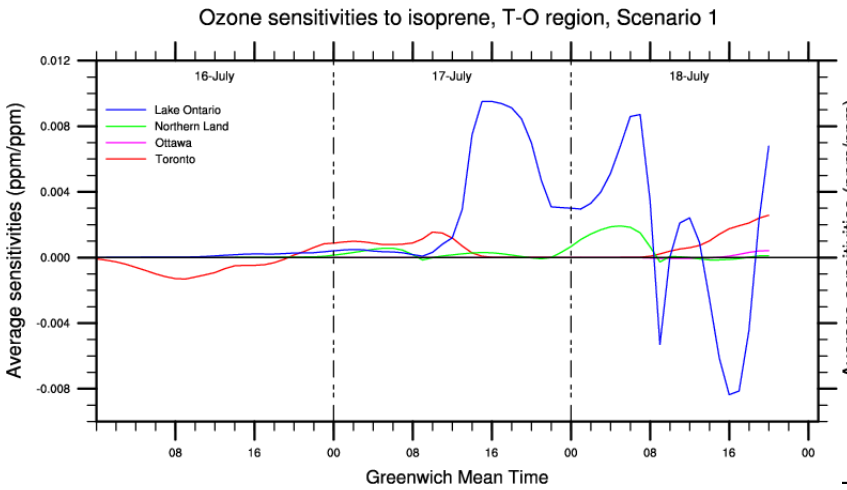
Ozone sensitivities to isoprene, T-O region, Scenario 1
Average sensitivities (ppm/ppm)
0.012
0.008
0.004
0.000
-0.004
-0.008
16-July
17-July
18-July
Lake Ontario
Northern Land
Ottawa
Toronto
08
16
00
Greenwich Mean Time

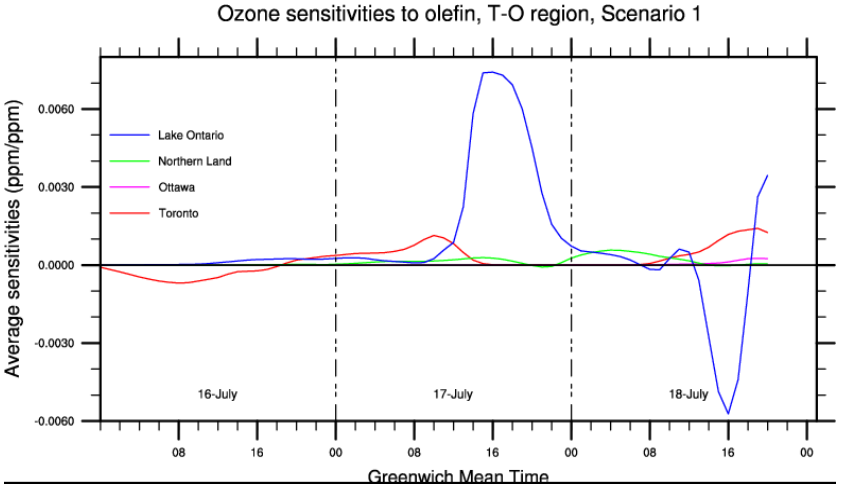
Ozone sensitivities to olefin, T-O region, Scenario 1
Average sensitivities (ppm/ppm)
0.0060
0.0030
0.0000
-0.0030
-0.0060
Lake Ontario
Northern Land
Ottawa
Toronto
16-July
17-July
18-July
08
16
00
Greenwich Mean Time

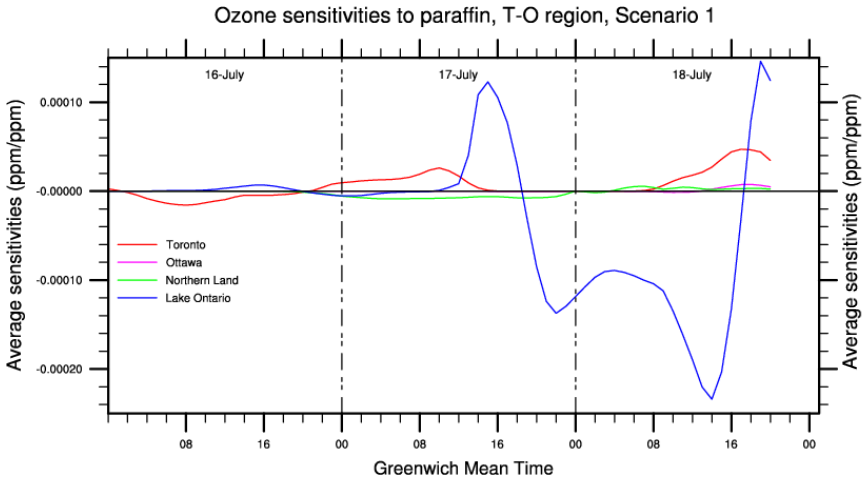
Ozone sensitivities to paraffin, T-O region, Scenario 1
Average sensitivities (ppm/ppm)
0.00010
-0.00000
-0.00010
-0.00020
16-July
17-July
18-July
Toronto
Ottawa
Northern Land
Lake Ontario
08
16
00
Greenwich Mean Time

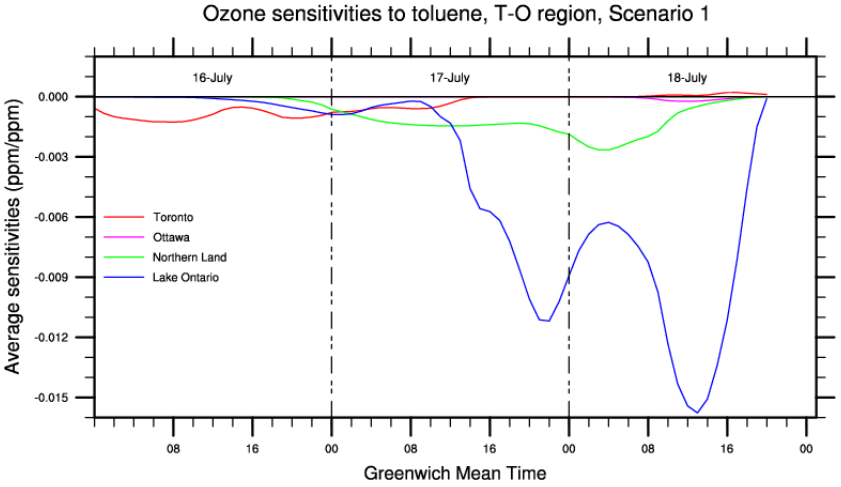
Ozone sensitivities to toluene, T-O region, Scenario 1
Average sensitivities (ppm/ppm)
0.000
-0.003
-0.006
-0.009
-0.012
-0.015
16-July
17-July
18-July
Toronto
Ottawa
Northern Land
Lake Ontario
08
16
00
Greenwich Mean Time

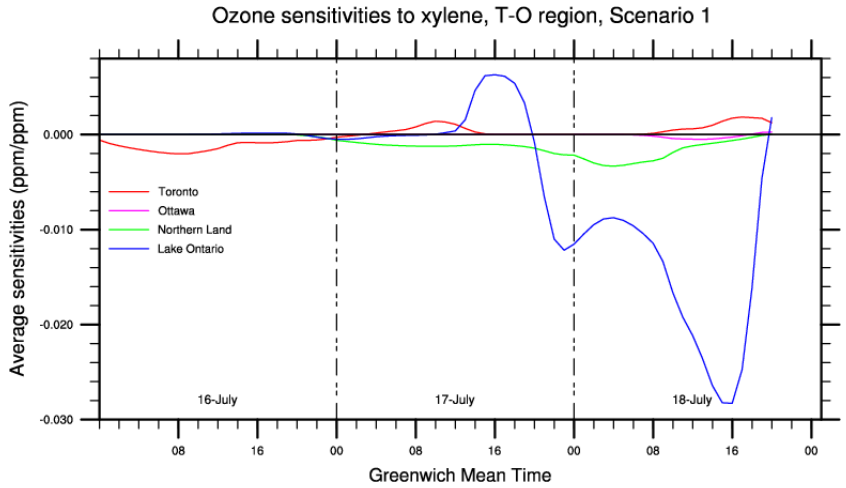

Figure 39. Time series of the average ozone sensitivity to CO and 8 VOC changes in 4 sub-regions of the Toronto-Ottawa region for Scenario 1. The 4 local regions are Toronto, Ottawa, northern land area, and central part of Lake Ontario.

Table 5. How a morning release of CO or VOCs enhances (+) or suppresses (-) local ozone formation at 17:00 local time in the 4 sub-regions of east-central Ontario in Scenario 1.

	CO	Aldehyde	Ethylene	Formaldehyde	Isoprene	Olefins	Paraffins	Toluene	Xylene
Toronto	+	+	+	+	+	+	+	+	+
Ottawa	+	+	+	+	+	+	+	+	+
Northern Land	+	-	+	+	+	+	-	-	-
Lake Ontario	+	-	+	+	-	-	+	-	-

5.3.3.4 Summary

The modified CMAQ-ADJ is used to run three scenarios studying the sensitivity of ozone level changes in east-central Ontario (Toronto-Ottawa region) with respect to precursors. The success of this approach leads credence to the validity of the modified CMAQ-ADJ model. The identification of the distinct features over different underlying surfaces associated with different VOC/NOx regimes for the 69-hour period further proves the current treatment of the advection and chemistry time-step is appropriate.

Under typical summer meteorological conditions, the ozone in east-central Ontario is sensitive to the pre-existing ozone in the upwind north direction of the T-O region. The ozone in this area can be advected to east-central Ontario to increase the ozone level there. Unlike the case in southwestern Ontario (W-T region), ozone changes in the Midwest U.S. and Ohio Valley does not influences the ozone level that much in east-central Ontario. NO emission in this industrialized region of the U.S. enhances the ozone formation in the T-O region 2 day to 69 hours later. Ozone level in east-central Ontario within the next 69 hours can be enhanced by increasing NO emission in northern Ontario as well. The calculation of the sensitivity to VOCs shows that except toluene, the other 7 VOC emissions in the U.S. side of the research domain enhance the ozone production in east-central Ontario in the next one day to 69 hours. Except sometimes in Toronto area where the VOC/NOx ratio is very small, toluene emission in almost all of the non-zero sensitivity regions tends to suppress the ozone level in the T-O region. The VOC response regions extend to the northern side of the research Domain 1 day to 69 hours before the assumed high ozone event in the T-O region. The sensitivity in the north area is mostly negative, which is associated with the high VOC/NOx ratios there. As there is not much anthropogenic VOCs in northern Ontario, biogenic isoprene advected from the north area then becomes an important sink for ozone in east-central Ontario.

Most of the Great Lake regions are in the upwind direction of the Toronto-Ottawa receptor region. The influence of lake breezes on pollutants has been detected in the first two scenarios. This suggests that when pollutants pass by lake regions, they can be trapped around the lake area until stronger large-scale wind starts to take effect. Ozone sensitivity to all precursors over the influencing lake areas tends to be larger than that on the surrounding land area (a similar phenomenon is seen in Scenario 3).

From about one day prior to the outbreak of the assumed high ozone event, the positive ozone sensitivity to pre-existing ozone increases in the local T-O receptor region. The largest sensitivity is over Lake Ontario for all scenarios, followed by the large northern land area in the T-O square, then

the two urban areas Toronto and Ottawa. A similar increasing trend also applies for the sensitivity to NO, but the average magnitude is largest around noon. In NOx–rich areas such as Toronto, increasing NO emission can suppress local ozone formation in the next few hours. The largest local response to CO and various VOCs also occurs several hours before the assumed high ozone episode in the afternoon. A local increase in CO, ethylene, or formaldehyde enhances the ozone formation by late afternoon. An increase in any of the selected carbon compounds in NOx-rich Toronto enhances the ozone formation in the next several hours in the late afternoon. Increasing VOCs except ethylene and formaldehyde over VOC-rich areas such as the central part of Lake Ontario from morning to one hour before the high ozone event suppresses ozone formation.

The magnitude of the ozone sensitivity to CO is much smaller than that to VOCs. This indicates that CO is not an important influencing factor of ozone level changes in east-central Ontario. The release of different VOCs to different locations at different times causes different ozone level changes in the T-O receptor region, which is due to the different properties of different VOCs. When the temperature is higher, a larger portion of carbon compounds contributes to the ozone in the receptor region than under low temperature conditions.

Chapter 6
Scope and future work

6.1 CMAQ/4D-Var and the modified CMAQ/4D-Var

Observations that are collected to provide initial/boundary conditions for atmospheric models are often spatially and temporally sparse, irregular, or incompatible with numerical models. Variational data assimilation is an approach to construct accurate initial conditions for forecast models by taking advantage of consistency constraints with laws of time evolution and physical properties, the observed information, and the model state (Bouttier and Courtier, 2005; Daley, 1993). Through minimizing a pre-defined cost function (objective function) that measures the differences in observations and model states, four-dimensional data assimilation (4D-Var) optimally combines the observation with the background estimate of the state of the atmosphere (a priori) and the dynamics and chemistry inside the atmospheric model involved. This optimized model state vector best fits both the observational data and the model states, it is the best possible representation of the true state at the time of the analysis (Wang et al., 2001).

4D-Var generalizes 3D-Var for observations that are distributed in time, it was first introduced to atmospheric chemistry by Fisher and Lary (1995). Elbern et al. (1997) used a gas-phase box model to prove the feasibility of 4D-Var for a tropospheric gas phase mechanism. Elbern and Schmidt (1999) developed and applied a variational method to assimilate various trace gas observations into chemical transport model EURAD-CTM2. This was the first full 4D-Var experiment for a comprehensive 3-D CTM. This 4D-Var system was used to assimilate ozone observations and optimize emission rates of non-observed various precursor constituents of ozone. They demonstrated that 4D-Var is a promising tool to analyze these emission rates under the condition that only ozone is observed (Elbern et al., 2000). They further used this 4D-Var system to optimize ozone initial conditions over central Europe (Elbern and Schmidt, 2001). Hakami et al. (2005) used the 4D-Var approach with the STEM-2K1 model to recover black carbon emissions over the Asian Pacific region. Meirink et al. (2006) used 4D-Var to optimize satellite measurements of methane emissions. Yumimoto and Uno (2006) developed the 4D-Var data assimilation system based on RAMS/CTM to optimize CO emissions over the East Asian using ground-based observation of CO concentration.

CMAQ-ADJ efficiently calculates the gradient of a cost function with respect to initial conditions. This makes the 4-dimensional data assimilation of CMAQ possible. (Singh and Sandu, 2007)

combined CMAQ-ADJ with the L-BFGS optimization package and provided the first 4-D variational data assimilation interface for CMAQ model.

The optimizer L-BFGS used by the 4D-Var of CMAQ is an iterative optimization software. It needs the values of both the cost function and its gradient as inputs to improve the approximation to the optimal analysis after each iteration. Singh and Sandu (2007) in the 4D-Var system of CMAQ used the original CMAQ-ADJ to calculate the gradients of the cost function. Therefore, this system has all the problems that the original CMAQ-ADJ has, i.e., it does not work properly in high resolution and its meteorological interface needs to be modified. To fix these problems, the modified CMAQ-ADJ is used to replace the original CMAQ-ADJ in 4D-Var of CMAQ (Singh and Sandu, 2007). All the code that is related to the modified CMAQ-ADJ is also re-written (new FORTRAN code is in Appendix D). A 6-hour test run in high resolution Domain 2 (Figure 4) from 14:00 GMT to 20:00 GMT July 16 2007 is conducted using the 4D-Var of CMAQ with the modified CMAQ-ADJ. The background field for all time steps is obtained by running CMAQ with a 10% perturabation added to the initial ozone with the other chemicals unchanged. The observations are based on the concentration field after running CMAQ from CMAQ simulations at 14:00 GMT July 16, it is assumed that there is a ground-level ozone observation every 4 columns and every 4 rows among the 156×96 grids of the research domain.

Figure 40 shows the difference between the assimilated ozone concentrations at 14:00 GMT July 16 and the mock observations. The general difference is very small, which means the optimized ozone concentrations are reasonable and can be used to represent the observations. The built-in convergence criteria used by the L-BFGS algorithm is satisfied after six iterations, i.e., the analysis will not improve significantly. The convergence criteria used in the model is "(fold - f) .le. factr*epsmch*ddum", i.e., the difference between the cost function in the previous iteration (fold) and the cost function in the current iteration (f) is the same as or less than the multiplication of "factr" (a number specified by user to control the accuracy), "epsmch" (the machine precision), and "ddum" (the largest among the absolute value of "fold", "f", and one). Considering the fact that moderate accuracy is enough for fluid problems, "factr" is set to 1.d+7 here. "Epsmch" is 2.220D-16, which is returned by the computer (the SHARCNET cluster Brown, www.sharcnet.ca) used in this test run.

The fact that the 6-hour test run in high resolution Domain 2 has automatically obtained the optimized ozone concentrations after six iterations, the modified CMAQ-ADJ can be judged to be successfully transplanted into the 4D-Var system for CMAQ.

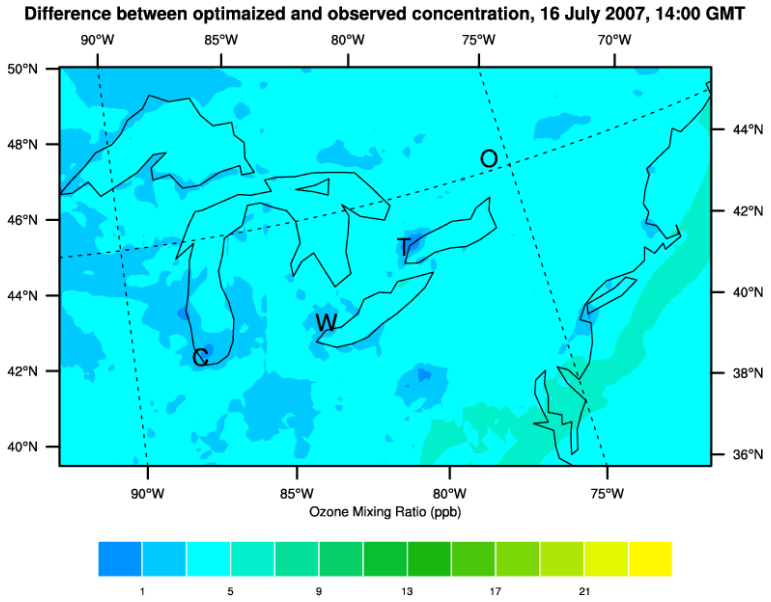

Figure 40. Difference between optimized and reference ozone concentration, in ppb.

6.2 Other future works

Current 4D-Var data assimilation of CMAQ uses the modified CMAQ-ADJ to calculate the first-order gradient of the cost function with respect to initial conditions. The first-order adjoint provides only necessary conditions for optimal solutions (Le Dimet et al., 2002). To ensure the optimal control in variational data assimilation and to speed up the convergence rate of the minimization, it is necessary to know the second-order gradient of the cost function (Giles and Pierce, 2000; Le Dimet et al., 2002; Wang et al., 1992), which is because Hessian (the matrix of second partial derivatives) of the cost function can be used to study the properties of local convexity which determines the implementation of the convergence of the algorithms of variational data assimilation problems (Le Dimet et al., 2002). In this sense, second-order adjoint for CMAQ-ADJ should be introduced in the future.

In this research, MM5 provided hourly (the first level time-step) meteorological data for the modified CMAQ. The model hence was driven by the same weather conditions for the adjoint integration for all the sync time-steps (the second level time-step) of the hour. In this sense, more consistent evolutions of adjoint variables can be expected if using online meteorological data. What's more, the offline meteorological data used in the current version of CMAQ-ADJ makes it difficult to

study the relationship between climate change and air quality issues, one has to consider a large number of meteorological conditions of different decades to simulate different climate change scenarios.

The modified CMAQ-ADJ is developed based on the CMAQ-ADJ of (Hakami et al., 2007). The gas phase chemical mechanism used in both CMAQ-ADJ and the modified CMAQ-ADJ is the basic CB4. It does not include aerosol or aqueous chemistry. When more new chemistry is introduced to CMAQ-ADJ such as the work by Zhao et al. (2011) (who introduced aerosols into the model), the corresponding code that deals with high-resolution simulation, meteorological interface, and chemistry time-step should also be modified. The new code provided in this thesis is module-based. It will therefore be easy to be incorporated into any new developments in CMAQ-ADJ.

Similar to all the other adjoint models, uncertainties exist in CMAQ-ADJ because the adjoint sensitivity analysis does not produce a complete source attribution and provides only a first-order analysis (Martien and Harley, 2006b). The accuracy of a sensitivity result greatly depends on synoptic situations, the size and structure of perturbation, and the simulation duration (Errico et al., 1993; Errico, 1997). When including more physical and chemical processes, the accuracy of adjoint integrations can be improved because "all-physics" in a tangent linear model improves the fit to the nonlinear models (Mahfouf, 1999). The accuracy of CMAQ will continue to improve when the following mechanisms or algorithms are included in new versions of CMAQ-ADJ: aerosol thermodynamics, aerosol dynamics, and aqueous chemistry. These works are parts of the ongoing project "a multiphase adjoint for CMAQ" by collaborators from Carleton University, Georgia Institute of Technology, University of Colorado, University of Iowa, University of Houston, Virginia Tech, Academy of Sciences of the Czech Republic, the U.S. EPA and NOAA (Zhao et al., 2010). This project also includes data assimilation, parallelization, and nesting. The modified CMAQ-ADJ in this thesis has made nesting possible through changing the checkpointing method from a fixed sync time-step to a model-calculated time-varying sync time-step.

Pinder and Hakami (2011) proposed future work related to the application of CMAQ-ADJ, i.e., to define different cost functions for different species at different locations and time, and to process the calculated sensitivities. The sensitivity calculated at different locations could provide a scientific basis for policy-makers to design air quality management and control strategies. In addition to its applications to sensitivity studies, further applications of the modified CMAQ-ADJ include source appointment, examination and estimation of the model parameters, and the application of 4-D variational data assimilation of CMAQ in high resolutions.

In all the scenarios used in this thesis, the ozone enhancements are assumed not to exceed by much the one-hour Ambient Air Quality Criterion of 80 ppb in Ontario (AQO2007, 2008). Due to the fact that extremely large ozone concentrations have been observed in smog episodes in urban areas such as Los Angeles where ozone level were as large as 580 ppb in 1970, 490 ppb in 1980, and 330 ppb in 1990 (Benoit Cushman-Roisin, 2010), very big perturbations can therefore be assigned when studying ozone sensitivity in polluted urban regions. For sensitivity study in smaller regions such as an urban area, a higher resolution than used in this study should be chosen. A higher resolution sensitivity study can discover more detailed phenomena than a coarse resolution case. When only the first-order derivatives are available in adjoint models, the accuracy of the sensitivity results depends on whether the linearized approximation is valid. The perturbation size should be infinitesimally small for small scale systems (Errico, 1997). Reasonable results in this thesis have shown that the perturbations used for the research area with 12 km resolution are appropriate. But one should be careful when choosing very large perturbations to study severe pollution using the first-order adjoint methods. Sensitivity analysis in this thesis has shown that the modified CMAQ-ADJ can identify the locations that contribute most significantly and compare the relative strengths of the chemical species to pollutants of interest. Combined with the knowledge of pollutant inventories, this model can also be used to determine pollutant sources of a specific region. For policy makers, the modified CMAQ-ADJ can be used to address environmental issues such as the ozone control or constrain emissions of other pollutants from their sources. This has demonstrated that the modified CMAQ-ADJ has the potential to address a wide range of scientific problems.

Chapter 7
Conclusions

Two tasks were focused upon in this thesis, the improvement of the CMAQ-ADJ (Hakami et al., 2007) and the application of the modified CMAQ-ADJ to ozone sensitivity study in southwestern Ontario and east-central Ontario. The CMAQ-ADJ in a 4-dimensional variational data assimilation (4D-Var) system for CMAQ model has been replaced by the modified CMAQ-ADJ.

The modified CMAQ-ADJ

Three major improvements were introduced to the original CMAQ-ADJ by adding new FORTRAN 90 code or modifying the existed FORTRAN 77 code. The first improvement is the use of a time-varying synchronization (sync) time-step for checkpointing data to replace the original fixed synchronization time-step for checkpointing data. The determination of the time-varying sync time-step is based on the model resolution and the meteorology (wind) of every output time-step, and is calculated by the model automatically. Using a time-varying sync time-step removes restrictions on meteorological conditions or resolution, especially high resolution and severe weather. This modification makes sensitivity studies in nested domains possible, so that materials from distant regions in the outer domain of the nested region can be transported to the high resolution inner domain.

The meteorological interface of the original CMAQ-ADJ was modified to enable the advection during the whole simulation period to be accurate and therefore enable long-range transport from distant locations. The third improvement that has been made to the model is the modification of the treatment of the checkpointing of the chemistry time-step, otherwise using an incorrect chemistry time-step will cause the modeled results to be unreasonable.

The modified CMAQ-ADJ is applied to the high resolution inner domain of two-level nested domains to study the impact of precursor species on ozone change in southwestern Ontario and east-central Ontario. Since there are no straightforward methods to examine the complex non-linear physics and chemistry in a model, these applications to ozone sensitivity are also the way to test the proposed improvements to the code.

The modified CMAQ-ADJ works automatically and effectively in the double-nested domain without aborting like the original CMAQ-ADJ. This shows that replacing the fixed sync time-step

with the time-varying sync time-step that is determined by the model algorithm has been successfully implemented. The evolution of the sensitivity fields with horizontal winds, the close relationship with the underlying surface features such as land, lakes, and large cities and the identification of the ozone formation features in different VOC/NOx regimes show that the modification to the meteorological interface is correct. By capturing the strong contrast of land, major water bodies, and urban areas this work showed that the chemistry time-step in the modified version of CMAQ has been implemented correctly.

The six case runs showed that meteorological conditions and underlying surface features in the pollutant pathway play an important role in influencing ozone perturbations in both southwestern and east-central Ontario. When there are no strong large-scale winds, the lake breezes trap pollutants. These pollutants are recycled around lakes to influence the southwestern and east-central Ontario ozone level in at least 69 hours. When strong large-scale scale winds take effect, pollutants can transport to the two selected Ontario regions from distant regions.

Influence of pre-existing ozone

The ozone changes in both southwestern Ontario and east-central Ontario are influenced by pre-existing ozone changes in the upwind direction. The ozone that is transported along the northern side of the Great Lakes Basin can enhance the ozone formation in Toronto-Ottawa region, but hardly influences ozone changes in southwestern Ontario.

Pre-existing ozone changes in the Midwest U.S. and Ohio Valley have little influence on ozone changes in east-central Ontario. The ozone level in southwestern Ontario (W-T region) can be enhanced by the transport of pre-existing ozone from industrialized regions in the U.S.. However, increasing ozone in the NOx-rich urban areas can suppress ozone level in both T-O and W-T regions after 2 days to 69 hours.

At all times, the magnitude of the ozone sensitivity over lake areas is larger than over land areas. The smallest sensitivity is in urban areas. On land, the target high ozone event responds more to pre-existing ozone changes at locations where there are large VOC emissions than those locations where the VOC emissions are smaller. Under all the weather conditions used in this thesis, when time approaches the outbreak of the high ozone event, the influencing region of pre-existing ozone approaches the receptor region. The average magnitude of the ozone sensitivity to pre-existing ozone increases with time at all local locations.

Influence of NO

Increasing NO emission in northern Ontario can enhance the ozone level in southwestern Ontario in the next 2 days and east-central Ontario in the next 69 hours. NO emission in the industrialized Midwest U.S. and Ohio Valley can enhance the ozone formation in southwestern Ontario in 1 to 3 days and in east-central Ontario in 2-3 days. Increasing NO emission in the areas associated with rich NO emission such as Toronto can suppress the ozone formation in the receptor regions.

Under both usual and unusual weather conditions, increased NO emission over lake areas has a larger influence to the ozone in the examined regions in Ontario than that increased in land areas. The average magnitude of the local ozone sensitivity with respect to NO within the receptor region generally increases with time and reaches to a peak in the morning or early afternoon before the high ozone episode. Similar to the influence of pre-existing ozone, in land areas, the target high ozone event responds greater to NO changes at locations where the VOC/NOx ratio is larger.

Influence of CO and VOCs

Under typical summer weather conditions, the influencing region of all VOCs extends to the northern part of the research Domain 24 to 69 hours before the assumed high ozone event in east-central Ontario. For ozone in southwestern Ontario, only the area of the influencing region of toluene and xylene in the north is competitive to that in the T-O region. The influencing area of the other VOCs is very small. Although the northern area can have a negative influence on ozone levels in the target regions, the lack of anthropogenic emissions there leaves the advection of biogenic VOCs as an important photochemical O_3 loss pathway from the north area. Isoprene emission from northern forest can suppress ozone level in east-central Ontario. It can also suppress ozone level in southwestern Ontario, but its influencing region is small.

Increased emission of all VOCs except toluene in the Midwest U.S. and Ohio Valley can enhance the ozone formation in southwestern Ontario and in east-central Ontario in the next 1 day to 69 hours. Toluene emissions here tend to suppress ozone production in the receptor regions.

The pollutants over lake regions tend to have larger contribution to ozone changes in the receptor regions than that over surrounding land areas under both weather conditions used in this study. As time approaches the target time, the influencing region approaches the receptor region and the influence of CO and VOCs becomes local. The largest magnitude (positive or negative) of the

average ozone sensitivity to all the carbon species usually appears in the morning to noon, several hours before the occurrence of the high ozone event in the late afternoon.

The response of ozone level to different VOCs is different. The ozone response to the release of various VOCs depends on the time and the location of the emission. For example, an increase in VOCs in the Toronto area where the VOC/NOx ratio is very low can cause the ozone level in east-central Ontario to decrease after 69 hours. In the same day as the high ozone event, increased VOCs emissions in urban areas almost always causes an increase in local ozone level in the late afternoon. Increasing VOCs except ethylene and formaldehyde to places with large VOC/NOx ratio such as the southern part of Lake Huron, the central part of Lake Ontario, and the land area in the northern part of Toronto-Ottawa region in the morning suppresses the local ozone level by late afternoon. An VOC change in the morning to noon in places that have extreme VOC/NOx ratios might be diagnostic for the prediction of local ozone event in the late afternoon. In places where the VOC/NOx regime is complex or with moderate VOC/NOx ratios, the ozone response to VOC changes is complex. The ozone sensitivity in such regions should be studied in fine resolution because a coarse resolution potentially averages away some small-scale features.

The magnitude of the sensitivity of ozone to carbon compounds is dependent on temperature. As reaction rates increase with temperature, a larger portion of carbon compounds in Scenario 1 can contribute to the ozone level in the two target squares than in Scenario 3. The influence of pre-existing ozone and NO on the target ozone changes does not change the magnitude under different temperature conditions.

Among all species, CO has the smallest contribution to ozone concentration in the receptor regions, but the ozone sensitivity to CO is always positive in this study. Once there is a forest fire somewhere in a non-zero sensitivity area, the emitted CO will always enhance the ozone formation in southwestern and east-central Ontario. Since the ozone sensitivity to CO is up to two to three orders of magnitude smaller than that to VOCs and NO, CO is very unlikely to be an important source of ozone enhancement mechanism in the W-T region and the T-O region. Forward sensitivity approaches can be used to examine how Ontario ozone responds to CO emissions such as from a forest fire.

Among all the species examined in this thesis, NO has the largest impact on the ozone level changes in both southwestern and east-central Ontario. Anthropogenic NO and VOC emissions in the Midwest U.S. and Ohio Valley can enhance the ozone concentrations in both the receptor regions after at least 69 hours. Even though the model results show that the ozone sensitivity to some species

is small, especially in the earlier hours of the simulation period, the continuous anthropogenic emissions from the polluted U.S. regions can accumulate and finally make a large contribution to the ozone level in southwestern and east-central Ontario.

Bibliography

Altshuller, A. P., A. F. Wartburg and R. A. Taft, The Interaction of Ozone with Plastic and Metallic Materials in A Dynamic Flow System, *International Journal of Air and Water Pollution, 4*(1-2), 70-78, 1961.

Andries, J. C., C. K. Rhee, R. W. Smith, D. B. Ross and H. E. Diem, Surface Study of Ozone Attack and Anti-Ozonant Protection of Carbon-Black Loaded Natural-Rubber Compounds, *Rubber Chemistry and Technology, 52*(4), 823-837, 1979.

Appel, K. W., A. B. Gilliland and S. Golam, Evaluation of the Community Multiscale Air Quality (CMAQ) model version 4.5: Sensitivities impacting model performance Part I - Ozone, *Atmospheric Environment, 41*(40), 9603-9615, 2007.

AQO2007, Air Quality in Ontario - 2007 Report, Air Monitoring & Reporting Section, Environmental Monitoring and Reporting Branch, Ontario Ministry of the Environment, 2008.

AQO2008, Air Quality in Ontario 2008 Report, Environmental Monitoring and Reporting Branch, Ontario Ministry of the Environment, 2010.

Atkinson, R., Gas-Phase Tropospheric Chemistry of Organic-Compounds - A Review, *Atmospheric Environment Part A-General Topics, 24*(1), 1-41, 1990.

Atkinson, R. and J. Arey, Gas-phase tropospheric chemistry of biogenic volatile organic compounds: a review, *Atmospheric Environment, 37*, S197-S219, 2003.

Baek, J., P. Saide, G. R. Carmichael, A. G. Carlton and C. O. Stanier, Developing forward and adjoint aqueous chemistry module for CMAQ with Kinetic PreProcessor, AAAR Conference, 2011.

BAQS, Border Air Quality Study - An Ambient Air Quality Overview for Southwestern Ontario (Summer 2007), pp. 1-34, Air Monitoring & Reporting Section, Environmental Monitoring and Reporting Branch, Ontario Ministry of the Environment, 2008.

Bell, M. L., F. Dominici and J. M. Samet, A meta-analysis of time-series studies of ozone and mortality with comparison to the national morbidity, mortality, and air pollution study, *Epidemiology, 16*(4), 436-445, 2005.

Benoit Cushman-Roisin, Ground-level ozone, Smog over Los Angeles, 2010.

Bergin, M. S., A. G. Russell and J. B. Milford, Quantification of Individual Voc Reactivity Using A Chemically Detailed, 3-Dimensional Photochemical Model, *Environmental Science & Technology, 29*(12), 3029-3037, 1995.

Bouttier, F. and P. Courtier, Data assimilation concepts and methods, ECMWF, 2005.

Brankov, E., R. F. Henry, K. L. Civerolo, W. Hao, S. T. Rao, P. K. Misra, R. Bloxam and N. Reid, Assessing the effects of transboundary ozone pollution between Ontario, Canada and New York, USA, *Environmental Pollution, 123*(3), 403-411, 2003.

Brasseur, G., J. J. Orlando and G. S. Tyndall, Atmospheric Chemistry and Global Change, Oxford Univ. Press, Oxford, 1999.

Brasseur, G. P., J. T. Kiehl, J. F. Muller, T. Schneider, C. Granier, X. X. Tie and D. Hauglustaine, Past and future changes in global tropospheric ozone: Impact on radiative forcing, *Geophysical Research Letters, 25*(20), 3807-3810, 1998.

Brook, J. R., L. M. Zhang, Y. F. Li and D. Johnson, Description and evaluation of a model of deposition velocities for routine estimates of dry deposition over North America. Part II: review of past measurements and model results, *Atmospheric Environment, 33*(30), 5053-5070, 1999.

Brulfert, G., O. Galvez, F. Yang and J. J. Sloan, A regional modelling study of the high ozone episode of June 2001 in southern Ontario, *Atmospheric Environment, 41*(18), 3777-3788, 2007.

Byrd, R. H., P. H. Lu, J. Nocedal and C. Y. Zhu, A Limited Memory Algorithm for Bound Constrained Optimization, *Siam Journal on Scientific Computing, 16*(5), 1190-1208, 1995.

Byun, D., OVERVIEW OF THE MULTI-SCALE COMMUNITY AIR QUALITY (CMAQ) MODELING SYSTEM (on line), *Institute for Multi-dimensional Air Quality Studies, University of Houston,* 1-17, 2002.

Byun, D. and K. L. Schere, Review of the governing equations, computational algorithms, and other components of the models-3 Community Multiscale Air Quality (CMAQ) modeling system, *Applied Mechanics Reviews, 59*(1-6), 51-77, 2006.

Byun, D. and J. Young, Governing Equations and Computational Structure of the Community Multiscale Air Quality (CMAQ) Chemical Transport Model, in Science Algorithms of the EPA Models-3 Community Multiscale Air Quality (CMAQ) Modeling System, edited by D. W. Byun and J. K. S. Ching, pp. 6-1-6-17, National Exposure Research Laboratory,U.S.EPA, 1999.

Byun, D. W., J. Young and J. Pleim, Numerical Transport Algorithms for the Community Multiscale Air Quality (CMAQ) Chemical Transport Model in Generalized Coordinates, in Science Algorithms of the EPA Models-3 Community Multiscale Air Quality (CMAQ) Modeling System, edited by D. W. Byun and J. K. S. Ching, pp. 1-55, National Exposure Research Laboratory,U.S.EPA, 1999.

Carter, W. P. L., Development of Ozone Reactivity Scales for Volatile Organic-Compounds, *Journal of the Air & Waste Management Association, 44*(7), 881-899, 1994.

Carter, W. P. L., Implementation of the SAPRC-99 chemical mechanism into the models-3 framework. Report to the United States Environmental Protection Agency, 2000.

Chameides, W. L., R. W. Lindsay, J. Richardson and C. S. Kiang, The Role of Biogenic Hydrocarbons in Urban Photochemical Smog - Atlanta As A Case-Study, *Science, 241*(4872), 1473-1475, 1988.

Chandra, S., J. R. Ziemke, P. K. Bhartia and R. V. Martin, Tropical tropospheric ozone: Implications for dynamics and biomass burning, *Journal of Geophysical Research-Atmospheres, 107*(D14), 2002.

Chou, C. C. K., S. C. Liu, C. Y. Lin, C. J. Shiu and K. H. Chang, The trend of surface ozone in Taipei, Taiwan, and its causes: Implications for ozone control strategies, *Atmospheric Environment, 40*(21), 3898-3908, 2006.

CMAQ, CMAQ v4.6 Operational Guidance Document, CMAS Center and Center for Environmental Modeling for Policy Development at The University of North Carolina at Chapel Hill, 2007.

Coats, C., The EDSS/Models-3 I/O API, 2005.

Comrie, A. C., The Climatology of Surface Ozone in Rural-Areas - A Conceptual-Model, *Progress in Physical Geography, 14*(3), 295-316, 1990.

Constable, J. V. H., A. B. Guenther, D. S. Schimel and R. K. Monson, Modelling changes in VOC emission in response to climate change in the continental United States, *Global Change Biology, 5*(7), 791-806, 1999.

Crutzen, P., Discussion of Chemistry of Some Minor Constituents in Stratosphere and Troposphere, *Pure and Applied Geophysics, 106*(5-7), 1385-1399, 1973.

Daescu, D. N., A. Sandu and G. R. Carmichael, Direct and adjoint sensitivity analysis of chemical kinetic systems with KPP: II - Numerical validation and applications, *Atmospheric Environment, 37*(36), 5097-5114, 2003.

Daley, R., Atmospheric Data Analysis, Cambridge University Press,REP edition, 1993.

Davidson, P. M., N. Seaman, K. Schere, R. A. Wayland, J. L. Hayes and K. F. Carey, National Air Quality Forecasting Capability: First Steps toward Implementation, paper presented at 6th Conference on Atmospheric Chemistry: Air Quality in Megacities, Seattle, WA, 2004.

Derwent, R. G., M. E. Jenkin and S. M. Saunders, Photochemical ozone creation potentials for a large number of reactive hydrocarbons under European conditions, *Atmospheric Environment, 30*(2), 181-199, 1996.

Derwent, R. G., M. E. Jenkin, S. M. Saunders and M. J. Pilling, Photochemical ozone creation potentials for organic compounds in northwest Europe calculated with a master chemical mechanism, *Atmospheric Environment, 32*(14-15), 2429-2441, 1998.

Dodge, M. C., Chemical oxidant mechanisms for air quality modeling: critical review, *Atmospheric Environment, 34*(12-14), 2103-2130, 2000.

Dunker, A. M., Efficient Calculation of Sensitivity Coefficients for Complex Atmospheric Models, *Atmospheric Environment, 15*(7), 1155-1161, 1981.

Dunker, A. M., The Decoupled Direct Method for Calculating Sensitivity Coefficients in Chemical-Kinetics, *Journal of Chemical Physics, 81*(5), 2385-2393, 1984.

Dunker, A. M., G. Yarwood, J. P. Ortmann and G. M. Wilson, Comparison of source apportionment and source sensitivity of ozone in a three-dimensional air quality model, *Environmental Science & Technology, 36*(13), 2953-2964, 2002a.

Dunker, A. M., G. Yarwood, J. P. Ortmann and G. M. Wilson, The decoupled direct method for sensitivity analysis in a three-dimensional air quality model - Implementation, accuracy, and efficiency, *Environmental Science & Technology, 36*(13), 2965-2976, 2002b.

Eder, B., D. W. Kang, R. Mathur, S. C. Yu and K. Schere, An operational evaluation of the Eta-CMAQ air quality forecast model, *Atmospheric Environment, 40*(26), 4894-4905, 2006.

Elbern, H. and H. Schmidt, A four-dimensional variational chemistry data assimilation scheme for Eulerian chemistry transport modeling, *Journal of Geophysical Research-Atmospheres, 104*(D15), 18583-18598, 1999.

Elbern, H. and H. Schmidt, Ozone episode analysis by four-dimensional variational chemistry data assimilation, *Journal of Geophysical Research-Atmospheres, 106*(D4), 3569-3590, 2001.

Elbern, H., H. Schmidt and A. Ebel, Variational data assimilation for tropospheric chemistry modeling, *Journal of Geophysical Research-Atmospheres, 102*(D13), 15967-15985, 1997.

Elbern, H., H. Schmidt, O. Talagrand and A. Ebel, 4D-variational data assimilation with an adjoint air quality model for emission analysis, *Environmental Modelling & Software, 15*(6-7), 539-548, 2000.

EPA-CMAQ, Community Multiscale Air Quality (CMAQ) - Description of Model Changes for the 2003 Release of the CMAQ Model (on line), *http://www. epa. gov/asmdnerl/CMAQ/release43. html*, 2009.

EPA-SMOKE, SMOKE v2.3.2 User's Manual, pp. 1-488, The institute for the Environment - The University of North Carolina at Chapel Hill, 2007.

Errico, R. M., What is an adjoint model?, *Bulletin of the American Meteorological Society, 78*(11), 2577-2591, 1997.

Errico, R. M., T. Vukicevic and K. Raeder, Examination of the Accuracy of A Tangent Linear-Model, *Tellus Series A-Dynamic Meteorology and Oceanography, 45A*(5), 462-477, 1993.

Faraji, M., Y. Kimura, E. McDonald-Buller and D. Allen, Comparison of the carbon bond and SAPRC photochemical mechanisms under conditions relevant to southeast Texas, *Atmospheric Environment, 42*(23), 5821-5836, 2008.

Fast, J. D. and W. E. Heilman, simulated sensitivity of seasonal ozone exposure in the Great Lakes region to changes in anthropogenic emissions in the presence of interannual variability, *Atmospheric Environment, 39*(29), 5291-5306, 2005.

FinlaysonPitts, B. J. and J. N. Pitts, Tropospheric air pollution: Ozone, airborne toxics, polycyclic aromatic hydrocarbons, and particles, *Science, 276*(5315), 1045-1052, 1997.

Fiore, A. M., L. W. Horowitz, D. W. Purves, H. Levy, M. J. Evans, Y. X. Wang, Q. B. Li and R. M. Yantosca, Evaluating the contribution of changes in isoprene emissions to surface ozone trends over the eastern United States, *Journal of Geophysical Research-Atmospheres, 110*(D12), 2005.

Fiore, A. M., D. J. Jacob, J. A. Logan and J. H. Yin, Long-term trends in ground level ozone over the contiguous United States, 1980-1995, *Journal of Geophysical Research-Atmospheres, 103*(D1), 1471-1480, 1998.

Fisher, M. and D. J. Lary, Lagrangian 4-Dimensional Variational Data Assimilation of Chemical-Species, *Quarterly Journal of the Royal Meteorological Society, 121*(527), 1681-1704, 1995.

Fishman, J. and V. G. Brackett, The climatological distribution of tropospheric ozone derived from satellite measurements using version 7 Total Ozone Mapping Spectrometer and Stratospheric Aerosol and Gas Experiment data sets, *Journal of Geophysical Research-Atmospheres, 102*(D15), 19275-19278, 1997.

Fishman, J., S. Solomon and P. J. Crutzen, Observational and Theoretical Evidence in Support of A Significant Insitu Photo-Chemical Source of Tropospheric Ozone, *Tellus, 31*(5), 432-446, 1979.

Foley, K. M., S. J. Roselle, K. W. Appel, P. V. Bhave, J. E. Pleim, T. L. Otte, R. Mathur, G. Sarwar, J. O. Young, R. C. Gilliam, C. G. Nolte, J. T. Kelly, A. B. Gilliland and J. O. Bash, Incremental testing of the Community Multiscale Air Quality (CMAQ) modeling system version 4.7, *Geoscientific Model Development, 3*(1), 205-226, 2010.

Forster, P., V. Ramaswarny, P. Artaxo, T. Berntsen, R. Betts, D. W. Fahey, J. Haywood, J. Lean, D. C. Lowe, G. Myhre, J. Nganga, R. Prinn, G. Raga, M. Schulz and R. Van Dorland, Changes in Atmospheric Constituents and in Radiative Forcing. In: Climate Change 2007: The physical Science Basis. Contribution of Working Group I to the Fourth Assessment Report of the Intergovernmental panel on Climate Change, edited by S. D. Solomon, D. Qin, M. Manning, Z. Chen, M. Marquis, K. B. Averyt, M. Tignor and H. L. Miller, Cambridge University Press, 2007.

Galvez, O., Synoptic-scale transport of ozone into Southern Ontario, *Atmospheric Environment, 41*(38), 8579-8595, 2007.

Gbor, P. K., D. Y. Wen, F. Meng, F. Q. Yang, B. N. Zhang and J. J. Sloan, Improved model for mercury emission, transport and deposition, *Atmospheric Environment, 40*(5), 973-983, 2006.

Gbor, P. K., D. Wen, F. Meng, F. Yang and J. J. Sloan, Modeling of mercury emission, transport and deposition in North America, *Atmospheric Environment, 41*(6), 1135-1149, 2007.

Geddes, J. A., J. G. Murphy and D. K. Wang, Long term changes in nitrogen oxides and volatile organic compounds in Toronto and the challenges facing local ozone control, *Atmospheric Environment, 43*(21), 3407-3415, 2009.

Geddes, J. A., J. G. Murphy and D. K. Wang, Long term changes in nitrogen oxides and volatile organic compounds in Toronto and the challenges facing local ozone control, *Atmospheric Environment, 43*(21), 3407-3415, 2009c.

Geron, C. D., A. B. Guenther and T. E. Pierce, An Improved Model for Estimating Emissions of Volatile Organic-Compounds from Forests in the Eastern United-States, *Journal of Geophysical Research-Atmospheres, 99*(D6), 12773-12791, 1994.

Gery, M. W., G. Z. Whitten, J. P. Killus and M. C. Dodge, A Photochemical Kinetics Mechanism for Urban and Regional Scale Computer Modeling, *Journal of Geophysical Research-Atmospheres, 94*(D10), 12925-12956, 1989.

Giering, R. and T. Kaminski, Recipes for adjoint code construction, *Acm Transactions on Mathematical Software, 24*(4), 437-474, 1998.

Giles, M. B. and N. A. Pierce, An introduction to the adjoint approach to design, *Flow Turbulence and Combustion, 65*(3-4), 393-415, 2000.

Gillani, N. V. and J. E. Pleim, Sub-grid-scale features of anthropogenic emissions of NOx and VOC in the context of regional Eulerian models, *Atmospheric Environment, 30*(12), 2043-2059, 1996.

Gipson, G. L., The Initial Concentration and Boundary Condition Processes, in Science Algorithms of the EPA Models-3 Community Multiscale Air Quality (CMAQ) Modeling System, edited by D. W. Byun and J. K. S. Ching, pp. 1-18, National Exposure Research Laboratory,U.S.EPA, 1999.

Gipson, G. L. and J. Young, Gas-Phase Chemistry, in Science Algorithms of the EPA Models-3 Community Multiscale Air Quality (CMAQ) Modeling System, pp. 8-1-8-35, National Exposure Research Laboratory,U.S.EPA, 1999.

Gison, G. L. and J. O. Young, Gas phase chemistry. In: Byun, D.W., Ching, J.K.S. (Eds.), Science Algorithms of the EPA Models-3 Community Multiscale Air Quality (CMAQ) Modeling System. EPA600/R99/030. U.S. Environmental Protection Agency, RTP NC, pp. 8-1-8-86, 1999.

Gou, T. Y., K. Singh and A. Sandu, Chemical Data Assimilation with CMAQ: Continuous vs. Discrete Advection Adjoints, 2009.

Grell, G. A., J. Dudhia and D. R. Stauffer, A description of the fifth-generation Penn State/NCAR Mesoscale Model (MM5), NCAR/TN-398+STR, 1994.

Gryparis, A., B. Forsberg, K. Katsouyanni, A. Analitis, G. Touloumi, J. Schwartz, E. Samoli, S. Medina, H. R. Anderson, E. M. Niciu, H. E. Wichmann, B. Kriz, M. Kosnik, J. Skorkovsky, J. M. Vonk and Z. Dortbudak, Acute effects of ozone on mortality from the "Air pollution and health: A European approach" project, *American Journal of Respiratory and Critical Care Medicine, 170*(10), 1080-1087, 2004.

Guenther, A., C. Geron, T. Pierce, B. Lamb, P. Harley and R. Fall, Natural emissions of non-methane volatile organic compounds; carbon monoxide, and oxides of nitrogen from North America, *Atmospheric Environment, 34*(12-14), 2205-2230, 2000.

Hakami, A., Direct sensitivity analysis in air quality models, Georgia Institute of Technology, 2003.

Hakami, A., D. K. Henze, J. H. Seinfeld, T. Chai, Y. Tang, G. R. Carmichael and A. Sandu, Adjoint inverse modeling of black carbon during the Asian Pacific Regional Aerosol Characterization Experiment, *Journal of Geophysical Research-Atmospheres, 110*(D14), 2005.

Hakami, A., D. K. Henze, J. H. Seinfeld, K. Singh, A. Sandu, S. T. Kim, D. W. Byun and Q. B. Li, The adjoint of CMAQ, *Environmental Science & Technology, 41*, 7807-7817, 2007.

Hakami, A., M. T. Odman and A. G. Russell, High-order, direct sensitivity analysis of multidimensional air quality models, *Environmental Science & Technology, 37*(11), 2442-2452, 2003.

Hakami, A., J. H. Seinfeld, T. F. Chai, Y. H. Tang, G. R. Carmichael and A. Sandu, Adjoint sensitivity analysis of ozone nonattainment over the continental United States, *Environmental Science & Technology, 40*(12), 3855-3864, 2006.

Harley, R. A., A. G. Russell, G. J. Mcrae, G. R. Cass and J. H. Seinfeld, Photochemical Modeling of the Southern California Air-Quality Study, *Environmental Science & Technology, 27*(2), 378-388, 1993.

Hastie, D. R., J. Narayan, C. Schiller, H. Niki, P. B. Shepson, D. M. L. Sills, P. A. Taylor, W. J. Moroz, J. W. Drummond, N. Reid, R. Taylor, P. B. Roussel and O. T. Melo, Observational evidence for the impact of the lake breeze circulation on ozone concentrations in Southern Ontario, *Atmospheric Environment, 33*(2), 323-335, 1999.

Heck, W. W., O. C. Taylor, R. Adams, G. Bingham, J. Miller, E. Preston and L. Weinstein, Assessment of Crop Loss from Ozone, *Journal of the Air Pollution Control Association, 32*(4), 353-361, 1982.

Henze, D. K., A. Hakami and J. H. Seinfeld, Development of the adjoint of GEOS-Chem, *Atmospheric Chemistry and Physics, 7*(9), 2413-2433, 2007.

Hogrefe, C., B. Lynn, K. Civerolo, J. Y. Ku, J. Rosenthal, C. Rosenzweig, R. Goldberg, S. Gaffin, K. Knowlton and P. L. Kinney, Simulating changes in regional air pollution over the eastern United States due to changes in global and regional climate and emissions, *Journal of Geophysical Research-Atmospheres, 109*(D22), 2004.

Horowitz, L. W., A. M. Fiore, G. P. Milly, R. C. Cohen, A. Perring, P. J. Wooldridge, P. G. Hess, L. K. Emmons and J. F. Lamarque, Observational constraints on the chemistry of isoprene nitrates over the eastern United States, *Journal of Geophysical Research-Atmospheres, 112*(D12), 2007.

Ito, K., S. F. De Leon and M. Lippmann, Associations between ozone and daily mortality - Analysis and meta-analysis, *Epidemiology, 16*(4), 446-457, 2005.

Johnson, C. E., D. S. Stevenson, W. J. Collins and R. G. Derwent, Role of climate feedback on methane and ozone studied with a coupled ocean-atmosphere-chemistry model, *Geophysical Research Letters, 28*(9), 1723-1726, 2001.

Johnson, D., D. Mignacca, D. Herod, D. Jutzi and H. Miller, Characterization and identification of trends in average ambient ozone and fine particulate matter levels through trajectory cluster analysis in eastern Canada, *Journal of the Air & Waste Management Association, 57*(8), 907-918, 2007.

Junge, C. E., Global Ozone Budget and Exchange Between Stratosphere and Troposphere, *Tellus, 14*(4), 363-377, 1962.

Kang, D. W., V. P. Aneja, R. Mathur and J. D. Ray, Nonmethane hydrocarbons and ozone in three rural southeast United States national parks: A model sensitivity analysis and comparison to measurements, *Journal of Geophysical Research-Atmospheres, 108*(D19), 2003.

Khattatov, B. V., J. C. Gille, L. V. Lyjak, G. P. Brasseur, V. L. Dvortsov, A. E. Roche and J. W. Waters, Assimilation of photochemically active species and a case analysis of UARS data, *Journal of Geophysical Research-Atmospheres, 104*(D15), 18715-18737, 1999.

Klink, K., Climatological mean and interannual variance of united states surface wind speed, direction and velocity, *International Journal of Climatology, 19*(5), 471-488, 1999.

Krupa, S. V. and W. J. Manning, Atmospheric Ozone - Formation and Effects on Vegetation, *Environmental Pollution, 50*(1-2), 101-137, 1988.

Kuhn, M., P. J. H. Builtjes, D. Poppe, D. Simpson, W. R. Stockwell, Y. Andersson-Skold, A. Baart, M. Das, F. Fiedler, O. Hov, F. Kirchner, P. A. Makar, J. B. Milford, M. G. M. Roemer, R. Ruhnke, A. Strand, B. Vogel and H. Vogel, Intercomparison of the gas-phase chemistry in several chemistry and transport models, *Atmospheric Environment, 32*(4), 693-709, 1998.

Lamb, B., A. Guenther, D. Gay and H. Westberg, A National Inventory of Biogenic Hydrocarbon Emissions, *Atmospheric Environment, 21*(8), 1695-1705, 1987.

Lamb, B., H. Westberg, G. Allwine and T. Quarles, Biogenic Hydrocarbon Emissions from Deciduous and Coniferous Trees in the United-States, *Journal of Geophysical Research-Atmospheres, 90*(ND1), 2380-2390, 1985.

Layer, R. W. and R. P. Lattimer, Protection of Rubber Against Ozone, *Rubber Chemistry and Technology, 63*(3), 426-450, 1990.

Le Dimet, F. X., I. M. Navon and D. N. Daescu, Second-order information in data assimilation, *Monthly Weather Review, 130*(3), 629-648, 2002.

Lelieveld, J. and F. J. Dentener, What controls tropospheric ozone?, *Journal of Geophysical Research-Atmospheres, 105*(D3), 3531-3551, 2000.

Lewis, A. C., N. Carslaw, P. J. Marriott, R. M. Kinghorn, P. Morrison, A. L. Lee, K. D. Bartle and M. J. Pilling, A larger pool of ozone-forming carbon compounds in urban atmospheres, *Nature, 405*(6788), 778-781, 2000.

Lin, C. Y. C., D. J. Jacob, J. W. Munger and A. M. Fiore, Increasing background ozone in surface air over the United States, *Geophysical Research Letters, 27*(21), 3465-3468, 2000.

Lippmann, M., Health-Effects of Tropospheric Ozone, *Environmental Science & Technology, 25*(12), 1954-1962, 1991.

Lippmann, M., Health-Effects of Tropospheric Ozone - Review of Recent Research Findings and Their Implications to Ambient Air-Quality Standards, *Journal of Exposure Analysis and Environmental Epidemiology, 3*(1), 103-129, 1993.

Liu, S. C., M. Trainer, F. C. Fehsenfeld, D. D. Parrish, E. J. Williams, D. W. Fahey, G. Hubler and P. C. Murphy, Ozone Production in the Rural Troposphere and the Implications for Regional and Global Ozone Distributions, *Journal of Geophysical Research-Atmospheres, 92*(D4), 4191-4207, 1987.

Logan, J. A., Tropospheric Ozone - Seasonal Behavior, Trends, and Anthropogenic Influence, *Journal of Geophysical Research-Atmospheres, 90*(ND6), 10463-10482, 1985.

Luecken, D. J., S. Phillips, G. Sarwar and C. Jang, Effects of using the CB05 vs. SAPRC99 vs. CB4 chemical mechanism on model predictions: Ozone and gas-phase photochemical precursor concentrations, *Atmospheric Environment, 42*(23), 5805-5820, 2008.

Lurmann, F. W., W. P. L. Carter and L. A. Coyner, A surrogate species chemical reaction mechanism for urban scale air quality simulation models Volume 1 EPA-600/3-87-014a, 1987.

Mahfouf, J. F., Influence of physical processes on the tangent-linear approximation, *Tellus Series A-Dynamic Meteorology and Oceanography, 51*(2), 147-166, 1999.

Mallet, V. and B. Sportisse, A comprehensive study of ozone sensitivity with respect to emissions over Europe with a chemistry-transport model, *Journal of Geophysical Research-Atmospheres, 110*(D22), 2005.

Martien, P. T. and R. A. Harley, Adjoint sensitivity analysis for a three-dimensional photochemical model: Application to Southern California, *Environmental Science & Technology, 40*(13), 4200-4210, 2006a.

Martien, P. T. and R. A. Harley, Adjoint sensitivity analysis for a three-dimensional photochemical model: Implementation and method comparison, *Environmental Science & Technology, 40*(8), 2663-2670, 2006b.

Mathur, R., J. O. Young, K. L. Schere and G. L. Gipson, A comparison of numerical techniques for solution of atmospheric kinetic equations, *Atmospheric Environment, 32*(9), 1535-1553, 1998.

Mcrae, G. J., W. R. Goodin and J. H. Seinfeld, Numerical-Solution of the Atmospheric Diffusion Equation for Chemically Reacting Flows, *Journal of Computational Physics, 45*(1), 1-42, 1982.

Meirink, J. F., H. J. Eskes and A. P. H. Goede, Sensitivity analysis of methane emissions derived from SCIAMACHY observations through inverse modelling, *Atmospheric Chemistry and Physics, 6*, 1275-1292, 2006.

Meng, F., B. Zhang, P. Gbor, D. Wen, F. Yang, C. Shi, J. Aronson and J. Sloan, Models for gas/particle partitioning, transformation and air/water surface exchange of PCBs and PCDD/Fs in CMAQ, *Atmospheric Environment, 41*(39), 9111-9127, 2007.

Menut, L., Adjoint modeling for atmospheric pollution process sensitivity at regional scale, *Journal of Geophysical Research-Atmospheres, 108*(D17), 2003.

Monks, P. S., Gas-phase radical chemistry in the troposphere, *Chemical Society Reviews, 34*(5), 376-395, 2005.

Mukammal, E. I., H. H. Neumann and T. J. Gillespie, Meteorological Conditions Associated with Ozone in Southwestern Ontario, Canada, *Atmospheric Environment, 16*(9), 2095-2106, 1982.

Muller, J. F. and T. Stavrakou, Inversion of CO and NOx emissions using the adjoint of the IMAGES model, *Atmospheric Chemistry and Physics, 5*, 1157-1186, 2005.

Napelenok, S. L., D. S. Cohan, M. T. Odman and S. Tonse, Extension and evaluation of sensitivity analysis capabilities in a photochemical model, *Environmental Modelling & Software, 23*(8), 994-999, 2008.

Olaguer, E. P., G. Yarwood, H. Jeffries and J. Smith, New Research for the Texas SIP: A Science-Policy Synthesis, pp. 1-55, Texas Environmental Research Consortium, 2005.

Philander, S. G., Is The Temperature Rising?, Princeton University Press, 1998.

Pierce, T., C. Geron, L. Bender, R. Dennis, G. Tonnesen and A. Guenther, Influence of increased isoprene emissions on regional ozone modeling, *Journal of Geophysical Research-Atmospheres, 103*(D19), 25611-25629, 1998.

Pinder, R. and A. Hakami, Development and Applications of CMAQ Adjoint, 2011.

Pironnea, O., Optimum Design in Fluid Mechanics, *Journal of Fluid Mechanics, 64*(JUN3), 97-110, 1974.

Reich, P. B. and R. G. Amundson, Ambient Levels of Ozone Reduce Net Photosynthesis in Tree and Crop Species, *Science, 230*(4725), 566-570, 1985.

Resler, J., K. Eben, P. Jurus and P. Krc, Inverse modeling of emissions using the CMAQ adjoint model, paper presented at The 7th Annual CMAS Conference, 2008.

Resler, J., K. Eben, P. Jurus and P. Krc, Assimilation of satellite-retrieved columns and ground-level observations of tropospheric compounds into the CMAQ CTM Model, 2009.

Rew, R., G. Davis, S. Emmerson, H. Davis, E. Hartnett and D. Heimbigner, The NetCDF Users Guide: Data Model, Programming Interfaces, and Format for Self-Describing, Portable Data. NetCDF Version 4.1.3, Unidata Program Center, 2011.

Roselle, S. J., K. L. Schere, J. E. Pleim and A. F. Hanna, Photolysis Rates for CMAQ, in Science Algorithms of the EPA Models-3 Community Multiscale Air Quality (CMAQ) Modeling System, edited by D. W. Byun and J. K. S. Ching, pp. 14-1-14-7, 1999.

Russell, A. and R. Dennis, NARSTO critical review of photochemical models and modeling, *Atmospheric Environment, 34*(12-14), 2283-2324, 2000.

Russell, A., J. Milford, M. S. Bergin, S. Mcbride, L. Mcnair, Y. Yang, W. R. Stockwell and B. Croes, Urban Ozone Control and Atmospheric Reactivity of Organic Gases, *Science, 269*(5223), 491-495, 1995.

Ryerson, T. B., M. Trainer, J. S. Holloway, D. D. Parrish, L. G. Huey, D. T. Sueper, G. J. Frost, S. G. Donnelly, S. Schauffler, E. L. Atlas, W. C. Kuster, P. D. Goldan, G. Hubler, J. F. Meagher and F. C. Fehsenfeld, Observations of ozone formation in power plant plumes and implications for ozone control strategies, *Science, 292*(5517), 719-723, 2001.

Sandu, A., D. N. Daescu and G. R. Carmichael, Direct and adjoint sensitivity analysis of chemical kinetic systems with KPP: Part I - theory and software tools, *Atmospheric Environment, 37*(36), 5083-5096, 2003.

Sandu, A., D. N. Daescu, G. R. Carmichael and T. F. Chai, Adjoint sensitivity analysis of regional air quality models, *Journal of Computational Physics, 204*(1), 222-252, 2005.

Seigneur, C., T. W. Tesche, P. M. Roth and L. E. Reid, Sensitivity of A Complex Urban Air-Quality Model to Input Data, *Journal of applied meteorology, 20*(9), 1020-1040, 1981.

Seinfeld, J. H. and S. N. Pandis, Atmospheric chemistry and physics : from air pollution to climate change, Wiley, New York ; Toronto, 1998.

Sillman, S., The relation between ozone, NOx and hydrocarbons in urban and polluted rural environments, *Atmospheric Environment, 33*(12), 1821-1845, 1999.

Sillman, S. and F. J. Samson, Impact of Temperature on Oxidant Photochemistry in Urban, Polluted Rural and Remote Environments, *Journal of Geophysical Research-Atmospheres, 100*(D6), 11497-11508, 1995.

Sillman, S., P. J. Samson and J. M. Masters, Ozone Production in Urban Plumes Transported Over Water - Photochemical Model and Case-Studies in the Northeastern and Midwestern United-States, *Journal of Geophysical Research-Atmospheres, 98*(D7), 12687-12699, 1993.

Singh, K. and A. Sandu, CMAQ_ADJv4.5: An adjoint model for EPA's Community Multiscale Air Quality(CMAQ), 2007.

Sistla, G., W. Hao, J. Y. Ku, G. Kallos, K. S. Zhang, H. T. Mao and S. T. Rao, An operational evaluation of two regional-scale ozone air quality modeling systems over the eastern United States, *Bulletin of the American Meteorological Society, 82*(5), 945-964, 2001.

Tao, Z. N., S. M. Larson, D. J. Wuebbles, A. Williams and M. Caughey, A summer simulation of biogenic contributions to ground-level ozone over the continental United States, *Journal of Geophysical Research-Atmospheres, 108*(D14), 2003.

Tarasick, D. W., V. E. Fioletov, D. I. Wardle, J. B. Kerr and J. Davies, Changes in the vertical distribution of ozone over Canada from ozonesondes: 1980-2001, *Journal of Geophysical Research-Atmospheres, 110*(D2), 2005.

Trainer, M., E. J. Williams, D. D. Parrish, M. P. Buhr, E. J. Allwine, H. H. Westberg, F. C. Fehsenfeld and S. C. Liu, Models and Observations of the Impact of Natural Hydrocarbons on Rural Ozone, *Nature, 329*(6141), 705-707, 1987.

Vautard, R., M. Beekmann and L. Menut, Applications of adjoint modelling in atmospheric chemistry: sensitivity and inverse modelling, *Environmental Modelling & Software, 15*(6-7), 703-709, 2000.

Vukicevic, T., Nonlinear and Linear Evolution of Initial Forecast Errors, *Monthly Weather Review, 119*(7), 1602-1611, 1991.

Vukicevic, T., Optimal initial perturbations for 2 cases of extratropical cyclogenesis, *Tellus Series A-Dynamic Meteorology and Oceanography, 50*(2), 143-166, 1998.

Vukicevic, T. and R. M. Errico, Linearization and Adjoint of Parameterized Moist Diabatic Processes, *Tellus Series A-Dynamic Meteorology and Oceanography, 45A*(5), 493-510, 1993.

Vukicevic, T. and P. Hess, Analysis of tropospheric transport in the Pacific Basin using the adjoint technique, *Journal of Geophysical Research-Atmospheres, 105*(D6), 7213-7230, 2000.

Vukovich, F. M. and J. Sherwell, An examination of the relationship between certain meteorological parameters and surface ozone variations in the Baltimore-Washington corridor, *Atmospheric Environment, 37*(7), 971-981, 2003.

Wang, K. Y., D. J. Lary, D. E. Shallcross, S. M. Hall and J. A. Pyle, A review on the use of the adjoint method in four-dimensional atmospheric-chemistry data assimilation, *Quarterly Journal of the Royal Meteorological Society, 127*(576), 2181-2204, 2001.

Wang, Y. H. and D. J. Jacob, Anthropogenic forcing on tropospheric ozone and OH since preindustrial times, *Journal of Geophysical Research-Atmospheres, 103*(D23), 31123-31135, 1998.

Wang, Z., I. M. Navon, F. X. Ledimet and X. Zou, The 2Nd-Order Adjoint Analysis - Theory and Applications, *Meteorology and Atmospheric Physics, 50*(1-3), 3-20, 1992.

Wen, D., Modelling of Atmospheric Mercury Emission, Transport, Transformation and deposition in North America, Ph.D. in Chemistry. University of Waterloo, 2006.

Wennberg, P. O. and D. Dabdub, Atmospheric chemistry - Rethinking ozone production, *Science, 319*(5870), 1624-1625, 2008.

West, J. J., V. Naik, L. W. Horowitz and A. M. Fiore, Effect of regional precursor emission controls on long-range ozone transport - Part 2: Steady-state changes in ozone air quality and impacts on human mortality, *Atmospheric Chemistry and Physics, 9*(16), 6095-6107, 2009.

Whiten, G., H. Hogo and J. Killus, The carbon-bond mechanism - a condensed kinetic mechanism for photochemical smog, *Environmental Science & Technology, 14*(6), 690-700, 1980.

Williams, E. J., A. Guenther and F. C. Fehsenfeld, An Inventory of Nitric-Oxide Emissions from Soils in the United-States, *Journal of Geophysical Research-Atmospheres, 97*(D7), 7511-7519, 1992.

Yang, R. J., A. G. Xia, D. V. Michelangeli, D. A. Plummer, L. Neary, J. W. Kaminski and J. C. McConnell, Evaluating a Canadian regional air quality model using ground-based observations in north-eastern Canada and United States, *Journal of Environmental Monitoring, 5*(1), 40-46, 2003.

Yang, Y. J., J. G. Wilkinson and A. G. Russell, Fast, direct sensitivity analysis of multidimensional photochemical models, *Environmental Science & Technology, 31*(10), 2859-2868, 1997.

Yap, D., D. T. Ning and W. Dong, An Assessment of Source Contributions to the Ozone Concentrations in Southern Ontario, 1979-1985, *Atmospheric Environment, 22*(6), 1161-1168, 1988.

Yarwood, G., S. Rao, M. Yocke and G. Z. Whitten, Updates to the Carbon Bond chemical mechanism: CB05. Final Report to the US EPA, RT-0400675, 2005.

Yu, S., R. Mathur, G. Sarwar, D. Kang, D. Tong, G. Pouliot and J. Pleim, Eta-CMAQ air quality forecasts for O-3 and related species using three different photochemical mechanisms (CB4, CB05, SAPRC-99): comparisons with measurements during the 2004 ICARTT study, *Atmospheric Chemistry and Physics, 10*(6), 3001-3025, 2010.

Yu, S. C., R. Mathur, K. Schere, D. W. Kang, J. Pleim and T. L. Otte, A detailed evaluation of the Eta-CMAQ forecast model performance for O-3, its related precursors, and meteorological parameters during the 2004 ICARTT study, *Journal of Geophysical Research-Atmospheres, 112*(D12), 2007.

Yumimoto, K. and I. Uno, Adjoint inverse modeling of CO emissions over Eastern Asia using four-dimensional variational data assimilation, *Atmospheric Environment, 40*(35), 6836-6845, 2006.

Zhang, L., E. M. Constantinescu, A. Sandu, Y. Tang, T. Chai, G. R. Carmichael, D. Byun and E. Olaguer, An adjoint sensitivity analysis and 4D-Var data assimilation study of Texas air quality, *Atmospheric Environment, 42*(23), 5787-5804, 2008.

Zhang, L., D. J. Jacob, M. Kopacz, D. K. Henze, K. Singh and D. A. Jaffe, Intercontinental source attribution of ozone pollution at western US sites using an adjoint method, *Geophysical Research Letters, 36*, 2009.

Zhao, S., A. Hakami, S. L. Capps, A. Nenes, T. Russel, J. Resler, T. Chai, D. Byun, M. Turner, D. K. Henze, P. Percell, J. Baek, C. Stanier, G. Carmichael, S. Napelenok, R. Prinn and A. Sandu, Development of a multiphase adjoint for CMAQ (in 2010 CMAS Conference), 2010.

Zhao, S., A. Hakami, M. Turner, D. K. Henze, S. L. Capps, T. Russel and A. Nenes, Development and integration of an aerosol adjoint model for CMAQ-ADJ (in 2011 CMAS Conference), 2011.

Zhu, C. Y., R. H. Byrd, P. H. Lu and J. Nocedal, Algorithm 778: L-BFGS-B: Fortran subroutines for large-scale bound-constrained optimization, *Acm Transactions on Mathematical Software, 23*(4), 550-560, 1997.

Zou, X., A. Barcilon, I. M. Navon, J. Whitaker and D. G. Cacuci, An Adjoint Sensitivity Study of Blocking in A 2-Layer Isentropic Model, *Monthly Weather Review, 121*(10), 2833-2857, 1993.

Appendix A

Reaction list of CB4 mechanism

[1] NO2 + hv --> NO + O

[2] O + [O2] --> O3

[3] O3 + NO --> NO2

[4] O + NO2 --> NO

[5] O + NO2 --> NO3

[6] O + NO --> NO2

[7] O3 + NO2 --> NO3

[8] O3 + hv --> O

[9] O3 + hv --> O1D

[10] O1D + [N2] --> O

[11] O1D + [O2] --> O

[12] O1D + [H2O] --> 2.000*OH

[13] O3 + OH --> HO2

[14] O3 + HO2 --> OH

[15] NO3 + hv --> 0.890*NO2 + 0.890*O + 0.110*NO

[16] NO3 + NO --> 2.000*NO2

[17] NO3 + NO2 --> NO + NO2

[18] NO3 + NO2 --> N2O5

[19] N2O5 + [H2O] --> 2.000*HNO3

[20] N2O5 --> NO3 + NO2

[21] NO + NO + [O2] --> 2.000*NO2

[22] NO + NO2 + [H2O] --> 2.000*HONO

[23] OH + NO --> HONO

[24] HONO + hv --> OH + NO

[25] HONO + OH --> NO2

[26] HONO + HONO --> NO + NO2

[27] OH + NO2 --> HNO3

[28] OH + HNO3 --> NO3

[29] HO2 + NO --> OH + NO2

[30] HO2 + NO2 --> PNA

[31] PNA --> HO2 + NO2

[32] PNA + OH --> NO2

[33] HO2 + HO2 --> H2O2

[34] HO2 + HO2 + [H2O] --> H2O2

[35] H2O2 + hv --> 2.000*OH

[36] H2O2 + OH --> HO2

[37] CO + OH --> HO2

[38] FORM + OH --> HO2 + CO

[39] FORM + hv --> 2.000*HO2 + CO

[40] FORM + hv --> CO

[41] FORM + O --> OH + HO2 + CO

[42] FORM + NO3 --> HNO3 + HO2 + CO

[43] ALD2 + O --> C2O3 + OH

[44] ALD2 + OH --> C2O3

[45] ALD2 + NO3 --> C2O3 + HNO3

[46] ALD2 + hv --> XO2 + 2.000*HO2 + CO + FORM

[47] C2O3 + NO --> NO2 + XO2 + FORM + HO2

[48] C2O3 + NO2 --> PAN

[49] PAN --> C2O3 + NO2

[50] C2O3 + C2O3 --> 2.000*XO2 + 2.000*FORM + 2.000*HO2

[51] C2O3 + HO2 --> 0.790*FORM + 0.790*XO2 + 0.790*HO2 + 0.790*OH

[52] OH --> XO2 + FORM + HO2

[53] PAR + OH --> 0.870*XO2 + 0.130*XO2N + 0.110*HO2 + 0.110*ALD2 + 0.760*ROR - 0.110*PAR

[54] ROR --> 1.100*ALD2 + 0.960*XO2 + 0.940*HO2 - 2.100*PAR + 0.040*XO2N + 0.020*ROR

[55] ROR --> HO2

[56] ROR + NO2 --> NTR

[57] OLE + O --> 0.630*ALD2 + 0.380*HO2 + 0.280*XO2 + 0.300*CO + 0.200*FORM + 0.020*XO2N + 0.220*PAR + 0.200*OH

[58] OLE + OH --> FORM + ALD2 + XO2 + HO2 - PAR

[59] OLE + O3 --> 0.500*ALD2 + 0.740*FORM + 0.330*CO + 0.440*HO2 + 0.220*XO2 + 0.100*OH - PAR

[60] OLE + NO3 --> 0.910*XO2 + 0.090*XO2N + FORM + ALD2 - PAR + NO2

[61] ETH + O --> FORM + 0.700*XO2 + CO + 1.700*HO2 + 0.300*OH

[62] ETH + OH --> XO2 + 1.560*FORM + HO2 + 0.220*ALD2

[63] ETH + O3 --> FORM + 0.420*CO + 0.120*HO2

[64] TOL + OH --> 0.080*XO2 + 0.360*CRES + 0.440*HO2 + 0.560*TO2

[65] TO2 + NO --> 0.900*NO2 + 0.900*HO2 + 0.900*OPEN + 0.100*NTR

[66] TO2 --> CRES + HO2

[67] CRES + OH --> 0.400*CRO + 0.600*XO2 + 0.600*HO2 + 0.300*OPEN

[68] CRES + NO3 --> CRO + HNO3

[69] CRO + NO2 --> NTR

[70] XYL + OH --> 0.700*HO2 + 0.500*XO2 + 0.200*CRES + 0.800*MGLY + 1.100*PAR + 0.300*TO2

[71] OPEN + OH --> XO2 + 2.000*CO + 2.000*HO2 + C2O3 + FORM

[72] OPEN + hv --> C2O3 + HO2 + CO

[73] OPEN + O3 --> 0.030*ALD2 + 0.620*C2O3 + 0.700*FORM + 0.030*XO2 + 0.690*CO + 0.080*OH + 0.760*HO2 + 0.200*MGLY

[74] MGLY + OH --> XO2 + C2O3

[75] MGLY + hv --> C2O3 + HO2 + CO

[76] ISOP + O --> 0.750*ISPD + 0.500*FORM + 0.250*XO2 + 0.250*HO2 + 0.250*C2O3 + 0.250*PAR

[77] ISOP + OH --> 0.912*ISPD + 0.629*FORM + 0.991*XO2 + 0.912*HO2 + 0.088*XO2N

[78] ISOP + O3 --> 0.650*ISPD + 0.600*FORM + 0.200*XO2 + 0.066*HO2 + 0.266*OH + 0.200*C2O3 + 0.150*ALD2 + 0.350*PAR + 0.066*CO

[79] ISOP + NO3 --> 0.200*ISPD + 0.800*NTR + XO2 + 0.800*HO2 + 0.200*NO2 + 0.800*ALD2 + 2.400*PAR

[80] XO2 + NO --> NO2

[81] XO2 + XO2 -->

[82] XO2N + NO --> NTR

[83] SO2 + OH --> SULF + HO2

[84] SO2 --> SULF

[85] XO2 + HO2 -->

[86] XO2N + HO2 -->

[87] XO2N + XO2N -->

[88] XO2N + XO2 -->

[89] ISPD + OH --> 1.565*PAR + 0.167*FORM + 0.713*XO2 + 0.503*HO2 + 0.334*CO + 0.168*MGLY + 0.273*ALD2 + 0.498*C2O3

[90] ISPD + O3 --> 0.114*C2O3 + 0.150*FORM + 0.850*MGLY + 0.154*HO2 + 0.268*OH + 0.064*XO2 + 0.020*ALD2 + 0.360*PAR + 0.225*CO

[91] ISPD + NO3 --> 0.357*ALD2 + 0.282*FORM + 1.282*PAR + 0.925*HO2 + 0.643*CO + 0.850*NTR + 0.075*C2O3 + 0.075*XO2 + 0.075*HNO3

[92] ISPD + hv --> 0.333*CO + 0.067*ALD2 + 0.900*FORM + 0.832*PAR + 1.033*HO2 + 0.700*XO2 + 0.967*C2O3

[93] ISOP + NO2 --> 0.200*ISPD + 0.800*NTR + XO2 + 0.800*HO2 + 0.200*NO + 0.800*ALD2 + 2.400*PAR

Rate Expression Rate Constant of CB4 mechanism:

k(1) uses photo table NO2_CBIV88 , scaled by 1.00000E+00 [0.00000E+00]

k(2) is a falloff expression using: [1.37387E-14]

k0 = 6.0000E-34 * (T/300)**(-2.30)

kinf = 2.8000E-12 * (T/300)**(0.00)

F = 0.60, n = 1.00

k(3) = 1.8000E-12 * exp(-1370.0/T) [1.81419E-14]

k(4) = 9.3000E-12 [9.30000E-12]

k(5) is a falloff expression using: [1.57527E-12]

k0 = 9.0000E-32 * (T/300)**(-2.00)

kinf = 2.2000E-11 * (T/300)**(0.00)

F = 0.60, n = 1.00

k(6) is a falloff expression using: [1.66375E-12]

k0 = 9.0000E-32 * (T/300)**(-1.50)

kinf = 3.0000E-11 * (T/300)**(0.00)

F = 0.60, n = 1.00

k(7) = 1.2000E-13 * exp(-2450.0/T) [3.22581E-17]

k(8) uses photo table NO2_CBIV88 , scaled by 5.30000E-02 [0.00000E+00]

k(9) uses photo table O3O1D_CBIV88 , scaled by 1.00000E+00 [0.00000E+00]

k(10) = 1.8000E-11 * exp(107.0/T) [2.57757E-11]

k(11) = 3.2000E-11 * exp(67.0/T) [4.00676E-11]

k(12) = 2.2000E-10 [2.20000E-10]

k(13) = 1.6000E-12 * exp(-940.0/T) [6.82650E-14]

k(14) = 1.4000E-14 * exp(-580.0/T) [1.99920E-15]

k(15) uses photo table NO2_CBIV88 , scaled by 3.39000E+01 [0.00000E+00]

k(16) = 1.3000E-11 * exp(250.0/T) [3.00805E-11]

k(17) = 2.5000E-14 * exp(-1230.0/T) [4.03072E-16]

k(18) is a falloff expression using: [1.26440E-12]

k0 = 2.2000E-30 * (T/300)**(-4.30)

kinf = 1.5000E-12 * (T/300)**(-0.50)

F = 0.60, n = 1.00

k(19) = 1.3000E-21 [1.30000E-21]

k(20) = k(18) / Keq, where Keq = 2.700E-27 * exp(11000.0/T) [4.36029E-02]

k(21) = 3.3000E-39 * exp(530.0/T) [1.95397E-38]

k(22) = 4.4000E-40 [4.39999E-40]

k(23) is a falloff expression using: [6.69701E-12]

k0 = 6.7000E-31 * (T/300)**(-3.30)

kinf = 3.0000E-11 * (T/300)**(-1.00)

F = 0.60, n = 1.00

k(24) uses photo table NO2_CBIV88 , scaled by 1.97500E-01 [0.00000E+00]

k(25) = 6.6000E-12 [6.60000E-12]

k(26) = 1.0000E-20 [1.00000E-20]

k(27) is a falloff expression using: [1.14885E-11]

k0 = 2.6000E-30 * (T/300)**(-3.20)

kinf = 2.4000E-11 * (T/300)**(-1.30)

F = 0.60, n = 1.00

k(28) is a special rate expression of the form: [1.47236E-13]

k = k0 + [k3[M] / (1 + k3[M]/k2)], where

k0 = 7.2000E-15 * exp(785.0/T)

k2 = 4.1000E-16 * exp(1440.0/T)

k3 = 1.9000E-33 * exp(725.0/T)

k(29) = 3.7000E-12 * exp(240.0/T) [8.27883E-12]

k(30) is a falloff expression using: [1.48014E-12]

k0 = 2.3000E-31 * (T/300)**(-4.60)

kinf = 4.2000E-12 * (T/300)**(0.20)

F = 0.60, n = 1.00

k(31) = k(30) / Keq, where Keq = 2.100E-27 * exp(10900.0/T) [9.17943E-02]

k(32) = 1.3000E-12 * exp(380.0/T) [4.65309E-12]

k(33) = 5.9000E-14 * exp(1150.0/T) [2.79783E-12]

k(34) = 2.2000E-38 * exp(5800.0/T) [6.23927E-30]

k(35) uses photo table HCHOmol_CBIV88 , scaled by 2.55000E-01 [0.00000E+00]

k(36) = 3.1000E-12 * exp(-187.0/T) [1.65514E-12]

k(37) = 1.5000E-13 * (1.0 + 0.6*Pressure) [2.40000E-13]

k(38) = 1.0000E-11 [1.00000E-11]

k(39) uses photo table HCHOrad_CBIV88 , scaled by 1.00000E+00 [0.00000E+00]

k(40) uses photo table HCHOmol_CBIV88 , scaled by 1.00000E+00 [0.00000E+00]

k(41) = 3.0000E-11 * exp(-1550.0/T) [1.65275E-13]

k(42) = 6.3000E-16 [6.30000E-16]

k(43) = 1.2000E-11 * exp(-986.0/T) [4.38753E-13]

k(44) = 7.0000E-12 * exp(250.0/T) [1.61972E-11]

k(45) = 2.5000E-15 [2.50000E-15]

k(46) uses photo table ALD_CBIV88 , scaled by 1.00000E+00 [0.00000E+00]

k(47) = 3.4900E-11 * exp(-180.0/T) [1.90766E-11]

k(48) = 2.6300E-12 * exp(380.0/T) [9.41356E-12]

k(49) = 2.0000E+16 * exp(-13500.0/T) [4.23268E-04]

k(50) = 2.5000E-12 [2.50000E-12]

k(51) = 6.5000E-12 [6.50000E-12]

k(52) = 1.1000E+02 * exp(-1710.0/T) [3.54242E-01]

k(53) = 8.1000E-13 [8.10000E-13]

k(54) = 1.0000E+15 * exp(-8000.0/T) [2.19325E+03]

k(55) = 1.6000E+03 [1.60000E+03]

k(56) = 1.5000E-11 [1.50000E-11]

k(57) = 1.2000E-11 * exp(-324.0/T) [4.04572E-12]

k(58) = 5.2000E-12 * exp(504.0/T) [2.82173E-11]

k(59) = 1.4000E-14 * exp(-2105.0/T) [1.19778E-17]

k(60) = 7.7000E-15 [7.70000E-15]

k(61) = 1.0000E-11 * exp(-792.0/T) [7.01080E-13]

k(62) = 2.0000E-12 * exp(411.0/T) [7.94340E-12]

k(63) = 1.3000E-14 * exp(-2633.0/T) [1.89105E-18]

k(64) = 2.1000E-12 * exp(322.0/T) [6.18715E-12]

k(65) = 8.1000E-12 [8.10000E-12]

k(66) = 4.2000E+00 [4.20000E+00]

k(67) = 4.1000E-11 [4.10000E-11]

k(68) = 2.2000E-11 [2.20000E-11]

k(69) = 1.4000E-11 [1.40000E-11]

k(70) = 1.7000E-11 * exp(116.0/T) [2.50901E-11]

k(71) = 3.0000E-11 [3.00000E-11]

k(72) uses photo table HCHOrad_CBIV88 , scaled by 9.04000E+00 [0.00000E+00]

k(73) = 5.4000E-17 * exp(-500.0/T) [1.00858E-17]

k(74) = 1.7000E-11 [1.70000E-11]

k(75) uses photo table HCHOrad_CBIV88 , scaled by 9.64000E+00 [0.00000E+00]

k(76) = 3.6000E-11 [3.60000E-11]

k(77) = 2.5400E-11 * exp(407.6/T) [9.97368E-11]

k(78) = 7.8600E-15 * exp(-1912.0/T) [1.28512E-17]

k(79) = 3.0300E-12 * exp(-448.0/T) [6.73819E-13]

k(80) = 8.1000E-12 [8.10000E-12]

k(81) = 1.7000E-14 * exp(1300.0/T) [1.33359E-12]

k(82) = 8.1000E-12 [8.10000E-12]

k(83) = 4.3900E-13 * exp(160.0/T) [7.51005E-13]

k(84) = 1.3600E-06 [1.36000E-06]

k(85) = 7.6700E-14 * exp(1300.0/T) [6.01684E-12]

k(86) = 7.6700E-14 * exp(1300.0/T) [6.01684E-12]

k(87) = 1.7300E-14 * exp(1300.0/T) [1.35712E-12]

k(88) = 3.4500E-14 * exp(1300.0/T) [2.70640E-12]

k(89) = 3.3600E-11 [3.36000E-11]

k(90) = 7.1100E-18 [7.11000E-18]

k(91) = 1.0000E-15 [1.00000E-15]

k(92) uses photo table ACROLEIN , scaled by 3.60000E-03 [0.00000E+00]

k(93) = 1.4900E-19 [1.49000E-19]

Appendix B

New FORTRAN code for the forward model of CMAQ-ADJ

```
!“nc_chk1_module.f90”:
! Revision History:
! August 2009 by Hongyan Dang
module nc_chk1_module
  implicit none
  save
      integer chk_status
      integer :: &
        chk_ncid    ,& !
        dat_varid   ,& !
        lon_varid   ,& !
        lat_varid   ,& !
        lev_varid
      integer :: &
        rec_dimid     ,& !
        lev_dimid     ,& !
        lon_dimid     ,& !
        lat_dimid     ,& !
        var_dimid     ,& !
        dat_dimid     ,& !
        date_dimid    ,& !
        time_dimid    ,& !
        dt_dimid      ,& !
        rhoj_dimid    ,& !
        chemstep_dimid ,& !
        syn_dimid
      integer :: tstep_varid   !
      integer :: &
        tflag_varid       ,& !
        JDATE_varid       ,& !
        JTIME_varid       ,& !
        conc_varid(36)    ,& !
        rhoj_varid        ,& !
        var_varid         ,& !
        chemstep_varid    ,& !
        syns_varid        ,& !
        rj_varid(6)         !
      integer :: nstep_cmaq  !
end module nc_chk1_module


!“nc_check.f90”:
! Revision History:
! August 2009 by Hongyan Dang
  subroutine nc_check(chk_status)
    use netcdf
    use nc_chk1_module
    implicit none

    integer, intent (in) :: chk_status
      if(chk_status /= nf90_noerr) then
        stop "Stopped when writting nc files."
      end if

  end subroutine nc_check


!“nc_chk1_putvar.f90”:
! Revision History:
! August 2009 by Hongyan Dang
! Note: There are 5 subroutines in this file:
!       nc_chk1_putvar
!       nc_chk1_putvar1
!       nc_chk1_putvar2
!       nc_chk1_putvar3
!       nc_chk1_putvar4
  subroutine nc_chk1_putvar(  &
                        nc_data_varid  &
                       , CGRID         &
                       , Nspecies      &
                       , nstep_nreps)
    use netcdf
    use nc_chk1_module
    USE GRID_CONF           ! horizontal & vertical domain specifications
```

```
    USE CGRID_SPCS          ! CGRID species number and offsets
    USE KPP_Integrator
    implicit none
!- Writing 4D data, a nc_lon X nc_lat X nc_lev lon-lat-lev grid, with unknown timesteps of
data.
    integer :: &
        nstep_nreps,&
        Nspecies

!- Program variables to hold the data we will write out.
    real, pointer :: CGRID(:,:,:,:)
    integer :: nc_data_varid
!- Start and count arrays to tell the netCDF library where to write data.
    integer :: start(4), count(4)
! These settings tell netcdf to write one timestep of data. (The
! setting of start(4) inside the loop below tells netCDF which
! timestep to write.)
 start = (/ 1, 1, 1, nstep_nreps /)
 count = (/ NCOLS, NROWS, NLAYS, 1 /)
!- These settings tell netCDF to write one timestep of data
!    do loop in syn.-time-step.
    call nc_check(nf90_put_var( &
                chk_ncid,  &
                nc_data_varid,  &
                CGRID(:,:,:,Nspecies),  &
                start=start,  &
                count=count  &
               ))
 end subroutine NC_CHK1_PUTVAR

! Hongyan Dang, August 2009.
  subroutine nc_chk1_putvar1( &
                      nc_data_varid  &
                    , RJ          &
                    , Nspecies      &
                    , nstep_nreps)
    use netcdf
    use nc_chk1_module
    USE GRID_CONF          ! horizontal & vertical domain specifications
    USE CGRID_SPCS         ! CGRID species number and offsets
    USE KPP_Integrator
    implicit none
!- Writing 4D data, a nc_lon X nc_lat X nc_lev lon-lat-lev grid, with unknown timesteps of
data.
```



```
    integer :: &
        nstep_nreps,&
        Nspecies
!- Program variables to hold the data we will write out.
    real, RJ(:,:,:,:)
    integer :: nc_data_varid
!- Start and count arrays to tell the netCDF library where to write data.
    integer :: start(4), count(4)
! These settings tell netcdf to write one timestep of data. (The
! setting of start(4) inside the loop below tells netCDF which
! timestep to write.)
 start = (/ 1, 1, 1, nstep_nreps /)
 count = (/ NCOLS, NROWS, NLAYS, 1 /)
!- These settings tell netCDF to write one timestep of data
!    do loop in syn.-time-step.
    call nc_check(nf90_put_var( &
                chk_ncid,  &
                nc_data_varid,  &
                RJ(:,:,:,Nspecies),  &
                start=start,  &
                count=count  &
               ))
 end subroutine NC_CHK1_PUTVAR1


! Hongyan Dang, August 2009.
  subroutine nc_chk1_putvar2( &
                      nc_data_varid  &
                    , v_nc          &
                    , nstep_nreps)
    use netcdf
    use nc_chk1_module
    USE GRID_CONF          ! horizontal & vertical domain specifications
    USE CGRID_SPCS         ! CGRID species number and offsets
    USE KPP_Integrator
    implicit none
!- Writing 4D data, a nc_lon X nc_lat X nc_lev lon-lat-lev grid, with unknown timesteps of
data.
    integer :: &
        nstep_nreps,&
        Nspecies
!- Program variables to hold the data we will write out.
    real, v_nc(:,:,:)
    integer :: nc_data_varid
```

```
!- Start and count arrays to tell the netCDF library where to write data.
    integer :: start(4), count(4)
    integer ::  count1(3)
! These settings tell netcdf to write one timestep of data. (The
! setting of start(4) inside the loop below tells netCDF which
! timestep to write.)
 start = (/ 1, 1, 1, nstep_nreps /)
 count = (/ NCOLS, NROWS, NLAYS, 1 /)
!- These settings tell netCDF to write one timestep of data
!    do loop in syn.-time-step.
    call nc_check(nf90_put_var( &
                chk_ncid,  &
                nc_data_varid,  &
                v_nc(:,:,:),  &
                start=start,  &
                count=count  &
               ))
 end subroutine NC_CHK1_PUTVAR2


! Hongyan Dang, August 2009.
  subroutine nc_chk1_putvar3( &
                      nc_data_varid  &
                    , v_nc1        &
                    , nstep_nreps)
    use netcdf
    use nc_chk1_module
    USE GRID_CONF           ! horizontal & vertical domain specifications
    USE CGRID_SPCS          ! CGRID species number and offsets
    USE KPP_Integrator
    implicit none
!- Writing 3D data, a nc_lon X nc_lat  lon-lat grid, with unknown timesteps of data.
    integer :: &
        nstep_nreps,&
        Nspecies
    INTEGER     JDATE       ! current model date, coded YYYYDD
    INTEGER     JTIME       ! current model time, coded HHMMSS
!- Program variables to hold the data we will write out.
    integer, v_nc1(1)
    integer :: nc_data_varid
!- Start and count arrays to tell the netCDF library where to write data.
    integer :: start(2), count(2)
! These settings tell netcdf to write one timestep of data. (The
! setting of start(4) inside the loop below tells netCDF which
! timestep to write.)
 start = (/ 1, nstep_nreps /)
 count = (/ 1, 1 /)
!- These settings tell netCDF to write one timestep of data
!    do loop in syn.-time-step.
    call nc_check(nf90_put_var( &
                chk_ncid,  &
                nc_data_varid,  &
                v_nc1,  &
                start=start,  &
                count=count  &
               ))
 end subroutine NC_CHK1_PUTVAR3


  subroutine nc_chk1_putvar4( &
                      nc_data_varid  &
                    , v_nc1)
    use netcdf
    use nc_chk1_module
    USE GRID_CONF           ! horizontal & vertical domain specifications
    USE CGRID_SPCS          ! CGRID species number and offsets
    USE KPP_Integrator
    implicit none
!- Program variables to hold the data we will write out.
    integer, v_nc1(1)
    integer :: nc_data_varid
!- Start and count arrays to tell the netCDF library where to write data.
    integer :: start(1), count(1)
! These settings tell netcdf to write one timestep of data. (The
! setting of start(4) inside the loop below tells netCDF which
! timestep to write.)
 start = (/ 1 /)
 count = (/ 1 /)
!- These settings tell netCDF to write one timestep of data
!    do loop in syn.-time-step.
    call nc_check(nf90_put_var( &
                chk_ncid,  &
                nc_data_varid,  &
                v_nc1,  &
                start=start,  &
                count=count  &
               ))
 end subroutine NC_CHK1_PUTVAR4
```

```
!“nc_chk1.f90”:
!- This program is to save CMAQ-ADJOINT variables to netCDF format without using IOAPI.
! Revision History:
! August 2009 by Hongyan Dang
    subroutine nc_chk1
    use netcdf
    use KPP_Integrator
    USE HGRD_DEFN          ! horizontal domain specifications
    USE VGRD_DEFN          ! vertical layer specifications
    USE HRDATA
    use nc_chk1_module
    implicit none
    include 'gc__spc.ext'
!- This is the name of the nc_check-point file we will create.
    character(len = *), parameter :: FILE_NAME = "fwd/cctm_fwdCHK.nc"
    integer, parameter :: &
       NDIMS1=1   ,& !
       NDIMS2=2   ,& !
       NDIMS3=3   ,& !
       NDIMS4=4   ,& !
       NRECS=2
    integer, dimension(1:NDIMS2) :: tflag_dimids
    integer, dimension(1:NDIMS2) :: jdate_dimids
    integer, dimension(1:NDIMS2) :: jtime_dimids
    integer, dimension(1:NDIMS4) :: rhoj_dimids
    integer, dimension(1:NDIMS4) :: nc_dimids
    integer, dimension(1:NDIMS4) :: chemstep_dimids
    integer, dimension(1:NDIMS1) :: syns_dimids
    integer, dimension(1:NDIMS4) :: rj_dimids
!- Writing 4D data, a 156 X 96 X 14 lon-lat-lev grid, with unknown timesteps of data.
    integer, parameter :: &
       nc_date  =  1  ,& ! number of time
       nc_time  =  1  ,& ! number of time
       nc_var   = 44  ,& ! 44 variables
       nc_rj    =  6  ,&
       nc_syn   =  1
    character (len = *), parameter :: &
       LON_NAME = "COL"       ,& !
       LAT_NAME = "ROW"       ,& !
       LEV_NAME = "LAY"       ,& !
       VAR_NAME = "VAR"       ,& !
       DATE_NAME = "DATE_SIZE"  ,& !
       TIME_NAME = "TIME_SIZE"  ,& !
       REC_NAME = "TSTEP"     ,& !
       DAT_NAME = "DATE-TIME"   ,& !
       SYN_NAME = "SYNC_SIZE"
!- Start and count arrays to tell the netCDF library where to write data.
    integer :: start(NDIMS4), count(NDIMS4)
!- Create 2+44 variables to save timestep and field values.
!-   these settings uses the definitions in "include SUBST_GC_SPC"
    character (len=*), parameter :: tflag_name       = "JDATEJTIME"
    character (len=16), parameter :: jdate_name      = "JDATE          "
    character (len=16), parameter :: jtime_name      = "JTIME          "     !
    character (len=16), parameter :: rhoj_name       = "RHOJ           "
    character (len=16), parameter :: chemstep_name   = "CHEMSTEP       "
    character (len=16), parameter :: nstep_nreps_name = "N_SYNS         "
    character (len=16) :: rj_name(6)
    data rj_name(1)/"RJ1           "/
    data rj_name(2)/"RJ2           "/
    data rj_name(3)/"RJ3           "/
    data rj_name(4)/"RJ4           "/
    data rj_name(5)/"RJ5           "/
    data rj_name(6)/"RJ6           "/
!- Totally (N_GC_SPC + 8 = 36 + 8 = 44) variables will be written to "CCTM_fwdCHK.nc".
    INTEGER,parameter ::   nc_GC_SPC=36, nc_GC_SPCD=nc_GC_SPC + 1
    CHARACTER (len=16)   nc_SPC(nc_GC_SPCD+8)
!- Units of the 44 variables
  character (len = *), parameter :: UNITS = "units"
  character (len = *), parameter :: VDESC = "var_desc"
!- Units of the coordinate variables.
  character (len = *), parameter :: LAT_UNITS = "degrees_north"
  character (len = *), parameter :: LON_UNITS = "degrees_east"
  character (len = *), parameter :: LEV_UNITS = " "
  character (len = *), parameter :: REC_UNITS = "second"
!- Units of the variables.
! character (len = *), parameter :: TFLAG_UNITS = "<YYYYDDDHHMMSS>"
  character (len = *), parameter :: JDATE_UNITS = "<YYYYDDD>"
  character (len = *), parameter :: JTIME_UNITS = "<MMSS> or <HMMSS> or <HHMMSS>"
  character (len = *), parameter :: CONC_UNITS = "ppmV"
  character (len = *), parameter :: RHOJ_UNITS = "m"
  character (len = *), parameter :: CHEMSTEP_UNITS = "min"
  character (len = *), parameter :: RJ_UNITS = " "
  character (len = *), parameter :: SYNS_UNITS = " "
!- Description of the variables.
  character (len = *), parameter :: TFLAG_VDESC = "Timestep-valid flags: YYYYDDDHHMMSS"
  character (len = *), parameter :: RHOJ_VDESC = "Advected air density X total Jacobian"
```

```
 character (len = *), parameter :: CHEMSTEP_VDESC = "Previous Rosenbrock time step"
 character (len = *), parameter :: SYNS_VDESC = "Total syncronization timesteps during the
simulation period"
 character (len = *), parameter :: RJ_VDESC = "Photolysis rates from tables"
 integer :: nc_i  ! used for do loops
    INTERFACE
      subroutine nc_check(chk_status)
        integer chk_status
      end subroutine nc_check
    END INTERFACE
!- Create the file.
    call nc_check( nf90_create(FILE_NAME, nf90_share, chk_ncid) )

!- Define the dimensions. The time dimension is defined to have unlimited
!- length - it can grow as needed.
    call nc_check( nf90_def_dim(chk_ncid, REC_NAME, NF90_UNLIMITED, rec_dimid ))
    call nc_check( nf90_def_dim(chk_ncid, DATE_NAME, nc_date, date_dimid ) )
    call nc_check( nf90_def_dim(chk_ncid, TIME_NAME, nc_time, time_dimid ) )
    call nc_check( nf90_def_dim(chk_ncid, VAR_NAME, nc_var, var_dimid ) )
    call nc_check( nf90_def_dim(chk_ncid, LEV_NAME, NLAYS, lev_dimid ) )
    call nc_check( nf90_def_dim(chk_ncid, LAT_NAME, NROWS, lat_dimid ) )
    call nc_check( nf90_def_dim(chk_ncid, LON_NAME, NCOLS, lon_dimid ))
    call nc_check( nf90_def_dim(chk_ncid, SYN_NAME, nc_syn, syn_dimid ))
!- Define the coordinate variables for lat, lon, lev, var, rec.
!- Through providing the address of the dimension ID:
!- (lat_dimid), (lon_dimid), (lev_dimid), (dat_dimid), and (rec_dimid).
!    call nc_check( nf90_def_var(chk_ncid, LAT_NAME, NF90_REAL, lat_dimid, lat_varid) )
!    call nc_check( nf90_def_var(chk_ncid, LON_NAME, NF90_REAL, lon_dimid, lon_varid) )
!    call nc_check( nf90_def_var(chk_ncid, LEV_NAME, NF90_REAL, lev_dimid, lev_varid) )
!- Assign units to coordiante variables.
!    call nc_check( nf90_put_att(chk_ncid, lat_varid, UNITS, LAT_UNITS) )
!    call nc_check( nf90_put_att(chk_ncid, lon_varid, UNITS, LON_UNITS) )
!    call nc_check( nf90_put_att(chk_ncid, lev_varid, UNITS, LEV_UNITS) )
!- Define arrays dimensions for the variables.
!    tflag_dimids    = (/ dt_dimid, rec_dimid /)
    JDATE_dimids    = (/ date_dimid, rec_dimid /)
    JTIME_dimids    = (/ time_dimid, rec_dimid /)
    nc_dimids       = (/ lon_dimid, lat_dimid, lev_dimid, rec_dimid/)
    rhoj_dimids     = (/ lon_dimid, lat_dimid, lev_dimid, rec_dimid/)
    chemstep_dimids = (/ lon_dimid, lat_dimid, lev_dimid, rec_dimid/)
    rj_dimids       = (/ lon_dimid, lat_dimid, lev_dimid, rec_dimid/)
    syns_dimids     = (/ syn_dimid /)
!- Define the netCDF variables for the concentration, Jacobians, and so on.
    call nc_check (nf90_def_var(chk_ncid, JDATE_name, NF90_REAL, &
              jdate_dimids, jdate_varid))
    call nc_check (nf90_def_var(chk_ncid, JTIME_name, NF90_REAL, &
              jtime_dimids, jtime_varid))
    do nc_i=1,nc_GC_SPC                                  ! nc_gc_spc=36
      chk_status =  nf90_def_var(chk_ncid, GC_SPC(nc_i), NF90_REAL, &
                nc_dimids, conc_varid(nc_i))
    enddo
    call nc_check (nf90_def_var(chk_ncid, rhoj_name, NF90_REAL, &
              rhoj_dimids, rhoj_varid))
    call nc_check (nf90_def_var(chk_ncid, chemstep_name, NF90_REAL, &
              chemstep_dimids, chemstep_varid))
    do nc_i=1,6
      call nc_check (nf90_def_var(chk_ncid, rj_name(nc_i), NF90_REAL,  &
                rj_dimids, rj_varid(nc_i)))
    enddo
    call nc_check (nf90_def_var(chk_ncid, nstep_nreps_name, NF90_REAL, &
              syns_dimids, syns_varid))
!- Assign units and variable description to the netCDF variables.
!    call nc_check (nf90_put_att(chk_ncid, tflag_varid, UNITS, TFLAG_UNITS))
!    call nc_check (nf90_put_att(chk_ncid, tflag_varid, VDESC, TFLAG_VDESC))
    call nc_check (nf90_put_att(chk_ncid, jdate_varid, UNITS, JDATE_UNITS))
    call nc_check (nf90_put_att(chk_ncid, jtime_varid, UNITS, JTIME_UNITS))
    do nc_i=1,nc_GC_SPC   ! nc_gc_spc=36
      call nc_check (nf90_put_att(chk_ncid, conc_varid(nc_i), UNITS, CONC_UNITS))
    enddo
    call nc_check (nf90_put_att(chk_ncid, rhoj_varid, UNITS, RHOJ_UNITS))
    call nc_check (nf90_put_att(chk_ncid, rhoj_varid, VDESC, RHOJ_VDESC))
    call nc_check (nf90_put_att(chk_ncid, chemstep_varid, UNITS, CHEMSTEP_UNITS))
    call nc_check (nf90_put_att(chk_ncid, chemstep_varid, VDESC, CHEMSTEP_VDESC))
    call nc_check (nf90_put_att(chk_ncid, syns_varid, UNITS, SYNS_UNITS))
    do nc_i=1,6
      call nc_check (nf90_put_att(chk_ncid, rj_varid(nc_i), UNITS, RJ_UNITS))
      call nc_check (nf90_put_att(chk_ncid, rj_varid(nc_i), VDESC, RJ_VDESC))
    enddo
    call nc_check (nf90_put_att(chk_ncid, syns_varid, VDESC, SYNS_VDESC))
!- End define mode.
    call nc_check( nf90_enddef(chk_ncid))
!- close the file
!    call nc_check( nf90_close(chk_ncid))
 end subroutine nc_chk1
```

Appendix C

New FORTRAN code for the backward model of CMAQ-ADJ

!“nc_adj_module.f90”:

```
module nc_adj_module
  implicit none
  save
      integer chk_status, &
        chk1_varid
      integer :: &
        chk_ncid    ,& !
         bg_ncid    ,& !
        obs_ncid    ,& !
        chkpt_ncid  ,& !
        bwd_ncid
      integer :: &
        adj_ncid    ,& !
        dat_varid   ,& !
        lon_varid   ,& !
        lat_varid   ,& !
        lev_varid
      integer :: &
        rec_dimid     ,& !
        lev_dimid     ,& !
        lon_dimid     ,& !
        lat_dimid     ,& !
        var_dimid     ,& !
        dat_dimid     ,& !
        date_dimid    ,& !
        time_dimid    ,& !
        dt_dimid      ,& !
        rhoj_dimid    ,& !
        chemstep_dimid ,& !
        syn_dimid       !
      integer :: tstep_varid   !
      integer :: &
        tflag_varid       ,& !
        jdate_varid       ,& !
        jtime_varid       ,& !
        conc_varid(36)    ,& !
        rhoj_varid        ,& !
        var_varid         ,& !
        chemstep_varid    ,& !
        syns_varid        ,& !
        rj_varid(6)         !
    integer :: nstep_cmaq  !
    integer, dimension(1:2) :: tflag_dimids
    integer, dimension(1:2) :: jdate_dimids
    integer, dimension(1:2) :: jtime_dimids
    integer, dimension(1:4) :: rhoj_dimids
    integer, dimension(1:4) :: nc_dimids
    integer, dimension(1:4) :: chemstep_dimids
    integer, dimension(1:1) :: syns_dimids
    integer, dimension(1:4) :: rj_dimids
    integer  nstep_nreps &
          , chk1_nstep_nreps(1) &
          , chk1_datime(1) &
          , chk1_JDATE(1) &
          , chk1_JTIME(1)
 end module nc_adj_module
```

!“nc_check.f90”:

```
! Hongyan. August 2009.
 subroutine nc_check(chk_status)
   use netcdf
   use nc_adj_module
   implicit none
   integer, intent (in) :: chk_status
    if(chk_status /= nf90_noerr) then
      stop "Stopped when writting nc files."
    end if
 end subroutine nc_check
```

!“nc_open_chk1.f90”:

```
    subroutine nc_open_chk1
    use netcdf
    use KPP_Integrator
    USE HRDATA
    use nc_adj_module
```

```
    implicit none
    include 'gc__spc.ext'
!- This is the name of the nc_check-point file to read.
    character(len = *), parameter :: FILE_NAME = "fwd/cctm_fwdCHK.nc"
    call nc_check( nf90_open(FILE_NAME, nf90_nowrite, chk_ncid) )
 end subroutine nc_open_chk1


!"nc_read_chk1.f90":
  subroutine nc_chk1_rd0(rd_chemstep_name, chemstep_data, nstep_nreps)
   use netcdf
   use nc_adj_module
   USE GRID_CONF          ! horizontal & vertical domain specifications
   USE CGRID_SPCS         ! CGRID species number and offsets
   USE KPP_Integrator
   implicit none
    character (len=16) rd_chemstep_name
    real :: chemstep_data(NCOLS, NROWS, NLAYS)
    integer :: nstep_nreps
    integer :: start1(4), count1(4)
    integer :: rd_chemstep_varid
    start1 = (/ 1, 1, 1, nstep_nreps /)
    count1 = (/ NCOLS, NROWS, NLAYS, 1 /)
     call nc_check( nf90_inq_varid(chk_ncid, rd_chemstep_name, rd_chemstep_varid))
     call nc_check( nf90_get_var(chk_ncid, rd_chemstep_varid &
            , chemstep_data(:,:,:), start1, count1          ))
  endsubroutine nc_chk1_rd0


  subroutine nc_chk1_rd1(nc_data_name, chk1_data, N_ic, nstep_nreps)
   use netcdf
   use nc_adj_module
   USE GRID_CONF          ! horizontal & vertical domain specifications
   USE CGRID_SPCS         ! CGRID species number and offsets
   USE KPP_Integrator
   implicit none
    character*16 nc_data_name
    real, intent(out) :: chk1_data(:,:,:,:)
    integer :: N_ic,nstep_nreps
    integer :: start1(4), count1(4)
    integer :: nc_data_varid
    start1 = (/ 1, 1, 1, nstep_nreps /)
    count1 = (/ NCOLS, NROWS, NLAYS, 1 /)
     call nc_check( nf90_inq_varid(chk_ncid, nc_data_name, nc_data_varid))
      call nc_check( nf90_get_var(chk_ncid, nc_data_varid &
             , chk1_data(:,:,:,N_ic), start1, count1          ))
  endsubroutine nc_chk1_rd1


  subroutine nc_chk1_rd2(Jdatime_name,datime_data, nstep_nreps)
   use netcdf
   use nc_adj_module
   implicit none
    character (len=16) jdatime_name  ! = "JDATE" or "JTIME"
    integer :: datime_data(1)
    integer :: nstep_nreps
    integer :: start2(2), count2(2)
    integer :: jdatime_varid
    start2 = (/ 1, nstep_nreps /)
    count2 = (/ 1, 1 /)
    call nc_check( nf90_inq_varid(chk_ncid, Jdatime_name, jdatime_varid))
     call nc_check( nf90_get_var(chk_ncid, jdatime_varid &
            , datime_data, start2, count2          ))
  endsubroutine nc_chk1_rd2


  subroutine nc_chk1_rd3(rd_nstep_nreps_name,chk1_nstep_nreps)
   use netcdf
   use nc_adj_module
   implicit none
    character(len=16) rd_nstep_nreps_name   ! = "N_SYNS"
    integer :: chk1_nstep_nreps(1)
    integer :: start3(1), count3(1)
    integer :: nstep_nreps_varid
    start3 = (/ 1 /)
    count3 = (/ 1 /)
     call nc_check( nf90_inq_varid(chk_ncid, rd_nstep_nreps_name, nstep_nreps_varid))
     call nc_check( nf90_get_var(chk_ncid, nstep_nreps_varid &
            , chk1_nstep_nreps, start3, count3          ))
  endsubroutine nc_chk1_rd3


!"nc_chk1_putvar.f90":
! Note: There are 4 subroutines in this file:
!       nc_chk1_putvar
!       nc_chk1_putvar1
!       nc_chk1_putvar2
!       nc_chk1_putvar3
```

```
! Hongyan Dang, August 2009.
  subroutine nc_chk1_putvar(  &
!                       bwd_ncid &
!                     , nc_data_varid  &
                      nc_data_varid  &
                     , CGRID        &
                     , Nspecies      &
                     , nstep_nreps)
    use netcdf
    use nc_adj_module
    USE GRID_CONF          ! horizontal & vertical domain specifications
    USE CGRID_SPCS         ! CGRID species number and offsets
    USE KPP_Integrator
    implicit none
!- Writing 4D data, a nc_lon X nc_lat X nc_lev lon-lat-lev grid, with unknown timesteps of
data.
    integer :: &
!       nc_lon,  nc_lat,  nc_lev, nc_time, &
        nstep_nreps,&
        Nspecies
!- Program variables to hold the data we will write out.
    real, pointer :: CGRID(:,:,:,:)
!    integer :: bwd_ncid
    integer :: nc_data_varid
!- Start and count arrays to tell the netCDF library where to write data.
    integer :: start(4), count(4)
! These settings tell netcdf to write one timestep of data. (The
! setting of start(4) inside the loop below tells netCDF which
! timestep to write.)
 start = (/ 1, 1, 1, nstep_nreps /)
 count = (/ NCOLS, NROWS, NLAYS, 1 /)
!- These settings tell netCDF to write one timestep of data
!    do loop in syn.-time-step.
    call nc_check(nf90_put_var( &
                bwd_ncid,  &
                nc_data_varid,  &
                CGRID(:,:,:,Nspecies),  &
                start=start,  &
                count=count  &
               ))
 end subroutine NC_CHK1_PUTVAR

! Hongyan Dang, August 2009.
  subroutine nc_chk1_putvar3( &
!                       bwd_ncid &
!                     , nc_data_varid  &
                      nc_data_varid  &
                     , v_nc1        &
                     , nstep_nreps)
    use netcdf
    use nc_adj_module
    USE GRID_CONF          ! horizontal & vertical domain specifications
    USE CGRID_SPCS         ! CGRID species number and offsets
    USE KPP_Integrator
    implicit none
!- Writing 3D data, a nc_lon X nc_lat  lon-lat grid, with unknown timesteps of data.
    integer :: &
       nstep_nreps,&
       Nspecies
    INTEGER     JDATE       ! current model date, coded YYYYDD
    INTEGER     JTIME       ! current model time, coded HHMMSS
 !- Program variables to hold the data we will write out.
    integer, v_nc1(1)
!    integer :: bwd_ncid
    integer :: nc_data_varid
!- Start and count arrays to tell the netCDF library where to write data.
    integer :: start(2), count(2)
! These settings tell netcdf to write one timestep of data. (The
! setting of start(4) inside the loop below tells netCDF which
! timestep to write.)
 start = (/ 1, nstep_nreps /)
 count = (/ 1, 1 /)
!- These settings tell netCDF to write one timestep of data
!    do loop in syn.-time-step.
    call nc_check(nf90_put_var( &
                bwd_ncid,  &
                nc_data_varid,  &
                v_nc1,  &
                start=start,  &
                count=count  &
               ))
 end subroutine NC_CHK1_PUTVAR3


  subroutine nc_chk1_putvar4( &
                      bwd_ncid &
                     , nc_data_varid  &
                     , v_nc1)
```

```
    use netcdf
    use nc_adj_module
    USE GRID_CONF          ! horizontal & vertical domain specifications
    USE CGRID_SPCS         ! CGRID species number and offsets
    USE KPP_Integrator
    implicit none
!- Program variables to hold the data we will write out.
    integer, v_nc1(1)
    integer :: bwd_ncid
    integer :: nc_data_varid

!- Start and count arrays to tell the netCDF library where to write data.
    integer :: start(1), count(1)
! These settings tell netcdf to write one timestep of data. (The
! setting of start(4) inside the loop below tells netCDF which
! timestep to write.)
 start = (/ 1 /)
 count = (/ 1 /)
!- These settings tell netCDF to write one timestep of data
!    do loop in syn.-time-step.
    call nc_check(nf90_put_var( &
              bwd_ncid,  &
              nc_data_varid,  &
              v_nc1,  &
              start=start,  &
              count=count  &
             ))
 end subroutine NC_CHK1_PUTVAR4


!"nc_chk1_bwd.f90":
!- This program is to save CMAQ-ADJOINT variables to netCDF format without using IOAPI.
!- Hongyan Dang, August 2009.
    subroutine nc_chk1_bwd
    use netcdf
    use KPP_Integrator
    USE HGRD_DEFN          ! horizontal domain specifications
    USE VGRD_DEFN          ! vertical layer specifications
    USE HRDATA
    use nc_adj_module
    implicit none
    include 'gc__spc.ext'
!- This is the name of the nc_check-point file we will create.
    character(len = *), parameter :: FILE_NAME = "bwd/cctm_bwdCHK.nc"
    integer, parameter :: &
       NDIMS1=1   ,& !
       NDIMS2=2   ,& !
       NDIMS3=3   ,& !
       NDIMS4=4   ,& !
       NRECS=2
!- Writing 4D data, a 156 X 96 X 14 lon-lat-lev grid, with unknown timesteps of data.
    integer, parameter :: &
       nc_date =  1  ,& ! number of time
       nc_time =  1  ,& ! number of time
       nc_var  = 44  ,& ! 44 variables
       nc_rj   =  6  ,&
       nc_syn  =  1
    character (len = *), parameter :: &
       LON_NAME = "COL"       ,& !
       LAT_NAME = "ROW"       ,& !
       LEV_NAME = "LAY"       ,& !
       VAR_NAME = "VAR"       ,& !
       DATE_NAME = "DATE_SIZE"  ,& !
       TIME_NAME = "TIME_SIZE"  ,& !
       REC_NAME = "TSTEP"     ,& !
       DAT_NAME = "DATE-TIME"   ,& !
       SYN_NAME = "SYNC_SIZE"
!- Start and count arrays to tell the netCDF library where to write data.
    integer :: start(NDIMS4), count(NDIMS4)
!- Create 2+44 variables to save timestep and field values.
!-   these settings uses the definitions in "include SUBST_GC_SPC"
    character (len=*), parameter :: tflag_name       = "JDATEJTIME"
    character (len=16), parameter :: jdate_name      = "JDATE         "
    character (len=16), parameter :: jtime_name      = "JTIME         "     !
    character (len=16), parameter :: rhoj_name       = "RHOJ          "
    character (len=16), parameter :: chemstep_name   = "CHEMSTEP      "
    character (len=16), parameter :: nstep_nreps_name = "N_SYNS        "
    character (len=16) :: rj_name(6)
    data rj_name(1)/"RJ1           "/
    data rj_name(2)/"RJ2           "/
    data rj_name(3)/"RJ3           "/
    data rj_name(4)/"RJ4           "/
    data rj_name(5)/"RJ5           "/
    data rj_name(6)/"RJ6           "/
!- Totally (N_GC_SPC + 8 = 36 + 8 = 44) variables will be written to "CCTM_fwdCHK.nc".
    INTEGER,parameter ::   nc_GC_SPC=36, nc_GC_SPCD=nc_GC_SPC + 1
    CHARACTER (len=16)   nc_SPC(nc_GC_SPCD+8)
!- Units of the 44 variables
```

```
  character (len = *), parameter :: UNITS = "units"
  character (len = *), parameter :: VDESC = "var_desc"

!- Units of the coordinate variables.
  character (len = *), parameter :: LAT_UNITS = "degrees_north"
  character (len = *), parameter :: LON_UNITS = "degrees_east"
  character (len = *), parameter :: LEV_UNITS = " "
  character (len = *), parameter :: REC_UNITS = "second"
!- Units of the variables.
! character (len = *), parameter :: TFLAG_UNITS = "<YYYYDDDHHMMSS>"
  character (len = *), parameter :: JDATE_UNITS = "<YYYYDDD>"
  character (len = *), parameter :: JTIME_UNITS = "<MMSS> or <HMMSS> or <HHMMSS>"
  character (len = *), parameter :: CONC_UNITS = "ppmV"
  character (len = *), parameter :: RHOJ_UNITS = "m"
  character (len = *), parameter :: CHEMSTEP_UNITS = "min"
  character (len = *), parameter :: RJ_UNITS = " "
  character (len = *), parameter :: SYNS_UNITS = " "
!- Description of the variables.
  character (len = *), parameter :: TFLAG_VDESC = "Timestep-valid flags: YYYYDDDHHMMSS"
  character (len = *), parameter :: RHOJ_VDESC = "Advected air density X total Jacobian"
  character (len = *), parameter :: CHEMSTEP_VDESC = "Previous Rosenbrock time step"
  character (len = *), parameter :: SYNS_VDESC = "Total syncronization timesteps during the
simulation period"
  character (len = *), parameter :: RJ_VDESC = "Photolysis rates from tables"
  integer :: nc_i  ! used for do loops
     INTERFACE
       subroutine nc_check(chk_status)
         integer chk_status
       end subroutine nc_check
     END INTERFACE

!- Create the file.
     call nc_check( nf90_create(FILE_NAME, nf90_share, bwd_ncid) )
!- Define the dimensions. The time dimension is defined to have unlimited
!- length - it can grow as needed.
     call nc_check( nf90_def_dim(bwd_ncid, REC_NAME, NF90_UNLIMITED, rec_dimid ))
     call nc_check( nf90_def_dim(bwd_ncid, DATE_NAME, nc_date, date_dimid ) )
     call nc_check( nf90_def_dim(bwd_ncid, TIME_NAME, nc_time, time_dimid ) )
     call nc_check( nf90_def_dim(bwd_ncid, VAR_NAME, nc_var, var_dimid ) )
     call nc_check( nf90_def_dim(bwd_ncid, LEV_NAME, NLAYS, lev_dimid ) )
     call nc_check( nf90_def_dim(bwd_ncid, LAT_NAME, NROWS, lat_dimid ) )
     call nc_check( nf90_def_dim(bwd_ncid, LON_NAME, NCOLS, lon_dimid ))
     call nc_check( nf90_def_dim(bwd_ncid, SYN_NAME, nc_syn, syn_dimid ))
!- Define the coordinate variables for lat, lon, lev, var, rec.
!- Through providing the address of the dimension ID:
!- (lat_dimid), (lon_dimid), (lev_dimid), (dat_dimid), and (rec_dimid).
!    call nc_check( nf90_def_var(bwd_ncid, LAT_NAME, NF90_REAL, lat_dimid, lat_varid) )
!    call nc_check( nf90_def_var(bwd_ncid, LON_NAME, NF90_REAL, lon_dimid, lon_varid) )
!    call nc_check( nf90_def_var(bwd_ncid, LEV_NAME, NF90_REAL, lev_dimid, lev_varid) )
!- Assign units to coordiante variables.
!    call nc_check( nf90_put_att(bwd_ncid, lat_varid, UNITS, LAT_UNITS) )
!    call nc_check( nf90_put_att(bwd_ncid, lon_varid, UNITS, LON_UNITS) )
!    call nc_check( nf90_put_att(bwd_ncid, lev_varid, UNITS, LEV_UNITS) )
!- Define arrays dimensions for the variables.
!    tflag_dimids    = (/ dt_dimid, rec_dimid /)
     JDATE_dimids    = (/ date_dimid, rec_dimid /)
     JTIME_dimids    = (/ time_dimid, rec_dimid /)
     nc_dimids       = (/ lon_dimid, lat_dimid, lev_dimid, rec_dimid/)
     rhoj_dimids     = (/ lon_dimid, lat_dimid, lev_dimid, rec_dimid/)
     chemstep_dimids = (/ lon_dimid, lat_dimid, lev_dimid, rec_dimid/)
     rj_dimids       = (/ lon_dimid, lat_dimid, lev_dimid, rec_dimid/)
     syns_dimids     = (/ syn_dimid /)
!- Define the netCDF variables for the concentration, Jacobians, and so on.
!    call nc_check (nf90_def_var(bwd_ncid, tflag_name, NF90_REAL, &
!              tflag_dimids, tflag_varid))
     call nc_check (nf90_def_var(bwd_ncid, JDATE_name, NF90_REAL, &
               jdate_dimids, jdate_varid))
     call nc_check (nf90_def_var(bwd_ncid, JTIME_name, NF90_REAL, &
               jtime_dimids, jtime_varid))
     do nc_i=1,nc_GC_SPC
       chk_status =  nf90_def_var(bwd_ncid, GC_SPC(nc_i), NF90_REAL, &
                 nc_dimids, conc_varid(nc_i))
     enddo
     call nc_check (nf90_def_var(bwd_ncid, rhoj_name, NF90_REAL, &
               rhoj_dimids, rhoj_varid))
     call nc_check (nf90_def_var(bwd_ncid, chemstep_name, NF90_REAL, &
               chemstep_dimids, chemstep_varid))
     do nc_i=1,6
       call nc_check (nf90_def_var(bwd_ncid, rj_name(nc_i), NF90_REAL,  &
                 rj_dimids, rj_varid(nc_i)))
     enddo
     call nc_check (nf90_def_var(bwd_ncid, nstep_nreps_name, NF90_REAL, &
               syns_dimids, syns_varid))

!- Assign units and variable description to the netCDF variables.
     call nc_check (nf90_put_att(bwd_ncid, jdate_varid, UNITS, JDATE_UNITS))
     call nc_check (nf90_put_att(bwd_ncid, jtime_varid, UNITS, JTIME_UNITS))
     do nc_i=1,nc_GC_SPC   ! nc_gc_spc=36
```

```
      call nc_check (nf90_put_att(bwd_ncid, conc_varid(nc_i), UNITS, CONC_UNITS))
    enddo
    call nc_check (nf90_put_att(bwd_ncid, rhoj_varid, UNITS, RHOJ_UNITS))
    call nc_check (nf90_put_att(bwd_ncid, rhoj_varid, VDESC, RHOJ_VDESC))
    call nc_check (nf90_put_att(bwd_ncid, chemstep_varid, UNITS, CHEMSTEP_UNITS))
    call nc_check (nf90_put_att(bwd_ncid, chemstep_varid, VDESC, CHEMSTEP_VDESC))
    call nc_check (nf90_put_att(bwd_ncid, syns_varid, UNITS, SYNS_UNITS))
    do nc_i=1,6
      call nc_check (nf90_put_att(bwd_ncid, rj_varid(nc_i), UNITS, RJ_UNITS))
      call nc_check (nf90_put_att(bwd_ncid, rj_varid(nc_i), VDESC, RJ_VDESC))
    enddo
    call nc_check (nf90_put_att(bwd_ncid, syns_varid, VDESC, SYNS_VDESC))
!- End define mode.
    call nc_check( nf90_enddef(bwd_ncid))
!- close the file
!    call nc_check( nf90_close(bwd_ncid))
 end subroutine nc_chk1_bwd


!“advstep_adj.F”:
    SUBROUTINE ADVSTEP_ADJ ( JDATE, JTIME, TSTEP, ASTEP, NREPS )
C Function:
C   This subroutine is added by Hongyan Dang to be used in the backward
C               to locate the corresponding meteorology data
C               for the corresponding output time-step.
C Revision history:
C   Hongyan Dang modified based on "SUBROUTINE ADVSTEP" of CMAQ model.
C   October 2009 by Hongyan Dang

    USE GRID_CONF          ! horizontal & vertical domain specifications
    USE SUBST_MODULES           ! stenex
    IMPLICIT NONE
C Includes:
    INCLUDE SUBST_CONST      ! constants
    INCLUDE SUBST_IOPARMS    ! I/O parameters definitions
    INCLUDE SUBST_IOFDESC    ! file header data structure
    INCLUDE SUBST_IODECL     ! I/O definitions and declarations
    INCLUDE SUBST_FILES_ID   ! file name parameters
C Arguments:
    INTEGER   JDATE        ! current model simulation date (YYYYDDD)
    INTEGER   JTIME        ! current model simulation time (HHMMSS)
    INTEGER   TSTEP( 2 )    ! time step vector (HHMMSS)
                  ! TSTEP(1) = local output step
                  ! TSTEP(2) = sciproc sync. step (chem)
    INTEGER   ASTEP( : )    ! layer advection step
    INTEGER   NREPS         ! sync time steps per output time step
C Parameter:  maximum Courant number allowed
    REAL, PARAMETER :: CC = 0.75
    INTEGER, SAVE :: MAXSYNC        ! force max TSTEP(2) (sec)
    INTEGER, SAVE :: MINSYNC        ! force min TSTEP(2) (sec)
    REAL, SAVE    :: SIGST          ! sigma_sync_top value
    INTEGER, SAVE :: ADVLAYR        ! adv=sync at least up to this level
C External Functions (not already declared by IODECL3.EXT):
    INTEGER, EXTERNAL :: SEC2TIME, TIME2SEC, SECSDIFF, ENVINT
    LOGICAL, EXTERNAL :: ENVYN, CURRSTEP
    REAL, EXTERNAL    :: ENVREAL
C Local variables:
    INTEGER, SAVE :: LOGDEV        ! unit number for log device
    LOGICAL, SAVE :: FIRSTIME = .TRUE.
    INTEGER, SAVE :: WSTEP = 0     ! wind file interpolation time step
    INTEGER, SAVE :: SDATE, STIME   ! wind file start date and time
    INTEGER, SAVE :: FDATE, FTIME   ! wind file current date and time
    INTEGER, SAVE :: FSTEP         ! wind file time step
    REAL, SAVE :: IDX1            ! 1/dx1
    REAL, SAVE :: IDX2            ! 1/dx2
    REAL WIND ( NCOLS+1,NROWS+1 )      ! Contravariant generic-velocity
    INTEGER     MINSECS           ! min TSTEP(2) (sec) that divides TSTEP(1)
    INTEGER     C, R, L
    INTEGER     EDATE, ETIME
    INTEGER     REP, ADV, STEP, T2, K
    INTEGER     SYNC, NADVS( NLAYS )
    LOGICAL     ADJFLG
    REAL       UOVDX( NLAYS )     ! max  component velocity / dXi
    REAL       MXUOVDX
    CHARACTER( 16 ) :: PNAME = 'ADVSTEP_ADJ'
    CHARACTER( 16 ) :: UORV
    CHARACTER( 96 ) :: XMSG = ' '
    INTEGER     STATUS           !  ENVINT status
    CHARACTER( 80 ) :: VARDESC     !  environment variable description
    CHARACTER( 80 ) :: MSG = ' '
C environment variable max sync step
    CHARACTER( 16 ) :: CTM_MAXSYNC = 'CTM_MAXSYNC'
C environment variable min sync step
    CHARACTER( 16 ) :: CTM_MINSYNC = 'CTM_MINSYNC'
C environment variable adv layer
    CHARACTER( 16 ) :: SIGMA_SYNC_TOP = 'SIGMA_SYNC_TOP'
    INTEGER MY_TEMP
    INTEGER, SAVE :: STARTCOL, ENDCOL
```

```
      INTEGER, SAVE :: STARTROW, ENDROW
!     integer mxcol, mxrow, mxlvl
!     real mxwind, vovdx( nlays )
      INTERFACE
        SUBROUTINE HCONTVEL ( FDATE, FTIME, FSTEP, LVL, UORV, WIND )
          IMPLICIT NONE
          INTEGER, INTENT( IN ) :: FDATE, FTIME, FSTEP, LVL
          CHARACTER( 16 ), INTENT( IN ) :: UORV
          REAL, INTENT( OUT ) :: WIND( :,: )
        END SUBROUTINE HCONTVEL
      END INTERFACE
      IF ( FIRSTIME ) THEN
        FIRSTIME = .FALSE.
        LOGDEV = INIT3()
        MAXSYNC = 720       ! default
        VARDESC = 'Maximum Synchronization Time Step (sec)'
        MAXSYNC = ENVINT( CTM_MAXSYNC, VARDESC, MAXSYNC, STATUS )
          IF ( STATUS .NE. 0 ) WRITE( LOGDEV, '(5X, A)' ) VARDESC
          IF ( STATUS .EQ. 1 ) THEN
            XMSG = 'Environment variable improperly formatted'
            CALL M3EXIT( PNAME, JDATE, JTIME, XMSG, XSTAT2 )
            END IF
!       MINSYNC = 300       ! default
        MINSYNC = 60        ! default
        VARDESC = 'Minimum Synchronization Time Step (sec)'
        MINSYNC = ENVINT( CTM_MINSYNC, VARDESC, MINSYNC, STATUS )
          IF ( STATUS .NE. 0 ) WRITE( LOGDEV, '(5X, A)' ) VARDESC
          IF ( STATUS .EQ. 1 ) THEN
            XMSG = 'Environment variable improperly formatted'
            CALL M3EXIT( PNAME, JDATE, JTIME, XMSG, XSTAT2 )
            END IF
        SIGST = 0.7         ! default
        VARDESC = 'Minimum layer limit for which adv = sync'
        SIGST = ENVREAL( SIGMA_SYNC_TOP, VARDESC, SIGST, STATUS )
          IF ( STATUS .NE. 0 ) WRITE( LOGDEV, '(5X, A)' ) VARDESC
          IF ( STATUS .EQ. 1 ) THEN
            XMSG = 'Environment variable improperly formatted'
            CALL M3EXIT( PNAME, JDATE, JTIME, XMSG, XSTAT2 )
            END IF
        IF ( VGTYP_GD .NE. VGSGPN3 .AND. VGTYP_GD .NE. VGSGPH3 ) THEN
          XMSG = 'Wrong vertical coordinate type'
          CALL M3EXIT( PNAME, JDATE, JTIME, XMSG, XSTAT2 )
          END IF
        IF ( SIGST .GT. VGLVS_GD( 2 ) .OR.
     &       SIGST .LT. VGLVS_GD( NLAYS + 1 ) ) THEN
          WRITE( XMSG, '( A, 1PE12.3 )' ) 'SIGMA_SYNC_TOP incorrect', SIGST
          CALL M3EXIT( PNAME, JDATE, JTIME, XMSG, XSTAT2 )
          END IF
        IF ( SIGST .EQ. VGLVS_GD( NLAYS + 1 ) ) THEN
          L = NLAYS
          ELSE
          DO K = 1, NLAYS
            IF ( SIGST .GE. VGLVS_GD( K+1 ) ) THEN
              IF ( SIGST - VGLVS_GD( K+1 ) .LE.
     &             VGLVS_GD( K ) - SIGST )  THEN
                L = K
                ELSE
                L = K - 1
                END IF
                GO TO 101
              END IF
            END DO
          END IF
101     CONTINUE
        ADVLAYR = L
        WRITE( LOGDEV, 92005 ) ADVLAYR
C Open wind field file and get header data
        IF ( .NOT. OPEN3( MET_DOT_3D, FSREAD3, PNAME ) ) THEN
          XMSG = 'Could not open ' // MET_DOT_3D // ' file'
          CALL M3EXIT( PNAME, JDATE, JTIME, XMSG, XSTAT0 )
          END IF

        IF ( .NOT. DESC3( MET_DOT_3D ) ) THEN
          XMSG = 'Could not get ' // MET_DOT_3D // ' file description'
          CALL M3EXIT( PNAME, JDATE, JTIME, XMSG, XSTAT1 )
          END IF
        SDATE = SDATE3D
        STIME = STIME3D
        FSTEP = TSTEP3D
C Check file data against COORD.EXT
        IF ( XCELL3D .NE. XCELL_GD .OR. YCELL3D .NE. YCELL_GD ) THEN
          XMSG = 'File grid sizes do not match CTM domain definition'
          CALL M3EXIT( PNAME, JDATE, JTIME, XMSG, XSTAT3 )
          END IF
C Get cell size in meters (from COORD.EXT)
        IF ( GDTYP_GD .EQ. LATGRD3 ) THEN
          IDX2 = 1.0 / (DG2M * YCELL_GD)
          IDX1 = 1.0 / (DG2M * XCELL_GD
```

```
     &         * COS( PI180*( YORIG_GD + YCELL_GD*FLOAT( NROWS/2 ))) )
          ELSE
          IDX1 = 1.0 / XCELL_GD
          IDX2 = 1.0 / YCELL_GD
          END IF
C Get the starting wind field: do not interpolate
        IF ( .NOT. CURRSTEP( JDATE, JTIME, SDATE, STIME, FSTEP,
     &                       FDATE, FTIME ) ) THEN
          XMSG = 'Cannot get step-starting date and time'
          CALL M3EXIT( PNAME, JDATE, JTIME, XMSG, XSTAT3 )
          END IF
        CALL SUBST_LOOP_INDEX ( 'C', 1, MY_NCOLS, 1, MY_TEMP,
     &                          STARTCOL, ENDCOL )
        CALL SUBST_LOOP_INDEX ( 'R', 1, MY_NROWS, 1, MY_TEMP,
     &                          STARTROW, ENDROW )
        END IF                  !  if firstime
C Compute the least number of equal time steps that satisfy the Courant
C condition (force TSTEP(2) to be no greater than 15 min.):
      STEP = TIME2SEC( TSTEP( 1 ) )
C Make sure STEP .GE. MINSYNC
      IF ( STEP .LT. MINSYNC ) THEN
        WRITE( LOGDEV,92009 ) STEP, MINSYNC
        XMSG = ' '
        CALL M3EXIT( PNAME, JDATE, JTIME, XMSG, XSTAT3 )
        END IF
C Make sure that MINSYNC divides STEP and is even
      DO REP = MINSYNC, STEP
        IF ( MOD( STEP, REP ) .EQ. 0 ) THEN
          MINSECS = REP
          IF ( MINSECS .NE. MINSYNC )
     &       WRITE( LOGDEV,92011 ) JDATE, JTIME, MINSYNC, MINSECS
          GO TO 201
          END IF
        END DO
C If you get here: could not determine satisfactory MINSECS
      WRITE( XMSG,94011 ) MINSYNC, STEP
      CALL M3EXIT( PNAME, JDATE, JTIME, XMSG, XSTAT3 )

201   CONTINUE
      WRITE( LOGDEV,92013 ) JDATE, JTIME
C Establish ending time for this Courant number calculation:
      EDATE = JDATE
      ETIME = JTIME
      CALL NEXTIME ( EDATE, ETIME, TSTEP( 1 ) )
```



```
      IF ( SECSDIFF( FDATE, FTIME, EDATE, ETIME ) .GT. 0 )
C Get the next wind field: do not interpolate
     &   CALL NEXTIME( FDATE, FTIME, FSTEP )
      UORV = 'X1VEL'
      DO L = 1, ADVLAYR
        CALL HCONTVEL ( FDATE, FTIME, WSTEP, L, UORV, WIND )
        UOVDX( L ) = -1.0
        DO R = 1, MY_NROWS
          DO C = STARTCOL, ENDCOL     !     DO C = 1, MY_NCOLS+1
            UOVDX( L ) = MAX( UOVDX( L ), ABS( WIND( C,R ) ) * IDX1 )
            END DO
          END DO
        END DO
      UORV = 'X2VEL'
      DO L = 1, ADVLAYR
        CALL HCONTVEL ( FDATE, FTIME, WSTEP, L, UORV, WIND )
        DO R = STARTROW, ENDROW       !  DO R = 1, MY_NROWS+1
          DO C = 1, MY_NCOLS
            UOVDX( L ) = MAX( UOVDX( L ), ABS( WIND( C,R ) ) * IDX2 )
            END DO
          END DO
        END DO
!     write( logdev,* ) 'vmax- c,r,l,wind: ', mxcol, mxrow, mxlvl, mxwind
      MXUOVDX = -1.0
      DO L = 1, ADVLAYR
        UOVDX( L ) = SUBST_GLOBAL_MAX ( UOVDX( L ) )
        IF ( UOVDX( L ) .GT. MXUOVDX ) MXUOVDX = UOVDX( L )
        END DO
C Determine sync step, S and adv step, A such that S = A and A satisfies the
C Courant condition (CC) up to layer ADVLAYR and such that S >= MINSYNC. If
C S should be < MINSYNC in order to satisfy the CC, set S = MINSYNC and adjust
C A to satisfy the CC and evenly divide S
      ADJFLG = .FALSE.
      DO REP = 1, STEP
        IF ( MOD( STEP, REP ) .EQ. 0 ) THEN  ! make TSTEP(2) divide TSTEP(1)
          SYNC = STEP / REP
          IF ( SYNC .LE. MAXSYNC ) THEN       ! force max TSTEP(2)
            ADV = SYNC
            IF ( MXUOVDX * FLOAT( ADV ) .LT. CC ) THEN
              IF ( SYNC .GE. MINSECS ) THEN  ! force min TSTEP(2)
                NREPS = REP
                ELSE   ! make ADV divide TSTEP(2) evenly
                SYNC = MINSECS
                NREPS = STEP / MINSECS
```

```
            IF ( MOD ( MINSECS,ADV ) .EQ. 0 ) THEN ! make ADV
              K = MINSECS / ADV          ! divide TSTEP(2)
              ELSE
              K = MINSECS / ADV + 1
              END IF
            ADV = MINSECS / K
            ADJFLG = .TRUE.
            END IF
          GO TO 301
          END IF     ! if Courant condition satisfied
        END IF     ! if SYNC .le. MAXSYNC
      END IF     ! if REP divides STEP evenly
    END DO     ! step loop
C If you get here: could not determine satisfactory advection time step.
    WRITE( LOGDEV,94013 ) TSTEP( 1 ), MXUOVDX
    XMSG = ' '
    CALL M3EXIT( PNAME, JDATE, JTIME, XMSG, XSTAT3 )
301   CONTINUE
  TSTEP( 2 ) = SEC2TIME( SYNC )
  DO L = 1, ADVLAYR
    ASTEP( L ) = SEC2TIME( ADV )
    NADVS( L ) = SYNC / ADV
    END DO
  IF ( ADJFLG ) THEN
    WRITE( LOGDEV,92019 ) MINSECS, TSTEP( 2 ), NREPS
    ELSE
    WRITE( LOGDEV,92021 ) TSTEP( 2 ), NREPS
    END IF
  UORV = 'X1VEL'
  DO L = ADVLAYR + 1, NLAYS
    CALL HCONTVEL ( FDATE, FTIME, WSTEP, L, UORV, WIND )
    UOVDX( L ) = -1.0
    DO R = 1, MY_NROWS
      DO C = STARTCOL, ENDCOL    !    DO C = 1, MY_NCOLS+1
        UOVDX( L ) = MAX( UOVDX( L ), ABS( WIND( C,R ) ) * IDX1 )
        END DO
      END DO
    END DO
  UORV = 'X2VEL'
  DO L = ADVLAYR + 1, NLAYS
    CALL HCONTVEL ( FDATE, FTIME, WSTEP, L, UORV, WIND )
    DO R = STARTROW, ENDROW       !  DO R = 1, MY_NROWS+1
      DO C = 1, MY_NCOLS
        UOVDX( L ) = MAX( UOVDX( L ), ABS( WIND( C,R ) ) * IDX2 )
        END DO
      END DO
    END DO
  DO L = ADVLAYR + 1, NLAYS
    UOVDX( L ) = SUBST_GLOBAL_MAX ( UOVDX( L ) )
    END DO
  T2 = TIME2SEC( TSTEP( 2 ) )
  DO L = ADVLAYR + 1, NLAYS
    ADV = T2 + 1
    DO REP = 1, STEP
      ADV = ADV - 1    ! subtract 1 sec
      IF ( UOVDX( L ) * FLOAT( ADV ) .LT. CC ) THEN
!   &                    ',  adv, uovdx: ', adv, uovdx( l )
        IF ( ADV .EQ. T2 ) THEN
          NADVS( L ) = T2 / ADV
          ELSE
          NADVS( L ) = T2 / ADV + 1
          END IF
        ASTEP( L ) = SEC2TIME( T2 / NADVS( L ) )
        GO TO 401
        END IF           !  if Courant condition satisfied
      END DO
C If you get here: could not determine satisfactory advection time step.
    WRITE( LOGDEV,94013 ) TSTEP( 1 ), L, UOVDX( L )
    XMSG = ' '
    CALL M3EXIT( PNAME, JDATE, JTIME, XMSG, XSTAT3 )
401   CONTINUE
    END DO   ! layer loop
  CALL NEXTIME( FDATE, FTIME, FSTEP*(-1) )   !Hongyan Dang added. oct23,2008
  WRITE( LOGDEV,92025 )
  DO L = NLAYS, 1, -1
    WRITE( LOGDEV,92027 ) L, ASTEP( L ), NADVS( L )
    END DO
  WRITE( LOGDEV,* ) ' '
  RETURN
C----------------  FORMAT  STATEMENTS   ------------------------------
92005 FORMAT (   5X, 'Top layer thru which sync step determined:', I3 )
92009 FORMAT ( / 5X, 'Output time step:', I8,
   &         1X, 'less than minimum synchronization step:', I8 )
92011 FORMAT ( / 5X, 'From ADVSTEP_ADJ - date/time: ', I8, '/', I6.6
   &       / 5X, 'Minimum Synchronization Step adjusted from:', I8,
   &         1X, 'to:', I8 )
92013 FORMAT ( / 5X, 'From ADVSTEP_ADJ - date/time: ', I8, '/', I6.6 )
92019 FORMAT ( / 5X, 'Synchronization step adjusted up to mimimum (SEC):', I7
```

```
     &        /46X, '(HHMMSS): ', I6.6
     &        / 5X, 'Number of Synchronization steps:', I3 /)
92021 FORMAT ( / 5X, 'Computed synchronization step (HHMMSS): ', I6.6
     &        / 5X, 'Number of Synchronization steps:', I3 /)
92025 FORMAT ( / 5X, 'Layer', 3X, 'Advection', 3X, 'per Sync'
     &        /11X, 'Step (HHMMSS)', 2X, 'Step' )
92027 FORMAT (   5X, I4, 6X, I6.6, 6X, I2 )
94011 FORMAT( / 5X, 'Starting from:', I6, ',',
     &         1X, 'could not determine minimum step that divides TSTEP',
     &         1X, 'for model step:', I7.6, ' HHMMSS')
94013 FORMAT( / 5X, 'Could not determine Courant-condition safe sync step',
     &         1X, 'for model step:', I7.6, ' HHMMSS',
     &         1X, 'in layer:', I3
     &       / 5X, '(Max vel)/(dX) =', 1PE10.3)
      END
```

Appendix D

New FORTRAN code for high resolution 4D-Var of CMAQ

```
 ! The subroutines “nc_check”, “ADVSTEP_ADJ”, “nc_chk1_putvar”, “nc_chk1_putvar1”,
!  “nc_chk1_putvar2”, “nc_chk1_putvar3”, and “nc_chk1_putvar4”
!   are same as those in Appendix B and are not replicated here.
! The subroutines “nc_chk1_rd0”, “nc_chk1_rd1”, “nc_chk1_rd2”, and “nc_chk1_rd3”
!  are same as those in Appendix C and are not replicated here.
!nc_adj_module.f90
! Hongyan. August 2009.
 module nc_adj_module

   implicit none
   save
       integer chk_status, &
          chk1_varid
       integer :: &
          chk_ncid    ,& !
           bg_ncid    ,& !
          obs_ncid    ,& !
          chkpt_ncid
       integer :: &
          adj_ncid    ,& !
          dat_varid   ,& !
          lon_varid   ,& !
          lat_varid   ,& !
          lev_varid
       integer :: &
          rec_dimid      ,& !
          lev_dimid      ,& !
          lon_dimid      ,& !
          lat_dimid      ,& !
          var_dimid      ,& !
          dat_dimid      ,& !
          date_dimid     ,& !
          time_dimid     ,& !
          dt_dimid       ,& !
          rhoj_dimid     ,& !
          chemstep_dimid ,& !
          syn_dimid         !
               integer :: tstep_varid   !
       integer :: &
          tflag_varid        ,& !
          jdate_varid        ,& !
          jtime_varid        ,& !
          conc_varid(36)     ,& !
          rhoj_varid         ,& !
          var_varid          ,& !
          chemstep_varid     ,& !
          syns_varid         ,& !
          rj_varid(6)           !

       integer :: nstep_cmaq  !

       integer, dimension(1:2) :: tflag_dimids
       integer, dimension(1:2) :: jdate_dimids
       integer, dimension(1:2) :: jtime_dimids
       integer, dimension(1:4) :: rhoj_dimids
       integer, dimension(1:4) :: nc_dimids
       integer, dimension(1:4) :: chemstep_dimids
       integer, dimension(1:1) :: syns_dimids
       integer, dimension(1:4) :: rj_dimids

       integer  nstep_nreps &
             , chk1_nstep_nreps(1) &
             , chk1_datime(1) &
             , chk1_JDATE(1) &
             , chk1_JTIME(1)

 end module nc_adj_module



!nc_open_chk.f90
  subroutine nc_open_chk
  use netcdf
  use nc_adj_module
  implicit none
     call nc_check( nf90_open("cctmCHK_L3obs.nc", nf90_nowrite, obs_ncid) )
     call nc_check( nf90_open("cctmCHK_L5bg.nc", nf90_nowrite, bg_ncid) )
  end subroutine nc_open_chk
```

```
!nc_close_chk.f90
      subroutine nc_close_chk
      use netcdf
      use nc_adj_module

      implicit none

      call nc_check( nf90_close(obs_ncid) )
      call nc_check( nf90_close(bg_ncid) )
      end subroutine nc_close_chk


!nc_chk1_obs.f90
!- This program is to save CMAQ-ADJOINT variables to netCDF format without using IOAPI.
!- Hongyan Dang, August 2009.
!
      subroutine nc_chk1_obs
      use netcdf
      Use KPP_Integrator
      USE HGRD_DEFN           ! horizontal domain specifications
      USE VGRD_DEFN           ! vertical layer specifications
      USE HRDATA
      use nc_adj_module
      implicit none
      include 'gc__spc.ext'
!     INCLUDE SUBST_GC_SPC    ! Gas chem species names and MWs
!- This is the name of the nc_check-point file we will create.
      character(len = *), parameter :: FILE_NAME = "cctmCHK_L3obs.nc"
      integer, parameter :: &
          NDIMS1=1    ,& !
          NDIMS2=2    ,& !
          NDIMS3=3    ,& !
          NDIMS4=4    ,& !
          NRECS=2
!     integer, dimension(1:NDIMS2) :: tflag_dimids
!     integer, dimension(1:NDIMS2) :: jdate_dimids
!     integer, dimension(1:NDIMS2) :: jtime_dimids
!     integer, dimension(1:NDIMS4) :: rhoj_dimids
!     integer, dimension(1:NDIMS4) :: nc_dimids
!     integer, dimension(1:NDIMS4) :: chemstep_dimids
!     integer, dimension(1:NDIMS1) :: syns_dimids
!     integer, dimension(1:NDIMS4) :: rj_dimids
!- Writing 4D data, a 156 X 96 X 14 lon-lat-lev grid, with unknown timesteps of data.
      integer, parameter :: &
          nc_date  =   1  ,& ! number of time
          nc_time  =   1  ,& ! number of time
          nc_var   =  44  ,& ! 44 variables
          nc_rj    =   6  ,&
          nc_syn   =   1
      character (len = *), parameter :: &
          LON_NAME = "COL"         ,& !
          LAT_NAME = "ROW"         ,& !
          LEV_NAME = "LAY"         ,& !
          VAR_NAME = "VAR"         ,& !
          DATE_NAME = "DATE_SIZE"  ,& !
          TIME_NAME = "TIME_SIZE"  ,& !
          REC_NAME = "TSTEP"       ,& !
          DAT_NAME = "DATE-TIME"   ,& !
          SYN_NAME = "SYNC_SIZE"

!- Start and count arrays to tell the netCDF library where to write data.
      integer :: start(NDIMS4), count(NDIMS4)

!- Create 2+44 variables to save timestep and field values.
!-    these settings uses the definitions in "include SUBST_GC_SPC"
      character (len=*), parameter :: tflag_name        = "JDATEJTIME"
      character (len=16), parameter :: jdate_name       = "JDATE          "
      character (len=16), parameter :: jtime_name       = "JTIME          "      !
      character (len=16), parameter :: rhoj_name        = "RHOJ           "
      character (len=16), parameter :: chemstep_name    = "CHEMSTEP       "
      character (len=16), parameter :: nstep_nreps_name = "N_SYNS         "
      character (len=16) :: rj_name(6)
      data rj_name(1)/"RJ1           "/
      data rj_name(2)/"RJ2           "/
      data rj_name(3)/"RJ3           "/
      data rj_name(4)/"RJ4           "/
      data rj_name(5)/"RJ5           "/
      data rj_name(6)/"RJ6           "/
!- Totally (N_GC_SPC + 8 = 36 + 8 = 44) variables will be written to "CCTM_fwdCHK.nc".
      INTEGER,parameter ::    nc_GC_SPC=36, nc_GC_SPCD=nc_GC_SPC + 1
      CHARACTER (len=16)   nc_SPC(nc_GC_SPCD+8)
!- Units of the 44 variables
  character (len = *), parameter :: UNITS = "units"
  character (len = *), parameter :: VDESC = "var_desc"
!- Units of the coordinate variables.
  character (len = *), parameter :: LAT_UNITS = "degrees_north"
  character (len = *), parameter :: LON_UNITS = "degrees_east"
  character (len = *), parameter :: LEV_UNITS = " "
  character (len = *), parameter :: REC_UNITS = "second"

!- Units of the variables.
```

```
! character (len = *), parameter :: TFLAG_UNITS = "<YYYYDDDHHMMSS>"
  character (len = *), parameter :: JDATE_UNITS = "<YYYYDDD>"
  character (len = *), parameter :: JTIME_UNITS = "<MMSS> or <HMMSS> or
<HHMMSS>"
  character (len = *), parameter :: CONC_UNITS = "ppmV"
  character (len = *), parameter :: RHOJ_UNITS = "m"
  character (len = *), parameter :: CHEMSTEP_UNITS = "min"
  character (len = *), parameter :: RJ_UNITS = " "
  character (len = *), parameter :: SYNS_UNITS = " "

!- Description of the variables.
  character (len = *), parameter :: TFLAG_VDESC = "Timestep-valid flags:
YYYYDDDHHMMSS"
  character (len = *), parameter :: RHOJ_VDESC = "Advected air density X total Jacobian"
  character (len = *), parameter :: CHEMSTEP_VDESC = "Previous Rosenbrock time step"
  character (len = *), parameter :: SYNS_VDESC = "Total syncronization timesteps during the
simulation period"
  character (len = *), parameter :: RJ_VDESC = "Photolysis rates from tables"

  integer :: nc_i  ! Used for do loops

     INTERFACE
       subroutine nc_check(chk_status)
         integer chk_status
       end subroutine nc_check
     END INTERFACE

!- Create the file.
     call nc_check( nf90_create(FILE_NAME, nf90_share, obs_ncid) )

!- Define the dimensions. The time dimension is defined to have unlimited
!- length - it can grow as needed.
     call nc_check( nf90_def_dim(obs_ncid, REC_NAME, NF90_UNLIMITED, rec_dimid ))
     call nc_check( nf90_def_dim(obs_ncid, DATE_NAME, nc_date, date_dimid ) )
     call nc_check( nf90_def_dim(obs_ncid, TIME_NAME, nc_time, time_dimid ) )
     call nc_check( nf90_def_dim(obs_ncid, VAR_NAME, nc_var, var_dimid ) )
     call nc_check( nf90_def_dim(obs_ncid, LEV_NAME, NLAYS, lev_dimid ) )
     call nc_check( nf90_def_dim(obs_ncid, LAT_NAME, NROWS, lat_dimid ) )
     call nc_check( nf90_def_dim(obs_ncid, LON_NAME, NCOLS, lon_dimid ))
     call nc_check( nf90_def_dim(obs_ncid, SYN_NAME, nc_syn, syn_dimid ))

!- Define the coordinate variables for lat, lon, lev, var, rec.
!- Through providing the address of the dimension ID:
!- (lat_dimid), (lon_dimid), (lev_dimid), (dat_dimid), and (rec_dimid).
!    call nc_check( nf90_def_var(obs_ncid, LAT_NAME, NF90_REAL, lat_dimid, lat_varid) )
!    call nc_check( nf90_def_var(obs_ncid, LON_NAME, NF90_REAL, lon_dimid, lon_varid)
)
!    call nc_check( nf90_def_var(obs_ncid, LEV_NAME, NF90_REAL, lev_dimid, lev_varid)
)
!- Assign units to coordiante variables.
!    call nc_check( nf90_put_att(obs_ncid, lat_varid, UNITS, LAT_UNITS) )
!    call nc_check( nf90_put_att(obs_ncid, lon_varid, UNITS, LON_UNITS) )
!    call nc_check( nf90_put_att(obs_ncid, lev_varid, UNITS, LEV_UNITS) )

!- Define arrays dimensions for the variables.
!    tflag_dimids    = (/ dt_dimid, rec_dimid /)
     JDATE_dimids    = (/ date_dimid, rec_dimid /)
     JTIME_dimids    = (/ time_dimid, rec_dimid /)
     nc_dimids       = (/ lon_dimid, lat_dimid, lev_dimid, rec_dimid/)
     rhoj_dimids     = (/ lon_dimid, lat_dimid, lev_dimid, rec_dimid/)
     chemstep_dimids = (/ lon_dimid, lat_dimid, lev_dimid, rec_dimid/)
     rj_dimids       = (/ lon_dimid, lat_dimid, lev_dimid, rec_dimid/)
     syns_dimids     = (/ syn_dimid /)

!- Define the netCDF variables for the concentration, Jacobians, and so on.
!    call nc_check (nf90_def_var(obs_ncid, tflag_name, NF90_REAL, &
!                tflag_dimids, tflag_varid))
     call nc_check (nf90_def_var(obs_ncid, JDATE_name, NF90_REAL, &
                 jdate_dimids, jdate_varid))
     call nc_check (nf90_def_var(obs_ncid, JTIME_name, NF90_REAL, &
                 jtime_dimids, jtime_varid))
     do nc_i=1,nc_GC_SPC                                    ! nc_gc_spc=36
       chk_status =  nf90_def_var(obs_ncid, GC_SPC(nc_i), NF90_REAL, &
                   nc_dimids, conc_varid(nc_i))
     enddo
     call nc_check (nf90_def_var(obs_ncid, rhoj_name, NF90_REAL, &
                 rhoj_dimids, rhoj_varid))
     call nc_check (nf90_def_var(obs_ncid, chemstep_name, NF90_REAL, &
                 chemstep_dimids, chemstep_varid))
     do nc_i=1,6
       call nc_check (nf90_def_var(obs_ncid, rj_name(nc_i), NF90_REAL,  &
                   rj_dimids, rj_varid(nc_i)))
     enddo
     call nc_check (nf90_def_var(obs_ncid, nstep_nreps_name, NF90_REAL, &
                 syns_dimids, syns_varid))

!- Assign units and variable description to the netCDF variables.
!    call nc_check (nf90_put_att(obs_ncid, tflag_varid, UNITS, TFLAG_UNITS))
!    call nc_check (nf90_put_att(obs_ncid, tflag_varid, VDESC, TFLAG_VDESC))

     call nc_check (nf90_put_att(obs_ncid, jdate_varid, UNITS, JDATE_UNITS))
```

```
      call nc_check (nf90_put_att(obs_ncid, jtime_varid, UNITS, JTIME_UNITS))
      do nc_i=1,nc_GC_SPC   ! nc_gc_spc=36
        call nc_check (nf90_put_att(obs_ncid, conc_varid(nc_i), UNITS, CONC_UNITS))
      enddo
      call nc_check (nf90_put_att(obs_ncid, rhoj_varid, UNITS, RHOJ_UNITS))
      call nc_check (nf90_put_att(obs_ncid, rhoj_varid, VDESC, RHOJ_VDESC))
      call nc_check (nf90_put_att(obs_ncid, chemstep_varid, UNITS, CHEMSTEP_UNITS))
      call nc_check (nf90_put_att(obs_ncid, chemstep_varid, VDESC, CHEMSTEP_VDESC))
      call nc_check (nf90_put_att(obs_ncid, syns_varid, UNITS, SYNS_UNITS))
      do nc_i=1,6
        call nc_check (nf90_put_att(obs_ncid, rj_varid(nc_i), UNITS, RJ_UNITS))
        call nc_check (nf90_put_att(obs_ncid, rj_varid(nc_i), VDESC, RJ_VDESC))
      enddo
      call nc_check (nf90_put_att(obs_ncid, syns_varid, VDESC, SYNS_VDESC))

!- End define mode.
      call nc_check( nf90_enddef(obs_ncid))

!- close the file
!     call nc_check( nf90_close(obs_ncid))

  end subroutine nc_chk1_obs


!nc_chk1_chkpt.f90
!- This program is to save CMAQ-ADJOINT variables to netCDF format without using IOAPI.
!- Hongyan Dang, August 2009.
!
      subroutine nc_chk1_chkpt

      use netcdf
      Use KPP_Integrator
      USE HGRD_DEFN           ! horizontal domain specifications
      USE VGRD_DEFN           ! vertical layer specifications
      USE HRDATA

      use nc_adj_module

      implicit none

      include 'gc__spc.ext'
!     INCLUDE SUBST_GC_SPC    ! Gas chem species names and MWs

!- This is the name of the nc_check-point file we will create.
      character(len = *), parameter :: FILE_NAME = "cctmCHK_chkpt.nc"
      integer, parameter :: &
          NDIMS1=1    ,& !
          NDIMS2=2    ,& !
          NDIMS3=3    ,& !
          NDIMS4=4    ,& !
          NRECS=2

!     integer, dimension(1:NDIMS2) :: tflag_dimids
!     integer, dimension(1:NDIMS2) :: jdate_dimids
!     integer, dimension(1:NDIMS2) :: jtime_dimids
!     integer, dimension(1:NDIMS4) :: rhoj_dimids
!     integer, dimension(1:NDIMS4) :: nc_dimids
!     integer, dimension(1:NDIMS4) :: chemstep_dimids
!     integer, dimension(1:NDIMS1) :: syns_dimids
!     integer, dimension(1:NDIMS4) :: rj_dimids

!- Writing 4D data, a 156 X 96 X 14 lon-lat-lev grid, with unknown timesteps of data.
      integer, parameter :: &
          nc_date  =  1  ,& ! number of time
          nc_time  =  1  ,& ! number of time
          nc_var   =  44 ,& ! 44 variables
          nc_rj    =  6  ,&
          nc_syn   =  1
      character (len = *), parameter :: &
          LON_NAME = "COL"         ,& !
          LAT_NAME = "ROW"         ,& !
          LEV_NAME = "LAY"         ,& !
          VAR_NAME = "VAR"         ,& !
          DATE_NAME = "DATE_SIZE"  ,& !
          TIME_NAME = "TIME_SIZE"  ,& !
          REC_NAME = "TSTEP"       ,& !
          DAT_NAME = "DATE-TIME"   ,& !
          SYN_NAME = "SYNC_SIZE"

!- Start and count arrays to tell the netCDF library where to write data.
      integer :: start(NDIMS4), count(NDIMS4)

!- Create 2+44 variables to save timestep and field values.
!-    these settings uses the definitions in "include SUBST_GC_SPC"
      character (len=*), parameter :: tflag_name        = "JDATEJTIME"
      character (len=16), parameter :: jdate_name       = "JDATE          "
      character (len=16), parameter :: jtime_name       = "JTIME          "      !
      character (len=16), parameter :: rhoj_name        = "RHOJ           "
      character (len=16), parameter :: chemstep_name    = "CHEMSTEP       "
      character (len=16), parameter :: nstep_nreps_name = "N_SYNS         "
      character (len=16) :: rj_name(6)
```

```
      data rj_name(1)/"RJ1           "/
      data rj_name(2)/"RJ2           "/
      data rj_name(3)/"RJ3           "/
      data rj_name(4)/"RJ4           "/
      data rj_name(5)/"RJ5           "/
      data rj_name(6)/"RJ6           "/

!- Totally (N_GC_SPC + 8 = 36 + 8 = 44) variables will be written to "CCTM_fwdCHK.nc".
      INTEGER,parameter ::    nc_GC_SPC=36, nc_GC_SPCD=nc_GC_SPC + 1
      CHARACTER (len=16)   nc_SPC(nc_GC_SPCD+8)

!- Units of the 44 variables
  character (len = *), parameter :: UNITS = "units"
  character (len = *), parameter :: VDESC = "var_desc"

!- Units of the coordinate variables.
  character (len = *), parameter :: LAT_UNITS = "degrees_north"
  character (len = *), parameter :: LON_UNITS = "degrees_east"
  character (len = *), parameter :: LEV_UNITS = " "
  character (len = *), parameter :: REC_UNITS = "second"

!- Units of the variables.
! character (len = *), parameter :: TFLAG_UNITS = "<YYYYDDDHHMMSS>"
  character (len = *), parameter :: JDATE_UNITS = "<YYYYDDD>"
  character (len = *), parameter :: JTIME_UNITS = "<MMSS> or <HMMSS> or
<HHMMSS>"
  character (len = *), parameter :: CONC_UNITS = "ppmV"
  character (len = *), parameter :: RHOJ_UNITS = "m"
  character (len = *), parameter :: CHEMSTEP_UNITS = "min"
  character (len = *), parameter :: RJ_UNITS = " "
  character (len = *), parameter :: SYNS_UNITS = " "

!- Description of the variables.
  character (len = *), parameter :: TFLAG_VDESC = "Timestep-valid flags:
YYYYDDDHHMMSS"
  character (len = *), parameter :: RHOJ_VDESC = "Advected air density X total Jacobian"
  character (len = *), parameter :: CHEMSTEP_VDESC = "Previous Rosenbrock time step"
  character (len = *), parameter :: SYNS_VDESC = "Total syncronization timesteps during the
simulation period"
  character (len = *), parameter :: RJ_VDESC = "Photolysis rates from tables"

  integer :: nc_i  ! Used for do loops

     INTERFACE
       subroutine nc_check(chk_status)
         integer chk_status
         end subroutine nc_check
     END INTERFACE

!- Create the file.
      call nc_check( nf90_create(FILE_NAME, nf90_share, chkpt_ncid) )

!- Define the dimensions. The time dimension is defined to have unlimited
!- length - it can grow as needed.
      call nc_check( nf90_def_dim(chkpt_ncid, REC_NAME, NF90_UNLIMITED, rec_dimid ))
      call nc_check( nf90_def_dim(chkpt_ncid, DATE_NAME, nc_date, date_dimid ) )
      call nc_check( nf90_def_dim(chkpt_ncid, TIME_NAME, nc_time, time_dimid ) )
      call nc_check( nf90_def_dim(chkpt_ncid, VAR_NAME, nc_var, var_dimid ) )
      call nc_check( nf90_def_dim(chkpt_ncid, LEV_NAME, NLAYS, lev_dimid ) )
      call nc_check( nf90_def_dim(chkpt_ncid, LAT_NAME, NROWS, lat_dimid ) )
      call nc_check( nf90_def_dim(chkpt_ncid, LON_NAME, NCOLS, lon_dimid ))
      call nc_check( nf90_def_dim(chkpt_ncid, SYN_NAME, nc_syn, syn_dimid ))

!- Define the coordinate variables for lat, lon, lev, var, rec.
!- Through providing the address of the dimension ID:
!- (lat_dimid), (lon_dimid), (lev_dimid), (dat_dimid), and (rec_dimid).
!     call nc_check( nf90_def_var(chkpt_ncid, LAT_NAME, NF90_REAL, lat_dimid,
lat_varid) )
!     call nc_check( nf90_def_var(chkpt_ncid, LON_NAME, NF90_REAL, lon_dimid,
lon_varid) )
!     call nc_check( nf90_def_var(chkpt_ncid, LEV_NAME, NF90_REAL, lev_dimid,
lev_varid) )
!- Assign units to coordiante variables.
!     call nc_check( nf90_put_att(chkpt_ncid, lat_varid, UNITS, LAT_UNITS) )
!     call nc_check( nf90_put_att(chkpt_ncid, lon_varid, UNITS, LON_UNITS) )
!     call nc_check( nf90_put_att(chkpt_ncid, lev_varid, UNITS, LEV_UNITS) )

!- Define arrays dimensions for the variables.
!     tflag_dimids    = (/ dt_dimid, rec_dimid /)
      JDATE_dimids    = (/ date_dimid, rec_dimid /)
      JTIME_dimids    = (/ time_dimid, rec_dimid /)
      nc_dimids       = (/ lon_dimid, lat_dimid, lev_dimid, rec_dimid/)
      rhoj_dimids     = (/ lon_dimid, lat_dimid, lev_dimid, rec_dimid/)
      chemstep_dimids = (/ lon_dimid, lat_dimid, lev_dimid, rec_dimid/)
      rj_dimids       = (/ lon_dimid, lat_dimid, lev_dimid, rec_dimid/)
      syns_dimids     = (/ syn_dimid /)

!- Define the netCDF variables for the concentration, Jacobians, and so on.
!     call nc_check (nf90_def_var(chkpt_ncid, tflag_name, NF90_REAL, &
!                 tflag_dimids, tflag_varid))
      call nc_check (nf90_def_var(chkpt_ncid, JDATE_name, NF90_REAL, &
                  jdate_dimids, jdate_varid))
```

```
      call nc_check (nf90_def_var(chkpt_ncid, JTIME_name, NF90_REAL, &
                  jtime_dimids, jtime_varid))
      do nc_i=1,nc_GC_SPC                                  ! nc_gc_spc=36
        chk_status =  nf90_def_var(chkpt_ncid, GC_SPC(nc_i), NF90_REAL, &
                    nc_dimids, conc_varid(nc_i))
      enddo
      call nc_check (nf90_def_var(chkpt_ncid, rhoj_name, NF90_REAL, &
                  rhoj_dimids, rhoj_varid))
      call nc_check (nf90_def_var(chkpt_ncid, chemstep_name, NF90_REAL, &
                  chemstep_dimids, chemstep_varid))
      do nc_i=1,6
        call nc_check (nf90_def_var(chkpt_ncid, rj_name(nc_i), NF90_REAL,  &
                    rj_dimids, rj_varid(nc_i)))
      enddo
      call nc_check (nf90_def_var(chkpt_ncid, nstep_nreps_name, NF90_REAL, &
                  syns_dimids, syns_varid))

!- Assign units and variable description to the netCDF variables.
!     call nc_check (nf90_put_att(chkpt_ncid, tflag_varid, UNITS, TFLAG_UNITS))
!     call nc_check (nf90_put_att(chkpt_ncid, tflag_varid, VDESC, TFLAG_VDESC))

      call nc_check (nf90_put_att(chkpt_ncid, jdate_varid, UNITS, JDATE_UNITS))
      call nc_check (nf90_put_att(chkpt_ncid, jtime_varid, UNITS, JTIME_UNITS))
      do nc_i=1,nc_GC_SPC   ! nc_gc_spc=36
        call nc_check (nf90_put_att(chkpt_ncid, conc_varid(nc_i), UNITS, CONC_UNITS))
      enddo
      call nc_check (nf90_put_att(chkpt_ncid, rhoj_varid, UNITS, RHOJ_UNITS))
      call nc_check (nf90_put_att(chkpt_ncid, rhoj_varid, VDESC, RHOJ_VDESC))
      call nc_check (nf90_put_att(chkpt_ncid, chemstep_varid, UNITS, CHEMSTEP_UNITS))
      call nc_check (nf90_put_att(chkpt_ncid, chemstep_varid, VDESC, CHEMSTEP_VDESC))
      call nc_check (nf90_put_att(chkpt_ncid, syns_varid, UNITS, SYNS_UNITS))
      do nc_i=1,6
        call nc_check (nf90_put_att(chkpt_ncid, rj_varid(nc_i), UNITS, RJ_UNITS))
        call nc_check (nf90_put_att(chkpt_ncid, rj_varid(nc_i), VDESC, RJ_VDESC))
      enddo
      call nc_check (nf90_put_att(chkpt_ncid, syns_varid, VDESC, SYNS_VDESC))

!- End define mode.
      call nc_check( nf90_enddef(chkpt_ncid))

!- close the file
!     call nc_check( nf90_close(chkpt_ncid))

  end subroutine nc_chk1_chkpt
```



```
!nc_chk1_bg.f90
!- This program is to save CMAQ-ADJOINT variables to netCDF format without using IOAPI.
!- Hongyan Dang, August 2009.
!
      subroutine nc_chk1_bg

      use netcdf
      Use KPP_Integrator
      USE HGRD_DEFN          ! horizontal domain specifications
      USE VGRD_DEFN          ! vertical layer specifications
      USE HRDATA

      use nc_adj_module

      implicit none

      include 'gc__spc.ext'
!     INCLUDE SUBST_GC_SPC    ! Gas chem species names and MWs

!- This is the name of the nc_check-point file we will create.
      character(len = *), parameter :: FILE_NAME = "cctmCHK_L5bg.nc"

      integer, parameter :: &
          NDIMS1=1    ,& !
          NDIMS2=2    ,& !
          NDIMS3=3    ,& !
          NDIMS4=4    ,& !
          NRECS=2

!     integer, dimension(1:NDIMS2) :: tflag_dimids
!     integer, dimension(1:NDIMS2) :: jdate_dimids
!     integer, dimension(1:NDIMS2) :: jtime_dimids
!     integer, dimension(1:NDIMS4) :: rhoj_dimids
!     integer, dimension(1:NDIMS4) :: nc_dimids
!     integer, dimension(1:NDIMS4) :: chemstep_dimids
!     integer, dimension(1:NDIMS1) :: syns_dimids
!     integer, dimension(1:NDIMS4) :: rj_dimids

!- Writing 4D data, a 156 X 96 X 14 lon-lat-lev grid, with unknown timesteps of data.
      integer, parameter :: &
          nc_date  =  1  ,& ! number of time
          nc_time  =  1  ,& ! number of time
          nc_var   =  44  ,& ! 44 variables
          nc_rj    =  6  ,&
          nc_syn   =  1
      character (len = *), parameter :: &
```

```
      LON_NAME = "COL"        ,& !
      LAT_NAME = "ROW"        ,& !
      LEV_NAME = "LAY"        ,& !
      VAR_NAME = "VAR"        ,& !
      DATE_NAME = "DATE_SIZE"  ,& !
      TIME_NAME = "TIME_SIZE"  ,& !
      REC_NAME = "TSTEP"      ,& !
      DAT_NAME = "DATE-TIME"   ,& !
      SYN_NAME = "SYNC_SIZE"

!- Start and count arrays to tell the netCDF library where to write data.
    integer :: start(NDIMS4), count(NDIMS4)

!- Create 2+44 variables to save timestep and field values.
!-   these settings uses the definitions in "include SUBST_GC_SPC"
    character (len=*), parameter :: tflag_name       = "JDATEJTIME"
    character (len=16), parameter :: jdate_name      = "JDATE          "
    character (len=16), parameter :: jtime_name      = "JTIME          "      !
    character (len=16), parameter :: rhoj_name       = "RHOJ           "
    character (len=16), parameter :: chemstep_name   = "CHEMSTEP       "
    character (len=16), parameter :: nstep_nreps_name = "N_SYNS         "
    character (len=16) :: rj_name(6)
    data rj_name(1)/"RJ1            "/
    data rj_name(2)/"RJ2            "/
    data rj_name(3)/"RJ3            "/
    data rj_name(4)/"RJ4            "/
    data rj_name(5)/"RJ5            "/
    data rj_name(6)/"RJ6            "/

!- Totally (N_GC_SPC + 8 = 36 + 8 = 44) variables will be written to "CCTM_fwdCHK.nc".
    INTEGER,parameter ::    nc_GC_SPC=36, nc_GC_SPCD=nc_GC_SPC + 1
    CHARACTER (len=16)   nc_SPC(nc_GC_SPCD+8)

!- Units of the 44 variables
  character (len = *), parameter :: UNITS = "units"
  character (len = *), parameter :: VDESC = "var_desc"

!- Units of the coordinate variables.
  character (len = *), parameter :: LAT_UNITS = "degrees_north"
  character (len = *), parameter :: LON_UNITS = "degrees_east"
  character (len = *), parameter :: LEV_UNITS = " "
  character (len = *), parameter :: REC_UNITS = "second"

!- Units of the variables.
! character (len = *), parameter :: TFLAG_UNITS = "<YYYYDDDHHMMSS>"
  character (len = *), parameter :: JDATE_UNITS = "<YYYYDDD>"
  character (len = *), parameter :: JTIME_UNITS = "<MMSS> or <HMMSS> or
<HHMMSS>"
  character (len = *), parameter :: CONC_UNITS = "ppmV"
  character (len = *), parameter :: RHOJ_UNITS = "m"
  character (len = *), parameter :: CHEMSTEP_UNITS = "min"
  character (len = *), parameter :: RJ_UNITS = " "
  character (len = *), parameter :: SYNS_UNITS = " "

!- Description of the variables.
  character (len = *), parameter :: TFLAG_VDESC = "Timestep-valid flags:
YYYYDDDHHMMSS"
  character (len = *), parameter :: RHOJ_VDESC = "Advected air density X total Jacobian"
  character (len = *), parameter :: CHEMSTEP_VDESC = "Previous Rosenbrock time step"
  character (len = *), parameter :: SYNS_VDESC = "Total syncronization timesteps during the
simulation period"
  character (len = *), parameter :: RJ_VDESC = "Photolysis rates from tables"

  integer :: nc_i  ! Used for do loops

     INTERFACE
       subroutine nc_check(chk_status)
         integer chk_status
       end subroutine nc_check
     END INTERFACE

!- Create the file.
    call nc_check( nf90_create(FILE_NAME, nf90_share, bg_ncid) )

!- Define the dimensions. The time dimension is defined to have unlimited
!- length - it can grow as needed.
    call nc_check( nf90_def_dim(bg_ncid, REC_NAME, NF90_UNLIMITED, rec_dimid ))
    call nc_check( nf90_def_dim(bg_ncid, DATE_NAME, nc_date, date_dimid ) )
    call nc_check( nf90_def_dim(bg_ncid, TIME_NAME, nc_time, time_dimid ) )
    call nc_check( nf90_def_dim(bg_ncid, VAR_NAME, nc_var, var_dimid ) )
    call nc_check( nf90_def_dim(bg_ncid, LEV_NAME, NLAYS, lev_dimid ) )
    call nc_check( nf90_def_dim(bg_ncid, LAT_NAME, NROWS, lat_dimid ) )
    call nc_check( nf90_def_dim(bg_ncid, LON_NAME, NCOLS, lon_dimid ))
    call nc_check( nf90_def_dim(bg_ncid, SYN_NAME, nc_syn, syn_dimid ))

!- Define the coordinate variables for lat, lon, lev, var, rec.
!- Through providing the address of the dimension ID:
!- (lat_dimid), (lon_dimid), (lev_dimid), (dat_dimid), and (rec_dimid).
!    call nc_check( nf90_def_var(bg_ncid, LAT_NAME, NF90_REAL, lat_dimid, lat_varid) )
!    call nc_check( nf90_def_var(bg_ncid, LON_NAME, NF90_REAL, lon_dimid, lon_varid)
)
!    call nc_check( nf90_def_var(bg_ncid, LEV_NAME, NF90_REAL, lev_dimid, lev_varid) )
```

```
!- Assign units to coordiante variables.
!     call nc_check( nf90_put_att(bg_ncid, lat_varid, UNITS, LAT_UNITS) )
!     call nc_check( nf90_put_att(bg_ncid, lon_varid, UNITS, LON_UNITS) )
!     call nc_check( nf90_put_att(bg_ncid, lev_varid, UNITS, LEV_UNITS) )

!- Define arrays dimensions for the variables.
!     tflag_dimids    = (/ dt_dimid, rec_dimid /)
      JDATE_dimids    = (/ date_dimid, rec_dimid /)
      JTIME_dimids    = (/ time_dimid, rec_dimid /)
      nc_dimids       = (/ lon_dimid, lat_dimid, lev_dimid, rec_dimid/)
      rhoj_dimids     = (/ lon_dimid, lat_dimid, lev_dimid, rec_dimid/)
      chemstep_dimids = (/ lon_dimid, lat_dimid, lev_dimid, rec_dimid/)
      rj_dimids       = (/ lon_dimid, lat_dimid, lev_dimid, rec_dimid/)
      syns_dimids     = (/ syn_dimid /)

!- Define the netCDF variables for the concentration, Jacobians, and so on.
!     call nc_check (nf90_def_var(bg_ncid, tflag_name, NF90_REAL, &
!                  tflag_dimids, tflag_varid))
      call nc_check (nf90_def_var(bg_ncid, JDATE_name, NF90_REAL, &
                  jdate_dimids, jdate_varid))
      call nc_check (nf90_def_var(bg_ncid, JTIME_name, NF90_REAL, &
                  jtime_dimids, jtime_varid))
      do nc_i=1,nc_GC_SPC                                    ! nc_gc_spc=36
        chk_status =  nf90_def_var(bg_ncid, GC_SPC(nc_i), NF90_REAL, &
                    nc_dimids, conc_varid(nc_i))
      enddo
      call nc_check (nf90_def_var(bg_ncid, rhoj_name, NF90_REAL, &
                  rhoj_dimids, rhoj_varid))
      call nc_check (nf90_def_var(bg_ncid, chemstep_name, NF90_REAL, &
                  chemstep_dimids, chemstep_varid))
      do nc_i=1,6
        call nc_check (nf90_def_var(bg_ncid, rj_name(nc_i), NF90_REAL,  &
                    rj_dimids, rj_varid(nc_i)))
      enddo
      call nc_check (nf90_def_var(bg_ncid, nstep_nreps_name, NF90_REAL, &
                  syns_dimids, syns_varid))

!- Assign units and variable description to the netCDF variables.
!     call nc_check (nf90_put_att(bg_ncid, tflag_varid, UNITS, TFLAG_UNITS))
!     call nc_check (nf90_put_att(bg_ncid, tflag_varid, VDESC, TFLAG_VDESC))

      call nc_check (nf90_put_att(bg_ncid, jdate_varid, UNITS, JDATE_UNITS))
      call nc_check (nf90_put_att(bg_ncid, jtime_varid, UNITS, JTIME_UNITS))
      do nc_i=1,nc_GC_SPC   ! nc_gc_spc=36
        call nc_check (nf90_put_att(bg_ncid, conc_varid(nc_i), UNITS, CONC_UNITS))
      enddo
      call nc_check (nf90_put_att(bg_ncid, rhoj_varid, UNITS, RHOJ_UNITS))
      call nc_check (nf90_put_att(bg_ncid, rhoj_varid, VDESC, RHOJ_VDESC))
      call nc_check (nf90_put_att(bg_ncid, chemstep_varid, UNITS, CHEMSTEP_UNITS))
      call nc_check (nf90_put_att(bg_ncid, chemstep_varid, VDESC, CHEMSTEP_VDESC))
      call nc_check (nf90_put_att(bg_ncid, syns_varid, UNITS, SYNS_UNITS))
      do nc_i=1,6
        call nc_check (nf90_put_att(bg_ncid, rj_varid(nc_i), UNITS, RJ_UNITS))
        call nc_check (nf90_put_att(bg_ncid, rj_varid(nc_i), VDESC, RJ_VDESC))
      enddo
      call nc_check (nf90_put_att(bg_ncid, syns_varid, VDESC, SYNS_VDESC))

!- End define mode.
      call nc_check( nf90_enddef(bg_ncid))

!- close the file
!     call nc_check( nf90_close(bg_ncid))

  end subroutine nc_chk1_bg
```